Department of Spatial Sciences

A Remote Sensing Based Approach to Enhance Food Security in the Greater Horn of Africa

Nathan Okoth Agutu

This thesis is presented for the Degree of
Doctor of Philosophy
of
Curtin University

August 2017

To the best of my knowledge and belief this thesis contains no material previously published by any other person except where due acknowledgement has been made. This thesis contains no material which has been accepted for the award of any other degree or diploma in any university.

Agutu Nathan

24-08-2017

"Sure I am this day we are masters of our fate, that the task which has been set before us is not above our strength; that its pangs and toils are not beyond our endurance. As long as we have faith in our own cause and an unconquerable will to win, victory will not be denied us."

- Winston S. Churchill

Acknowledgements

I would like to express my profound gratitude and appreciation to my supervisory team of Professor Joseph L. Awange, Dr. Robert Corner, and Associate Professor John B. K. Kiema for their guidance and contributions during the course of this PhD.

I am grateful to Curtin University for financing this PhD through - Curtin Strategic International Research Scholarship (CSIRS) without which this journey would not have been possible. I would also like to register my deepest appreciations to the Department of Spatial Sciences for providing me with a conducive environment and further support as my enrolling area.

Further, I am thankful to my home University, Jomo Kenyatta University of Agriculture and Technology, for granting me study leave during the duration of this PhD and the department of Geomatic Engineering and Geospatial Information Systems for their continued support.

Last but not least, I would like to thank my family members who have stood by me in the course of this journey from lower levels up to this moment. Finally, am grateful to the Almighty God for seeing me through this journey.

Abstract

Greater Horn of Africa (GHA), one of the most food insecure regions in the world, descends into acute food insecurity with catastrophic consequences whenever droughts occur due to its reliance on rain-fed agriculture. Other than droughts, other major causes of food insecurity in the region include, e.g., conflicts, high population growth, low crop yield due to poor water control, climate change and/or variability, and poverty. With climate change impacts and high population growth projected to exacerbate the food insecurity situation in the GHA region, this thesis examined agricultural drought and groundwater exploitation related issues to enhance food security. Specifically, the thesis (i) characterized agricultural droughts (1982 – 2013) and assessed the utility of agricultural drought indicators over the region, (ii) explored the impact of topography on agricultural drought characterization, (iii) examined the characteristics of model and reanalysis soil moisture products over the region, and (iv) explored the possibility of using Gravity Recovery and Climate Experiment (GRACE) to monitor large scale groundwater changes and their potential for irrigation, in view of the region lacking in-situ groundwater measurements. To achieve the aforementioned objectives, the thesis made use of the following analysis methods; standardized indices and anomalies, rotated principal component analysis (RPCA), partial least squares regression (PLSR), generalized three-cornered hat (TCH) method, Tylor diagrams, Pearson correlations, independent component analysis (ICA), and least squares trend analysis.

All the employed products (precipitation, soil moisture, vegetation condition index, and terrestrial water storage) showed largely consistent spatio-temporal drought patterns over lowland and relatively low rainfall areas of Eastern Kenya, Eastern Ethiopia, and Somalia compared to higher topography changing areas e.g., Ethiopian highlands. Further, the rainfall products were largely consistent over the whole region and had the highest areas under drought closely followed by soil moisture products, which had different areas, while VCI had the least areas

under drought. The drought cycle (onset, peak, and cessation) was observed to be registered first by rainfall then VCI/soil moisture and finally the TWS products. Finally, other than VCI (with 0-4 months lag) the rest of the product had inconsistent lags (differing from one drought episode to the other) in relation to drought cycle as picked by rainfall and amongst themselves.

Following agricultural drought characterization, the indicators were regressed on national annual crop production to evaluate their effectiveness in capturing agricultural droughts. Results showed CHIRPS, GPCC, and VCI explaining relatively higher variability in national annual crop production over Kenya, Uganda, Tanzania, and Ethiopia. Further, of the soil moisture products, FLDAS consistently explained relatively high percentage of variability in annual crop production over the region. In contrast, MERRA-2, ERA-Interim, and CPC explained higher percentage of variability in national annual crop production in only one or two countries. This inconsistency in the percentage of variability in national annul crop production explained is closely related to that observed in drought characterization above.

In response to the low consistency of spatio-temporal drought patterns over rapidly changing topographical areas observed in drought characterization above, coupled with reported complex topography - precipitation relationship over upper GHA, the study evaluated the impacts of topography on drought characterization. Results showed spatio-temporal drought patterns being influenced by topography of the region, especially over upper GHA where topography is a major factor. In addition, topography and gauge density (spatial distribution and availability) were found to influence the spatial extent and intensity of drought events as captured by rainfall products. In comparison, the drought spatial extent and intensity as captured by the soil moisture products were influenced by forcing precipitation and model thresholds. The influence of topography on drought characterization by the soil moisture products were largely through the forcing precipitation. Finally, the impacts were observed to be higher during moderate

and extreme droughts compared to severe droughts for both rainfall and soil moisture products.

Due to the inconsistent performance of the soil moisture products in drought characterization and evaluation of utilities observed above, and lack of in-situ soil moisture monitoring network over the region coupled with its critical role in agricultural drought monitoring, the study evaluated characteristics of major model soil moisture products. Uncertainties analyses showed higher magnitude of uncertainties in the soil moisture products over high rainfall areas and low uncertainties over low rainfall areas of GHA. Higher proportion of these uncertainties originated from uncertainties in magnitudes of spatial variability than uncertainty in spatial patterns. In addition, interannual variability analysis showed higher magnitude of uncertainties across the soil moisture products during wet seasons than dry ones over Ethiopian highlands and South Sudan for annual, MAM, JJAS, and OND means. On the other hand, Sudan, EA, East Ethiopia and Somalia had higher uncertainties during dry seasons than wet ones for the interannual variability analysis of annual, MAM, JJAS, and OND mean. Also, the spatio-temporal modes (PCA decomposed) of the soil moisture products were consistent with rainfall modes (also PCA decomposed) over the region except for GLDAS-VIC, CPC, GLDAS-CLM, and GLDAS-Mosaic, which missed the variability associated with the second rainfall (OND) over EA. Overall, FLDAS-Noah and MERRA-2 were consistently of lower uncertainties over the whole region while CPC had the highest uncertainty.

Finally, due to the importance of groundwater irrigated agriculture in enhancing food productivity, the study explored the use of GRACE for large scale groundwater monitoring to aid sustainable groundwater irrigation. From the GRACE-derived and ICA localized groundwater changes, the study identified the following aquifers (and/or groundwater areas); Nubian sandstone, Karoo Carbonate, Upper Nile, Ethiopian highlands, Lake Tana region, Kenya-Somalia, Central Tanzania, Karoo sandstone, and Ruvuma. All the

temporal evolutions of the identified aquifers, except Nubian sandstone and Kenya-Somalia, showed annual (cyclic) patterns indicating annual (yearly) recharge cycle. Further, least squares trend analysis of groundwater temporal evolution revealed increasing groundwater levels for Ethiopian highlands, Lake Tana region, and Kenya-Somalia; stable groundwater levels for Upper Nile, Karoo Carbonate, and Central Tanzania; and decreasing groundwater level changes for Nubian Sandstone and Ruvuma. In addition, the results showed limited/very low association between temporal groundwater levels and climate variability indices (ENSO and IOD), highlighting the advantage provided by groundwater under the influence of climate change. Finally, based on water availability (from GRACE), water quality (measured by total dissolved substance) and dominant soil types, potential for groundwater irrigated agriculture results showed low potentials for Nubian Sandstone and Kenya-Somalia areas; low to moderate potentials for Karoo Carbonate, Lake Tana region, central Tanzania, and Ruvuma; moderate to high potentials for Upper Nile and Karoo Sandstone; and high potential for Ethiopian highland.

The results of this study are crucial as they extend the understanding of agricultural drought over the region and could possibly contribute to enhancement of food security when applied to agricultural drought monitoring frameworks; development of food security early warning systems; enhancement of mobilization, management, and distribution of relief food; sustainable groundwater exploitation; and enhancement of groundwater irrigated agriculture.

Contents

1 Introduction

1.1 Food Security: A Definition

Food and Agricultural Organization (FAO) defines food security as a situation that exists when all the people, at all the times, have physical, economic, and social access to sufficient, safe, and nutritious food that meets their dietary requirements and food preference for an active and healthy life (see, e.g., *Schmidhuber and Tubiello*, 2007; *Boko et al.*, 2007). This definition has further been extended to include the following four major concepts/dimensions (*McCalla*, 1999; *Schmidhuber and Tubiello*, 2007; *Boko et al.*, 2007):

(i) Food availability - indicated by the amount of food that can be directly produced e.g., domestic production, imports, food aids etc,.

(ii) Food access - ability of the population to purchase appropriate food i.e., economic prosperity and market forces.

(iii) Food utilization - encompasses all food safety and quality aspects of nutrition.

(iv) Food stability - ability of individuals to withstand temporary shocks in food availability cycle and income.

Further, food security is layered in levels from household, national, to global with household food security building up to national which builds up to global but the reverse does not hold hence food security should be solved at the household level (*McCalla*, 1999).

1.2 Food Security Dynamics in Greater Horn of Africa

Over Greater Horn of Africa (GHA), food security is linked to agriculture, which is the major economic sector employing approximately 65% of the labor force, contributing up to about 42% of the countries' gross domestic products, and where

smallholder subsistence farmers contribute about 90% (*Adhikari et al.*, 2015). The vast majority of the smallholder farmers are dependent on rain-fed agriculture for their livelihood (*Shiferaw et al.*, 2014). As a result, agriculture is both a source of food and income, and directly determines the food security vulnerability of the majority of GHA population. The GHA is one of the most food-insecure regions in the world with over 70 million people living in areas prone to food shortages (*Technical Cooperation Department*, 2000). The per capita food availability over Sub-Sahara Africa, of which GHA is part of, has been below the world's average due to a combination of various factors e.g., high population growth rate, slow and sometimes negative growth rate in agricultural production, climate variability, and poverty (*McCalla*, 1999). The main causes of food insecurity over GHA include, e.g., natural hazards (frequent droughts and occasional floods), conflicts, population growth, fragile ecosystems, low agricultural productivity, climate change and/or variability, and poverty (see, e.g., *McCalla*, 1999; *Technical Cooperation Department*, 2000; *Niang et al.*, 2014; *Agola and Awange*, 2014).

Of the natural hazards listed above, drought is the main cause of food insecurity over GHA and represents one of the most natural triggers of malnutrition and famine (*Technical Cooperation Department*, 2000; *FAO*, 2011; *Mpelasoka et al.*, 2018). It affects all the four dimensions of food security; availability, accessibility, utilization, and stability. As most of GHA region is either arid or semi-arid with low, unreliable, and unevenly distributed rainfall, droughts have always been part of the climate system of the region though recent studies (see, e.g., *Ibrahim*, 1988; *Olsson*, 1993; *Gebrehiwot et al.*, 2011; *Edossa et al.*, 2010; *Williams and Funk*, 2011; *Lyon*, 2014; *Nicholson*, 2014a; *Niang et al.*, 2014; *Mpelasoka et al.*, 2018) suggest that they are increasing in intensity and frequency. Due to the heavy reliance on rain-fed agriculture, therefore, the region has always been plunged into food shortages whenever droughts strike and the food production system remains vulnerable (see, e.g., *Rojas et al.*, 2011; *Loewenberg*, 2011; *IFRC*, 2011; *OEA*, 2011a,b). Drought

impacts on agriculture include crop losses, lower yields in both crops and livestock productions, increased livestock deaths, increase in insect infestation and plant and animal diseases. Its impact on human health ranges from increased risk of food and water shortages to increased risk of malnutrition and a higher risk of water and food borne diseases (*FAO*, 2011; *Shiferaw et al.*, 2014; *Niang et al.*, 2014). In addition, drought has always led to increased food prices as supplies are reduced with severe effects on the poor and the most vulnerable (*Demombynes and Kiringai*, 2011; *FAO*, 2011). Indirectly, it has led to economic losses in growth of countries in the region (*Shiferaw et al.*, 2014). These impacts of drought on food security over the region are exacerbated by the effects of high population growth rate.

Africa has the highest population growth rate and is projected to remain highest among the continents (*United Nations*, 2015), while within the continent, GHA has the 2nd highest population growth rate after Central African region (*Ashton and Turton*, 2009). This rapidly growing population has a huge implication on food security when considered in conjunction with poverty and inadequate policies (*Shiferaw et al.*, 2014). High population growth rate increases pressure on limited and fragile land resources leading to unsustainable resource exploitation, which results in environmental degradation (*Technical Cooperation Department*, 2000; *Shiferaw et al.*, 2014; *Adhikari et al.*, 2015). The increasing population also drives fragmentation of landholdings leading to increased stress on smallholder and subsistence agriculture (*Morton*, 2007). The increased pressure on food producing system by the increasing population makes GHA so vulnerable that any small shock on the food production system (rain-fed agriculture), e.g., caused by droughts or armed conflicts, rapidly makes the region food insecure.

Armed conflicts within and between countries in the region is another factor contributing to food insecurity (see, e.g., *Technical Cooperation Department*, 2000; *Peace Bulletin*, 2003; *Rowhani et al.*, 2011; *Scheffran and Battaglini*, 2011).

Conflicts and food insecurity are closely linked with each triggering the other as a struggle for resources increase due to population pressure. As food security is linked to smallholder rain-fed subsistence agriculture, any factor that prevents the population from day to day farming e.g., conflict directly leads to food insecurity. Also, conflicts have displaced a large portion of the population of some countries in the region e.g., Somalia and South Sudan. The displaced population now residing in refugee camps across other countries put additional pressure on food resources of those countries thus making them vulnerable to food insecurity. In addition, conflicts disrupt food marketing and distribution systems. Finally, due to the conflicts in this region, the governments have allocated millions of dollars in to military expenditure and equipments, money that would have otherwise been spent on mitigating the impacts of drought-driven food insecurity.

Low agricultural productivity has also contributed to food insecurity of GHA region, i.e., the region has one of the lowest yields in the world (*Adhikari et al.*, 2015; *Technical Cooperation Department*, 2000; *FAO*, 2011). The low productivity has been attributed to lack of water control as only less than 1% of the cultivatable land is irrigated as compared to other regions e.g., Asia with approximately 37% (see, e.g., *Siebert et al.*, 2010; *Adhikari et al.*, 2015). This lack of irrigation makes the region vulnerable to rainfall variability and also may discourage farmers from having additional investments in quality seeds and fertilizers due to uncertainties in rainfall hence low productivity in crops. In addition to low agricultural productivity, being dependent on small range of crops and/or pastoralism due to lack of irrigation and access to markets makes the farmers in the region vulnerable to food insecurity. Finally, the limited data and/or analytical capacities of governments to respond quickly to the changing environment most of the time do rapidly compound the bad food security situation. Other factors that have indirectly impacted on the food security of the region include neglecting of pastoralism by the governments, uneven effects of market liberalization, weak infrastructure, poor health, and low standard of

education. The effects of the aforementioned factors on food insecurity are likely to be exacerbated by the impact of climate change and/or variability.

At macro-level, climate change and/or variability affect food security through its broader influence on investment, adoption of agricultural technology, aggregated food production, market prices and economic development, which in turn determine the ability of individuals, communities, and nations to produce and purchase food (*Zimmerman and Carter*, 2003; *Shiferaw et al.*, 2014). Climate change, such as periods of droughts and floods as well as long term changes, may either directly or indirectly impact on the four dimensions of food security (see, e.g., *Schmidhuber and Tubiello*, 2007; *Boko et al.*, 2007; *Niang et al.*, 2014); its impact on food availability, access, and nutrient is summarized in Figure 1.1. Its impact on food stability is through changes in food availability and access (*Boko et al.*, 2007; *Niang et al.*, 2014). Further, climate change and/or variability is projected to aggravate the frequency, severity, spatial extents, and duration of drought events and associated impacts (*Wilhite and Pulwarty*, 2005; *FAO*, 2011; *Schmidhuber and Tubiello*, 2007; *Shiferaw et al.*, 2014). In addition, climate change related precipitation variability is projected to increase irrigation water demand (*Shiferaw et al.*, 2014). The increase in frequency and severity of extreme events, i.e., floods and droughts, and increased irrigation water demand are likely to further decrease crop water availability and threaten the productivity of rain-fed agriculture over the region (e.g., *Shiferaw et al.*, 2014) thus increased food insecurity.

1.3 Enhancement of Food Security in GHA

For a region where livelihood is closely intertwined with climate variability through the dependence of large portion of the population on subsistence rain-fed agriculture, monitoring of drought development and provision of timely drought information is essential for drought risk reduction (*Sheffield et al.*, 2014). The enhancement of drought monitoring systems through accurate and

consistent drought indicators together with forecast information should allow droughts to be predicted earlier, their impact areas to be delineated more accurately, and impacts on crops diagnosed before harvest (*Thenkabail et al.*, 2004). Making drought monitoring tools, e.g., drought indices, part of comprehensive early warning system (EWS) can provide decision makers with improved and timely information. This would allow decision makers to assess food security indicators to detect major changes in food availability and advice on the likely occurrence of food crises due to drought in advance of a severe

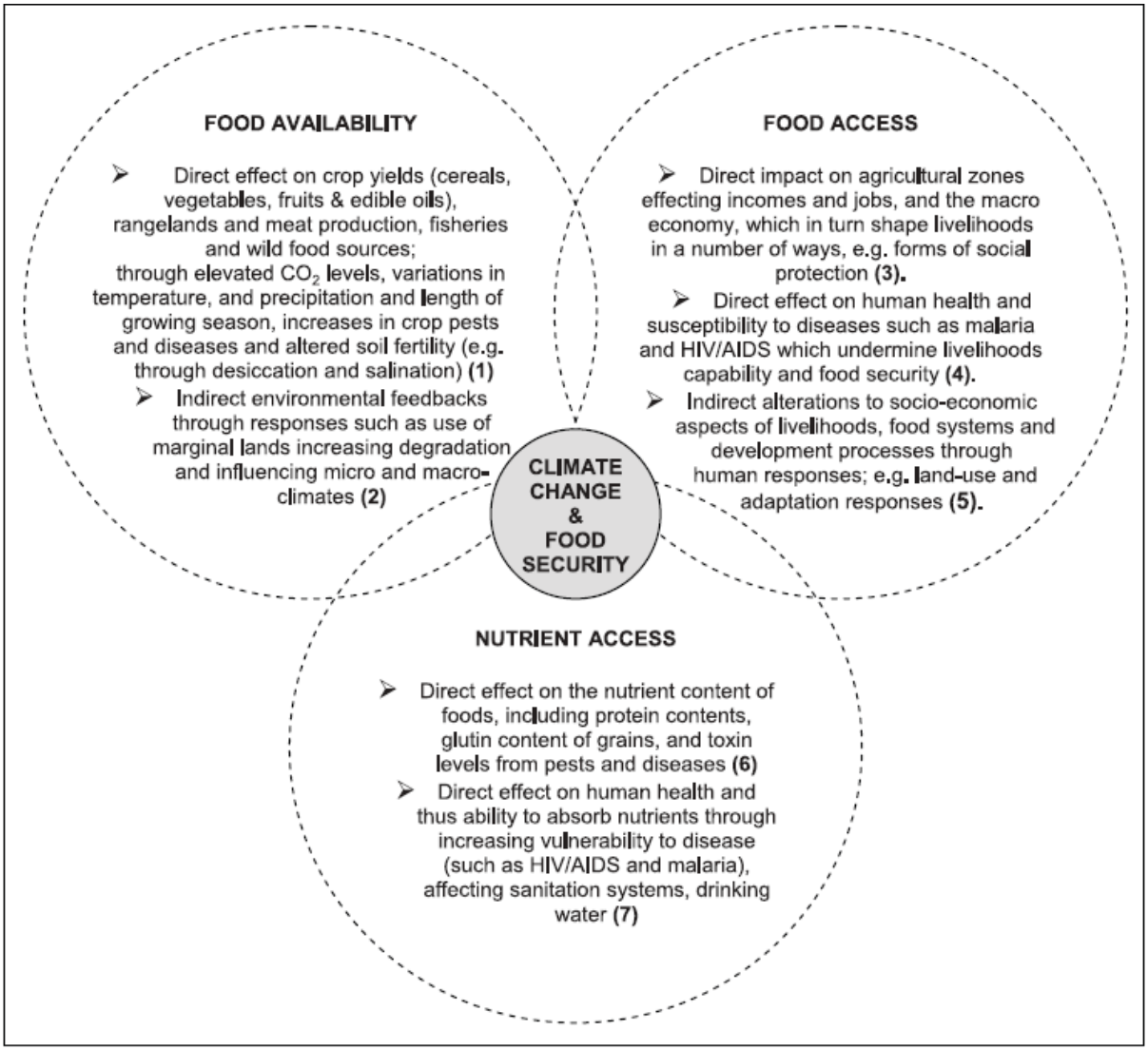

Figure 1.1: Linkages between climate change in Africa and the three major components/dimensions of food security. Adopted from *Boko et al.* (2007).

event (*Tadesse et al.*, 2008). Alternatively, adopting a risk management approach to drought management could drastically reduce its impacts. The risk management approach stresses the development of monitoring and EWS, the assessment of drought risks and implementation of drought mitigation and preparedness activities before the occurrence of the drought (*Tadesse et al.*, 2008). All these measures eventually contribute to the enhancement of food security through drought monitoring.

Some of the food insecurity causing issues over GHA such as low yield, climate change and/or impact of rainfall variability on rain-fed agriculture, and low per capita food production (outlined in section 1.2) could be addressed through sustainable groundwater irrigation. This follows from evidence of the growing importance and spatial extent, especially in arid and semi-arid areas of Sub-Sahara Africa, of groundwater irrigated agriculture (*Foster and Shah*, 2012; *Villholth*, 2013). This growth is driven by small scale farmers (i.e., having less than 2 ha), who have been attracted to groundwater irrigated agriculture due to the following benefits; groundwater respond to farmers demand for reliable and flexible irrigation water supply, better and more appropriate and cost effective drilling and pump technology, and services and markets making groundwater irrigated agriculture feasible. Also, the response of crops to fertilizer is higher where the supply of irrigation water (groundwater) is assured compared to rain-fed agriculture. In addition, the reliability and flexibility of groundwater allows farmers to take risk of investing in fertilizer, which in return substantially increases their crop productivity (*Moench et al.*, 2003).

In order to ensure sustainable exploitation of groundwater, there is need for its (i.e., aquifer) continuous monitoring over time so as to aid decision makers with a better understanding of long-term sustainability of the aquifers and to assess the impacts of climate change on the groundwater level changes (*Alley*, 2007). Unsustainable exploitation of groundwater would result in depletion with catastrophic consequences for the region. These consequences varying

considerably in occurrence and intensity with hydrogeological setting, would include but not limited to (*Konikow and Kendy*, 2005; *Foster and Shah*, 2012; *Döll et al.*, 2014); counterproductive competition between irrigation users, conflicts between rural and urban drinking water provisions making it more difficult to achieve millennium development goals, impacts on natural aquifer discharge (e.g., spring flow and natural river flow) which results cumulatively in un-acceptable impact on downstream water flow, degradation of important water-dependent ecosystems, salination of aquifers, and troublesome land subsidence due to settlement of inter-bedded aquitards in alluvial and/or lacustrine formations. These consequences would lead to reduced food production hence food insecurity.

1.4 Statement of the Problem

The GHA countries rely heavily on rain-fed subsistence agriculture, which has increasingly become vulnerable to drought events (see, e.g., *Rojas et al.*, 2011; *Loewenberg*, 2011; *Stampoulis et al.*, 2016; *Gebrehiwot et al.*, 2011; *Ibrahim*, 1988; *Olsson*, 1993) hence food insecure. The magnitude and severity of the impacts of drought-induced food insecurity in the region emphasizes the need for agricultural drought indicators that would provide comprehensive, clear, reliable, accurate, and consistent spatial extent drought monitoring in order to aid planning and mitigation of agricultural drought impacts. Other than droughts, higher population growth rate and negative impacts of climate change and/or variability on rain-fed agriculture and surface water are further threats to food security of the region (*McCalla*, 1999; *Technical Cooperation Department*, 2000; *Niang et al.*, 2014).

Agricultural drought monitoring in the region has been hampered by insufficient and/or lack of in-situ rainfall measurements. The sparse and/or uneven distribution of rain gauges cannot adequately capture the spatial variability of precipitation. In addition, the existing records have gaps and lack

consistency (*Nicholson*, 2014a; *Rojas et al.*, 2011; *Naumann et al.*, 2014). This insufficiency of in-situ measurements has been contributed by the following reasons among others: (i) the region being too big - with over 6.2 *million* km^2 of land, most of the in-situ gauge stations are located in high-densely populated areas hence the sparse and uneven distribution; (ii) conflicts - violence and armed conflicts running in the region has hampered establishment and maintenance of in-situ station, this is well illustrated by the distribution of global precipitation climatology centre (GPCC) rain gauge stations (see, Chapter 4 Fig. 4.1d; Somalia, South Sudan, and Sudan have low density of stations due to running conflicts); and (iii) governmental bureaucracy - with several different governments in the region, it is almost impossible to bring together all the rainfall records in their possession. This deficiency in in-situ measurements has seen researchers augment the little available in-situ measurements with satellite, reanalysis and/or model products. Even though these products provide consistent, homogeneous, and wide coverage (*Damberg and AghaKouchak*, 2014), they have shortcomings whose impacts on drought analysis are unknown.

Worse than rainfall monitoring situation, the GHA region does not have in-situ monitoring network for soil moisture despite it being a better indicator of agricultural drought. This situation has led to uncertainties in soil moisture products (models and reanalyses) over the region remaining largely unknown. This has led to low uptake of the soil moisture products in drought studies as reflected by the lower number of soil moisture drought-related studies in comparison to rainfall, despite the fact that soil moisture is the only indicator of the moisture situation between rainfall deficit and plant reaction time (e.g., *AghaKouchak et al.*, 2015).

Even though a number of studies (e.g., *Naumann et al.*, 2014; *Kurnik et al.*, 2011; *Clark et al.*, 2003; *Yang et al.*, 2014a; *Dutra et al.*, 2013; *Anderson et al.*, 2012; *Nicholson*, 2014a; *AghaKouchak*, 2015; *Awange et al.*, 2016b; *Lyon*, 2014;

Gedif et al., 2014; *Viste et al.*, 2013; *Kurnik et al.*, 2011; *Gebrehiwot et al.*, 2011; *Edossa et al.*, 2010) have analyzed drought over the region, very few of them (e.g., *Shukla et al.*, 2014; *Mwangi et al.*, 2014; *Anderson et al.*, 2012; *Rojas et al.*, 2011; *Agutu et al.*, 2017) have analyzed agricultural drought. Of the few that have analyzed agricultural drought, only *Agutu et al.* (2017) has evaluated the utility of satellite-gauge merged precipitation, reanalysis and model soil moisture, vegetation condition index, and terrestrial water storage in characterizing agricultural drought over GHA. For a region that faces food insecurity each time a drought event occurs, it is of utmost importance to evaluate the utility of available drought indicators. Moreover, other than fewer studies analyzing agricultural drought, little is known about the impacts of topography on drought characterization despite the fact that topography has been shown to influence rainfall variability over the region. Various studies (e.g., *Dinku et al.*, 2007, 2008; *Romilly and Gebremichael*, 2011) have shown the influence of topography, especially over Upper GHA (Sudan, South Sudan, Ethiopia, and Somalia), on rainfall variability as represented by gauges and/or satellite-based methods.

The problems of limited in-situ measurements are not restricted to precipitation and soil moisture only, GHA also has inadequate groundwater monitoring infrastructure leading to a lack of long-term groundwater level changes data (see, e.g., *Comte et al.*, 2016). This has resulted in an inadequate understanding of the long-term sustainability of groundwater (aquifers) as sources of long-term water supply. In addition, the impact of climate change and/or variability on groundwater level changes remains largely unknown due to lack of monitoring (*Becker et al.*, 2010; *Alley*, 2007). Sustainability of groundwater and knowledge of impacts of climate change on groundwater level changes are important for the region as groundwater is the only source of water that can be used to bridge the deficit in food production through groundwater irrigated agriculture. This deficit results from increased food demand due to

high population growth and the negative impact of climate change and/or variability on per capita food production and surface water sources (*Moore and Williams*, 2014; *Funk and Brown*, 2009; *Voll and Voll*, 2016).

1.5 Motivation and Objectives

Motivated by the shortcomings discussed in section 1.4 above, this study aimed at

(i) Investigating the suitability of several multi-satellites, models and reanalysis data in agricultural drought assessment (1982-2013). In this context, precipitation products (gauge interpolated and gauge-satellite merged), model and reanalyses soil moisture products, vegetation condition index, and reanalysis and satellite terrestrial water storage, are analysed using a combination of rotated principal component analysis and partial least squares regression. These products are used to characterise agricultural droughts in terms of severity, duration, and spatial (aerial) extents. The study evaluates how well the employed products capture agricultural droughts over the region as reflected by national annual crop production (wheat and maize) during the study period.

(ii) Investigating the impacts of topography on agricultural drought characterization. Here, apart from seeking to understand the impacts of topography on spatio-temporal drought patterns, the study also analyzes the consistency of percentage of areas under drought and different drought intensities.

(iii) Understanding the characteristics of common model and reanalysis soil moisture products over the region by evaluating the uncertainties in selected soil moisture products using generalized three-cornered hat (TCH) method. In addition, the study investigates the uncertainty characteristics by considering the relationship between the individual soil moisture

products and their ensemble mean in annual and seasonal means time laps using Taylor diagram. Finally, the spatio-temporal decompositions of the soil moisture products are compared to rainfall variability.

(iv) Testing the utility of Gravity Recovery and Climate Experiment (GRACE) as a viable tool in monitoring groundwater level changes and their potentials for irrigated agriculture. To achieve this, independent component analysis is employed to localize GRACE-derived groundwater changes into their respective groundwater locations and analyze the corresponding temporal variabilities and their links to climate variability. In addition, the study examines irrigation potential of the groundwater localized regions by investigating GRACE-derived groundwater temporal variability, water quality information, groundwater (aquifer) hydrogeological properties, and dominant soil properties in those regions.

1.6 Thesis Outline

The remainder of the thesis is organized as follows. Chapter 2 contains an overview of GHA, a detailed description of the datasets, and the statistical analysis methods used in the thesis to achieve the objectives above . Due to topographical characteristics of GHA, drought characterization is evaluated in two parts; part one dealing with lower parts of GHA (East Africa (EA); Kenya, Uganda, Tanzania, Rwanda, and Burundi) constitute Chapter 3 while part two dealing with Upper GHA (UGHA; Sudan, South Sudan, Ethiopia, Somalia, Djibouti, and Eritrea) comprise Chapter 4.

Chapter 3 deals with agricultural drought characterization and evaluation of the effectiveness of drought indicators over EA using national annual crop production. The results of this Chapter has recently been published in *Remote Sensing of Environment* (*Agutu et al.*, 2017, see Appendix). Chapter 4 investigates the impact of topography on agricultural drought characterization

by focusing on the impact of topography on spatio-temporal drought patterns, mean differences in the percentage of areas under drought and different drought intensities. In addition, the effectiveness of various products to capture agricultural drought over only Ethiopia is presented is presented as the rest of the countries in UGHA combine rain-fed and irrigated agriculture. Chapter 5 presents analyses of uncertainties and variabilities in model and reanalysis soil moisture products over GHA.

Chapter 6 presents the use of GRACE in monitoring groundwater level changes. The chapter focusses on temporal characteristics of the groundwater level changes, their link to climate variabilities and the potential to support groundwater irrigated agriculture. Finally, Chapter 7 links the major findings of the thesis to enhancement of food security over GHA and outlines potential areas for future research.

2 Data and Methods

2.1 Greater Horn of Africa and its Characteristics

Greater Horn of Africa (GHA; Fig. 2.1) comprises of 11 countries; Sudan, South Sudan, Ethiopia, Eritrea, Djibouti, Somalia, Kenya, Uganda, Tanzania, Rwanda, and Burundi. Kenya, Uganda, Tanzania, Rwanda, and Burundi are collectively referred to as East Africa (EA) while Sudan, South Sudan, Ethiopia, Eritrea, Djibouti, and Somalia are referred to as Upper Greater Horn of Africa (UGHA) in this thesis.

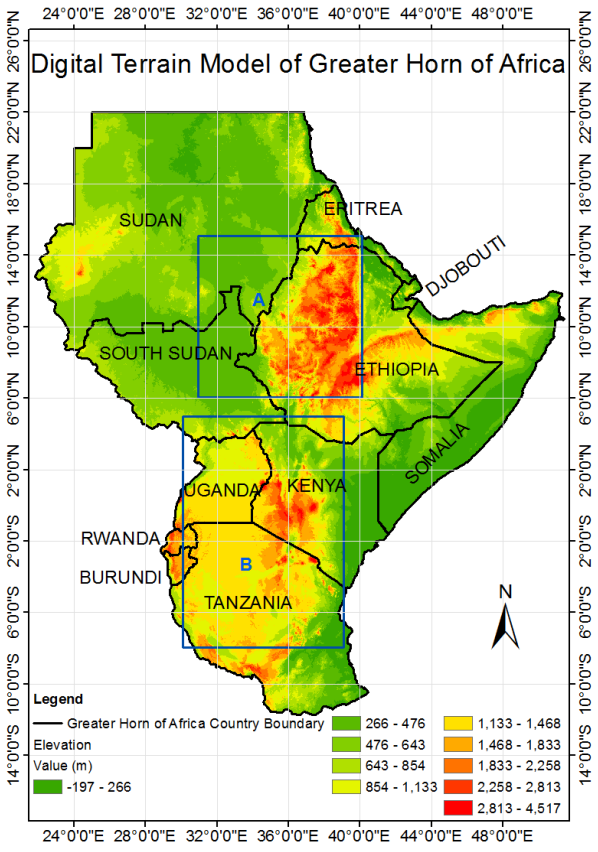

Figure 2.1: Greater Horn of Africa (GHA) region; Elevation variation from Shuttle Radar Topographical Mission (SRTM, source:http://www.cgiar-csi.org/data/srtm-90m-digital-elevation-database. Rectangular boxes A (Ethiopian highlands) and B (EA) indicate regions over which soil moisture spatial averages were taken for chapter 5.

Greater Horn of Africa region covers approximately 6.2 *million* km^2 and

is inhabited by over 350 million people majority of whom are dependent on subsistence rain-fed agriculture (*EACS*, 2014). With exception of Uganda, only between $4\% - 10\%$ of the GHA land is classified as arable with the rest being arid or semi-arid (*Technical Cooperation Department*, 2000).

The region's most prominent physical feature is the East Africa Rift System, comprising of main and western branches. The main branch, Great Rift Valley, cuts the region from Ethiopian Danakali plain to Lakes Turkana, Naivasha, and Magadi in Kenya and through Tanzania downwards to Mozambique. The western branch, Western Rift valley, extends northwards form the northern end of Lake Malawi in a great arc that includes Lakes Rukwa, Tanganyika, Kivu, Edwards, and Albert (*The Editors of Encyclopædia Britannica*, 2017). It is associated with the highlands over Ethiopia and Kenya (Fig. 2.1). The complex terrain over Ethiopian highlands and neighboring lands have been reported to be a hindrance to accurate and/or proper rainfall representation by both satellite and gauge-derived rainfall products due to complex rainfall-terrain relationships (see e.g., *Dinku et al.*, 2007, 2008; *Romilly and Gebremichael*, 2011).

Greater Horn of Africa has two distinct rainfall regimes, which are best captured/shown by principle component analysis decomposition of its rainfall. The unimodal rainfall (Fig. 2.2a EOF 1; over Sudan, South Sudan, Ethiopian Highlands, Djibouti, Eritrea, and northern Somalia) and bimodal rainfall (Fig. 2.2b EOF 2; over southern and eastern Ethiopia, Kenya, southern Somalia, Uganda, Tanzania, Rwanda, and Burundi) both largely associated with progression of the Inter-Tropical Convergence Zone (ITCZ) across the region (*Bowden and Semazzi*, 2007; *Nicholson*, 2014b).

The unimodal rainfall (Fig. 2.2c PC1; June – September (JJAS) with peaks in July/August) results from moisture migration from the rain forest regions of the Congo Basin as a result of westerly winds and thermal low pressure of ITCZ (*Williams et al.*, 2012). It forms the bulk of the rainfall received over GHA region.

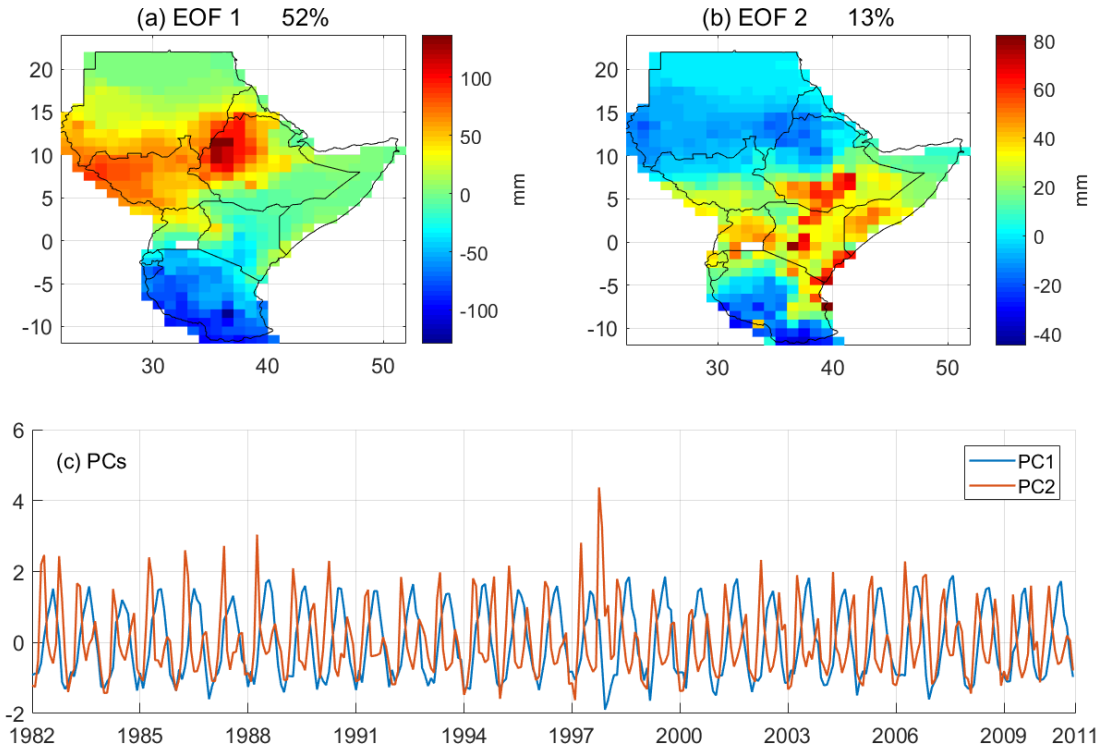

Figure 2.2: GHA principal component analysis-derived precipitation spatio-temporal variability. The decomposed precipitation was from Global Precipitation Climatology Centre (GPCC) from 1982 - 2010. The uni-modal rainfall is captured by EOF 1 and PC1 while the bi-modal rainfall is captured by EOF 2 and PC2. EOF 1 and EOF 2 corresponds to PC1 and PC2, respectively.

The bimodal rainfall (Fig. 2.2c PC2) comprises of March – May (MAM; long rain, peaks in April) and October – December (OND; short rains, peaks in November) with the latter having larger interannual variability. The short rains are more associated with sea surface temperature anomaly forcings of which El Niño-Southern oscillation (ENSO) and Indian Ocean Dipole (IOD) are the dominant sources of variability (*Bowden and Semazzi*, 2007). IOD has higher influence over the short rain as compared to ENSO (*Saji et al.*, 1999; *Williams and Funk*, 2011). The interannual variability of the long rains is controlled majorly by Madden-Julian Oscillation and tropical Walker circulation (*Williams and Funk*, 2011).

2.2 Data

In order to achieve the objectives outlined in section 1.5, the following datasets/products were employed; precipitation, model and reanalysis soil moisture, terrestrial water storage, model groundwater, climate indices, vegetation condition index, and national annual crop production.

2.2.1 Precipitation

The following Precipitation products were used in this thesis: Global Precipitation Climatology Centre (GPCC), Climate Hazard Group InfraRed Precipitation with Stations (CHIRPS), Climate Hazard Group InfraRed Precipitation (CHIRP), and Tropical Rainfall Measuring Mission (TRMM).

2.2.1.1 CHIRPS

CHIRPS is a quasi-global (50°S – 50°N) high resolution, 0.05°, daily, pentad, dekad, and monthly precipitation data set produced from a combination of in-situ station observations and satellite precipitation estimates based on Cold Cloud Duration (CCD) observations to represent sparsely gauged regions. It has been primarily developed to support agricultural drought monitoring (see *Funk et al.* (2015) for a detailed description). Monthly precipitation data, version 2.0, from 1982 to 2013 was downloaded from ftp://ftp.chg.ucsb.edu/pub/org/chg/products /CHIRPS-2.0/. CHIRPS precipitation was found to have correlation of greater than 0.75 with GPCC over the GHA region (see, e.g., *Funk et al.*, 2015) and has subsequently been used in a number of drought and hydrology related studies in the region (see, e.g., *Pricope et al.*, 2013; *Shukla et al.*, 2014; *McNally et al.*, 2016).

2.2.1.2 CHIRP

Similar to CHIRPS, CHIRP is a quasi-global (50°S – 50°N) high resolution, 0.05°, daily, pentad, dekad, and monthly precipitation data set. It is a satellite only precipitation product based on satellite Cold Cloud Duration (CCD) observations. Monthly precipitation data from 1982 to 2013 was downloaded from ftp://ftp.chg.ucsb.edu/pub/org/chg/products/CHIRP/ for drought characterization. See *Funk et al.* (2015) for more details.

2.2.1.3 GPCC

GPCC (*Schneider et al.*, 2014) full data reanalysis version 7, 0.5° spatial resolution, monthly land surface precipitation from 1982 to 2013 downloaded from ftp://ftp.dwd.de/pub/data/gpcc/html/fulldata_v7_doi_download.html was used in addition to CHIRPS and CHIRP for drought analysis. It is a purely gauge gridded product based on 75,000 rain gauge stations worldwide, that feature record durations of 10 years or longer (see, *Schneider et al.*, 2014). It has been used in several drought related studies both globally and in GHA region (see, e.g., *Kurnik et al.*, 2011; *Funk et al.*, 2014; *Ziese et al.*, 2014; *Dutra et al.*, 2014).

2.2.1.4 TRMM

TRMM (*Kummerow et al.*, 2000; *Huffman et al.*, 2007) is a joint US–Japan satellite mission providing precipitation measurement covering 50° N to 50° S. The precipitation product is based on multiple satellite estimates and rain gauge observation analysis (for more details, see e.g., *Kummerow et al.*, 2000; *Huffman et al.*, 2007). Precipitation estimate for 2003 – 2014 downloaded from National Aeronautics and Space Administration's Goddard Earth Sciences Data and Information Services Center (http://mirador.gsfc.nasa.gov) was used to aid understanding of groundwater trends. TRMM 3B43 (V7) given as monthly precipitation rate (mm/h) at 0.25° spatial resolution was converted to monthly

totals before subsequent analysis. *Dinku et al.* (2007) have shown that it is suitable to be used in the region.

2.2.2 Soil Moisture

The following soil moisture products were used in the thesis: second Modern-Era Retrospective analysis for Research and Applications (MERRA-2), European Centre for Medium-Range Weather Forecasts Interim Re-Analysis (ERA-Interim), Global Land Data Assimilation System (GLDAS), Famine Early Warning System Network (FEWS NET) Land Data Assimilation System (FLDAS), and Climate Prediction Center (CPC).

2.2.2.1 MERRA-2

MERRA-2 is a NASA atmospheric reanalysis since 1980 that replaced the original MERRA-reanalysis (*Decker et al.*, 2012; *Rienecker et al.*, 2011) using upgraded version of Goddard Earth Observing System Model, version 5.12.4 (GEOS 5.12.4), data assimilation system (*Bosilovich et al.*, 2016). Key components of the system include GEOS-5 atmospheric model and an updated Gridpoint Statistical Interpolation (GSI) analysis scheme. The updates enable MERRA-2 to ingest several important new data types e.g., new microwave sounders and hyperspectral infra-red radiance. Unlike MERRA, MERRA-2 uses observation based precipitation data as a forcing for land surface parametrization. Over Africa, Climate Prediction Center Merged Analysis of Precipitation (CMAP; a satellite-gauge merged product) is used due to limitations of available gauge observations (*Bosilovich et al.*, 2015). Because of the improved assimilation system (updates to the treatment of canopy interception) and better forcing data, MERRA-2 has improved soil moisture estimates over MERRA (*Bosilovich et al.*, 2015). Monthly 0.625° by 0.5° root zone soil moisture from 1982 to 2013 was downloaded from https://gmao.gsfc.nasa.gov/reanalysis/MERRA-2/data_access/.

2.2.2.2 ERA-Interim

ERA-Interim (*Decker et al.*, 2012; *Dee et al.*, 2011) is a global reanalysis from ECMWF, produced through sequential assimilation scheme advancing forward in time using 12 hourly analyses cycle. In each cycle, available observations are combined with prior information from a forecast model to estimate the evolving state of global atmosphere and its underlying surface. ERA-Interim data assimilation key system is the 12 hours 4D-Var of the upper atmosphere, which uses forecast model (Integrated Forecast system – IFS) to constrain the state evolution within each analysis window and update bias correction estimate parameters needed for majority of satellite derived radiance observations. The IFS comprises three fully coupled components for atmosphere, land surface, and ocean waves. The analysis of surface parameters over land and ocean are done separately from atmospheric analysis (*Decker et al.*, 2012; *Dee et al.*, 2011). Unlike MERRA-2, it does not use ground based observation to force land surface based parametrization. Monthly (monthly means of daily means) soil moisture, from 1982 to 2013, at 0.25° spatial resolution was downloaded from http://apps.ecmwf.int/datasets/data/interim-full-moda/levtype=sfc/.

The three layers of soil moisture from 0 to 1 meter were aggregated into one soil moisture product before subsequent analyses. ERA-Interim has been found to have a good skill in capturing surface soil moisture variability, though it tends to overestimate soil moisture, especially over dry lands (*Albergel et al.*, 2012). In addition, it has been used in a number of studies globally and in GHA region (see, e.g., *Balsamo et al.*, 2009; *Dee et al.*, 2011; *Decker et al.*, 2012; *Dutra et al.*, 2013; *Viste et al.*, 2013; *Mwangi et al.*, 2014).

2.2.2.3 GLDAS

GLDAS - is a global, high resolution, offline (uncoupled to the atmosphere) terrestrial modelling system that incorporates satellite and ground-based observations in order to produce optimal fields of land surface states and fluxes

in real time (*Rodell et al.*, 2004). It drives the following land surface models (LSMs):

(i) Noah – a one-dimensional model that evaluates the surface energy and water budgets to calculate the distribution of moisture in the soil column (*Anderson et al.*, 2012). It has been used operationally in National Centers for Environmental Prediction (NCEP) models since 1996 with continued improvements (*Rodell et al.*, 2004). GLDAS-Noah version 2 was used in this thesis.

(ii) Mosaic – basically divides each model grid into mosaic of tiles based on vegetation distribution within the cell followed by surface flux estimation in manner similar to that described by *Sellers et al.* (1986), for more details see *Rodell et al.* (2004).

(iii) Community Land Model (CLM) – a combination of superior components from National Center for Atmospheric research (NCAR) land surface model, the Biosphere-Atmosphere Transfer Scheme (BATS), and LSM of the Institute of Atmospheric physics of the Chinese Academy of Sciences (*Rodell et al.*, 2004).

(iv) Variable Infiltration Capacity (VIC) — a semi-distributed macroscale hydrological model originally developed at the University of Washington. It balances water and energy budgets at grid while taking into account proportions of bare soils and vegetation (*Liang et al.*, 1994; *Bi et al.*, 2016). It is the main model used by African Flood and Drought Monitor (*Sheffield et al.*, 2014) and a prototype for FEWS NET seasonal agricultural drought forecasting system (*Shukla et al.*, 2014).

Instance of Noah used in this study was forced by Princeton global meteorological forcing data of *Sheffield et al.* (2006), which is constructed by combining a suite of global observation-based data set with NCEP/NCAR reanalysis. Instances of CLM, VIC, and Mosaic used in this study were forced

by a combination of different forcing data sets covering various durations (see, *LDAS*, 2016). The forcing data for the duration 1995 - 1997 is reported to have relatively high uncertainty (*LDAS*, 2016). Monthly 1° spatial resolution GLDAS soil moisture variants (Noah, VIC, CLM, and mosaic) from 1982 to 2010 were downloaded from http://disc.sci.gsfc.nasa.gov/services/grads-gds/gldas. Similar to ERA-Interim, individual layers of soil moisture from 0 to 1 meter depth were aggregated into one soil moisture product before further processing.

2.2.2.4 FLDAS

FLDAS – is a custom instance of NASA Land Information System (LIS), adapted to work with domains, data streams and monitoring, and forecast systems associated with food security assessment in data sparse, developing country settings (*Rui and McNally*, 2016; *McNally et al.*, 2017). FLDAS is driven by Noah and VIC LSMs. Both Noah and VIC implementation used in this study were from a simulation runs forced by soil moisture and other state fields from MERRA-2 and CHIRPS. FLDAS, Noah 0.1° spatial resolution and VIC 0.25° spatial resolution, monthly soil moisture from 1982 to 2013 downloaded from https://ldas.gsfc.nasa.gov/FLDAS/FLDASdownload.php were used.

2.2.2.5 CPC

CPC – a one layer bucket water balance model based on Climate Prediction Center (CPC) 1700 global rain gauge observations and NCAR Climate Data Assimilation System (CDAS) reanalysis temperature. The accuracy of the output (soil moisture) is dependent entirely on the quality of the precipitation (*van den Dool et al.*, 2003; *Fan and van den Dool*, 2004). Monthly mean 0.5° spatial resolution soil moisture, version 2, for the duration 1982 – 2013 downloaded from the National Oceanic & Atmospheric Administration's (NOAA) Earth System Research Laboratory database

(http://www.esrl.noaa.gov/psd/data/gridded/data.cpcsoil.html) was used. CPC soil moisture simulates the seasonal and inter-seasonal annual variability reasonably well over GHA region (see, *Dirmeyer et al.*, 2004).

2.2.3 Terrestrial Water Storage (TWS)

2.2.3.1 GRACE-derived TWS and Groundwater

GRACE satellite mission has been in space since 2002 providing global monthly temporal gravity variations in the form of spherical harmonic coefficients (see, e.g., *Tapley et al.*, 2004; *Wouters et al.*, 2014). Centre for Space Research's (CSR) release five (RL05) monthly spherical harmonic coefficients for the duration 2003 – 2014, downloaded from International Centre for Global Earth Models (http://icgem.gfz-potsdam.de/ICGEM/shms/monthly/csr-rl05/) were used in this thesis. Since GRACE does not sense the geo-centre motion, degree one coefficients were replaced by those provided by *Swenson et al.* (2008) while degree two coefficients, which are affected by tidal aliasing errors were replaced by those provided by *Cheng et al.* (2013). The gravitational potential was then converted into equivalent water heights following *Wahr et al.* (1998). In order to remove stripes and spurious patterns in the spherical harmonic coefficients, a decorrelation and non-isotropic DDK2 filter (see, e.g., *Kusche*, 2007; *Kusche et al.*, 2009) was applied. The impacts of the filter on the resulting synthesised GRACE TWS was alleviated through the application of a scale factor developed from GLDAS TWS following *Landerer and Swenson* (2012). The synthesised GRACE-derived TWS over GHA comprise of changes from accumulated soil moisture, groundwater, surface water, and biomass/canopy water content. It is referred to as GTWS in the subsequent Chapters and has been used in a number of drought related studies both globally and in GHA region (see, e.g., *Chen et al.*, 2009; *Long et al.*, 2013; *Awange et al.*, 2016b).

For GRACE-derived groundwater, the following components were eliminated from the GRACE TWS; surface water changes, soil moisture, and

biomass/canopy water content. Surface water changes from the major lakes in the region were removed through integration of lake level changes from satellite altimetry and lake kernel (coefficient) function to generate a gridded time series of surface water changes. In addition, the biomass/canopy water content and soil moisture changes were then corrected for using GLDAS model estimates. GLDAS estimates (Noah monthly 1° by 1° soil moisture, TWS, and canopy water content products from 2003 to 2014) used in GRACE processing as outlined above were also downloaded from http://disc.sci.gsfc.nasa.gov/services/grads-gds/gldas.

Monthly lake level variations from Jason-1, Jason-2/OSTM, and TOPX/ POSEIDON altimetry, products of United States Department of Agriculture downloaded from http://www.pecad.fas.usda.gov/cropexplorer/global_reservoir/ were used to remove surface water variations from GRACE TWS as outlined above and further discussed in Chapter 6. The monthly lake variations, from 2003 to 2014 for Lakes Victoria, Turkana, Tana, Tanganyika, and Malawi were used as they are the dominant surface water bodies in the region and were the only ones with up to date altimetry level variations.

Other than the Centre for Space Research (CSR) GRACE solutions used in this thesis, other GRACE solutions are produced by the following processing centers NASA's Jet Propulsion Laboratory (JPL), Deutsches GeoForschungsZentrum (GFZ), and CNES/Groupe de Recherches de Ge'ode'sie Spatiale (CNES/GRGS). The differences in these solutions arise from varying processing strategies and tuning parameters (*Sakumura et al.*, 2014). These differences both in water heights and annual amplitudes are within the overall error of GRACE data and there is no significant biases between the solutions (*Sakumura et al.*, 2014; *Barletta et al.*, 2013). CSR solution was used in this thesis because it had the lowest scatter about the ensemble mean of the four solutions (see, e.g., *Sakumura et al.*, 2014).

2.2.3.2 MERRA-2 Total Land Water Storage

MERRA-2 total land water storage from 1982 to 2013, at 0.5° latitude by 0.625° longitude downloaded from https://gmao.gsfc.nasa.gov/reanalysis/MERRA-2/data_access/ was used in addition to GTWS. It does not include canopy water content and groundwater. It is referred to as MTWS in the subsequent Chapters.

2.2.4 WaterGap Hydrological Model (WGHM) Groundwater

WGHM simulates monthly continental water flows and storages as well as human water use for all land areas of the globe except Antarctica, at a spatial resolution of 0.5° by 0.5° (*Döll et al.*, 2014). Its inputs include GPCC v6 monthly rainfall, monthly data on temperature, cloud cover, and the number of wet days. The model applies a simple water balance approach (see *Döll et al.* (2014) for more detailed description). WGHM groundwater model variants IRR_70_S (deficit irrigation at only 70% of optimal irrigation with groundwater recharge from surface bodies) and NOUSE_S (no water use at all assumed with groundwater recharge from surface bodies) are used in this thesis to evaluate GRACE-derived groundwater changes. IRR_70_S has been found to best represent groundwater changes in several locations over the globe by *Döll et al.* (2014). WGHM groundwater changes from 2003 – 2009 were downloaded from http://www.uni-frankfurt.de/49903932/7_GWdepletion?.

2.2.5 Climate Indices

Dominant climate indices, Indian Ocean Dipole (IOD; *Ashok et al.*, 2003; *Saji et al.*, 1999) and El Niño-Southern Oscillation (ENSO; *Wolter and Timlin*, 2011), known to influence rainfall variability over GHA (*Bowden and Semazzi*, 2007; *Williams and Funk*, 2011) were investigated on their association with soil moisture variability and groundwater level changes. IOD represents the east-west temperature gradient across tropical Indian Ocean and is defined by Dipole Mode Index (DMI) while ENSO defines sea surface temperature

anomalies in the Pacific. Multivariate ENSO Index (MEI) defined based on sea-level pressure, zonal and meridional components of the surface wind, sea surface temperature, surface air temperature, and total cloudiness fraction of the sky (see, e.g. *Wolter and Timlin*, 2011) was used in the study. Both DMI and MEI from 1982 to 2010 were downloaded from https://climatedataguide.ucar.edu/climate-data.

2.2.6 Vegetation Condition Index (VCI)

Long term series of NOAA Advanced Very High Resolution Radiometer (AVHRR) NDVI dataset 1982 – 2013, from NASA's Global Inventory and Modelling Systems (http://ecocast.arc.nasa.gov/data/pub/gimms/3g.v0/) was used to compute VCI (*Kogan*, 1995). The data comprised of 15 days maximum composites at 5-arc-minute spatial resolution (for a detailed description, see e.g., *Tucker et al.*, 2005; *Pinzon and Tucker*, 2014). VCI is advantageous as it is able to isolate weather related vegetation stress (*Kogan*, 1995; *Quiring and Ganesh*, 2010; *Rojas et al.*, 2011), which within the study area, would correspond to water availability. It is computed as (*Kogan*, 1995)

$$VCI_i = 100 * \frac{NDVI_i - NDVI_{min}}{NDVI_{max} - NDVI_{min}}, \tag{2.1}$$

where $NDVI_i$ is the monthly $NDVI$, $NDVI_{max}$ and $NDVI_{min}$ are multi-year maximum and minimum $NDVI$, respectively.

AVHRR NDVI has been used extensively globally and over Africa for drought and other related studies (see, e.g., *Verdin et al.*, 2005; *Rojas et al.*, 2011; *Dorigo et al.*, 2012; *Guan et al.*, 2012; *Chen et al.*, 2014).

2.2.7 National Annual Crop Production

National annual maize and wheat production data for Kenya, Uganda, Tanzania, and Ethiopia downloaded from Food and Agriculture Organization (FAO) data portal (http://www.fao.org/faostat/en/#data/QC) was used to

evaluate the effectiveness of various satellite/model drought indices in capturing agricultural droughts. Even though this data set undergoes several quality checks along the processing chain (see, e.g., *Kasnakoglu and Mayo*, 2004), lack of direct production/yield reporting from farmers to government agencies in developing countries (e.g., GHA region countries) means there is some level of uncertainty in the production data used. Even with the uncertainties, this data is still the most credibl and readily available.

These uncertainties are more likely to be systematic than random year to year variations (due to wet/dry conditions) due to the fact that the government reported figures are analyzed and compared against FAO forecast and modeled estimates (*Kasnakoglu and Mayo*, 2004). The modeled and forecast estimates are based on magnitude of cropped areas, rainfall conditions, vegetation indices among other variables. In addition, the data is further quality controlled thereby reducing the systematic uncertainties that may be present in them hence there is likely to be very low impact of these uncertainties on evaluation of the indices. Also, as our interest is on majorly the comparative performance of the indices, any systematic and or random errors would have the same impacts on all of them hence negligible impact on our analyses.

Given that GLDAS variant soil moisture products and GRACE TWS have a spatial resolution of 1° x 1°, all the other products (except annual crop production and climate indices) were scaled to the same spatial resolution before analysis. Also, as the analyses were limited to 1 meter nominal depth (approximation for root zone soil moisture), the depth of each soil moisture layer was used as weight in aggregating total moisture to 1 meter depth following *Li* (2007). For example, considering a land surface model comprising of two soil layers; $0 - 10\ cm$ and $10 - 200\ cm$, with θ_1 and θ_2 volumetric soil moisture, respectively, the following equation was used to scale the soil moisture to top 1 m (*Li*, 2007).

$$W = 0.1 \times \theta_1 + 0.9 \times \theta_2, \tag{2.2}$$

where W represent volumetric soil moisture in the top 1 m, 0.1 and 0.9 are soil moisture depths for layers 1 and 2, respectively. 0.9 is used to sum up the layer to 1 m, i.e., $(1 - 0.1 = 0.9)$.

Other datasets in the form of meteorological drought index, agricultural drought index, and integrated meteorological and agricultural drought index providing global drought information can also be obtained from https://www.nature.com/articles/sdata20141.

2.3 Statistical Analysis Methods

The statistical methods employed in this study are summarised in Table 2.1 and discussed below.

Table 2.1: Table summarizing the statistical methods used in the thesis

Method	Chapters Applied	Reason*
Principal Component Analysis (PCA)	3, 4, and 5	It is the most widely used spatio-temporal analysis method in atmospheric sciences. In addition, it has been used in numerous drought studies
Partial Least Squares Regression Analysis (PLSR)	3 and 4	Its ability to handle data with collinearity, noise, and multiple variables over ordinary multi-linear regression.
Generalized three-cornered Hat (TCH) method	5	Does not require prior knowledge of variables in order to evaluate uncertainties. Its uncertainties are independent of the chosen reference dataset and are related to the respective datasets and not their ensemble mean, hence ease of interpretation.
Independent Component Analysis (ICA)	6	High ability to localize spatio-temporal signals as compared to other methods e.g., PCA.
Multiple-Comparison: Bonferroni Method	4	N/A
Analysis of Variance (ANOVA)	3 and 4	N/A
Linear trend	6	N/A
Correlation Analysis	3, 4, 5, and 6	N/A
W-test	3 and 4	Interest only on departure from normality. W-test is the simplest and most direct method.

* Advantages of the chosen methods in comparison to other methods, where applicable.

2.3.1 Principal Component Analysis

Principal component analysis (PCA, *Hannachi et al.*, 2007; *Jolliffe*, 2002; *Preisendorfer*, 1988; *Wilks*, 2006; *Lorenz*, 1956) is one of the most widely used methods in atmospheric sciences for pattern extraction and dimensionality reduction. It has been used in drought studies (e.g., *Santos et al.*, 2010; *Raziei*

et al., 2009; *Sigdel and Ikeda*, 2010) to decompose spatial-temporal fields such as standardized precipitation index (SPI) or standardized soil moisture index (SSI), into spatial patterns and their corresponding temporal evolutions.

Following from *Hannachi et al.* (2007), for a gridded data set composed of space time field $\mathbf{X}(t, \mathbf{s})$ representing the value of the field $\mathbf{X}$, such as SPI or SSI at a time t and spatial location $\mathbf{s}$. The value of the field at discrete time t_i and grid point $\mathbf{s}_j$ is denoted x_{ij} for $i = 1, ..., n$ and $j = 1, ..., p$. The field can then be represented by a data matrix as

$$\mathbf{X} = (\mathbf{x}_1, \mathbf{x}_2, ..., \mathbf{x}_n)^T = \begin{bmatrix} x_{11} & x_{12} & ... & x_{1p} \\ x_{21} & x_{22} & ... & x_{2p} \\ ... & ... & ... & ... \\ ... & ... & .... & .... \\ x_{n1} & x_{n2} & ... & x_{np} \end{bmatrix}, \tag{2.3}$$

where $\mathbf{x}_t = (x_{t1}, x_{t2}, ..., x_{tp})^T, t = 1, ..., n$, represent the value of the field at time t. The anomaly field or departure from climatology at $(t, \mathbf{s}_k), t = 1, ..., n, and\ k = 1, ..., p$ is defined as

$$x_{tk}^{'} = x_{tk} - \frac{1}{n}\sum_{k=1}^{n} x_{ki}, \tag{2.4}$$

Denoting the anomaly field by $\mathbf{X}$, the sample covariance of the data is then defined as

$$\mathbf{S} = \frac{1}{n}\mathbf{X}^T\mathbf{X}, \tag{2.5}$$

which contains the covariances $\mathbf{s}_{ij},\ i, j = 1, ..., p$, between the time series of the field at any pair of grid points $(\mathbf{s}_i, \mathbf{s}_j)$. The aim of PCA is to find an uncorrelated linear combination of different variables that explains maximum variance, that is, to find a unit-length direction $\mathbf{u} = (u_1, u_2, ..., u_p)^T$ such that $\mathbf{Xu}$ has maximum variability. This yields:

$$max(\mathbf{u}^T\mathbf{S}\mathbf{u}),\ subject\ to\ \mathbf{u}^T\mathbf{u} = 1, \tag{2.6}$$

The spatial patterns and temporal evolutions are thus obtained as the solution to the eigenvalue problem

$$\mathbf{S}\mathbf{u} = \lambda^2\mathbf{u}, \tag{2.7}$$

The k^{th} spatial pattern is simply the k^{th} eigenvector $\mathbf{u}_K$ of $\mathbf{S}$. The corresponding eigenvalue $\lambda_k^2, k = 1, ..., p$ is then

$$\lambda_k^2 = \mathbf{u}_k^T\mathbf{S}\mathbf{u}_k = \frac{1}{n}\|\mathbf{X}\mathbf{u}_k\|^2, \tag{2.8}$$

and hence the measure of the variance of the data accounted for in the direction of $\mathbf{u}_K$. The variance accounted for can be expressed in percentage as

$$\frac{100\lambda_k^2}{\sum_{k=1}^{p}\lambda_k^2}, \tag{2.9}$$

The projection of the anomaly field, $\mathbf{X}$, on to the k^{th} spatial pattern (eigenvector) $\mathbf{u} = (u_1, u_2, ..., u_p)^T$ i.e., $\mathbf{a}_k = X\mathbf{u}_k$ is the k^{th} temporal evolution (principal component) whose elements $a_{tk},\ t = 1, ..., n$ are given by:

$$a_{tk} = \sum_{j=1}^{p} x_{tj}\mathbf{u}_{kj}. \tag{2.10}$$

So the k^{th} eigenvalue, λ_k^2, represent the variance of the k^{th} temporal evolution $\mathbf{a}_k = (a_{1k}, a_{2k}, ..., a_{nk})^T$. In order to improve the interpretability of the resulting spatial patterns and spread the variances explained, the resulting spatial patterns are rotated. Given $p \times m$ matrix $\mathbf{U}_m = (\mathbf{u}_1, \mathbf{u}_2, ..., \mathbf{u}_m)$ of leading m spatial patterns, the rotation is achieved by seeking an $m \times m$ rotation matrix $\mathbf{R}$ to construct the spatial patterns according to:

$$\mathbf{B} = \mathbf{U}_m\Re, \tag{2.11}$$

where $\Re$ is either $\mathbf{R}$ *or* $(\mathbf{R})^{-1}$ depending on the type of rotation chosen. The

criterion for choosing the rotation matrix $\mathbf{R}$ is what constitutes the rotation algorithm or the simplicity criterion and is expressed by maximization problem

$$max\ f(\mathbf{U}_m\Re), \tag{2.12}$$

over a specific subset or class of $m \times m$ square rotation matrix. This chapter employed VARIMAX criterion (*Kaiser*, 1958; *Forina et al.*, 1988; *Jolliffe*, 1995), see *Hannachi et al.* (2007); *Forina et al.* (1988); *von Storch and Zwiers* (1999) for other rotation criterions. Designating the elements of the spatial patterns matrix $\mathbf{B}$ in equation 2.11 i.e., $\mathbf{b}_{ij} = [\mathbf{B}]_{ij}$, then the VARIMAX orthogonal rotation maximizes a simplicity criterion according to

$$max\ \left(f(\mathbf{B}) = \sum_{k=1}^{m} \left[p \sum_{j=1}^{p} \mathbf{b}_{jk}^4 - \left(\sum_{j=1}^{p} \mathbf{b}_{jk}^2 \right)^2 \right] \right), \tag{2.13}$$

where m is the number of spatial patterns chosen for rotation. The quantity in the square brackets in equation 2.13 is proportional to the (spatial) variance of the square of the rotated vectors $\mathbf{b}_k = (b_{1k}, b_{2k}, ..., b_{pk})$. For more information on rotated PCA, see, e.g., *Schönemann* (1958); *Richman* (1986); *von Storch and Zwiers* (1999); *Hannachi et al.* (2007).

2.3.2 Partial Least Squares Regression (PLSR)

PLSR is a regression technique in which the response variables are regressed on the predictor scores. The scores (few new variables) are linear combinations of the original predictor variables (*Wold et al.*, 2001; *Geladi and Kowalski*, 1986). The generation of the scores takes into account the variability in the dependent variable ensuring that only those components of the independent variables that are related to the dependent variables are used in the regression (*Geladi and Kowalski*, 1986). It is a generalization of the multiple linear regression (MLR), but unlike MLR, it can analyze data with collinearity (correlated), noisy, and

with numerous predictor variables (*Wold et al.*, 2001), hence its use in the current study.

Following from *Abdi et al.* (2013) and *Vinzi et al.* (2010), given a data sample consisting of n samples of independent variables $\mathbf{X} \in \mathbf{R}^{n\times p}$ and dependent variables (responses) $\mathbf{Y} \in \mathbf{R}^{n\times q}$, the aim of PLSR is to define orthogonal latent components in $\mathbf{R}^p$ and then use such latent components as predictors for $\mathbf{Y}$ in an ordinary least squares framework. The general model behind PLSR is $\mathbf{X} = \mathbf{T}\mathbf{P}^T + \mathbf{E}$ *and* $\mathbf{Y} = \mathbf{T}\mathbf{Q}^T + \mathbf{F}$, where $\mathbf{T}$ is the latent component matrix, $\mathbf{P}$ and $\mathbf{Q}$ are the loading matrices, $\mathbf{E}$ and $\mathbf{F}$ are the residual terms.

Assuming that $\mathbf{X}$ and $\mathbf{Y}$ have been centered, for a univariate $\mathbf{Y}$ i.e., $q = 1$, PLSR successively finds $\mathbf{X}$ weights $R = [\mathbf{r}_1, \mathbf{r}_2, ..., \mathbf{r}_K]$ as the solution to the constrained optimization (*Abdi et al.*, 2013)

$$\mathbf{r}_k = \arg\max_{\mathbf{r}} \left\{ \mathbf{r}^{\mathrm{T}} \mathbf{X}_{(\mathrm{k}-1)}^{\mathrm{T}} \mathbf{Y}_{\mathrm{k}-1} \mathbf{Y}_{\mathrm{k}-1}^{\mathrm{T}} \mathbf{X}_{(\mathrm{k}-1)} \mathbf{r} \right\} \quad \text{subject to,} \quad \mathbf{r}^{\mathrm{T}}\mathbf{r} = 1, \tag{2.14}$$

where $\mathbf{X}_{(k-1)}$ is the matrix of residuals (i.e., the deflated matrix) from the regression of the $\mathbf{X}$-variables on the first $k-1$ latent components, and $\mathbf{X}_0 = \mathbf{X}$. Due to the deflation of the data after each iteration for finding the weight vector $\mathbf{r}_k$, the orthogonality constraint is satisfied by construction. These weights are then used to find the orthogonal latent components $\mathbf{T} = \mathbf{X}_{(k-1)}\mathbf{R} = \mathbf{X}\mathbf{W}$, where $\mathbf{W}$ is the matrix containing the weights to be applied to the original variable in order to obtain the latent components.

For a fixed number of components, the response variable $\mathbf{Y}$ is predicted in an ordinary least square regression model where the latent components play the role of the exogenous variables

$$\arg\min_{\mathbf{Q}} \left\{ \left\| \mathbf{Y} - \mathbf{T}\mathbf{Q}^{\mathrm{T}} \right\|_2 \right\} = \left(\mathbf{T}^{\mathrm{T}}\mathbf{T} \right)^{-1} \mathbf{T}^{\mathrm{T}}\mathbf{Y}, \tag{2.15}$$

This provides the regression coefficients $\hat{\beta}^{PLS} = \mathbf{W}\hat{\mathbf{Q}}^T$ for the model

$\mathbf{Y} = \mathbf{X}\hat{\beta}^{PLS} + \mathbf{F}$. The objective function in equation 2.14 can be interpreted as maximizing the squared covariance between $\mathbf{Y}$ latent component: $corr^2(\mathbf{Y}, \mathbf{X}_{k-1}\mathbf{r}_k)\text{var}(\mathbf{X}_{k-1}\mathbf{r}_k)$. Further description and formulation can be found in *Abdi et al.* (2013); *Vinzi et al.* (2010); *Helland* (2004); *van Huffel* (1997).

2.3.3 Generalized Three-cornered Hat (TCH) Method

Due to lack of in-situ soil moisture over GHA, generalized TCH method (*Premoli and Tavella*, 1993; *Tavella and Premoli*, 1994; *Galindo et al.*, 2001) was adopted to evaluate the noise/uncertainties within the model and reanalysis soil moisture products. The method enables evaluation of uncertainties through comparison of the soil moisture products against each other. Given N moisture time series $\{\mathbf{X}^i\}, i = 1..., N$, the generalized TCH method splits them into (*Awange et al.*, 2016a)

$$\mathbf{X}^i = \mathbf{P} + \varepsilon^i, \quad \forall i = 1, ..., N, \tag{2.16}$$

where $\mathbf{P}$ is the part common to all the soil moisture products i.e., the signal, and ε is the part unique to each product i.e., the uncertainty. Adopting say for example FLDAS-Noah as the reference time series, the difference between the soil moisture products and it can be expressed as (*Koot et al.*, 2006)

$$\mathbf{Y}^{iN} \equiv \mathbf{X}^i - \mathbf{X}^N = \varepsilon^i - \varepsilon^N, \quad i = 1, ..., N-1, \tag{2.17}$$

where $\mathbf{X}^N$ is FLDAS-Noah series. As demonstrated by *Tavella and Premoli* (1994) and *Awange et al.* (2016a), the results are independent of the chosen reference time series. From the differences, the covariance matrix is computed as (*Koot et al.*, 2006)

$$\mathbf{S}^{ij} \equiv Cov(\mathbf{Y}^{iN}, \mathbf{Y}^{jN}), \quad i, j = 1, ..., N-1, \tag{2.18}$$

which due to bi-linearity can be expressed as

$$\mathbf{S}^{ij} = \mathbf{R}^{ij} - \mathbf{R}^{iN} - \mathbf{R}^{jN} + \mathbf{R}^{NN}, \quad i, j = 1, ..., N-1, \tag{2.19}$$

where $\mathbf{R}^{ij}$ is the unknown $N \times N$ covariance matrix of the individual noises (uncertainties), $\mathbf{R}^{ij} = Cov(\varepsilon^i, \varepsilon^j)$. By definition, the matrices $\mathbf{S}$ and $\mathbf{R}$ are real and symmetric, and have $(N-1)N/2$ and $(N+1)N/2$ independent parameters, respectively, hence equation 2.19 is underdetermined. From equation 2.19 there are N free parameters ($\mathbf{R}$) to be chosen from, $\mathbf{R}^{1N}, ..., \mathbf{R}^{NN}$, i.e., the covariance between the noise of each series and noise of reference series, and in terms of which the solution of other unknowns (noise) is expressed by rearranging equation 2.19 as (*Koot et al.*, 2006)

$$\mathbf{R}^{ij} = \mathbf{S}^{ij} + \mathbf{R}^{iN} + \mathbf{R}^{jN} - \mathbf{R}^{NN}, \quad i, j = 1, ..., N-1, \tag{2.20}$$

A constraint on the solution domain for determining the free parameters is that the estimated covariance matrix $\mathbf{R}$ must be positive definite. A condition satisfied if and only if (*Tavella and Premoli*, 1994)

$$Det(\mathbf{R}) > 0, \tag{2.21}$$

In addition, the parameters are chosen in such a manner that the sum of the estimated correlations between all the time series is minimal. Mathematically, this is equivalent to minimizing the following objective function (*Galindo et al.*, 2001)

$$F(\mathbf{R}^{1N}, ..., \mathbf{R}^{NN}) = \sum_{i<j}^{N} \frac{[\mathbf{R}^{ij}(\mathbf{R}^{1N}, ..., \mathbf{R}^{NN})]^2}{[\mathbf{R}^{ii}(\mathbf{R}^{1N}, ..., \mathbf{R}^{NN})][\mathbf{R}^{jj}(\mathbf{R}^{1N}, ..., \mathbf{R}^{NN})]}, \tag{2.22}$$

An algorithm for the minimization function can be found in *Galindo et al.* (2001). Once the free parameters were estimated, the $\mathbf{R}$ matrix was then completely

determined from equation 2.20.

This method is closely related to triple collocation analysis (*Caires and Sterl*, 2003; *Janssen et al.*, 2007; *McColl et al.*, 2014) in that they both analyze uncertainties. Their major difference being that whereas TCH analyzes the differences between the datasets with a designated reference (one of the datasets), triple collocation analyses the differences between the datasets and their ensemble mean. Both of these methods have been used in atmospheric sciences for uncertainty analyses for dataset validation, objective data merging etc., (see, e.g., *Anderson et al.*, 2012; *Yilmaz et al.*, 2014; *Gruber et al.*, 2016; *Awange et al.*, 2016a; *Dong and Crow*, 2017; *Miyaoka et al.*, 2017). Results of uncertainty analysis by these two methods using selected soil moisture products over the region showed similar trends but different magnitudes (see Table 8.1 in the Appendix). However, from their formulation, TCH was preferred in this thesis due to the fact that its uncertainties are independent of the reference dataset chosen and also they are related to the respective datasets and not their ensemble mean, hence ease of interpretation.

2.3.4 Independent Component Analysis (ICA)

ICA, a blind source signal separation technique in which mixed stochastic random signals are separated into stochastically independent sources (see, e.g., *Comon*, 1994; *Cardoso*, 1999; *Forootan and Kusche*, 2013) is mathematically quantified as (*Martín-Clemente et al.*, 2004)

$$\mathbf{X}(t) = \mathbf{A}\mathbf{S}(t), \tag{2.23}$$

where $\mathbf{X}(t)$ is the $N \times 1$ random vector of observations, $\mathbf{A}$ is the unknown $N \times N$ mixing matrix, and $\mathbf{S}(t)$ the random vector of unobserved sources. Its solution lies in finding a separating matrix $\mathbf{B}$ such that $\mathbf{BA} = \mathbf{G}$ has one and only one

non-zero element per column and row such that the recovered sources

$$\mathbf{Y}(t) = \mathbf{B}\mathbf{X}(t) = \mathbf{G}\mathbf{S}(t), \tag{2.24}$$

are the original ones up to permutation and scaling. For formulation, detailed description, and application to GRACE-derived signals see, e.g., *Forootan and Kusche* (2013); *Cardoso* (1998); *Cardoso and Souloumian* (1993); *Frappart et al.* (2011); *Awange et al.* (2014); *Boergens et al.* (2014); *Ndehedehe et al.* (2016).

2.3.5 Analysis of Variance (ANOVA)

ANOVA is a statistical method for multiple comparison among means while holding the probability of type I error (rejection of a true null hypothesis) constant at a preselected level (*Kutner*, 2005; *King*, 2010). ANOVA analysis can be carried out to investigate the effect of $1, ..., n$ treatments on the samples, leading to $1, ..., n$ -Way ANOVA. Below is formulation of a One-Way ANOVA following *Bingham and Fry* (2010)

$$\mathbf{X}_{ij} = \mu_i + \epsilon_{ij} \quad (i = 1, ..., r, \quad j = 1, ..., r), \quad \epsilon_{ij} \quad iid \quad N(0, \sigma^2). \tag{2.25}$$

Here μ_i is the main effect for the ith treatment, the null hypothesi being H_0 : $\mu_i = ... = \mu_r = \mu$, and σ^2 is the unknown variance. It then follows that (*Bingham and Fry*, 2010),

$$\sigma^2 := E[(\mathbf{X} - E\mathbf{X})^2] = E[\mathbf{X}^2] - (E\mathbf{X})^2 \tag{2.26}$$

and its sample counterpart

$$\mathbf{S}^2 := \overline{(\mathbf{X} - \overline{\mathbf{X}})^2} = \overline{\mathbf{X}^2} - \overline{\mathbf{X}}^2. \tag{2.27}$$

Denoting T, $\mathbf{T}_i$ for the grand total and group totals, defined as (*Bingham and Fry*, 2010)

$$T := \sum_i \sum_j \mathbf{X}_{ij}, \qquad \mathbf{T}_i := \sum_j \mathbf{X}_{ij} \tag{2.28}$$

so

$$\overline{X} = T/n, \qquad n\overline{X}^2 = T^2/n : \tag{2.29}$$

$$SS = \sum_i \sum_j \mathbf{X}_{ij}^2 - T^2/n, \tag{2.30}$$

$$SST = \sum_i \mathbf{T}_i^2/n_i - T^2/n, \quad MST = SST/(r-1), \tag{2.31}$$

$$SSE = SS - SST = \sum_i \sum_j \mathbf{X}_{ij}^2 - \sum_i \mathbf{T}_i^2/n_i, \quad MSE = SSE/(n-r), \tag{2.32}$$

which leads to computation of the F-statistics as

$$F = MST/MSE. \tag{2.33}$$

The formulation above can be extended to N-Way ANOVA depending on the treatments to be studied (for more details on this extension, see e.g., *Bingham and Fry*, 2010; *Kutner*, 2005; *Milliken and Johnson*, 1993).

2.3.6 Multiple Comparison: Bonferroni Method

The Bonferroni method of multiple comparison uses critical values from student's t-distribution after an adjustment to compensate for multiple comparisons (*Hochberg and Tamhane*, 1987; *Toothaker*, 1993). It rejects $H_0 : \alpha_j$ *at the* $\frac{\alpha}{2\binom{k}{2}}$ significance levels, where k is the number of groups if (*Toothaker*, 1993)

$$|t| = \frac{\overline{\mathbf{y}}_i - \overline{\mathbf{y}}_j}{\sqrt{MSE\left(\frac{1}{n_i} + \frac{1}{n_j}\right)}} > \frac{t_\alpha}{2\binom{k}{2}^{N-k}}, \tag{2.34}$$

where N is the total number of observations and k the number of groups.

2.3.7 Linear Trends

Through linear regression model of the form (*Rencher and Schaalje*, 2007)

$$\mathbf{y}_i = \beta_0 + \beta_1 \mathbf{t}_i + \varepsilon_i, \quad i = 1, ..., n, \tag{2.35}$$

where $\mathbf{y}$ is a random variable running over time $\mathbf{t}$, the coefficients β_0 (intercept) and β_1 (linear trend) were determined through least squares. The significance of the linear trend β_j was determined through hypothesis testing $H_0 : \beta_j = 0$, where the test variable (*Rieser et al.*, 2010):

$$\mathbf{t}_j = \frac{\beta_j}{\sqrt{\sigma_{jj}}} \sim \mathbf{t}_{n-p} \tag{2.36}$$

followed a student-t distribution.

2.3.8 Correlation Analysis

The correlation (association) between two random variables $\mathbf{A}$ and $\mathbf{B}$ each of N scalar observations is expressed through Pearson Correlation coefficient defined as (*Fisher*, 1944; *Kendall and Stuart*, 1963)

$$\rho(\mathbf{A}, \mathbf{B}) = \frac{1}{N-1} \sum_{i=1}^{N} \left(\frac{\mathbf{A}_i - \mu_A}{\sigma_A} \right) \left(\frac{\mathbf{B}_i - \mu_B}{\sigma_B} \right), \tag{2.37}$$

where μ_A and σ_A are the mean and standard deviations of $\mathbf{A}$, respectively, and μ_B and σ_B are mean and standard deviation of $\mathbf{B}$, respectively.

2.3.9 W–test

W-test (*Shapiro and Wilk*, 1965) is a well established and powerful test of departure from normality (*Royston*, 1992). The W statistic provide a generally superior omnibus measure of non-normality (*Shapiro et al.*, 1968). Suppose $y_1 < y_2 < ... < y_n$ is an ordered sample of size n to be tested for non-normality. The W-statistic is defined as (*Royston*, 1992)

$$W = \left(\sum \mathbf{a}_i \mathbf{y} i\right)^2 \Big/ \sum (\mathbf{y}_i - \overline{y})^2 \tag{2.38}$$

where $\mathbf{a} = (a_1, ..., a_n)^T$ is such that $(n-1)^{-\frac{1}{2}} \sum \mathbf{a}_i \mathbf{y} i$ is the best linear unbiased estimate (BLUE) of the standard deviation of $\mathbf{y}_i$, assuming normality. The exact value of a is

$$\mathbf{a} = (\mathbf{m}^T \mathbf{V}^{-1} \mathbf{V}^{-1} \mathbf{m})^{-\frac{1}{2}} \mathbf{m}^T \mathbf{V}^{-1} \tag{2.39}$$

where $\mathbf{V}$ is the covariance matrix of the order statistics of a sample of n standard normal random variables with expectation vector $\mathbf{m}$.

3 Assessing the Suitability of Selected Agricultural Drought Indicators in East Africa

3.1 Introductory Remarks

East Africa (EA; Kenya, Uganda, Tanzania, Rwanda, and Burundi) relies heavily on rain-fed subsistence agriculture, which is increasingly becoming vulnerable to frequent drought events (see, e.g., *Rojas et al.*, 2011; *Loewenberg*, 2011; *Stampoulis et al.*, 2016). Furthermore, the impacts of drought are compounded by high levels of poverty, conflicts, population migration, and lack of social infrastructure across the region, triggering famine cycles every time an episode occurs (*Nicholson*, 2014a; *Kurnik et al.*, 2011; *Loewenberg*, 2011; *IFRC*, 2011; *OEA*, 2011a,b). As drought is in part a naturally recurrent feature in EA, there is a need for comprehensive and reliable monitoring in order to aid planning and mitigation of drought impacts. Since frequency and severity of droughts are likely to intensify with climate change (e.g., *Williams and Funk*, 2011), the need to characterize droughts in terms of duration, severity, frequency, and spatial extent is critical.

Comprehensive characterization of drought in EA, like in many other places around the world, faces a number of challenges with respect to use of in-situ precipitation data. For instance, often spatial variability in precipitation cannot be adequately captured due to sparse and uneven spatial distribution of rain gauges. Furthermore, gaps in individual rainfall records, and at times lack of consistency due to poor handling complicate the use of precipitation data (*Nicholson*, 2014a; *Rojas et al.*, 2011; *Naumann et al.*, 2014). In many studies, this led to the replacement or augmentation of in-situ rainfall data with remotely sensed precipitation, reanalysis, and model outputs, providing consistent and homogeneous data with global coverage at various spatial scales that are suitable for drought monitoring (*Damberg and AghaKouchak*, 2014). However, these products can have considerable discrepancies and limitations in

representing rainfall at local and regional scales (*Rojas et al.*, 2011; *Naumann et al.*, 2014; *Damberg and AghaKouchak*, 2014; *Hong et al.*, 2006; *AghaKouchak et al.*, 2009).

In addition to precipitation (gauge and gauge-satellite merged) and soil moisture (model and reanalyses) products, normalised difference vegetation index (NDVI, *Rousel et al.*, 1974; *Tucker*, 1979) and Gravity Recovery and Climate Experiment (GRACE) total water storage (TWS, *Tapley et al.*, 2004) have been used to monitor drought. NDVI has been used directly or in its derivative form to monitor impacts of drought on vegetation health (e.g., *Kogan*, 1995; *Rhee et al.*, 2010; *Bayarjargal et al.*, 2006). In EA, it has been used, e.g., by *Anyamba and Tucker* (2005), *Anderson et al.* (2012), and *Nicholson* (2014a), while the use of GRACE satellite temporal gravity measurements (see, e.g., *Wouters et al.*, 2014; *Tapley et al.*, 2004) in EA has been limited to monitoring changes in TWS (e.g., *Swenson and Wahr*, 2009; *Awange et al.*, 2008; *Becker et al.*, 2010; *Awange et al.*, 2013), and recently drought analysis (*Awange et al.*, 2016b).

Currently, drought studies carried out in the EA region range from purely precipitation based (e.g., *Naumann et al.*, 2014; *Kurnik et al.*, 2011; *Clark et al.*, 2003), a combination of precipitation and climate models (e.g., *Yang et al.*, 2014a; *Dutra et al.*, 2013), to precipitation in combination with soil moisture and/or NDVI (e.g., *Anderson et al.*, 2012; *Nicholson*, 2014a; *AghaKouchak*, 2015). Some of the aforementioned studies and few others (see, e.g., *Shukla et al.*, 2014; *Mwangi et al.*, 2014; *Anderson et al.*, 2012; *Rojas et al.*, 2011) have examined agricultural drought using standardised precipitation index (SPI), NDVI, and/or soil moisture. However, for a region like EA, where the majority of the population depends on subsistence rain-fed agriculture, additional studies focussing on agricultural drought impacts, e.g., related to crop production, would be more relevant and beneficial to the population. Therefore, this Chapter focuses on both the characterization of drought behavior in general and

agricultural drought in particular using various indicators (precipitation, soil moisture, NDVI, and TWS) derived from multi-satellite remote sensing, reanalysis, and model products. Further, this Chapter evaluates the utility of these products using national annual crop production, which has so far not been done by the aforementioned studies.

To support agricultural drought monitoring from diverse indicators, it is imperative to identify and provide information on the most effective agricultural drought indicator or a combination of indicators for the EA region. Therefore, the objectives of this Chapter are: (i) to characterize agricultural droughts in terms of severity, duration, and spatial (areal) extent using the following products; gauge and satellite-gauge merged precipitation, model and reanalysis soil moisture, vegetation condition index, and reanalysis and GRACE TWS, and (ii) evaluate how well these products capture agricultural droughts in the region as reflected by national annual crop production data (wheat and maize) during the 1983 - 2013 period. This chapter only deals with Kenya, Uganda, Tanzania. Ethiopia is evaluated in the next chapter while Sudan and Somalia are not evaluated as they practice both rain-fed and irrigated agriculture.

To the best of my knowledge, this is the first comprehensive study to assess the potential of these remotely sensed products, reanalysis data, and land surface model outputs to monitor agricultural droughts in the EA region. Moreover, this Chapter proposes for the first time the possibility of using GRACE satellite products for agricultural drought monitoring in EA thus providing a link between TWS and crop production. The contents of this Chapter has been published in *Agutu et al.* (2017) and is here reproduced with minor changes with the publisher's permission.

The Chapter is organized as follows. In section 3.2, a summary of the dataset used is presented followed by a discussion of the methodology. The results are presented and discussed in section 3.3 and the Chapter is summarized in section 3.4.

3.2 Data and Methods

The dataset used in this Chapter is summarized in Table 3.1 below, while their detailed description are given in Chapter 2.

Table 3.1: A summary of the dataset used in this Chapter and Chapter 4.

	Data	Temporal resolution	Spatial resolution	Period used
Precipitation	GPCC	Monthly	0.5°× 0.5°	1982 - 2013
	CHIRPS	Monthly	0.05°× 0.05°	1982 - 2013
	CHIRP	Monthly	0.05°× 0.05°	1982 - 2013
Soil moisture	MERRA-2	Monthly	0.625° × 0.5°	1982- 2013
	ERA-Interim	Monthly	0.25°× 0.25°	1982 - 2013
	GLDAS	Monthly	1°× 1°	1982 - 2010
	FLDAS (Noah and VIC)	Monthly	0.1°× 0.1°	1982 - 2013
	CPC	Monthly	0.5°× 0.5°	1982 - 2013
TWS	GRACE	Monthly	1°× 1°	2003 - 2013
	MERRA-2	Monthly	0.625° × 0.5°	1982 - 2013
VCI	NDVI	15 days	0.083° × 0.083°	1982 - 2013
Crop production	Crop production	Annual	National	1982 - 2013

Note: CHIRP and FLDAS VIC are not used in this Chapter.

Due to the existence of a link between agricultural drought and 1 to 6 months precipitation anomalies (e.g., *Kurnik et al.*, 2011; *Elagib*, 2013; *Svoboda et al.*, 2012; *Rouault and Richard*, 2003), Standardised Indices (SI, e.g., SPI; *McKee et al.*, 1993) were derived to characterise agricultural drought using precipitation, VCI, TWS, and soil moisture products. Similarly, Standardized Anomalies (SA)/Z-scores (*Wu et al.*, 2001) were computed to characterize drought from GTWS due to its short duration. The resulting SI and/or SA were then subjected to rotated principal component analysis to obtain their most dominant spatial and temporal drought variabilities. Finally, the temporal variabilities were subjected to partial least-squares regression analysis to determine how well they captured drought variability. In order to satisfy the normality conditions of standardization and ANOVA, all the unstandardised data were tested for normality using W-test (*Shapiro et al.*, 1968) and found to be normally distributed. Even though other generalized tests such as

Kolmogorov–Smirnov test can evaluate departure from known or empirical distribution, the study opted for W-test as it is specific to departure from normality.

Given the differences in the variables used, comparison of drought information was primarily carried out between various products of the same variables, e.g., between precipitation products, or soil moisture products, or TWS. Notwithstanding the differences between the variables, links/relations in drought information across the various products were explored since drought progresses from deficiencies in rainfall followed by moisture through to TWS.

3.2.1 Agricultural Drought Characterization

3.2.1.1 Standardized Precipitation Index (SPI)

SPI (*McKee et al.*, 1993), one of the most preferred drought indices due to its numerous advantages such as simplicity (only requires one input), standardised nature, and flexibility of use on different time scales e.g., 1, 3, 6, 9, 12-month (see, e.g., *AghaKouchak*, 2015; *Svoboda et al.*, 2012, and the references therein), expresses precipitation anomalies with respect to its long term average. Its computation involves fitting a gamma probability distribution function to precipitation time series followed by transformation of the accumulated gamma probability distribution to the cumulative distribution function of the standard normal distribution (see, e.g., *Naresh Kumar et al.*, 2009; *Farahmand and AghaKouchak*, 2015). For the case of two parameter gamma distribution, SPI derivation proceeds as (*Farahmand and AghaKouchak*, 2015)

$$G(x) = \frac{1}{\beta^{\alpha}\Gamma(\alpha)} x^{\alpha-1} e^{-\frac{\alpha}{\beta}}, \tag{3.1}$$

where $\Gamma(\alpha)$ is the gamma function, x, denotes precipitation accumulation, α and β are shape and scale parameters, respectively. The cumulative probability $G(x)$ can then be simplified to (*McKee et al.*, 1993)

$$G(x) = \frac{1}{\Gamma(\alpha)} \int t^{\alpha-1} e^{-t} dt. \tag{3.2}$$

Since equation 3.2 is not valid for zero precipitation, it is then modified to

$$H(x) = q + (1 - q)G(x), \tag{3.3}$$

where q and $(1 - q)$ are the probabilities of zero ($x = 0$) and non-zero ($x \neq 0$) precipitations, respectively. SPI is then computed by transforming $H(x)$ into a normal distribution with mean of 0 and standard deviation of 1 (*McKee et al.*, 1993). Due to the sensitivity of the computed SPI values to the fitted parametric distribution, especially at the tail ends of the distribution (see, *Quiring*, 2009), a non-parametric SPI fitting method was adopted in this study (see, e.g., *Farahmand and AghaKouchak*, 2015, and the references therein).

This is obtained through the use of empirical Gringorten plotting position (*Gringorten*, 1963) as:

$$p(x_i) = \frac{i - 0.44}{n + 0.12}, \tag{3.4}$$

where n is the sample size, i denotes the rank of non-zero precipitation data from the smallest, and $p(x_i)$ the corresponding empirical probability. The output of Eqn. 3.4 is then transformed into standardised index as (*AghaKouchak*, 2015)

$$SI = \phi^{-1}(p), \tag{3.5}$$

where SI is SPI, or standardised soil moisture index (SSI), or standardised vegetation condition index (SVCI), or standardised terrestrial water storage index (STWSI) depending on the variable under consideration, ϕ is the standard normal distribution function, and p is the probability derived from Eqn. 3.4. This approach was implemented using Standardized Drought Analysis Toolbox (SDAT, *Farahmand and AghaKouchak* (2015)) and the SPI drought limit categories (intensities) proposed by *Agnew* (2000) used (Table 3.2). For

this study, a drought episode begins any time SPI is continuously less than −0.84 for a period of at least three months, and ends when SPI value exceeds −0.84. The various drought intensities (moderate, severe, and extreme) are then said to occur when the values in Table 3.2 are attained. The resulting standardized indices in this study were SPI, standardised soil moisture index (SSI), standardised vegetation condition index (SVCI), and standardised terrestrial water storage index (STWSI).

Table 3.2: Drought categories according to SPI values (*Agnew*, 2000). Drought is defined as when the SPI value is constantly less than -0.84 for a period of at least 3 months.

SPI	Drought Category
>1.65	extremely wet
>1.28	severely wet
>0.84	moderately wet
>- 0.84 and <0.84	normal
<-0.84	moderate drought
<-1.28	severe drought
<-1.65	extreme drought

3.2.1.2 Standardized Anomalies (SA)

As already pointed out, due to the short time frame of GRACE product, SA instead of SI was computed for characterizing agricultural drought. Here, the 3 and 6 months GTWS time series cumulations were obtained in a manner similar to those of the Standardized Precipitation Index (*McKee et al.*, 1993). For example, a three months' cumulation for January involves adding November and December of the previous year to the current January resulting in a new time series while six months for January would involve adding August to December of previous year onto the current January thereby forming a 6 months cumulation time series. Due to seasonality in precipitation, soil moisture, TWS, and NDVI dataset (*Yang et al.*, 2014b), GTWS anomalies were calculated by removing the monthly mean from the 1, 3, and 6 month time series. The anomalies were then divided by the

standard deviation for the duration of the data (e.g., *Peters et al.*, 2002), i.e.,

$$\mathrm{XS}_{ijk} = \frac{\mathrm{X}_{ijk} - \frac{1}{n}\sum_{k=1}^{n} \mathrm{X}_{ijk}}{\sigma_{ij}}, \tag{3.6}$$

where XS_{ijk} is the monthly standardized GTWS anomaly for location i, month j, and year k; X_{ijk} is the monthly GTWS for location i, month j, and year k; n is the length of GTWS in years; and σ_{ij} is the multi-year standard deviation for location i, month j. The resulting standardized anomalies (z-scores), express the deviation of the GTWS above or below the mean value and has been used to monitor drought in various studies (e.g., *Wu et al.*, 2001; *Agnew and Chappell*, 1999; *Lough*, 1997; *Katz and Glantz*, 1986). Positive values indicate wet conditions, 0 indicate normal (average) conditions while negative values indicate drought conditions (*Wu et al.*, 2001).

In order to demonstrate the consistency between SPI and SA in characterizing drought over the region, the study compared the spatio-temporal decompositions of CHIRPS-derived SPI and CHIRPS-derived SA over the study region. This comparison showed similar spatio-temporal drought patterns (See Figs. 3.1 and 3.3 for CHIRPS-derived SPI spatio-temporal drought patterns). Further, Pearson correlations between the SI and SA temporal patterns were greater than 0.95 over the region. Due to the close association between SA and SI (see also, *Wu et al.*, 2001), the SPI drought limit categories (Table 3.2) were used to differentiate the various SA drought intensities.

3.2.1.3 Principal Component Analysis (PCA)

In this Chapter, PCA (see Chapter 2 for formulation and details) was applied to the 1, 3, 6-month time scales of SI and SA. Log-eigenvalue (LEV) diagrams (*Jolliffe*, 2002) were used to determine and retain the significant components that were then rotated through VARIMAX rotation (*Kaiser*, 1958; *Forina et al.*, 1988; *Jolliffe*, 1995) for better localization. The resulting spatial patterns were

normalised by multiplying with the standard deviation of their corresponding rotated principal components (RPC) series, while the RPCs' were normalised by dividing with their respective standard deviations.

3.2.1.4 Percentage of Areas Under Drought

The resulting rotated spatio-temporal SI/SA (3-months' time scale; from section 3.2.1.3) were reconstituted and the percentage of pixels under various drought intensities (following drought limit categories in Table 3.2) determined for every month.

3.2.2 Assessing the Effectiveness of Drought Indicators Using National Annual Crop Production

Since national annual crop production data had national spatial resolution (they are country level datasets), rotated spatio-temporal drought patterns were re-computed but in this case for each country and not the whole region as in section 3.2.1. For each country, SI/SA values for each month of the year over the entire duration were extracted from the rotated principal components. For example, considering Kenya with four significant GRACE SA rotated principal components, each component comprising of 120 values/months (2004 to 2013), corresponding to January, February, ..., December were extracted resulting in four 10 by 12 matrices, i.e., 10 years of data for every month of the year. The resulting four matrices were concatenated to a 10 by 48 matrix, which served as the predictor variable in the PLSR (See Chapter 2 for details) against national annual crop production data (maize/wheat) as the response variable. This was done for 1, 3, and 6 month SI/SA time scales for all the variables/indicators across Kenya, Uganda, and Tanzania.

3.3 Results and Discussion

3.3.1 Spatio-temporal Drought Patterns

The PCA decomposition of SI/SA showed spatial and temporal patterns, which became very distinct upon applying varimax rotation as compared to unrotated components (data not shown). Integrating the spatial and temporal patterns of the SIs/SAs, and using the drought category definitions in Table 3.2, percentage of areas under various drought intensities were evaluated. The results presented and discussed here are for the 3-month time scale only, as this was representative of the results for the 1 and 6-month time scales.

3.3.1.1 Spatial Variability

The four most significant components in terms of explaining the total variability from RPCA of SI/SA revealed four distinct spatial patterns across all products (Figs. 3.1 and 3.2). While the rest of the products had distinct region 3 (the dry eastern part of Kenya), GPCC had a contrast between the dry and the wet part of the region in form of a dipole pattern (Fig. 3.1). This pattern is similar to that of 2nd EOF of *Schreck and Semazzi* (2004) that was attributed to decadal variability, in their decomposition of region's rainfall. In addition, the dipole pattern could have been made more prominent by the gauge distribution (see Fig. 8.1 in the Appendix); the western side has high gauge density and availability compared to the eastern side, this is likely to translate into the dipole pattern when the gauge values are interpolated into gridded equivalents. In addition, the spatial patterns of ERA-Interim and to some extent of GLDAS in region 2 were different from those of other products. The geographical coverage of these spatial patterns is summarized in Table 3.3.

The four RPCs explained between 38% (SVCI) and 96% (GTWS SA) of the total variance of the respective original SI/SA variables (Table 3.4). Most of the products had the highest and the lowest variabilities explained in regions 3

and 4, respectively (Table 3.4). This could be attributed to the fact that region 3 covering almost the entire region of Kenya (in those indicators showing it highest) is wet and dry on the western and eastern parts of the country, respectively, hence has high variability due to the presence of wet and dry extremes. On the other hand, region 4 is relatively wet and receives consistent rainfall resulting in a smaller variation in SI/SA.

Table 3.3: Geographical coverage of SI/SA spatial patterns (Figs. 3.1 and 3.2).

Region	Countries/Areas
1	Lake Victoria, Uganda, and western Kenya
2	Western Tanzania, Rwanda, and Burundi
3	Eastern Kenya
4	Eastern and southern Tanzania

Table 3.4: Proportion of variances explained by various spatial patterns across the four regions (Figs. 3.1 and 3.2, and Table 3.3 for the regions). Many of the products explain highest and lowest variabilities in regions 3 and 4, respectively. In addition, MERRA-2 and MTWS appear very close.

Region	CHIRPS	GPCC	VCI	MTWS	GTWS	ERA-Interim	GLDAS	CPC	MERRA-2	FLDAS
Region 1	15.26	12.07	8.24	13.86	29.88	18.91	11.79	10.29	13.61	14.86
Region 2	14.62	13.15	10.01	18.13	24.58	10.78	15.75	16.46	17.72	15.77
Region 3	15.26	13.67	12.57	21.44	21.58	14.32	14.22	21.80	21.98	18.21
Region 4	10.60	11.64	6.94	13.67	19.77	20.05	16.72	13.27	14.64	12.64
Total	55.53	50.53	37.77	67.10	95.81	64.06	58.48	61.83	67.95	61.48

3.3.1.2 Temporal Patterns

The temporal evolutions of the spatial patterns in regions 1 to 4 (Figs. 3.1 and 3.2) from the rotated PCA are shown in Figures 3.3 and 3.4. In general, the temporal evolutions (interpreted in conjunction with Figures 3.1 and 3.2, and

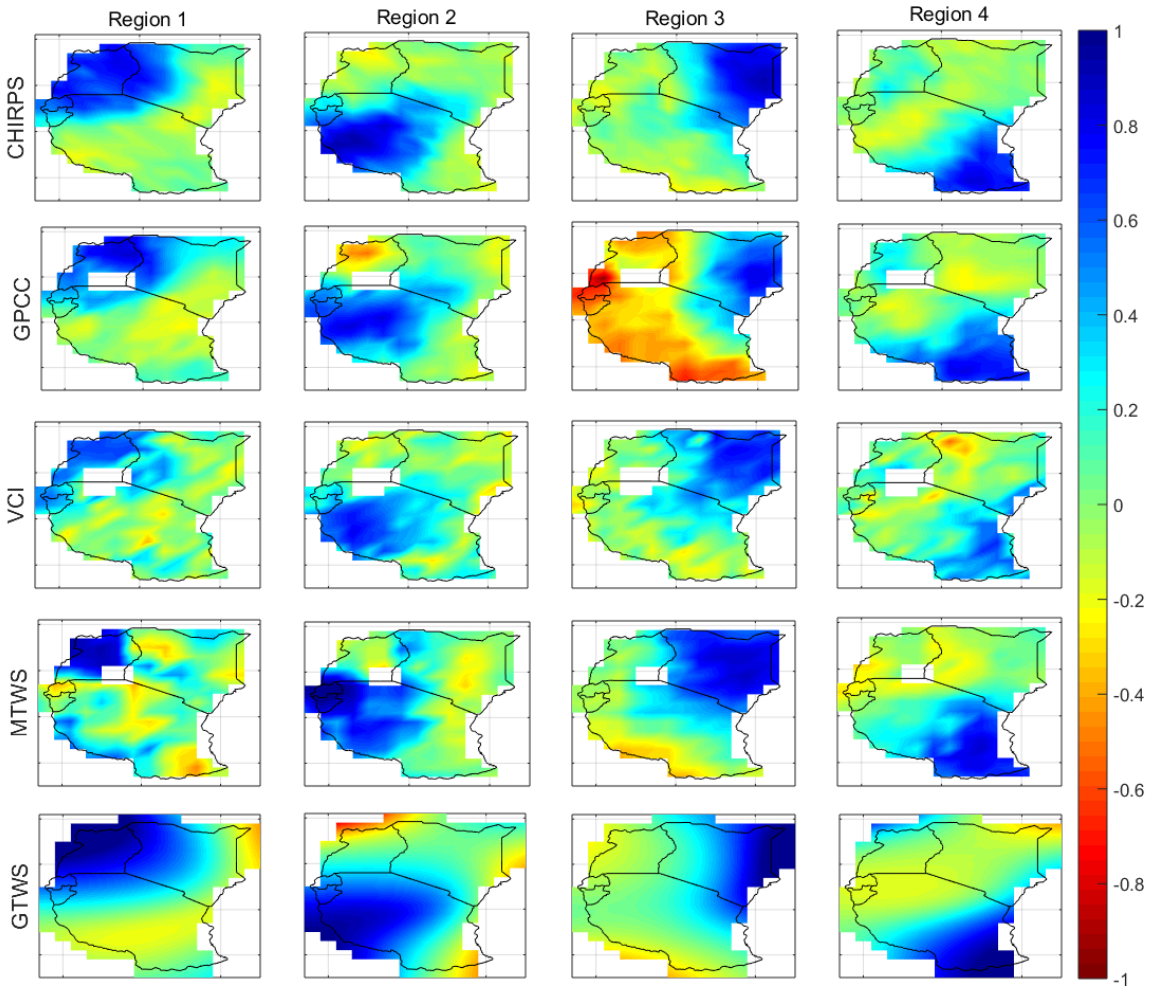

Figure 3.1: Rotated principal component spatial patterns of standardized indices/anomalies (SI/SA). Rows denote products while columns denote regions (also see Table 3.3). The spatial patterns have been scaled to ± 1, thus the temporal evolutions shown in Figure 3.3 indicate the actual magnitude of SI/SA for regions where the spatial patterns have values close to ± 1. The spatial patterns are interpreted in conjunction with temporal evolutions in Fig. 3.3 and represent drought spatial patterns any time the temporal evolutions falls below -0.84, as in Table 3.2. The white rectangular area in all the images except CHIRPS and GTWS is Lake Victoria.

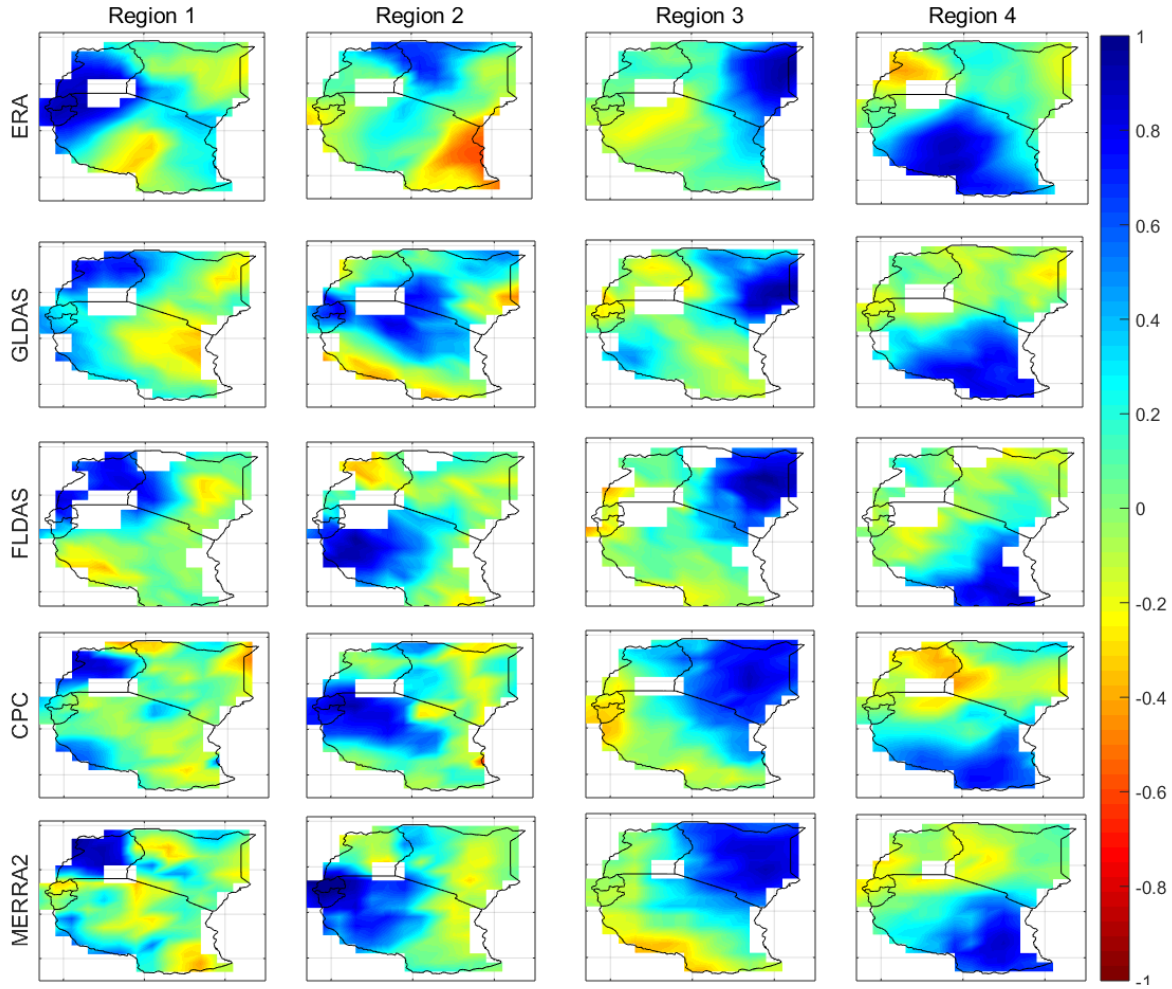

Figure 3.2: Rotated principal component spatial patterns of standardized soil moisture indices (SSI). Rows denote products while columns denote regions (also see Table 3.3). The spatial patterns have been scaled to ± 1, thus the temporal evolutions shown in Figure 3.4 indicate the actual magnitude of SSI for regions where the spatial patterns have values close to ± 1. The spatial patterns are interpreted in conjunction with temporal evolutions in Fig. 3.4 and represent drought spatial patterns any time the temporal evolutions falls below -0.84, as in Table 3.2. Patterns are consistent with those in Fig. 3.1 except for ERA-Interim and to some extent GLDAS in region 2. The white rectangular area in all the images is Lake Victoria.

Table 3.2) show most of the regions suffering from severe to extreme drought in 1984/1985, 1999, 2000, 2005/2006, and 2010/2011. These and other drought episodes captured in these figures are consistent with documented drought

episodes in the EA region (e.g., *Masih et al.*, 2014; *Nicholson*, 2014a; *IFRC*, 2011).

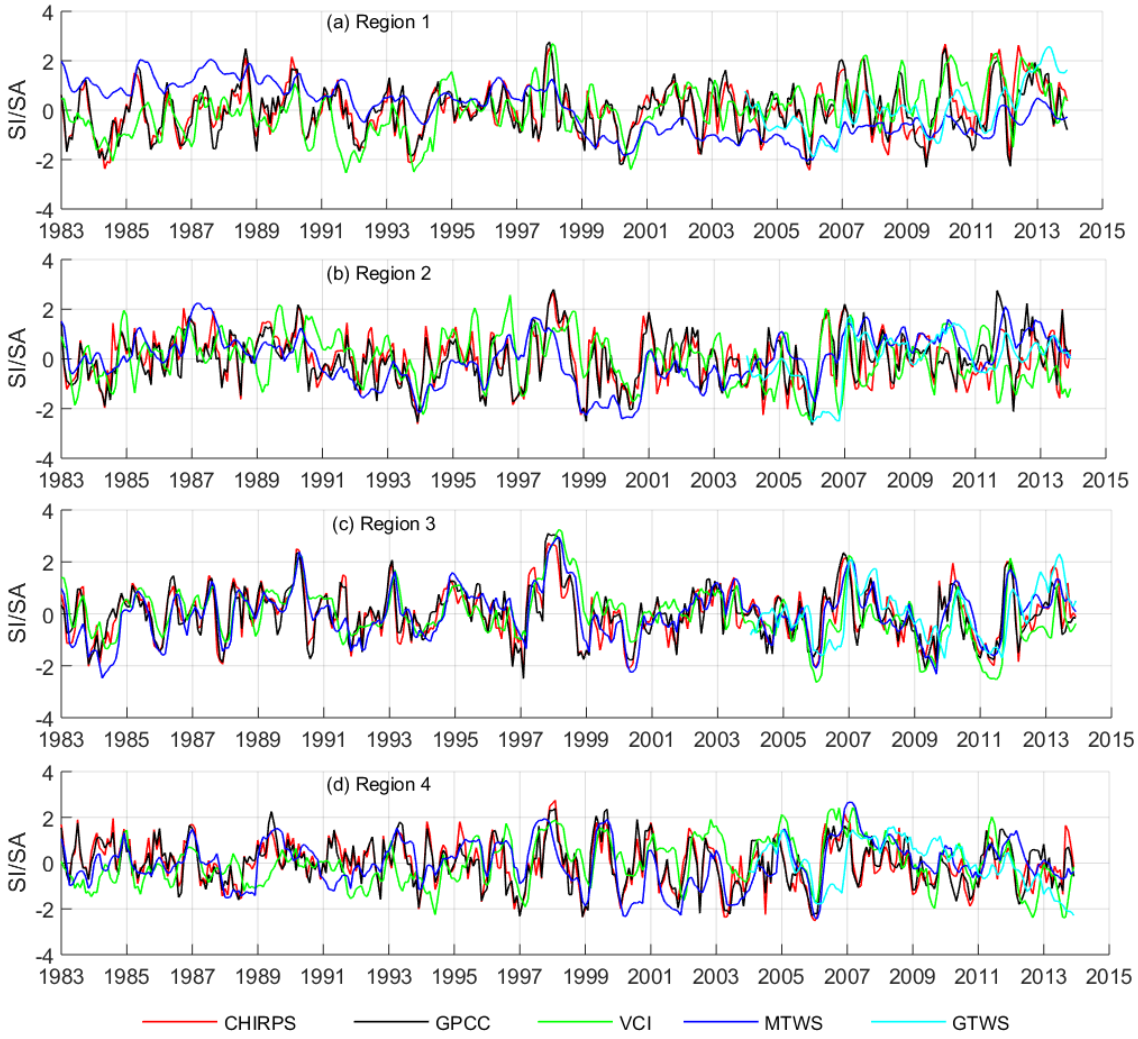

Figure 3.3: Temporal evolutions of SA/SI spatial patterns in Figure 3.1. The temporal evolutions are interpreted in conjunction with Table 3.2, to classify drought and/or wet conditions. Rainfall products (CHIRPS and GPCC) exhibit similar consistent performance across the region. Also, all the products exhibit consistent performance in region 3, while VCI and GTWS show some lag in relation to rainfall.

All the products had similar performance in region 3 (Figs. 3.3c and 3.4c), which may be attributed to the relatively flat terrain (Fig. 2.1) coupled with relatively less rainfall hence good performance by the models and rainfall products. The performance of the rainfall products (CHIRPS and GPCC) were

almost identical over the entire study region as a result of both containing in-situ rainfall (CHIRPS has satellite-derived precipitation estimates in addition to in-situ data while GPCC is purely gridded in-situ product, see e.g., *Schneider et al.*, 2014; *Funk et al.*, 2015). In relation to the rainfall products, the remaining products (VCI, soil moisture, and TWS) showed delayed (lagged) response in the temporal evolution. This is clearly visible in Figure 3.3a in which MTWS appears like a low pass filtered version of the CHIRPS/GPCC signals. This behavior could be due to a delayed response of terrestrial water storage changes to rainfall and soil moisture changes. Finally, the soil moisture products seemed to form largely two classes/categories with ERA-Interim, FLDAS, and GLDAS in one category and CPC and MERRA-2 on the other, especially considering region 1 (Fig. 3.4a).

Other than seasonality induced variability which is depicted across all the modes, due to the fact that all the variables analyzed directly depend on rainfall, the variability of the modes appears also to be influenced by occurrence of extreme events (droughts and floods). The frequent successions of extreme dry (droughts) and wet (flooding) conditions over the region are contributed by the regional climate, which is characterized by high interannual variation in precipitation numbers (*Segele et al.*, 2009; *Souverijns et al.*, 2016). The general precipitation climatology over the region is extremely heterogeneous, due to the complexity of large scale controls e.g., topography, lakes, maritime influence and seasonal dynamics of tropical circulation (Fig. 2; *Nicholson*, 2016). These could also be the reasons for the regionalization as observed in Figs. 3.1 and 3.2. As for the extreme wet events e.g., 1997, 2006, and 2011 research (e.g., *Nicholson*, 2016, 2015; *Hastenrath et al.*, 2010, 2007) have associated their occurrences to surface and 200 mbar zonal winds over the central equatorial Indian Ocean, sea surface temperature in Niño 3.4 and the Indian Ocean Zone mode, while the extreme dry events (droughts e.g., 2009, 2010, and 2011 among other years) have been associates with the equatorial westerlies over the Indian Ocean.

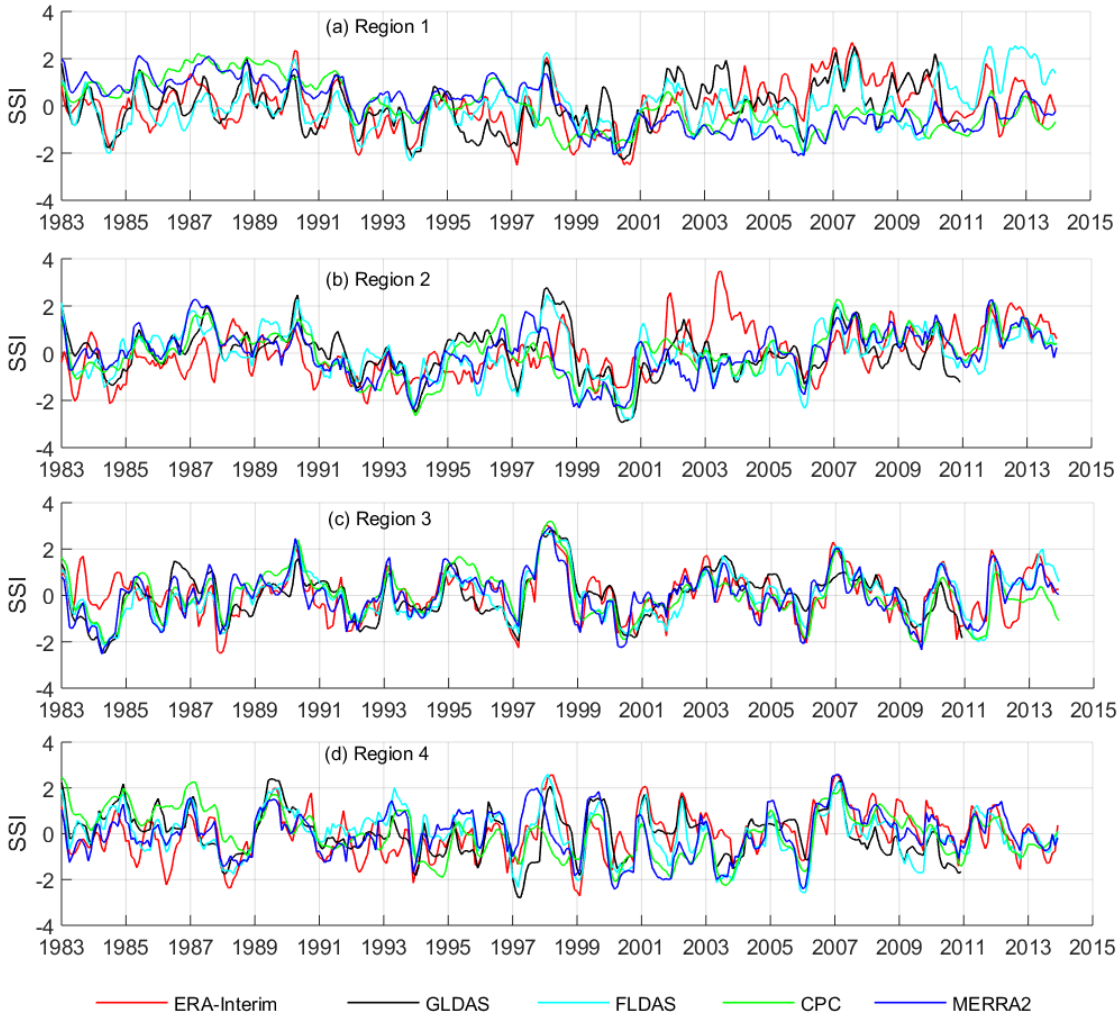

Figure 3.4: Temporal evolutions of SSI spatial patterns in Figure 3.2. The temporal evolutions are interpreted in conjunction with Table 3.2, to classify drought and/or wet conditions. All the moisture products have consistent performance in region 3 while in the rest of the regions, the soil moisture products seemed to form largely two classes/categories with ERA-Interim, FLDAS, and GLDAS in one category and CPC and MERRA-2 on the other, especially considering region 1 (a).

Further, correlation analysis between the drought indices revealed close relationships between various products e.g., CHIRPS and GPCC, MERRA-2, MTWS, and CPC, across the regions (Table 3.5 and Fig. 3.5). The close relationship between MTWS and MERRA-2 is similar to that between CHIRPS and GPCC, since MTWS include aspects of soil moisture captured by MERRA-2 in addition to greater depth of soil water content. Furthermore, the

significant and high correlations between the drought indices in region 3 support similar performance observed in Figures 3.3c and 3.4c. VCI had weak negative correlation trends with the following products: MTWS, MERRA-2, and CPC in region 1 due to these products showing a pre-dominantly wet pre-1993 and dry post-1999 that was opposite to the general VCI trend.

Table 3.5: Relationship between the drought indices by regions. Regions are as in Fig. 3.1. Non-significant correlations are in italics ($p < 0.05$). Region 3 has the strongest relationships with all values being significant. Also, note the high correlations between the following products across the regions: GPCC and CHIRPS; and MTWS, MERRA-2, and CPC. (MTWS - MERRA-2 TWS, GTWS - GRACE TWS).

	CHIRPS	GPCC	VCI	MTWS	ERA	CPC	MERRA2	FLDAS	GLDAS	GTWS
CHIRPS	1	**0.8991**	0.4907	0.1203	0.4255	0.1073	0.2052	0.7300	0.5106	0.3196
GPCC	**0.8619**	1	0.4250	0.1288	0.4505	0.1266	0.2161	0.6120	0.5454	0.2433
VCI	0.2832	0.1918	1	-0.1082	0.4366	-0.1091	*-0.0690*	0.6737	0.527	0.3658
MTWS	0.3922	0.4683	0.2152	1	*0.0526*	**0.8437**	**0.9910**	0.1888	*0.0359*	0.7939
ERA	*0.0947*	0.2525	*-0.1041*	0.3628	1	0.1788	0.1138	0.5229	0.6664	*-0.1708*
CPC	0.2970	0.3962	0.2410	**0.8714**	0.4240	1	**0.8482**	0.1370	0.0976	0.5036
MERRA2	0.4546	0.5310	0.1889	**0.9864**	0.3791	**0.8513**	1	0.2431	*0.0810*	0.7352
FLDAS	0.6324	0.6352	0.4079	0.7372	0.2704	0.6844	0.7212	1	0.6365	0.7047
GLDAS	0.4141	0.4499	0.4494	0.5911	0.3352	0.6274	0.5583	0.6940	1	*0.0643*
GTWS	0.1101	0.0776	0.1863	0.7310	0.5553	0.6465	0.6651	0.4429	0.4505	1
CHIRPS	1	**0.9267**	0.5771	0.7388	0.6827	0.5622	0.7921	0.5914	0.4727	0.3796
GPCC	**0.8959**	1	0.5733	0.7023	0.6797	0.5583	0.7589	0.5377	0.4782	0.2643
VCI	0.2740	0.2788	1	0.7895	0.6614	**0.8072**	0.7636	0.7144	0.6837	0.6688
MTWS	0.4808	0.4919	0.4735	1	0.7195	**0.8676**	**0.9912**	**0.8604**	0.7316	0.6209
ERA	0.4095	0.3615	0.5310	0.5082	1	0.6686	0.7307	0.6937	0.6083	0.5950
CPC	0.4003	0.3978	0.2787	0.6799	0.3201	1	**0.8267**	**0.8335**	0.7513	0.6861
MERRA2	0.5482	0.5534	0.4569	**0.9837**	0.5250	0.6692	1	**0.8256**	0.6903	0.5743
FLDAS	0.6516	0.6312	0.4592	0.7627	0.5595	0.6161	0.7465	1	**0.8302**	0.7693
GLDAS	0.5047	0.5016	0.4130	0.4736	0.5432	0.5496	0.4578	0.7438	1	0.5598
GTWS	0.0196	0.0609	0.4195	0.4637	0.4334	0.4860	0.4200	0.2699	*-0.0189*	1

Note: Red (region 1), blue (region 2), green (region 3), brown (region 4).

3.3.1.3 Drought Intensity Area Analyses

In order to gain further insight into the spatial extent of the drought events and their intensities, the spatial and temporal patterns (Figs. 3.1, 3.2, 3.3, and 3.4) were integrated and using drought limit categories in Table 3.2, percentage of areas under drought (by intensity) were evaluated and results presented in Figure 3.6. Overall, the rainfall products (CHIRPS and GPCC) had on average, the highest estimate of percentage areas under drought closely followed by the

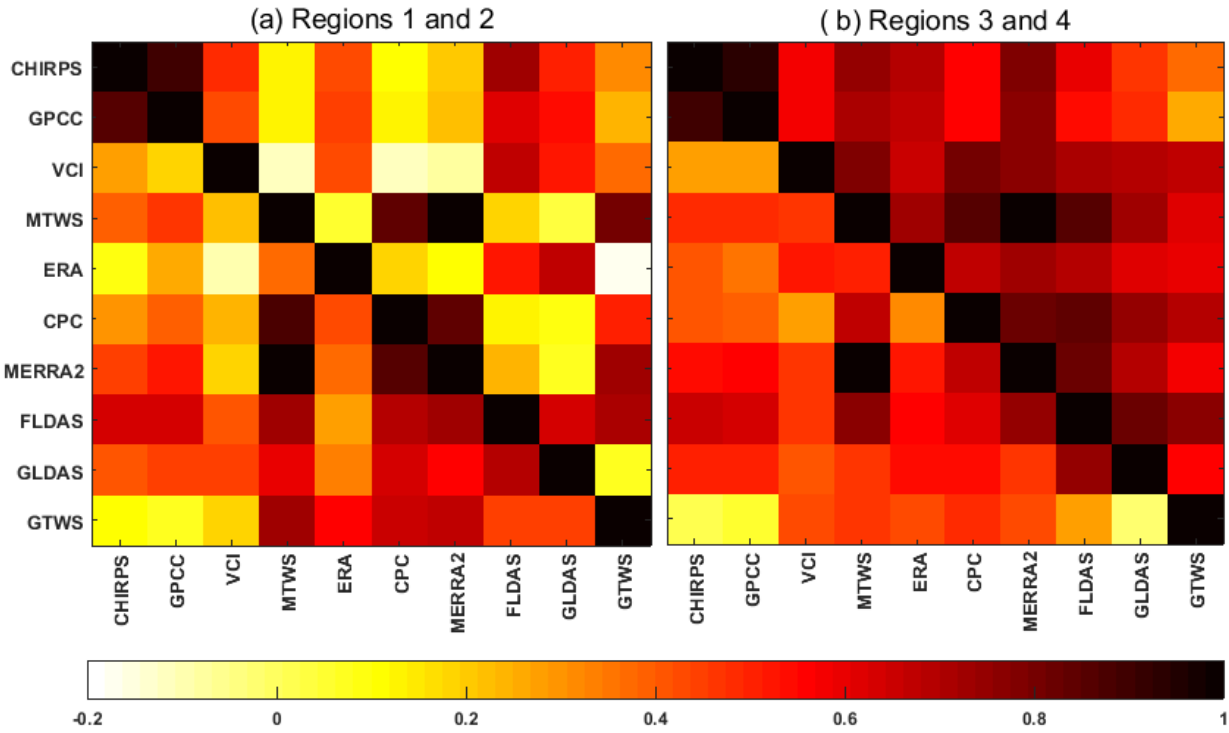

Figure 3.5: Correlation shaded plot between drought indices by region; (a) upper triangle - region 1, lower triangle - region 2; and (b) upper triangle - region 3, and lower triangle - region 4. Region 3 has the strongest relationships. Also, note the high correlations between the following products across the regions: GPCC and CHIRPS; and MTWS, MERRA-2, and CPC. (MTWS - MERRA-2 TWS, GTWS - GRACE TWS).

soil moisture products whereas VCI had the lowest estimates (average means of 13.09%, 11.90%, and 5.5%, respectively, at $F(2, 2212) = 19.7220$, $p = 3.2384 \times 10^{-9}$). One reason for the rainfall products showing more areas as being under drought may be that meteorological drought is a binary event (present or absent) which is not affected by modulating factors unlike the other drought indicators e.g., VCI. VCI-based droughts, unlike meteorological droughts, are modulated by soil characteristics (water holding capacity) and/or plant (vegetation) type. Thus, for example, there could be meteorological drought over an area but due to soil water retention capacity and/or vegetation with deep roots capable of drawing water from deep soils (underground),VCI indicates no drought condition, hence the smaller area under drought. Since the

soil moisture products and MTWS are modelled from rainfall and other additional inputs, their estimates of percentage areas under drought are likely to follow closely those of rainfall. However, the soil moisture products had statistically significantly different percent of areas under drought amongst themselves as was determined by one way ANOVA ($F(4, 1250) = 3.5410$, $p = 0.0070$).

The observed differences in percentage of drought areas between the various soil moisture products arise from differences in; (i) forcing precipitation, (ii) the ways in which the individual hydrological models partition precipitation into run-off and evapotranspiration, and (iii) water holding capacities, the last two of which impacts on the modelled soil moisture sensitivities to precipitation variability (*Shukla et al.*, 2014). The contribution of forcing precipitation on the differences in percentage of areas is highlighted by the differences in areas presented by GLDAS and FLDAS, products of the same model (Noah) but different forcing precipitation, hence different drought spatial extents and cycles. Of all the model forcing parameters, precipitation is the key factor determining the characteristics of the resulting soil moisture (see, e.g., *Entin et al.*, 1999; *Dirmeyer et al.*, 1999, 2004; *Mo et al.*, 2012), hence the areal extents under drought.

The MERRA-2 products show similar patterns and are closer to CPC (Fig. 3.6d, e, and h) while GLDAS is closer to ERA-interim as had been observed from the correlations (Table 3.5) and in the temporal evolutions (Figs. 3.3 and 3.4). FLDAS appear to be in between the two groups. Also, the lag in drought detection (already noted in Figures 3.3 and 3.4) becomes more evident with the rainfall products detecting drought onset and duration first, followed by VCI/soil moisture products, and finally the TWS products. This would be attributed to time delayed response in moisture accumulation from rainfall through soil moisture, vegetation, and finally to changes in TWS during both the start and cessation of rainfall. In addition, the rainfall product

(Fig. 3.6 a and b) also indicate the post-1999 period as having more drought events with higher intensity than the pre-1999 period. On average, the post-1999 period had at least 10%[1] more drought events compared to the pre-1999 period. This is in line with other drought and climate studies that observed a decline in rainfall since 1999 and increased drought frequencies (see,

[1]Number of drought episodes in the pre and post 1999 were counted, and their difference converted to percentage. This was done for the two rainfall products and average taken. Same was done for the rest of the products.

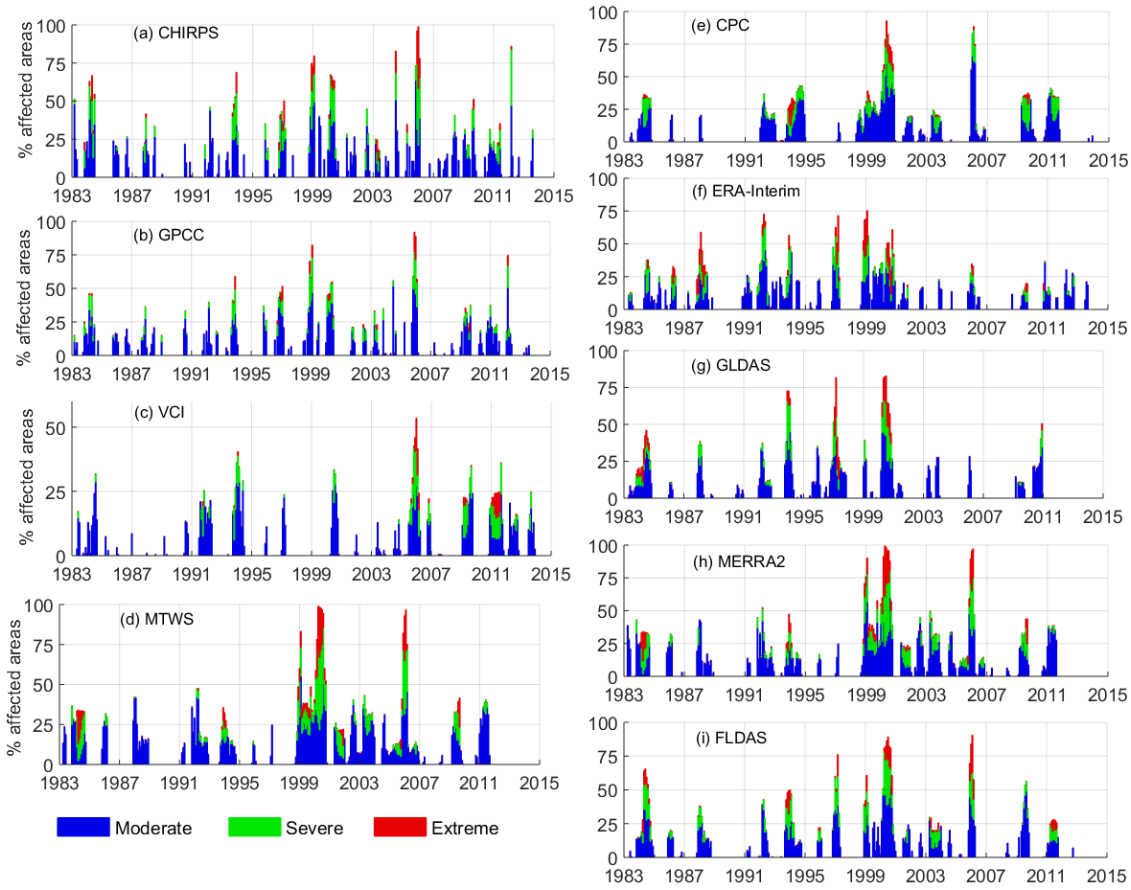

Figure 3.6: Percentage of area affected by various drought intensities during the period 1983 – 2013. Percentage areas are computed by integrating the regional spatial and temporal patterns (Figs. 3.1, 3.2, 3.3, and 3.4) then determining percentage of pixels under each drought category as per Table 3.2. The rainfall products have the highest percentage areas under drought followed closely by soil moisture products and finally the lowest percentage areas are by VCI. In addition to the soil moisture products having different percentage areas under drought, CPC is consistent with MERRA-2, GLDAS is consistent with ERA-Interim while FLDAS is in between.

Lyon and DeWitt, 2012; *Lyon*, 2014; *Yang et al.*, 2014a). In contrast, the other products (Fig. 3.6 c – i) did not reflect any meaningful increase in drought events (with VCI, moisture and TWS products having an average increase of 0%, 1.5%, and 0%, respectively). Also, GLDAS seems to have underestimated the 2005 - 2006 drought in terms of both duration and intensity as compared to the rest of the soil moisture products.

Further, GTWS returned higher percentage of areas under drought on average than MTWS as confirmed by one way ANOVA (25.307 *vs* 9.8147 *at* $F(1, 138) = 16.1064$, $p = 0.0001$) though with almost equal percentage of areas at drought peaks, at which GTWS lagged MTWS by $0 - 3$ *months* in the detection of drought onset and cessation (Fig. 3.7a and b). Since MTWS is modelled on precipitation and other input without groundwater while GTWS is observed, the lack of groundwater in MTWS probably explains why it does not properly account for the buffer effect, hence possible lag by GRACE in detecting the onset and cessation of drought. In addition, GTWS shows drought episodes in the post 2012 period while MTWS does not (see, Fig. 3.7).

The drought severity is consistent among the products as evidenced by the majority of the areas being under moderate drought followed by severe drought and then extreme according to the definition of SPI (see, e.g., Figs. 3.6 and 3.7 ; *McKee et al.*, 1993). All the products captured different severity levels except MTWS and MERRA-2, which had similar severity levels as a result of overlapping formulation. The differences in severity levels among the other products could be attributed to the different formulation of the products and to the fact that they represent droughts in different environments with different impacting factors, e.g., soil properties influence the severity of drought as captured by the soil moisture products while rainfall characteristics (amount, intensity, and duration) influence the drought severity as captured by rainfall products.

Finally, from the knowledge gained in the analyses above, the droughts of 1983 – 1984, 2005 – 2006, and 2010 – 2011 were closely examined using selected

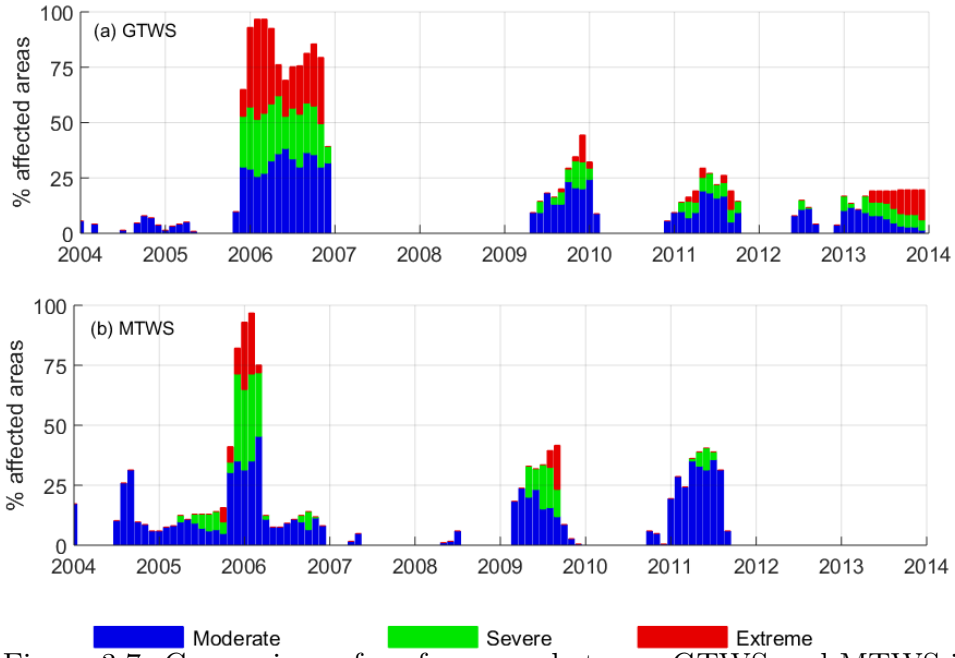

Figure 3.7: Comparison of performance between GTWS and MTWS in terms of percentage of areas affected by various drought categories. Percentage areas are computed as in Fig. 3.6. They have consistent performance, with GTWS having a lag in drought detection probably due to groundwater that is lacking in MTWS.

indicators in order to quantify the above-observed lags in drought cycles (Table 3.6, Fig. 3.8). These drought years have been selected for further analysis because they had more severe impacts in the region (see, e.g., *Shukla et al.*, 2014; *Masih et al.*, 2014; *Spinage*, 2012). From this analysis, VCI had a lag of 0 – 4 months in relation to CHIRPS in picking drought cycle (onset, peak, and cessation) while the soil moisture products (CPC, ERA-Interim, GLDAS, FLDAS, and MERRA-2) had inconsistent lags amongst themselves, and in relation to CHIRPS for the considered drought episodes (e.g., Table 3.6, Fig. 3.8). Soil moisture, being an integration of rainfall anomalies over time (*Dutra et al.*, 2008; *Sheffield and Wood*, 2008), is expected to have a lag in response to rainfall behavior throughout the hydrological cycle hence the soil moisture products and VCI (an indicator of moisture availability to vegetation) lag rainfall in the analysis.

The inconsistency in the lags by the soil moisture products, similar to observed

Table 3.6: Drought lags (in months) by various products in relation to CHIRPS drought cycle (onset, peak, and cessation). Negative values indicate the respective product had drought cycle before CHIRPS while dash indicate products not available during that particular drought. The lags were quantified from selected droughts of 1983 - 1984, 2005 - 2006, and 2010 - 2011, see Fig. 3.8.

Year/Drought cycle	VCI	CPC	ERA	GLDAS	FLDAS	MTWS/ MERRA2	GTWS
1983 - 1984/ Onset	1	1	6	-1	0	0	-
1983 - 1984/ Peak	3	0	3	2	1	-6	-
1983 - 1984/ Cessation	2	4	5	4	5	3	-
2005 - 2006/ Onset	1	5	4	7	5	-1	6
2005 - 2006/ Peak	0	1	0	1	1	1	1
2005 - 2006/ Cessation	2	>5	5	1	2	>5	>5
2010 - 2011/ Onset	3	1	2	-	3	2	4
2010 - 2011/ Peak	3	-3	-7	-	0	0	-1
2010 - 2011/ Cessation	4	3	-4	-	3	2	3

inconsistency in the percentage of areas under drought (Fig. 3.6), could be due to the different model forcing parameters used in generating various products in addition to different model thresholds as discussed above. Finally, the TWS products had different lags with GTWS having longer lag (Fig. 3.7). This longest lag from GTWS could be due to the fact that it is the last in the transition from rain event to moisture accumulation, and eventually groundwater change over time. Also, the under-characterization of the 2005 - 2006 drought by GLDAS already observed in Figure 3.6g is clearer in Figure 3.8b.

3.3.2 Assessing the Effectiveness of Drought Indicators Using National Annual Crop Production

In order to assess the effectiveness of the indicators in capturing agricultural droughts, partial least square regression (PLSR) models were fitted with indices as the predictors and national annual crop production data as the responses. The model with the lowest estimated mean squared prediction error was adopted in each case and the proportion of variability explained (R^2) used for comparison. As production is known to be related to water availability at various stages of crops growth (*Steduto et al.*, 2012; *Hane and Pumphrey*, 1984), and water being a major

growth determinant in the EA region (*Barron et al.*, 2003), a good relationship is expected between drought indices that capture (characterize) drought well and crop production over the considered duration of time.

Because crop production data is reported at country level (national) while the generalization in section 3.3.1 (Figs. 3.1 and 3.2) had signals across countries, SIs/SAs were re-computed for each country and the resulting rotated principal components reconstructed and used in PLSR with country level crop production data. The SIs were computed for the long term duration (1983 – 2013) and SAs for the short term (2004 – 2013). The latter duration though shorter, was

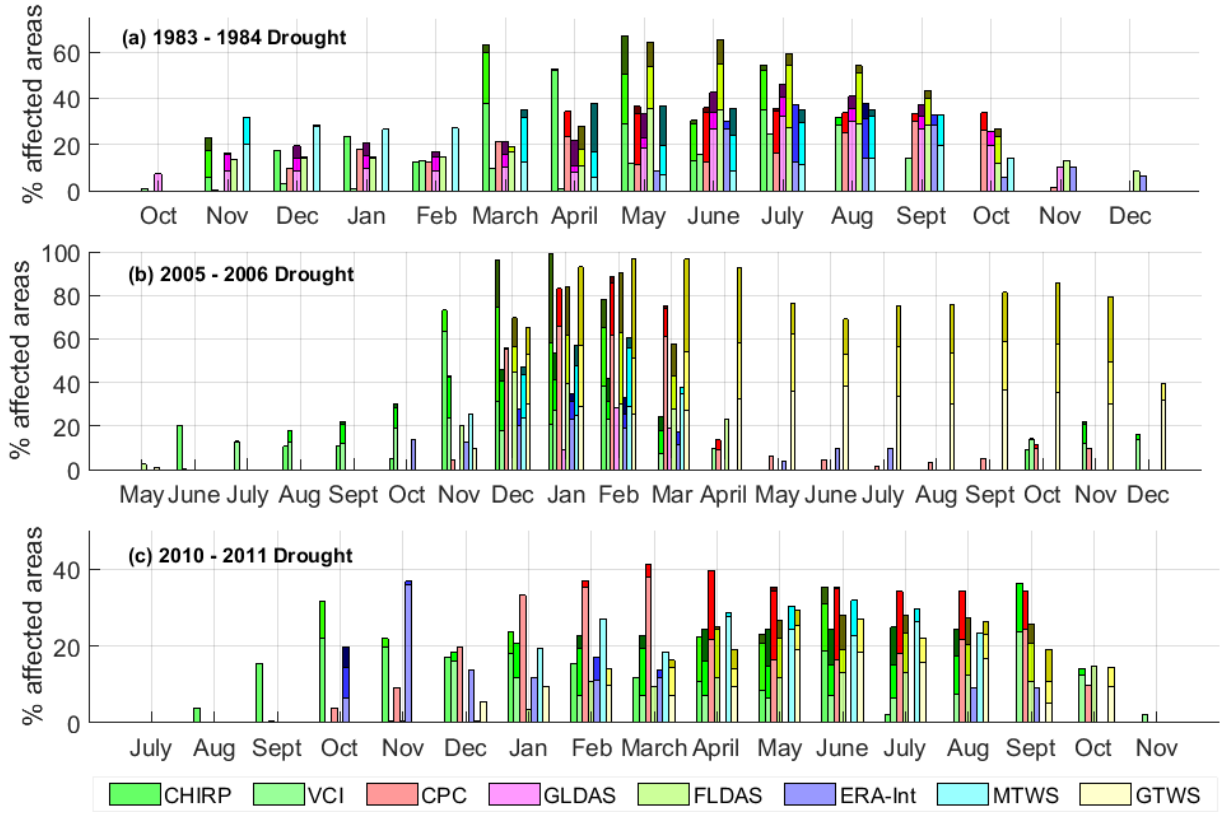

Figure 3.8: Percentage of areas affected by various drought intensities during the 1983 – 1984, 2005 – 2006, and 2010 – 2011 drought episodes. Each bar has up to 3 colour grades (gradients) representing from bottom moderate, severe, and extreme droughts at the top. Percentage areas are computed as in Figure 3.6 but only for the duration of drought. VCI has a lag of about 0 – 4 months in identifying the drought cycle in relation to CHIRPS. The rest of the products have inconsistent lags in relation to rainfall across the three drought episodes.

necessitated by the need to compare the performance of GRACE SA against the other products. The proportions of variabilities explained (R^2) from the regression using the short duration (SAs) should be interpreted with caution due to the short length of the data used.

For Kenya, other than GLDAS and ERA, the rest of the products performed fairly well for the period 1983 – 2013 with CHIPS, GPCC, and VCI explaining up to 94%, 73%, and 89%, respectively, of the total annual variability in crop (wheat and maize) production (Fig. 3.9a). Similarly for Tanzania, CHIRPS, GPCC, and VCI explained up to 96%, 85%, and 89%, respectively, of the total annual variability in crop (wheat and maize) production (Fig. 3.9b). Finally in Uganda, other than GLDAS, all the other products performed well with CHIRPS, ERA, FLDAS, and MTWS explaining up to 88%, 92%, 84%, and 77%, respectively, of the total annual variability in crop (wheat and maize) production (Fig. 3.9c). The poor performance of GLDAS in Kenya and Uganda compared to the other soil moisture products could be linked to poor performance in drought characterization as was observed in section 3.3.1.3 and Figures 3.6g and 3.8b. Most of the products explained higher proportions of annual variability in crop production (R^2) in 1-month standardized anomalies followed by 3 then 6-months. Also, the close performance of MERRA-2 and MTWS witnessed in drought characterization (section 3.3.1.2 and Table 3.5) is evident in the amount of variabilities explained by these products across the region.

CHIRPS performed generally better than GPCC across the region (Fig. 3.9a-c). This could be attributed to the fact that in addition to rain gauge input, CHIRPS has satellite-derived rainfall estimates for areas with less or no rain gauge information unlike GPCC with only rain gauge measured rainfall hence its performance is dependent on gauge density and terrain changes (see, e.g., *Schneider et al.*, 2014; *Funk et al.*, 2015). Compared to the rainfall products (CHIRPS and GPCC), the soil moisture products explained less variability in annual crop production over EA region except in Uganda where

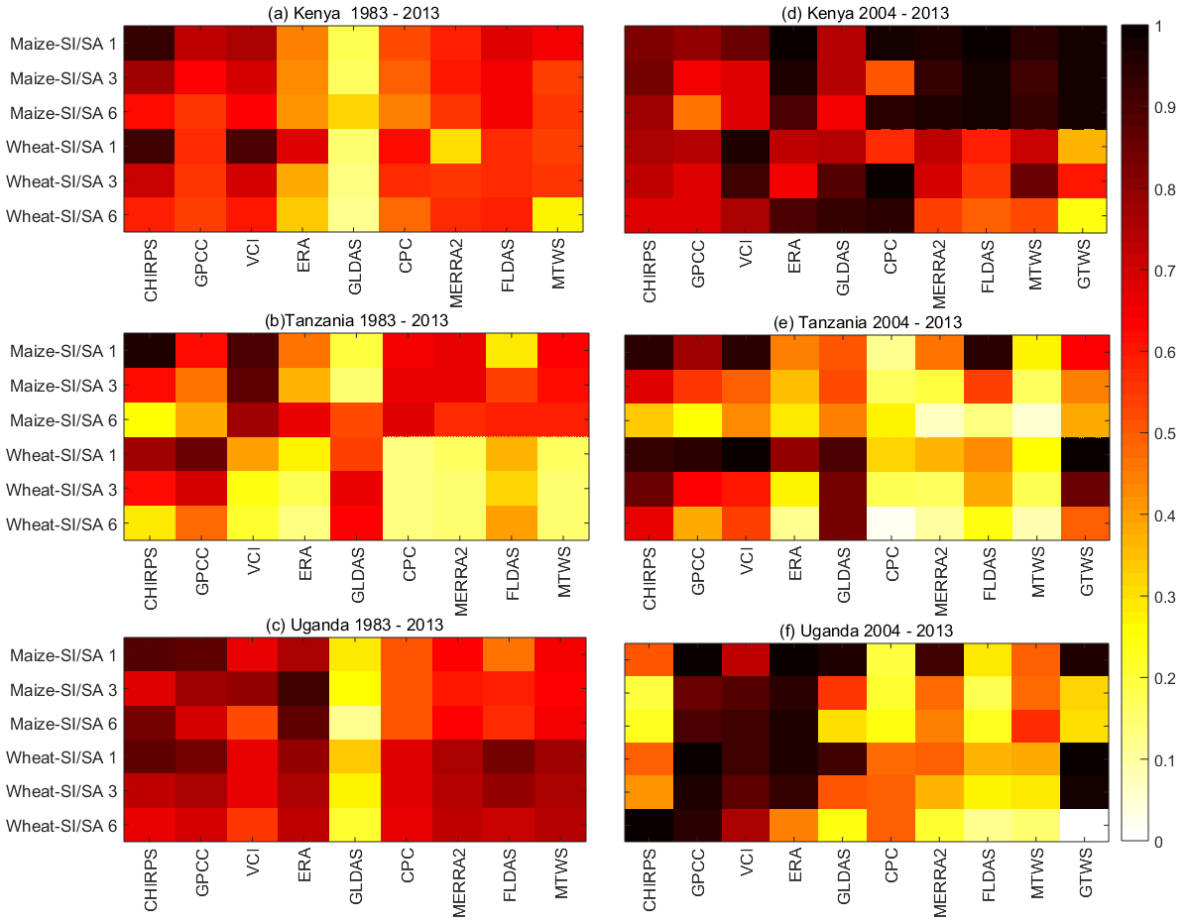

Figure 3.9: Proportions of variability in national annual crop (maize and wheat) production (R^2) explained by various drought indices for Kenya, Tanzania, and Uganda. CHIRPS, GPCC, and VCI consistently explains relatively higher variabilities in crop production, while the soil moisture products have inconsistent performance (a, b, and c). The figures d, e, and f should be interpreted with caution as the datasets used to fit the models are only 10 years long. Both SI and SA are computed at annual scales. The y axis indicates the crop (maize/wheat), SI (for a, b, and c), and SA (for d, e and f) while 1,3 and 6 indicate the standardization time scales for the indicators on the x axis.

the performance of ERA-Interim was almost as good as rainfall-derived indicators. Since soil moisture products represent the rainfall that remains after run-off and evaporation, the effective water available to the plants (crops), they are expected to explain higher variabilities in the annual crop production than rainfall thus their poor performance could be linked to how well they fit the region. In addition, the inconsistent performance of the soil moisture products (CPC, ERA-Interim, GLDAS, FLDAS, and MERRA-2) and MTWS across the

EA region in explaining the annual variability in crop production could be linked to the inconsistencies observed in the drought characterization as discussed in Section 3.3.1.2.

Overall, the good performance of FLDAS over GLDAS across the study region despite both being products of the same model (Noah) is due to the fact that for FLDAS, the Noah model was forced by CHIRPS, a precipitation product designed for the region. On the other hand, GLDAS's Noah was forced by Princeton global meteorological forcing data of *Sheffield et al.* (2006), a global product. This could also explain the difference in the performance of GLDAS across the three countries, since forcing precipitation has been shown to determine to a large extent the properties of model derived soil moisture (see, e.g., *Dirmeyer et al.*, 1999, 2004; *Entin et al.*, 1999). The magnitudes of the annual variabilities in crop production explained by FLDAS could be a pointer to difficulties faced by Noah in correctly partitioning precipitation into moisture, run-off, and evapotranspiration as per natural occurrence in the EA region.

Though based on a short duration data set (10 years), GRACE SA has mixed performance between wheat and maize across the countries but does better than or equals to soil moisture products across the region (Fig. 3.9d-f). The performance could be attributed to the fact that over a shorter duration of time such as the one considered (i.e., 1-, 3-, and 6-months anomalies), the bulk of the variation in the GRACE TWS occurs in the soil moisture compartment, which is more sensitive to climate variability than groundwater change (e.g., *Yang et al.*, 2014b). This shows the potential of GRACE product to monitor agricultural drought although longer duration of dataset is essential.

Results from regression analysis should be interpreted with caution though, as the relationship between production and climate conditions (water availability) only hold if other factors in the production chain are held constant, e.g., areas under cultivation over the period considered and technical factors of production (e.g., fertilizers, crop cultivars, pesticides). In addition, production response to

water at any stage of growth can be modified by various factors e.g., diseases, weeds, insects, crop variety (*Steduto et al.*, 2012; *Hane and Pumphrey*, 1984), hence, results should not be generalized to other areas.

3.4 Concluding Remarks

This Chapter characterized agricultural drought over EA region using precipitation products (CHIRPS and GPCC), soil moisture products (CPC, ERA-Interim, MERRA-2, FLDAS, and GLDAS), and TWS products (MERRA-2 and GRACE). This was accomplished through standardized indices/anomalies and rotated principal component analyses. In addition, the Chapter carried out partial least squares regression (PLSR) analysis over Kenya, Uganda, and Tanzania to assess the utility of these products in capturing agricultural drought in these countries. Drought characterization resulted in the following major findings:

(i) The rainfall products (CHIRPS and GPCC) were similar and consistent over the entire region, while all the other products were consistent over region 3 (dry lowland eastern Kenya).

(ii) In terms of percentage of areas under drought, the rainfall products (CHIRPS and GPCC) covered the highest areas closely followed by the soil moisture products, whereas VCI covered the least percentage areas under drought.

(iii) Drought cycle (onset, peak, and cessation) detection was in the order; rainfall, VCI/soil moisture, and TWS. In addition, VCI had 0-4 months lag in detecting drought cycle in relation to rainfall products while the soil moisture and TWS products had inconsistent lag varying from one drought to the next.

(iv) Soil moisture products had different results (both lag and areas under drought), with ERA-Interim being closer to GLDAS, MERRA-2 being close

to CPC while FLDAS was in between. GLDAS under-characterized the 2005 - 2006 drought to under 2 months in comparison to over 7 months of ERA and CPC.

(v) TWS products were consistent with GTWS having few months lag probably due to groundwater that is missing in MTWS.

In assessing the utility of the various indicators in capturing agricultural drought using national annual crop production:

(i) CHIRPS, GPCC, and VCI had consistent performance in explaining relatively high proportions of variabilities in national annual crop production in Kenya, Tanzania, and Uganda over the duration of the study.

(ii) The Chapter identified the following indicators as suitable for agricultural drought monitoring/characterization for the region during the study period; (a) for Kenya: CHIRPS, GPCC, VCI, MERRA-2, FLDAS, and MTWS; (b) for Uganda: CHIRPS, GPCC, VCI, FLDAS, ERA, MERRA-2, and MTWS; and (c) for Tanzania: CHIRPS, GPCC, VCI, FLDAS, GLDAS, and ERA.

(iii) The lack of consistency observed from the soil moisture products in drought characterization was also evident in the amount of variability explained in the national annual crop production by them across the region.

(iv) GTWS showed potential in explaining the variability in national annual crop production, albeit a longer period of dataset is required to evaluate its potential.

Further studies need to be undertaken to determine how well the model soil moisture products (CPC, ERA-Interim, MERRA-2, FLDAS, and GLDAS) and MTWS fit the region. Also, caution should be exercised in generalizing these results as production response to water at any different stages of crops growth can be modified by several factors. The next Chapter characterizes droughts over the

Upper GHA and explores the influence (impact) of topography on spatio-temporal drought patterns and percentage of areas under drought, while the uncertainties in the soil moisture products are explored in Chapter 5.

4 Gauge Density and Topographical Influence on the Consistency of Drought Characterization over UGHA

4.1 Introductory Remarks

A majority of the population of the Upper Greater Horn of Africa (UGHA; Sudan, South Sudan, Ethiopia, Djibouti, Eritrea, and Somalia) relies heavily on subsistence agriculture, an activity that has been frequently impacted by droughts leaving the population vulnerable to famine (*Gebrehiwot et al.*, 2011; *Ibrahim*, 1988; *Olsson*, 1993). Further consequences of drought in UGHA include; population displacement, rise in food prices, malnutrition and health related complications (*Edossa et al.*, 2010; *Taffesse et al.*, 2012; *Ibrahim*, 1988; *Viste et al.*, 2013). In addition, due to the fact that agriculture is largely rain-fed in Ethiopia and combination of rain-fed and irrigated in Sudan and Somalia (e.g., *Bewket*, 2009; *Elagib and Elhag*, 2011; *Longley et al.*, 2001), drought occurrence frequently lead to large-scale crop failures and losses of livestock. The magnitude and severity of drought impacts in the region emphasize the need for drought indicators that provide a clear, accurate, and consistent picture of drought extents.

Several studies have characterized and analysed droughts in the region from meteorological, agricultural to hydrological (see, e.g., *Awange et al.*, 2016b; *Lyon*, 2014; *Nicholson*, 2014a; *Gedif et al.*, 2014; *Dutra et al.*, 2013; *Viste et al.*, 2013; *Anderson et al.*, 2012; *Kurnik et al.*, 2011; *Gebrehiwot et al.*, 2011; *Edossa et al.*, 2010). These studies have analysed droughts based on rainfall (in-situ, satellite-derived, and a combination of both), soil moisture (model and re-analysis), normalised difference vegetation index (NDVI), and Gravity Recovery and Climate Experiment (GRACE) terrestrial water storage (TWS). As was discussed in Chapter 3 section 3.1, limitations associated with in-situ rainfall leads to use of satellite and/or satellite-gauge merged products, which

provide consistent, homogeneous, and wide coverage (e.g., *Agutu et al.*, 2017, and the references therein). However, these satellite precipitation and the other aforementioned products do have inherent errors and uncertainties, e.g., errors arising from retrieval algorithms, data acquisition and post-processing, estimation from cloud top reflectance, model limitations, and infrequent satellite overpasses (see, e.g., *Damberg and AghaKouchak*, 2014; *Hong et al.*, 2006; *AghaKouchak et al.*, 2009; *Rojas et al.*, 2011; *Naumann et al.*, 2014). Even though the above uncertainties can be reduced through standardization (e.g., SPI or percentiles) over time (*McNally et al.*, 2016), the impact of UGHA topography on these products and subsequent propagation of these impacts on drought characterization is largely unknown.

The complex topography-precipitation relationship in the UGHA region, especially over Ethiopia, has been reported in several studies (e.g., *Dinku et al.*, 2007, 2008; *Romilly and Gebremichael*, 2011). Topography has been found to be a major factor influencing rainfall distribution, and as such, has been a problem to both satellite-derived and gauge gridded (dependent on gauge density and topography) rainfall products. Satellite derived rainfall products employ either infrared or passive microwave techniques to determine the amount of rainfall (*Dinku et al.*, 2007, 2008), both of which are impacted by topography especially for convective rainfall as is found in this region. Even though various satellite derived rainfall product have been merged with in-situ gauge-derived components in order to reduce impact of topography and/or scale them, the varying density of in-situ gauge stations (spatial distribution and monthly availability) available has also lead to variation between various products.

The complex topography-precipitation relationship is expected to extend to soil moisture since it is an integration of rainfall anomalies over time (*Sheffield and Wood*, 2008). Furthermore, the quality of a model/reanalysis soil moisture is majorly determined by the precipitation product it is forced by and the individual model characteristics. The individual model characteristics range from different

operating thresholds for soil wetness, e.g., different mean values, variances, to hydrologically critical thresholds, e.g., points where evaporation occur at the potential rates or where surface run-off begins (*Dirmeyer et al.*, 2004). Despite the significant impacts of topography and gauge density on rainfall and soil moisture products, majority of drought studies in the region (including the aforementioned) using these products have not addressed the impacts of topography and gauge density on drought analysis results.

The failure of drought studies in the region to analyze and/or incorporate impacts of topography and gauge density on analyses results could lead to confusion and reduced confidence on drought analysis results due to inconsistencies between various indicators. The inconsistencies would arise from propagation of varying impacts of topography and gauge density on different products, during drought characterization. To this end, this Chapter considered the impact of topography and gauge density on agricultural drought analysis using rainfall, soil moisture, vegetation condition index, and TWS products. Specifically, in relation to topography and gauge density, the Chapter explored (i) spatio-temporal drought patterns, (ii) consistency of percentage of areas under drought, (iii) consistency of percentage of areas under different drought intensities, and (iv) effectiveness of various drought indicators in capturing agricultural drought over Ethiopia using national annual crop (wheat and maize) production. Drought spatial extents has not received much attention from researchers like other drought attributes e.g., intensity, frequency, and probability (*Lyon*, 2004). Therefore, this Chapter focusses on drought spatial extent due to its critical role in continuous monitoring for improving drought response plans and early warning systems, and quantifying drought impacts among other uses (see, e.g., *Tallaksen and van Lanen*, 2004; *Wilhite et al.*, 2014).

The remainder of the Chapter is organized as follows. In section 4.2, an overview of UGHA topography is given, with the data used in this Chapter

discussed in Chapter 2 and summarised in Table 3.1, followed by methodology in section 4.3. In section 4.4, the results and discussion are presented. Finally, the Chapter is concluded in section 4.5.

4.2 UGHA Topography

The UGHA countries of Ethiopia, Sudan (Sudan and South Sudan), and Somalia (Fig. 4.1a) have varied topographical characteristics:

Ethiopia with an area of approximately $1,127,127\ km^2$ has the most diverse topography ranging from highlands, the Rift Valley, to dry lowlands, with elevations ranging from –125 m at Danakil depression to 4620 m at RasDejen (*Enyew and Steeneveld*, 2014). Over 45% of the country is dominated by high plateaus (highlands) with a chain of mountain ranges that is divided by the Rift Valley system (*Enyew and Steeneveld*, 2014; *Rencher and Schaalje*, 2007). The highlands have wide varying topography over small topographical areas with the following common landscapes: hilltops, steep and moderate sloping lands, relatively flat plateaus, and valley bottoms both wide and narrow (*Rencher and Schaalje*, 2007). The Rift Valley highlights the complex topographical change within Ethiopia and splits the center of the country in a southeast–southwest direction creating highlands on both sides (*Dinku et al.*, 2007, 2008; *Romilly and Gebremichael*, 2011). The topography on the south-eastern side of the highlands descend and levels off towards the border with Somalia, while the most mountainous terrain is found to the northwest of the rift valley system. Topography plays a significant role in the climate of Ethiopia, creating diverse micro-climates ranging from hot deserts over the lowlands to cool highlands. Though the effect of topography on rainfall is evident, their relationship is not straightforward as some parts of north-western lowlands receive more rainfall than adjacent highlands (*Dinku et al.*, 2008).

The topography over Sudan (Sudan and South Sudan) can be broadly categorized as vastly flat and/or undulating plains interposed by several widely

separated ranges of hills and mountains (*Mutasim and Elgizouli*, n.d; *Zaroug*, 2000). High mountains do occur in the far south (South Sudan) and the country's northeast and western areas (*Voll and Voll*, 2016). The hills in the south are grouped in large masses such as the Nuba Mountains and the Ingessans hills; the Imatong and Dongotona mountains also in the south rise to over 3000 m (*Zaroug*, 2000).

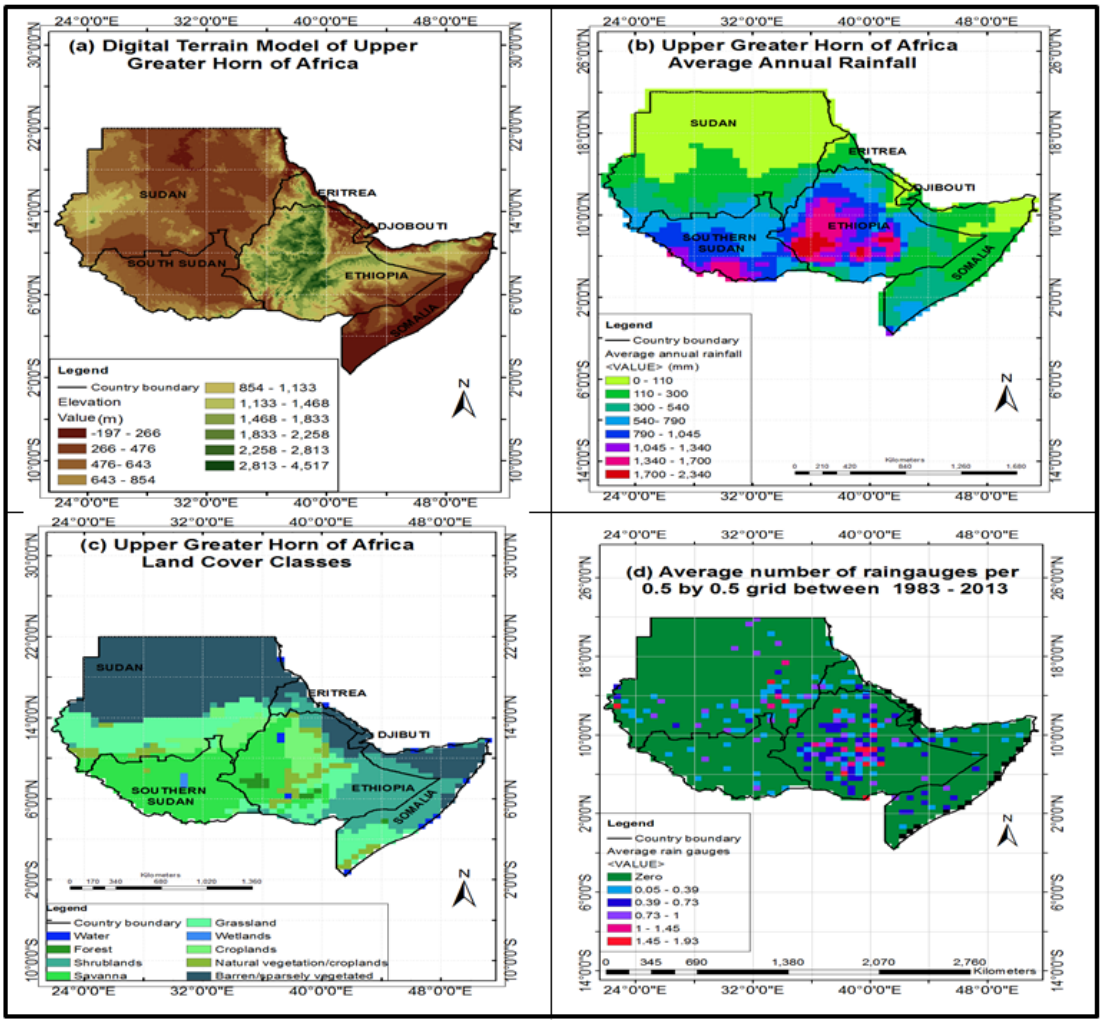

Figure 4.1: Upper Greater Horn of Africa (UGHA) region; (a) Elevation variation from Shuttle Radar Topographical Mission (SRTM, source:http://www.cgiar-csi.org/data/srtm-90m-digital-elevation-database), (b) Average annual rainfall, (c) Land cover types (modified from: http://e4ftl01.cr.usgs.gov/MOTA/MCD12Q1.051/), and (d) Average number of rain gauges per 0.5° by 0.5° grids between 1983 - 2013, used in deriving Global Precipitation Climatology Centre (GPCC) rainfall.

For Somalia, the country's topography can largely be divided into two major regions; the north characterized by incised highlands sloping towards the ocean and the South, where the low tablelands fall away to the wide coastal plains (*Lee*, 2007). It is relatively flat compared to Ethiopia and South Sudan.

For this chapter, the UGHA region is divided into three classes based on topographical characteristics; high changing/complex topography of Ethiopia, medium changing topography of South Sudan, and flat topography of Sudan and Somalia.

4.3 Methods

4.3.1 Spatio-temporal Drought Patterns

The spatio-temporal drought patterns were evaluated in a manner similar to Chapter 3 section 3.2.1, i.e., SI/SA was used to categorize drought then RPCA used to regionalize the drought patterns. See Chapters 2 and 3 for more details.

4.3.2 Consistency in Percentage of Areas Under Drought

The percentage of areas under drought and different drought intensities were evaluated for Ethiopia, Sudan, South Sudan, and Somalia through determination of the percentage of pixels under various drought categories following Table 3.2. Differences in percentage areas under drought and different drought intensities between various products during 1983 – 1984, 1987, 1999, 2009, and 2010 – 2011 drought events were then evaluated for each country.

In order to evaluate the impact of gauge density, the differences between CHIRPS and GPCC derived percentages of areas under drought were evaluated (Eqn 4.1). The in-situ stations in CHIRPS (global historical networks and global teleconnection networks) are all in GPCC plus other more stations (see, *Schneider et al.*, 2014; *Funk et al.*, 2015), though the number of stations available on monthly basis differs hence the variations in areas under drought. For the mean differences

due to topography, the following differences were evaluated

$$CHIRPS_{(\%\ area\ under\ drought)} - GPCC_{(\%\ area\ under\ drought)} = Influence\ of\ gauge\ density \tag{4.1}$$

$$CHIRP_{(\%\ area\ under\ drought)} - CHIRPS_{(\%\ area\ under\ drought)} - Influence\ of\ gauge\ density = Influence\ of\ topography \tag{4.2}$$

Equation 4.2 arises from the fact that CHIRP, a satellite only product, determines precipitation from cold cloud duration (CCD; *Funk et al.* (2015)) and the regional topography has been known to greatly hamper the satellite products (*Dinku et al.*, 2007, 2008; *Romilly and Gebremichael*, 2011). CHIRPS on the other had has gauge derived rainfall estimates in addition to CCD estimates; the inclusion of gauge derived estimates serve to correct/scale the CCD estimates to their proper values. This implies that the difference between CHIRPS and CHIRP contain the influence of both gauge and topography.

In addition, the following differences were evaluated for soil moisture products; FLDASN (FLDAS NOAH) – FLDASV (FLDAS VIC), FLDASN – MERRA2, MERRA2 – ERA, and FLDASN – GLDAS. The differences between the soil moisture products were taken to explore issues related to the role of forcing precipitation vis-a-vis model differences among other factors in contributing to the inconsistencies in areas under drought.

These differences were then analyzed using ANOVA and Bonferroni multiple comparison methods (see Chapter 2 for details and formulation). The analyses were used to explore how the following factors contribute to the differences in percentages of areas under drought across the region; (i) Gauge density (ii) physical characteristics (topography of each country)(iii) products (rainfall vis-a-vis moisture; different rainfall and soil moisture products), (iv) Forcing precipitation and model types.

4.3.3 Assessing the Effectiveness of Various Drought Indicators over Ethiopia

Similar to Chapter 3 section 3.2.2, the national annual crop (wheat and maize) production were regressed on drought indicators through PLSR and in each instance the model with lowest mean squared prediction error was adopted. It's the proportion of variability explained (R^2) by these models that's is reported. See Chapters 2 and 3 for more details.

4.4 Results and Discussion

4.4.1 Results

4.4.1.1 Spatio-temporal Drought Patterns

The regionalization of SI/SA through rotated principal component analysis resulted in 4 largely consistent and significant spatio-temporal patterns across majority of the drought indicators (Figs. 4.3 and 4.4). When assessed in relation to Figure 4.1, the spatial patterns of the rainfall products (CHIRPS, CHIRP, and GPCC) were largely similar across the regions and followed topography, while those of VCI and MTWS largely followed land cover classes, and GTWS patterns followed both rainfall and land cover classes (Fig. 4.2, compared to Fig. 4.1a-c). All the products showed consistent patterns over region 3, a region of relatively lowland flat topography with low-moderate rainfall (see, Fig. 4.1a and b). For the soil moisture products, the spatial patterns roughly resembled those of rainfall and/or land cover patterns except for CPC spatial patterns (Fig. 4.3, compared to Fig. 4.1b and c). Also, the region 4 spatial patterns were different across the soil moisture products (Fig. 4.4), with MERRA2's spatial pattern resembling that of MTWS in region 4 (Fig. 4.3). Similar to the patterns of the rainfall group (Fig. 4.3), there is consistency among the soil moisture products over region 3 (i.e., lowland region

of low to moderate rainfall) though not as close as in the rainfall group.

The proportion of variances of the SI/SA explained by these components is tabulated in Table 4.1. The majority of the rainfall products had the lowest variability in region 4 while the majority of the soil moisture products had the lowest variability in region 3. Region 4, from rainfall products, comprises mostly Ethiopian highlands; a region with lots of rainfall most of the year hence low variability in SPI while regions 3 comprises relatively dry regions with low soil moisture most of the year hence lowest variability in SSI. On the other hand, maximum variability as seen in Table 4.1 differed across products with no clear majority in any particular region. VCI had regions 1 and 3 explaining equal magnitudes of variability probably due to similar vegetation types in the vast areas of the two locations (Fig. 4.2 vis-a-vis Fig. 4.1c). On the basis of the total variabilities explained, CHIRPS and GPCC were almost equal but lower than CHIRP while the soil moisture products fell into 3 categories i.e., FLDASV (43%); GLDAS, ERA-Interim, and FLDASN (50 – 55%); and CPC and MERRA2 (66 – 67%), see Table 4.1.

Table 4.1: Variances explained in each region by each product. Regions are as shown in Figures 4.2 and 4.3.

Region	CHIRPS	CHIRP	GPCC	VCI	MERRA TWS	GRACE TWS	ERA-Interim	GLDAS	CPC	MERRA2	FLDASN	FLDASV
Region 1	10.03	15.78	13.68	8.08	17.50	14.28	15.84	9.95	30.47	18.01	17.53	13.85
Region 2	10.16	8.86	8.41	12.07	20.45	24.35	12.72	15.97	17.52	19.70	10.66	11.27
Region 3	11.38	11.10	11.00	8.05	12.66	23.34	10.91	10.39	8.56	13.20	12.06	10.81
Region 4	8.73	11.81	8.21	10.74	14.52	21.32	16.23	14.44	10.71	15.22	11.93	7.09
Total	40.03	47.55	41.3	38.94	65.13	83.29	55.70	50.75	67.26	66.13	52.18	43.02

FLDASN - FLDAS NOAH, and FLDASV - FLDAS VIC.

The temporal evolutions of the spatial patterns in Figures 4.3 and 4.4, showed region-wide agricultural drought events in the years 1983/1985, 1986/1987, 1990/1991, 2000, 2005/2006, 2009/2010, and 2010/2011 (see Figs. 4.4 and 4.5). These and other drought episodes captured in these figures are consistent with drought episodes in the region as reported by previous studies (e.g., *Viste et al.*, 2013; *Gebrehiwot et al.*, 2011; *Elagib and Elhag*, 2011;

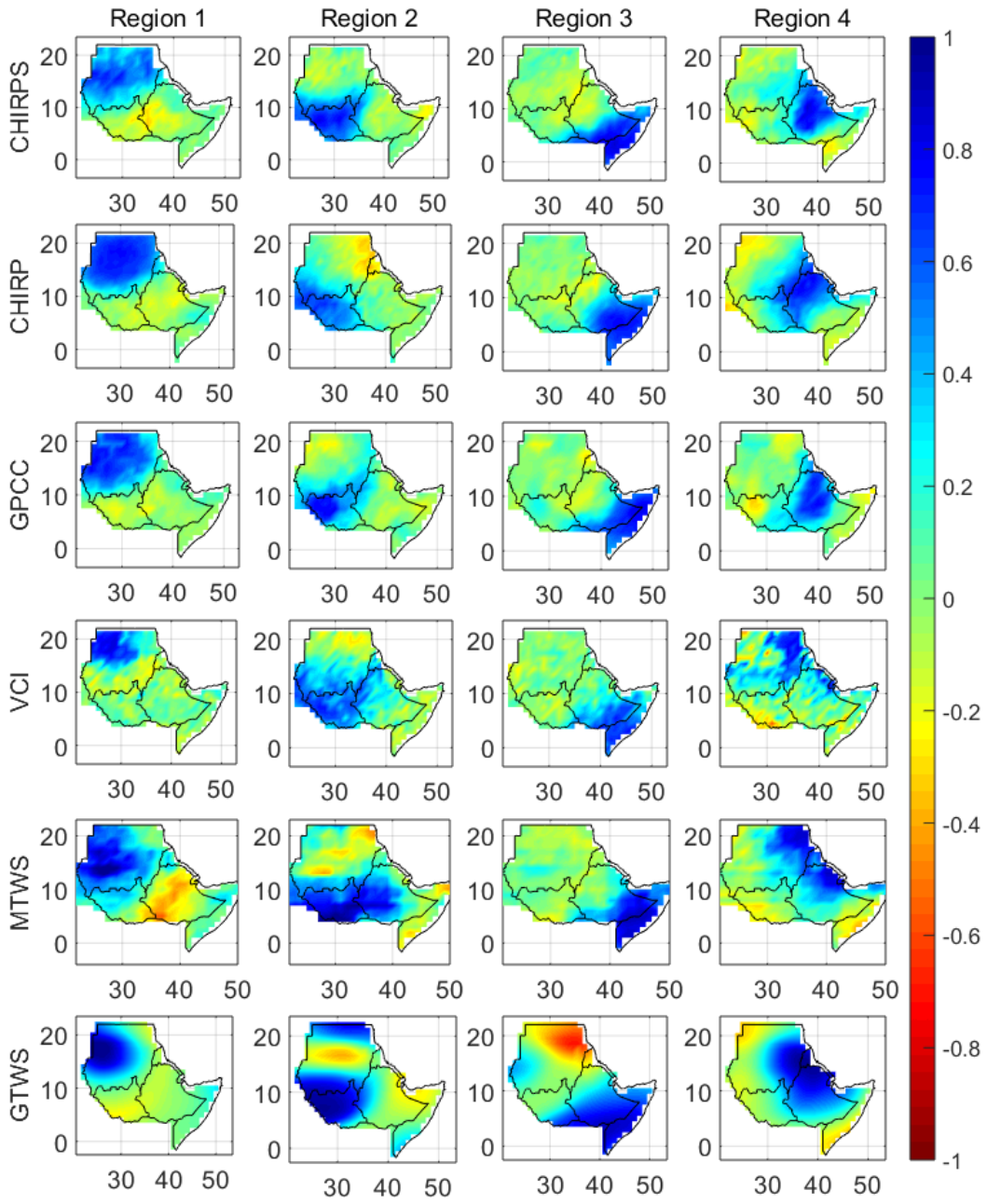

Figure 4.2: Rotated principal component spatial patterns of standardized indices/anomalies (SI/SA). Rows denote products while columns denote region. The spatial patterns have been scaled to ± 1, thus the temporal evolutions shown in Figure 4.4 indicate the actual magnitude for the regions where the spatial patterns have values close to ± 1. The spatial patterns are interpreted in conjunction with temporal evolutions in Figure 4.4 and represent drought spatial patterns any time the temporal evolutions falls below -0.84, as in Table 3.2.

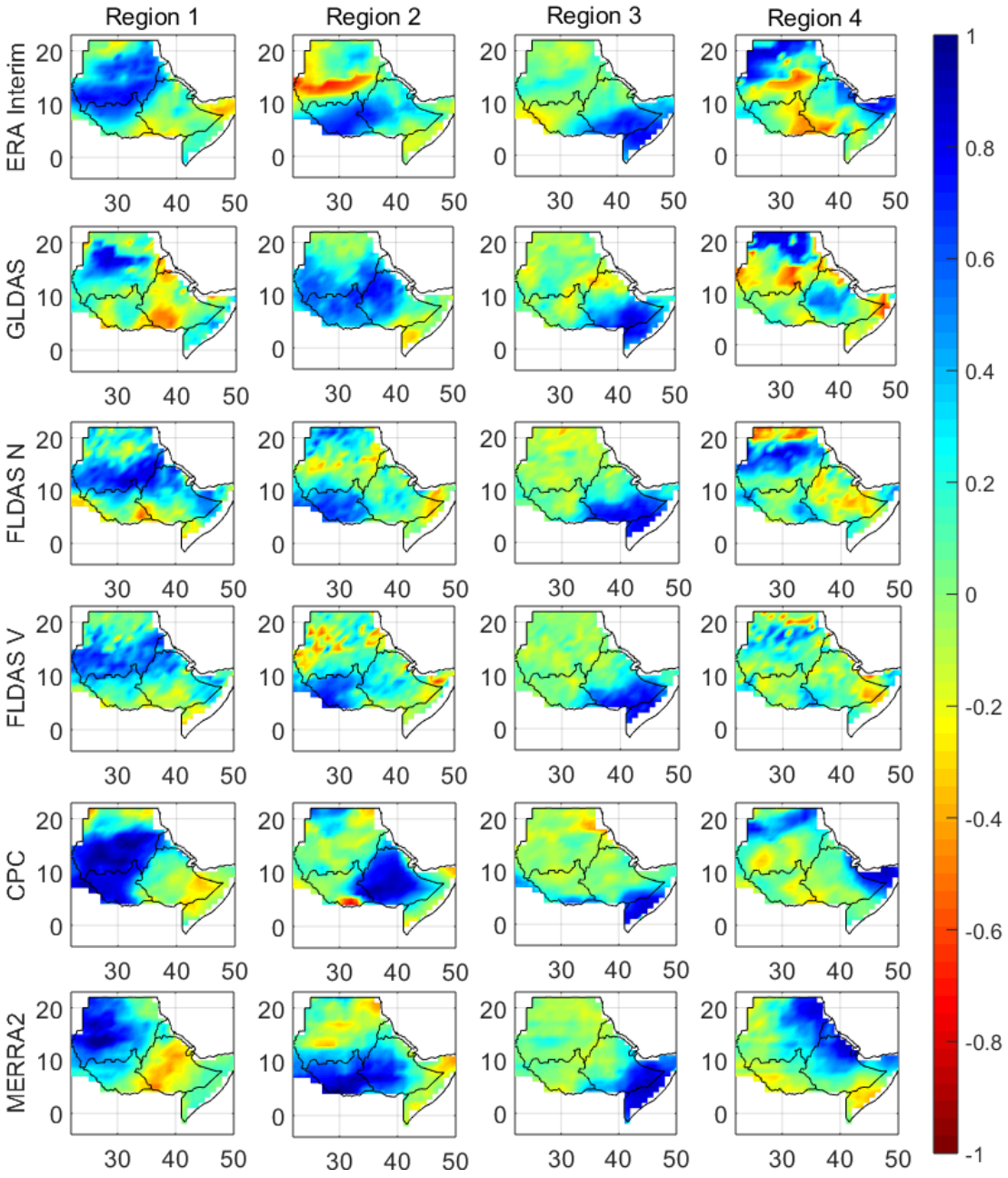

Figure 4.3: Rotated principal component spatial patterns of standardized soil moisture indices (SSI). Rows denote products while columns denote region. The spatial patterns have been scaled to ± 1, thus the temporal evolutions shown in Figure 4.5 indicate the actual magnitude for the regions where the spatial patterns have values close to ± 1. The spatial patterns are interpreted in conjunction with temporal evolutions in Figure 4.5 and represent drought spatial patterns any time the temporal evolutions falls below -0.84, as in Table 3.2.

Nicholson, 2014a; *Williams and Funk*, 2011; *Masih et al.*, 2014).

Of the rainfall products, CHIRPS and GPCC were similar across all the regions with little differences evident in regions 1 and 2 (Fig. 4.4a and b) though they were significantly different from CHIRP across the region (Fig. 4.4). This could be attributed to the fact that both CHIRPS and GPCC contain in-situ rainfall (rain gauge products) while CHIRP is only satellite derived hence differences depends on how well these products estimate rainfall across the region, which is a function of topographical changes (see, e.g., *Dinku et al.*, 2007, 2008; *Romilly and Gebremichael*, 2011). Also, FLDASN and FLDASV were largely close across the whole region (Fig. 4.5).

Over the duration considered, all the indicators were found to be consistent in region 3 more than the rest of the UGHA regions (Figs. 4.4 and 4.5), a pattern that was also noticed in the spatial maps (Figs. 4.2 and 4.3). This could be attributed to the facts that this region, a relatively flat region with moderate rainfall (Fig. 4.1a and b) does not have much topographical influence on the products as compared to high rainfall/rapid terrain changing regions like region 4 (Fig. 4.2) and region 2 (Fig. 4.3). The satellite and model-based products seems to work consistently well under flat topography and lower rainfall ranges while GPCC interpolation also seems to be good. The soil moisture products were most different in region 2 (Fig. 4.3 and Fig. 4.5b), which could be attributed to the failure of the models to capture the complex topography-rainfall relationship in the region. Also, the large difference between the temporal evolutions across the soil moisture-based indicators compared to the rainfall indicators could be a pointer to greater inconsistency in the drought information as represented by the soil moisture based indicators. Region 4 of SSI (Fig. 4.5) represent the region with the largest difference in temporal evolution possibly due to different spatial patterns as observed from the spatial SSI patterns (Fig. 4.3).

In general, some isolated performances are also observed from MTWS and GLDAS. MTWS appears to have a shift with pre-1999 being predominantly wet

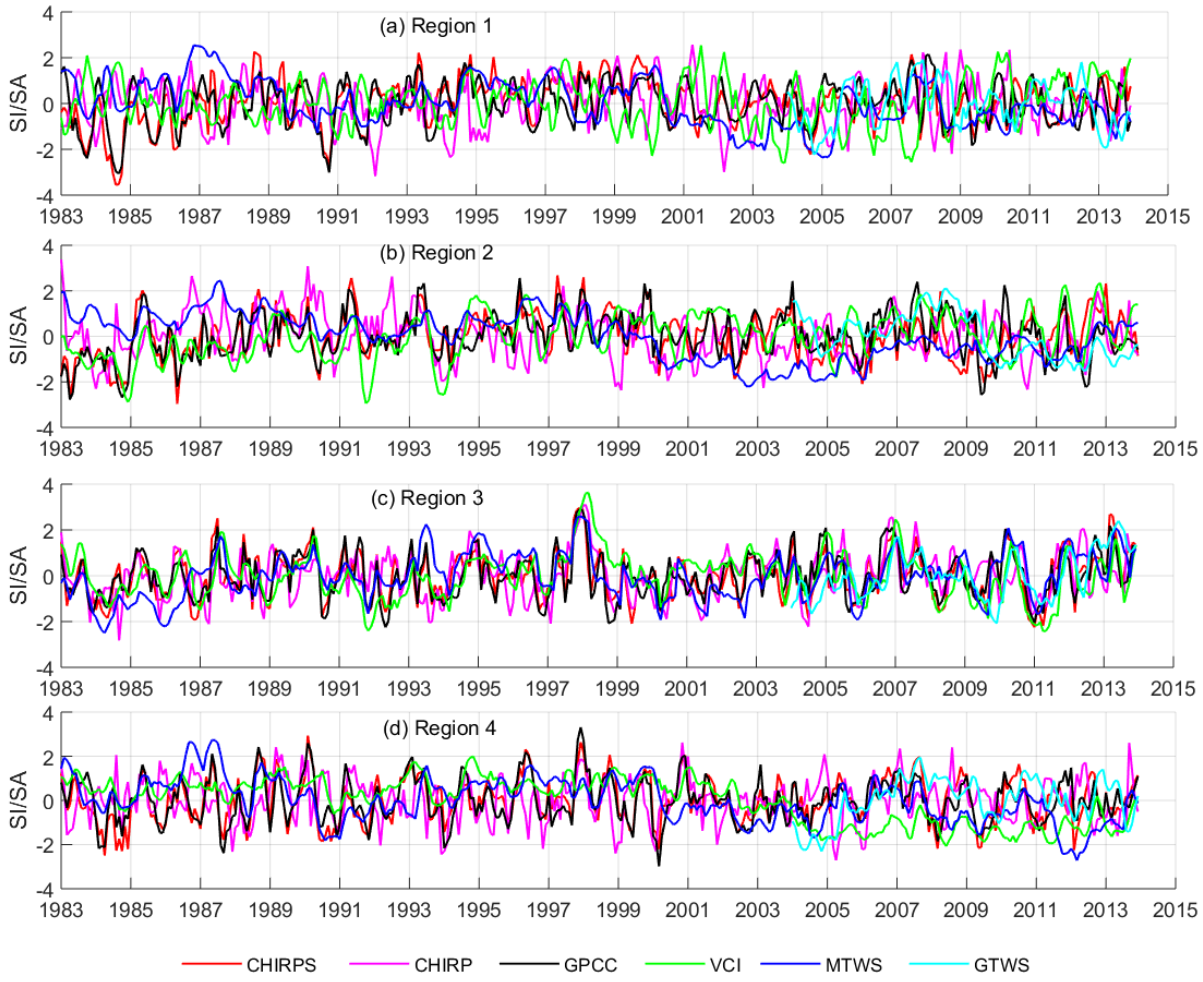

Figure 4.4: Temporal evolution of SA/SI spatial patterns in Fig. 4.2. Drought conditions occur when SI/SA falls below -0.84 continuously for at least three months, as in Table 3.2.

and dry afterward (Fig. 4.4a and b), while GLDAS appears to have issues in regions 2 and 4 though consistent with other products in region 3 (Fig. 4.5). Also, CPC and MERRA2 were closer over the region. Further, there was a lag in drought events from rainfall to VCI/soil moisture followed by MTWS and eventually GTWS.

Finally, the relationships between the temporal patterns of the SI/SA (Figs. 4.4 and 4.5) analyzed through Pearson correlation are shown in Table 4.2 and Fig. 4.6. From the correlation coefficients, there is high consistency between the following products across the region; CHIRPS and GPCC, FLDASN and

FLDASV, MTWS and MERRA2, and MTWS and CPC. In addition, the majority of the products have on average highest correlations in region 3 signifying consistent performance. These are consistent with the results outlined above (see Figs. 4.2, 4.3, 4.4, and 4.5). For the rainfall group, while CHIRPS and GPCC have the lowest correlation in region 2, CHIRPS and CHIRP, and GPCC and CHIRP have the lowest correlation in region 1. However, the soil moisture group do not have any particular region in which the majority of products had lowest correlations as values varied with product pairs and region.

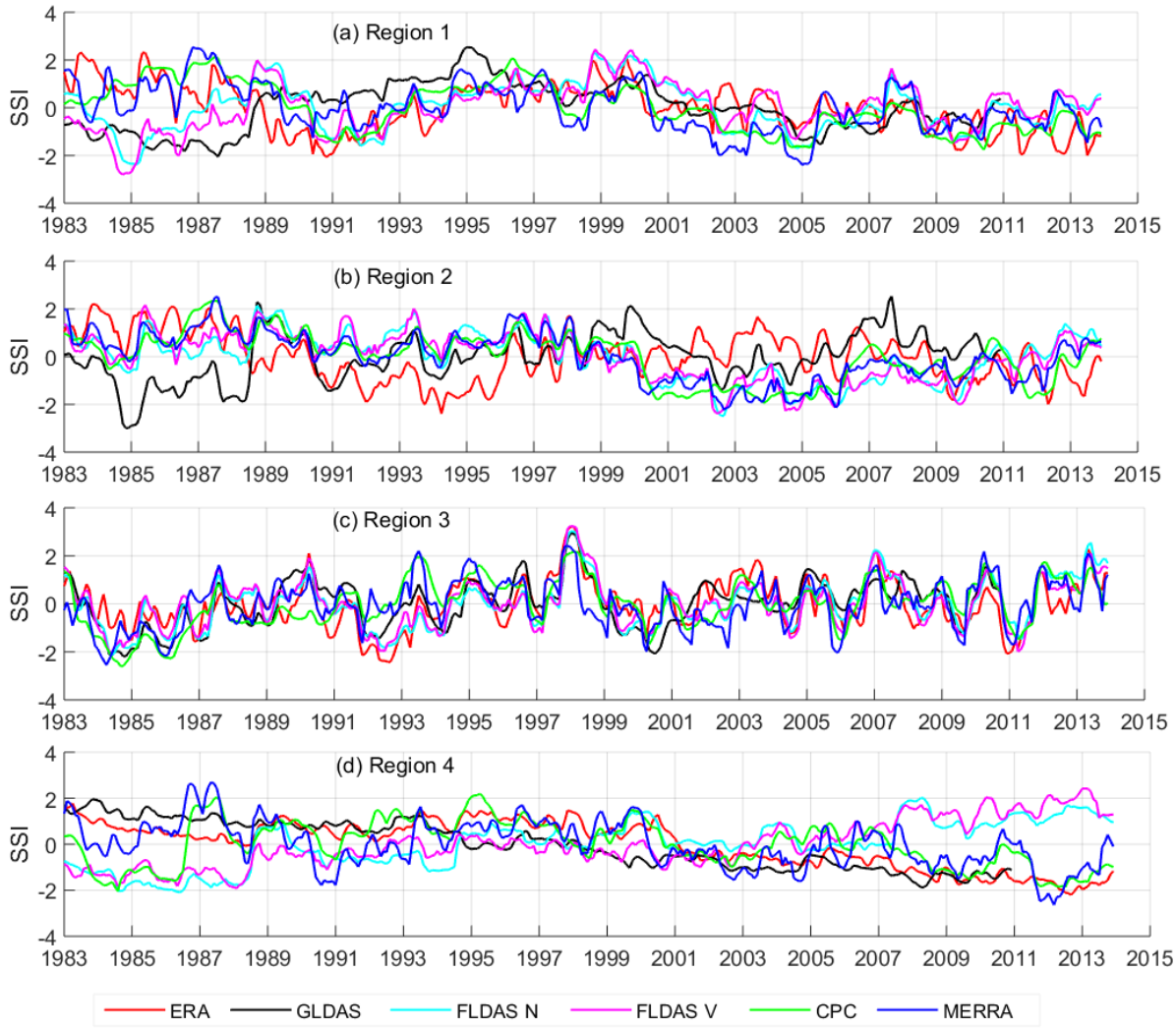

Figure 4.5: Temporal evolution of SSI spatial patterns in Fig. 4.3. Drought conditions occur when SSI falls below -0.84 continuously for at least three months, as in Table 3.2.

Table 4.2: Correlation between temporal drought patterns. Regions are as in Figures 4.2 and 4.3. Non-significant correlations are in italics ($p < 0.05$).

	CHIRPS	CHIRP	GPCC	VCI	MTWS	GTWS	ERA	GLDAS	FLDASN	FLDASV	CPC	MERRA2
CHIRPS	1	***0.0436***	**0.7825**	0.1466	0.2445	*0.0258*	0.1571	0.3544	0.4329	0.5559	*0.0906*	0.2388
CHIRP	***0.0917***	1	***0.0685***	*0.0969*	*0.0883*	*0.0246*	0.1032	*0.0195*	0.1230	*0.0978*	*0.0997*	*0.0886*
GPCC	**0.7392**	***0.0826***	1	0.1544	0.2032	*0.0121*	0.1061	0.1696	0.2644	0.4006	*0.0355*	0.2045
VCI	0.3434	0.1080	0.4003	1	0.1234	0.2081	*0.0890*	*0.0683*	*0.0287*	*0.0998*	*0.0217*	0.1168
MTWS	0.2202	0.2440	*0.0663*	*0.0711*	1	**0.5698**	0.4410	*0.0735*	0.4240	0.2454	**0.7836**	**0.9980**
GTWS	0.1591	*0.0487*	0.3580	0.3295	***0.0862***	1	0.2535	0.2791	0.3900	0.3637	0.4700	0.5620
ERA	*0.0072*	*0.0154*	*0.0934*	*0.0505*	0.1315	0.5353	1	**0.1280**	**0.2648**	**0.1777**	**0.6097**	**0.4405**
GLDAS	0.2693	*0.0737*	0.3905	0.5556	*0.0275*	0.3166	**0.1440**	1	**0.5061**	**0.5253**	***0.0143***	***0.0555***
FLDASN	0.4016	0.2338	0.1654	*0.0915*	0.8171	0.3292	***0.0431***	**0.1254**	1	**0.8847**	**0.4182**	**0.4011**
FLDASV	0.4102	0.1981	0.1865	*0.0498*	0.8848	0.3092	***0.0207***	***0.0268***	**0.9276**	1	**0.1794**	**0.2232**
CPC	0.1536	0.2841	*0.0673*	*0.0761*	**0.8949**	*0.0352*	**0.1083**	***0.0340***	**0.7143**	**0.7545**	1	**0.7797**
MERRA2	0.2470	0.2601	*0.0976*	*0.0633*	**0.9954**	*0.0762*	**0.1478**	***0.0297***	**0.8034**	**0.8805**	**0.8825**	1
CHIRPS	1	**0.5532**	**0.8554**	0.5416	0.5673	0.4293	0.5355	0.4223	0.5230	0.5905	0.3812	0.5830
CHIRP	**0.1027**	1	**0.4797**	0.3631	0.3633	0.1816	0.4134	0.3463	0.4305	0.4512	0.3261	0.3689
GPCC	**0.8512**	**0.1567**	1	0.4937	0.5424	0.2789	0.4775	0.3868	0.4466	0.5029	0.3357	0.5481
VCI	0.1347	*0.0529*	0.1723	1	0.4833	0.5429	0.7822	0.6051	0.7029	0.7948	0.4646	0.4751
MTWS	0.3383	*0.0420*	0.2307	0.5113	1	**0.5507**	0.5262	0.6055	0.6158	0.6377	**0.7726**	**0.9931**
GTWS	*0.1644*	*0.0535*	*0.1104*	0.2154	**0.2512**	1	0.6778	0.5798	0.8418	0.7897	0.5803	0.4997
ERA	*0.0548*	*0.0543*	0.1022	0.7942	0.5521	*0.1760*	1	**0.5936**	**0.7709**	**0.8030**	**0.4953**	**0.5082**
GLDAS	*0.0309*	*0.0550*	*0.0916*	0.6188	0.4139	0.4649	**0.7365**	1	**0.8044**	**0.7690**	**0.6605**	**0.5770**
FLDASN	0.1204	*0.0073*	*0.0232*	0.3540	0.3142	0.4085	**0.6083**	**0.7613**	1	**0.9655**	**0.6223**	**0.5665**
FLDASV	0.1434	*0.0200*	*0.0872*	0.6056	0.3885	0.5152	**0.7098**	**0.7280**	**0.8199**	1	**0.6147**	**0.6127**
CPC	0.2282	*0.0012*	0.1171	0.4497	**0.5732**	0.1865	**0.5591**	**0.1256**	***0.0607***	**0.2177**	1	**0.7501**
MERRA2	0.3387	*0.0361*	0.2228	0.5165	**0.9970**	0.2556	**0.5641**	**0.4160**	**0.2993**	**0.3830**	**0.5964**	1

Note: Red (region 1), blue (region 2), green (region 3), brown (region 4).

4.4.1.2 Consistency of Areas Under Drought

In order to analyze the consistency of areas under drought from rainfall and soil moisture products, this Chapter considered the mean differences in areas under drought between various products during 1983 - 1984, 1987, 1999, 2009, and 2010-2011 drought events. These drought events were considered as they had significant impacts on the region (see, e.g., *Viste et al.*, 2013; *Gebrehiwot et al.*, 2011; *Elagib and Elhag*, 2011; *Masih et al.*, 2014). In addition, spatial correlations of the respective Standardized Indices (SPIs and SSIs) during these drought events were used to support the analysis of the mean differences.

Overall, the rainfall products had higher mean differences in the percentage of areas under drought than soil moisture products (Figs. 4.7 and 4.9), i.e., 15.7% vis-a-vis 12.6% at $F(1,2338) = 28.5176$, with $p < 0.0001$. However, the reverse would be true if only gauge based precipitation products (CHIRPS and GPCC) were considered (overall mean percentage difference would be 9.7% as opposed to

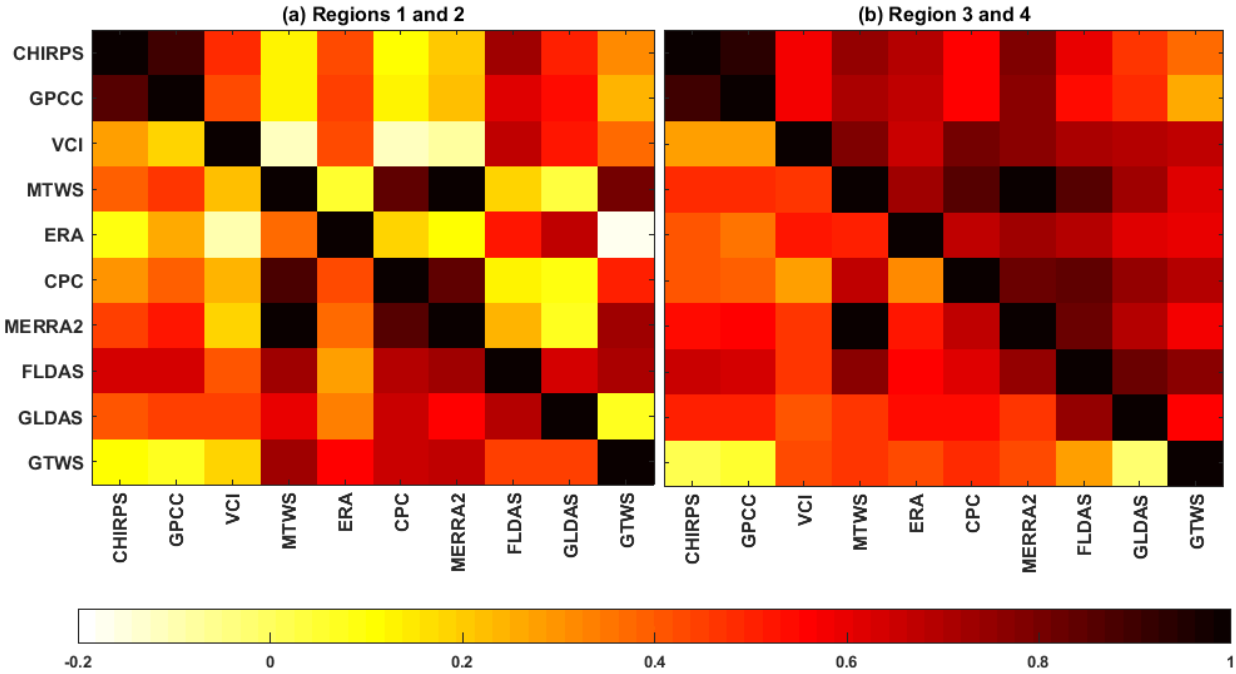

Figure 4.6: Correlation shaded plot between drought indices by region; (a) upper triangle - region 1, lower triangle - region 2; and (b) upper triangle - region 3, and lower triangle - region 4. Region 3 has the strongest relationships.Also, note the high correlation between the following products across the region; CHIRPS and GPCC, FLDASN and FLDASV, MTWS and MERRA2, and MTWS and CPC.

15. 9%). The larger mean difference is attributed to the inclusion of CHIRP, a satellite only product that seems to have problems capturing the regional precipitation well.

From the rainfall products, the mean differences in percentage of areas under drought due to the gauge density (spatial distribution and temporal availability) was lowest in Ethiopia, followed by South Sudan and Sudan, and highest in Somalia (Fig. 4.7). This was inversely related to the gauge density of both GPCC and CHIRPS (see, Figs. 4.1d and 8.2) and was further supported by relatively high correlation coefficients over Ethiopia vis-à-vis lower coefficients over Somalia (Fig. 4.8 a). Finally, the mean differences in percentage of areas under drought due to topographical variations were lowest over Somalia (an area of low topographical variation), and highest over South Sudan with Ethiopia and Sudan being in between Fig. 4.7. This was supported by relatively higher

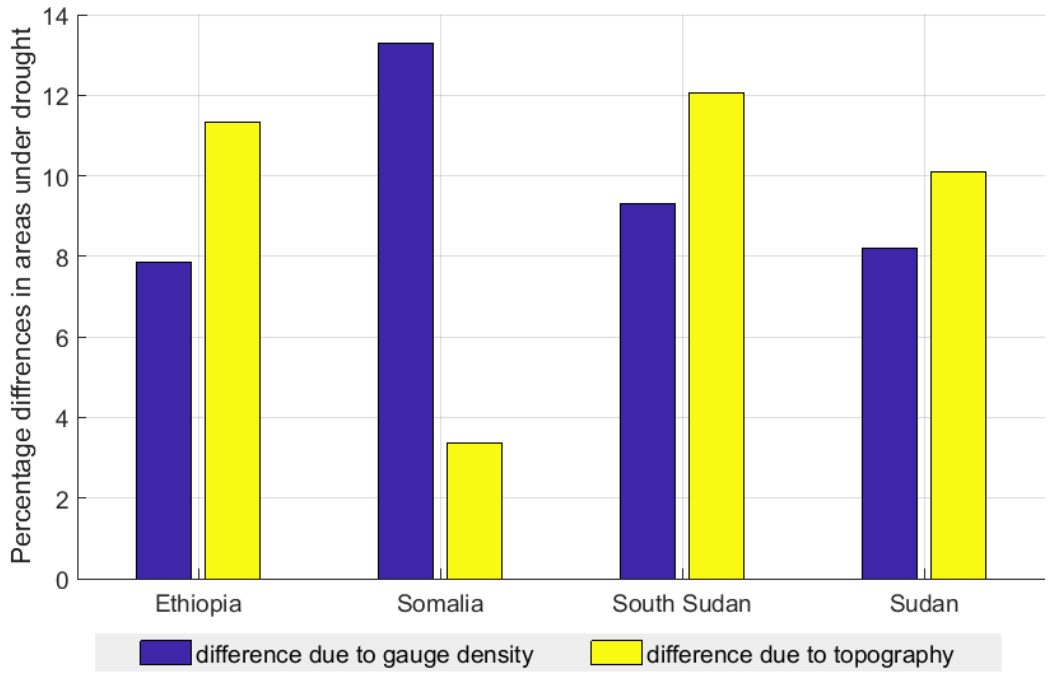

Figure 4.7: Mean percentage differences in areas under drought due to gauge density and topography over UGHA.

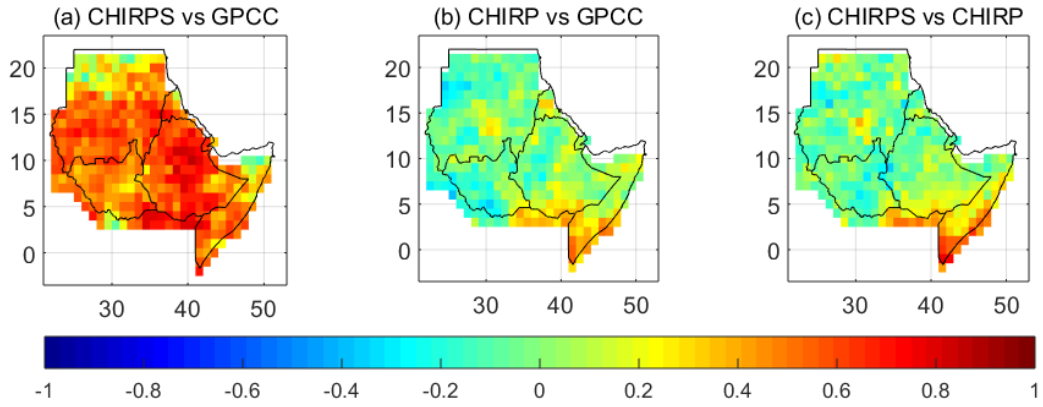

Figure 4.8: SPI spatial correlations for the 1983 - 1984, 1987, 1999, 2009, and 2010-2011 drought events. The correlations are a function of gauge density (a), and topography (b and c).

correlation coefficients over Somalia compared to the rest of the regions (Fig. 4.8, b and c)

For the soil moisture products, the mean differences in percentage of areas under drought between various products depended on the products under consideration ($F(3, 1292) = 61.92$, $p < 0.0001$) and the specific region (country)

being considered ($F(3, 1292) = 28$, $p < 0.0001$; Fig. 4.9). Different models with similar forcing precipitation translated into lower mean percentage difference in areas under drought across the entire region than similar models with different forcing precipitations (FLDASN-FLDASV vis-a-vis FLDASN-GLDAS; Fig. 4.9). This was also reflected by the higher correlation between FLDASN and FLDASV SSIs' compared to FLDASN and GLDAS SSIs' during the considered drought events (Fig. 4.10a and d). The mean difference in the percentage of areas under drought between reanalysis products was lower than that between a reanalysis and a normal model product except over Somalia (MERRA-ERA vis-a-vis FLDASN-MERRA) as also shown by higher correlations between MERRA and ERA SSI than between FLDASN and MERRA (Fig. 4.9 and Fig. 4.10b and c) during the considered drought events. The relatively higher difference in mean areas under drought between MERRA and ERA over

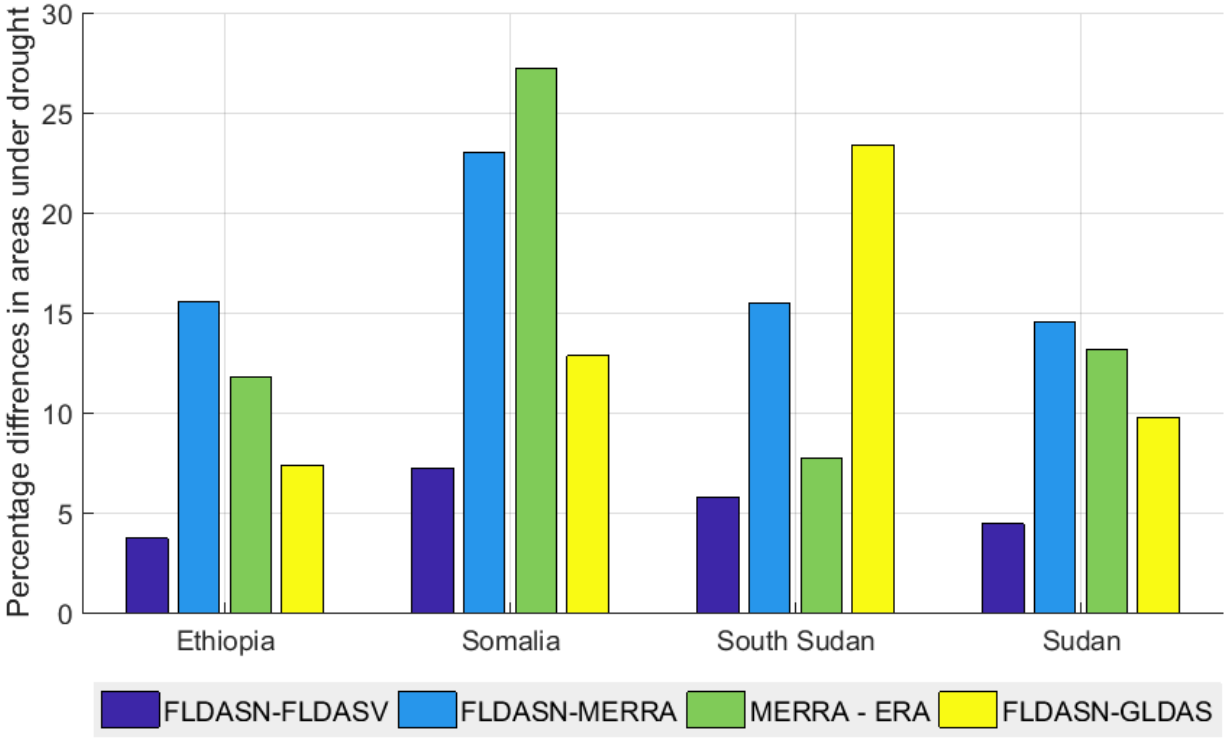

Figure 4.9: Mean percentage differences in areas under drought from soil moisture products. Lower mean percentage differences are observed from models forced by same precipitation products (FLDASN and FLDASV) .

Somalia, also reflected by low correlations (Figs. 4.9 and 4.10c) could be attributed to the tendency of ERA to overestimate soil moisture, especially over dry areas as was shown by *Albergel et al.* (2012). A combination of different models with different forcing precipitation products (FLDASN-MERRA and MERRA-ERA) had the highest mean difference in the percentage of areas under drought while different models forced with similar precipitation (FLDASN-FLDASV) had the lowest mean difference in the percentage of areas under drought across the region. This was supported by higher correlation between FLDASN and FLDSV SSIs' in comparison to the relatively lower correlations between FLDASN and MERRA2, and MERRA2 and ERA SSIs' (Fig. 4.10a, b, and c). Finally, concerning the regional variability of the mean percentage differences in areas under drought, Somalia had the highest mean differences while Ethiopia had the least mean differences on the majority of product differences considered (Fig. 4.9).

4.4.1.3 Consistency in Drought Intensity Information

In addition to the areas under drought, it is important to assess the extent to which each area is affected hence this section analyses the differences in drought intensity between various products used in section 4.4.1.2 for the same drought episodes i.e., 1983 - 1984, 1987, 1999, 2009, and 2010-2011 drought events.

On average, the mean difference in areas under different drought intensities from rainfall products was higher than those from soil moisture products when the whole region was considered in entirety (6.164% vis-a-vis 5.2021% at $F(1, 7018) = 33.91, p < 0.0001$) (Figs. 4.11 and 4.12). The mean differences in percentage of areas under different drought intensities (moderate, severe, and extreme) from rainfall products varied with product pairs under consideration ($F(2, 3088) = 41.13$, $p < 0.0001$), the country ($F(3, 3088) = 4.79$, $p < 0.0001$), and the drought intensity category ($F(2, 3088) = 91.6$, $p < 0.0001$) being considered (Fig. 4.11).

For the rainfall products, similar to the case of mean difference in areas under

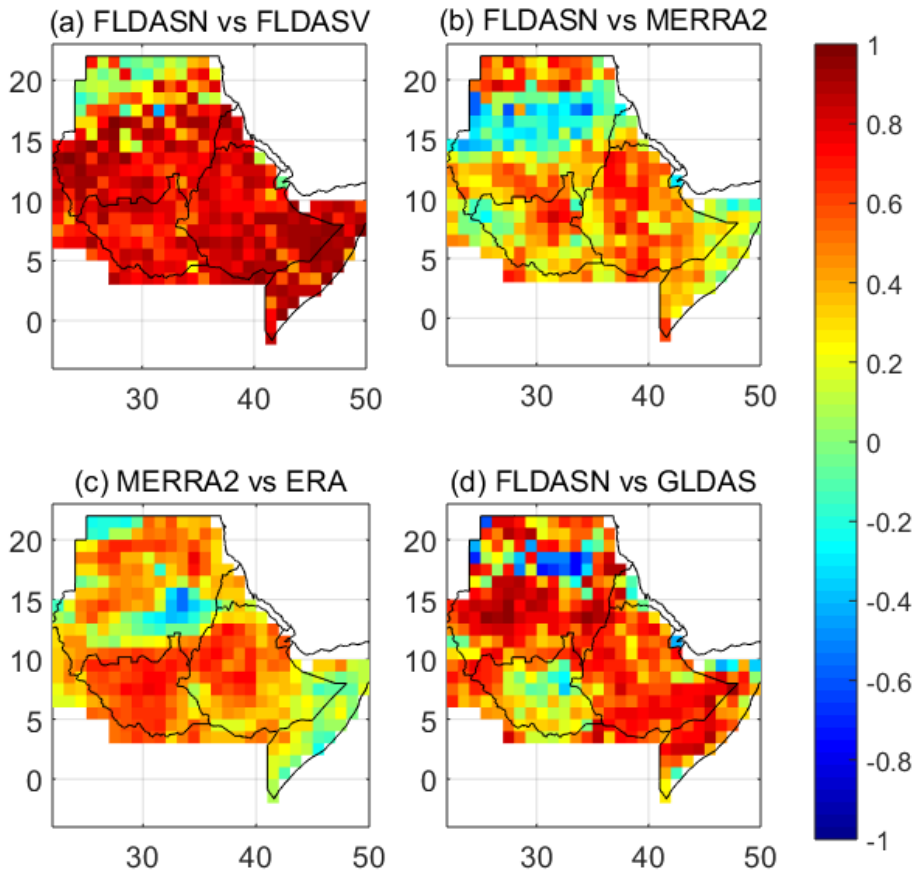

Figure 4.10: SSI spatial correlations for 1983 - 1984, 1987, 1999, 2009, and 2010-2011 drought events. FLDASN - FLDAS NOAH, and FLDASV - FLDAS VIC.

drought (see, section 4.4.1.2), the mean difference in percentage of areas under various intensities due to gauge density was lowest in Ethiopia and highest in Somalia, with Sudan and South Sudan being in between (Fig. 4.11). In addition, the mean difference in percentage of areas under various drought intensities due to topography was lowest over Somalia and largely the same over the remaining countries (Fig. 4.11).

Similar to the case of the precipitation products, the mean differences in percentage of areas under different drought intensities from soil moisture products were dependent on products pairs ($F(3, 3915) = 77.16$, $p < 0.0001$), the country ($F(3, 3915) = 49.5$, $p < 0.0001$), and the intensity category

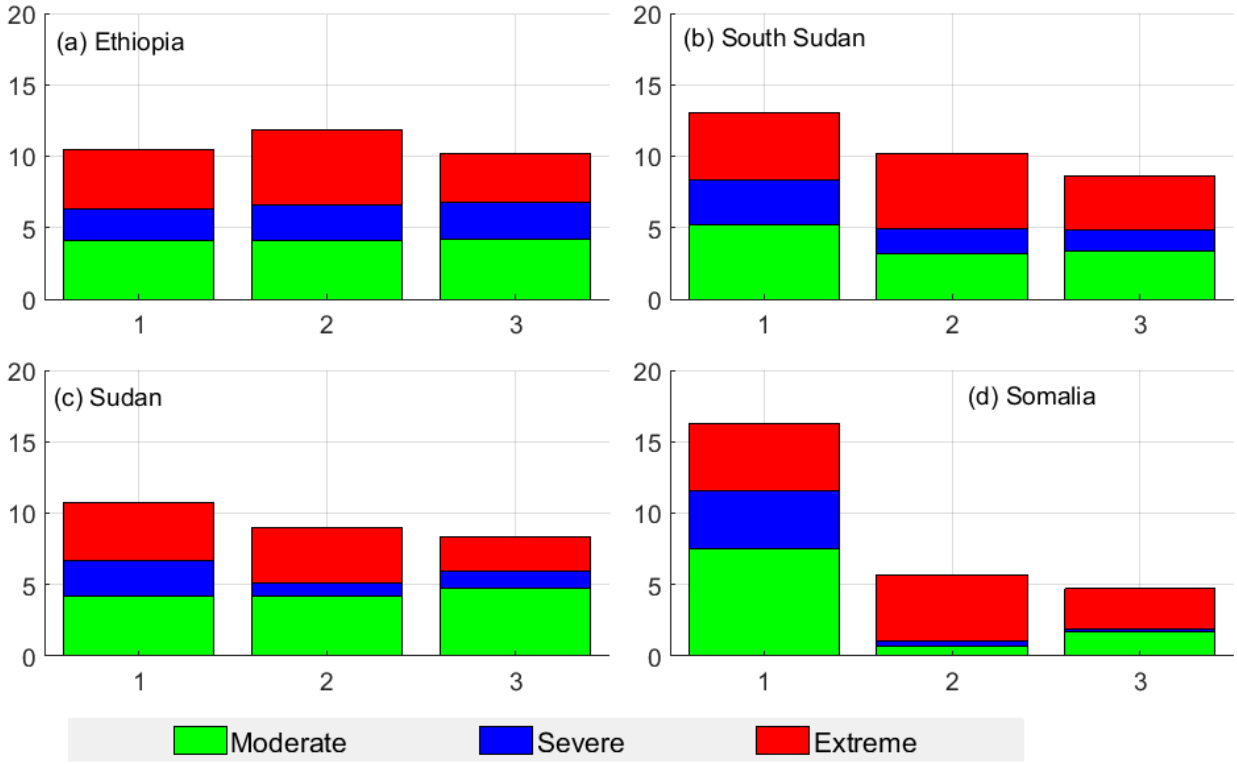

Figure 4.11: Mean differences in percentage of areas under different drought intensities during 1983 - 1984, 1987, 1999, 2009, and 2010-2011 drought events. The differences are due to gauge density (1) and topography (2 and 3).

($F(2, 3915) = 30.06$, $p < 0.0001$) under consideration (Fig. 4.12). The mean differences in the percentage of areas under different drought intensities were lower for FLDASN-FLDASV compared to the rest of the soil moisture pairs across the regions. The mean differences in the percentage of areas under various drought intensities were lowest in Ethiopia and highest over Somalia (Fig. 4.12 a and d). Like in the case of rainfall products, the mean differences in areas under different drought intensities were lower under severe droughts compared to moderate and extreme, across the countries for all the soil moisture product differences except for FLDASN – GLDAS. As with the case of differences in the percentage of areas under drought above, similar precipitation forcing with different models contributed to lower differences in intensity information compared to similar models with different forcing precipitations (FLDASN-FLDASV vis-a-vis FLDASN-GLDAS; Fig. 4.12).

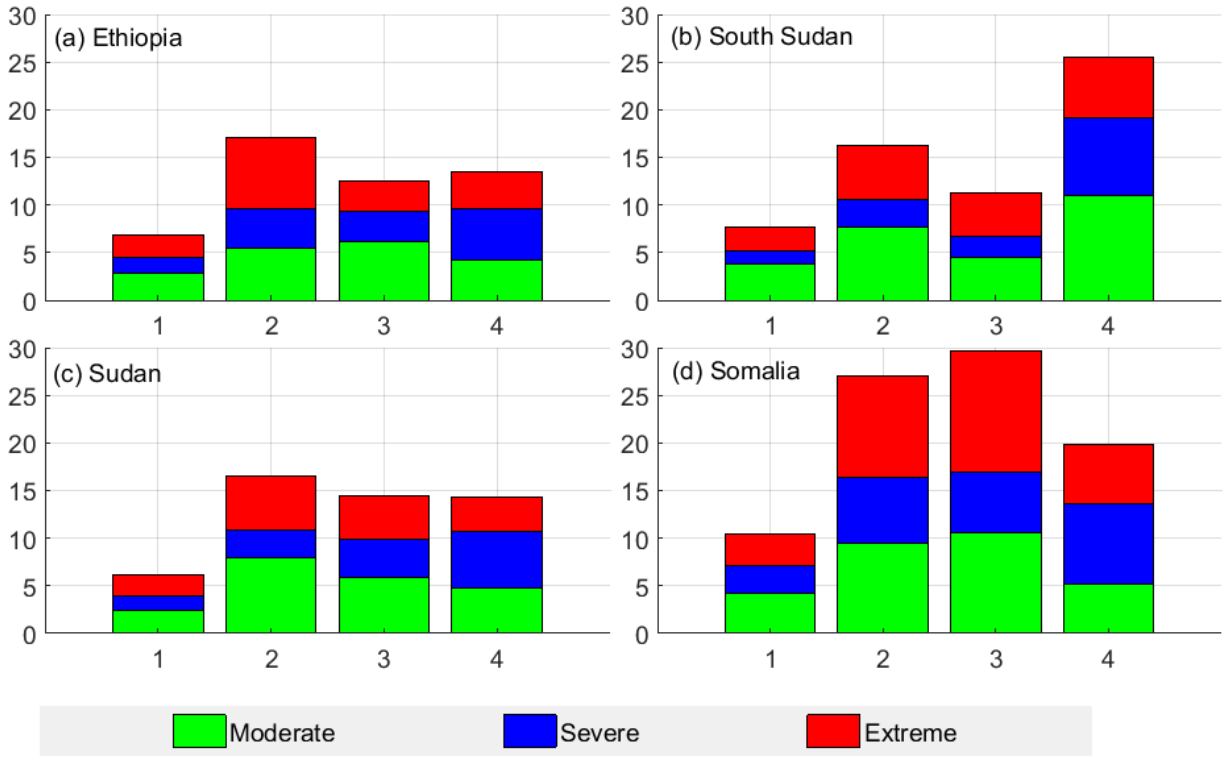

Figure 4.12: Mean differences in percentage of areas under different drought intensities during 1983 - 1984, 1987, 1999, 2009, and 2010-2011 drought events. (1 = FLDASN - FLDASV, 2 = FLDASN - MERRA2, 3 = MERRA - ERA, and 4 = FLDASN - GLDAS. FLDASN - FLDAS NOAH, and FLDASV - FLDAS VIC).

4.4.1.4 Evaluating the Effectiveness of Drought Indicators in Capturing Agricultural Drought

Whereas Chapter 3 (see, also *Agutu et al.*, 2017) evaluated the effectiveness of drought indicators in capturing agricultural drought over East Africa, here, only over Ethiopia is evaluated as Sudan, South Sudan, and Somali carry out both rain-fed and irrigated agriculture (*Elagib and Elhag*, 2011; *Larsson*, 1996) and therefore their annual crop production does not tally with natural water changes in the environment as represented by the indicators.

Both SI (computed using approximately 30 years length of data) and SA (computed using approximately 10 years length of data) were regressed with national annual crop (maize and wheat) production and the model with lowest mean prediction error had its proportion of variability explained (R^2) reported

(Fig. 4.13). As was done in Chapter 3, SA was necessitated by the need to compare how GTWS performs in relation to other indicators.

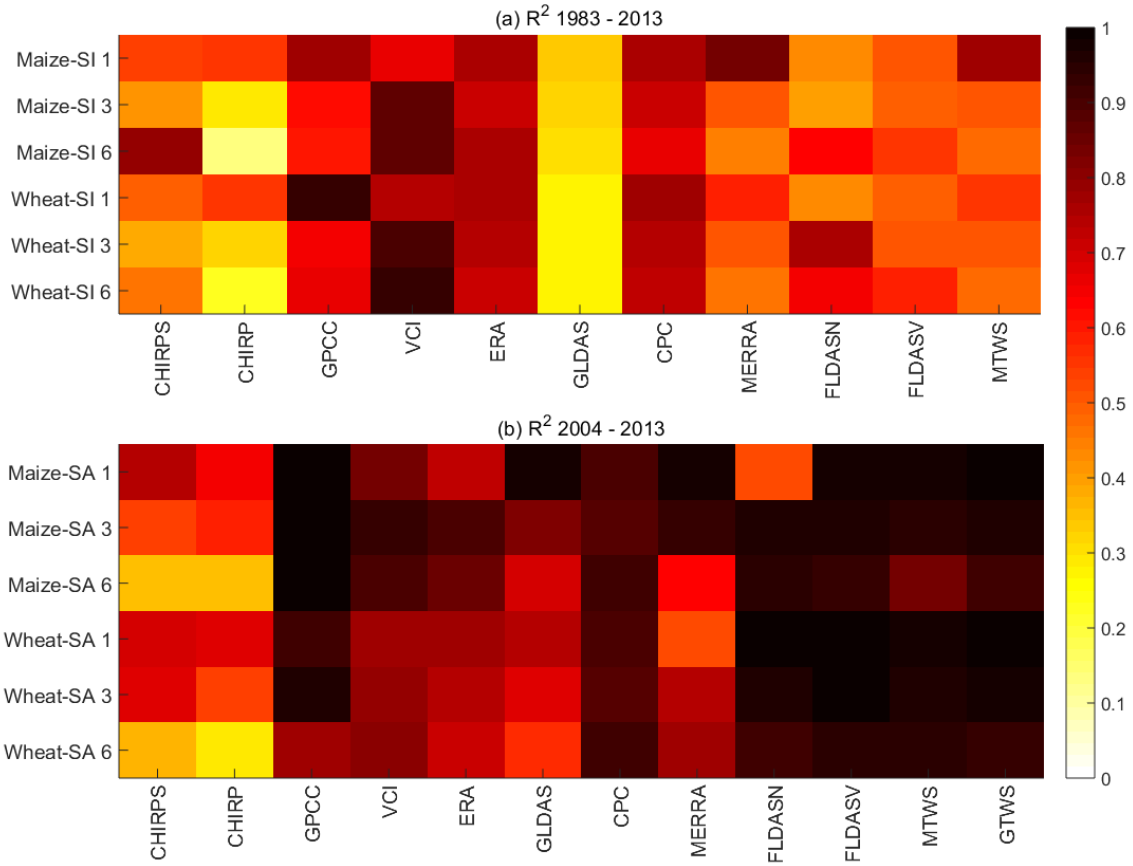

Figure 4.13: Proportions of variability in national annual crop (maize and wheat) production (R^2) explained by various drought indices over Ethiopia. VCI, GPCC, ERA, CPC, FLDASN, and FLDASV explained relatively higher variabilities in crop production, while GLDAS explained lowest variability. Figure (b) should be interpreted with caution as the datasets used to fit the models are only 10 years long. Both SI and SA are computed at annual scales. The y axis indicates the crop (maize/wheat), while 1,3 and 6 indicate the standardization time scales for the indicators on the x axis.

Based on SI regression with national annual crop production, all the indicators explained over 50% of variability in the national annual crop production (in most instances) except CHIRP and GLDAS (Fig. 4.13a). These results are largely consistent with those of *Bewket* (2009) and *Funk et al.* (2003) who found a good correlation between crops (teff, wheat, and maize) production and monthly rainfall anomalies over Ethiopia. VCI performed exceptionally well

explaining between 67% and 93% of the variability in national annual crop production. GPCC explained higher percentage of variability in national annual crop production than CHIRPS, which explained higher variability than CHIRP. For the soil moisture products, ERA and CPC performed better than the rest, FLDASN and FLDASV explained largely equal variabilities while GLDAS explained the least variability in national annual crop production.

SA regression generally explained higher variabilities in annual crop productions than SI (Fig 4.13b), possibly due to the shorter duration considered. GTWS performed exceptionally well explaining between $92\% - 99\%$ of the variability in national annual crop production. In addition, FLDASN, FLDASV, CPC, VCI, and GPCC also explained high variabilities. Like in SI regression, GPCC outperformed CHIRPS, which outperformed CHIRP while FLDASN and FLDASV explained almost equal variabilities. Also, FLDASN explained more variability than GLDAS. The SA regression results should be interpreted with caution due to the shorter duration of the data considered.

The regression results, as pointed out in Chapter 3, should not be generalized to other areas and time periods since the relationship between production (yield) and climate condition (water availability) only holds if production factors e.g., areas under cultivation, and farm management practices, remain constant.

4.4.2 Discussion

The spatial patterns of rainfall, VCI, TWS, and majority of the soil moisture products derived drought indicators have been seen to mimic rainfall distribution and/or land cover patterns (Figs. 4.2 and 4.3 vis-a-vis Fig. 4.1b–c) both of which are majorly influenced by topographical changes (terrain variations). Topography is a major factor influencing rainfall distribution (see, e.g., *Dinku et al.*, 2007, 2008; *Romilly and Gebremichael*, 2011) and to a large extent the land cover classes over the region (*Kurnik et al.*, 2011). The spatial variability of soil moisture is dependent on the scales under consideration i.e., at large scales, soil

moisture spatial variability is chiefly determined by soil types, topography, and vegetation types while at small scales, precipitation and evapotranspiration play major roles (*Entin et al.*, 2000; *Huang et al.*, 2012). This explains the closeness of the majority of the SSI spatial patterns to the land cover classes and/or spatial rainfall distribution (Fig. 4.3 compared to Fig. 4.1a–c).

Region 3 (southeastern Ethiopia and Somalia) had high consistency in spatial and temporal patterns, largely equal percentage of variabilities explained by rainfall and moisture products, and high average correlation among different products (Figs. 4.2, 4.3, 4.4c, and 4.5c, and Tables 4.1 and 4.2). These could be attributed to relatively flats topography of the region coupled with low rainfall. The combination of flat topography and low rainfall does not seem to give much challenge to the different products in capturing spatio-temporal drought information from the region, hence the high consistency.

The variation in the mean differences in percentage of areas under drought due to gauge density was inversely related to the gauge density of both GPCC and CHIRPS (Figs. 4.7, 4.1d, and 8.2). The mean percentage differences were lowest over Ethiopia and highest over Somalia (7.9% vis-a-vis 13.3%). Ethiopia has the highest gauge density from both GPCC and CHIRPS while Somalia has the lowest (Figs. 4.1d, and 8.2). Even though GPCC and CHIRPS have in-situ gauge measurements from global historical networks and global teleconnection networks (*Schneider et al.*, 2014; *Funk et al.*, 2015), the fluctuation in monthly number of stations available to each (see, e.g., variation in number of available stations for CHIRPS in Fig. 8.2) is the major source of this difference. In addition, this variation could also be contributed by the additional in-situ stations incorporated in GPCC but absent in CHIRPS (see, e.g., *Schneider et al.*, 2014; *Funk et al.*, 2015).

Other than gauge density, topographical factors were also found to contribute to the mean difference in percentage areas under drought (Figs. 4.7 and 4.1a). Somalia had the lowest mean difference in percentage of areas under

drought (3.4%) while Ethiopia (11.3%) and South Sudan (12%) had highest mean differences. This could be due to the fact that Somalia with low topographical variation has low influence on how various products characterize rainfall while Ethiopia and South Sudan with rapid changing topography presents difficulty to various products (Fig. 4.1a). In general, the performance of GPCC is affected by systematic errors (errors associated with systematic gauge-measurements) and sampling errors associated with gauge densities (see, e.g., *Schneider et al.*, 2014). The sampling errors are dependent on orography, season and type of rainfall, of which topography plays a large role hence differing performance across the regions. CHIRPS being a combination of satellite-based precipitation and in-situ observations, has its performance dependent on how well the infrared cold cloud duration (CCD) observed precipitation estimates correspond to the actual rainfall and how effective the merging is done, while CHIRP purely depends on CCD (*Funk et al.*, 2015). The degree of correspondence between the CCD estimated rainfall and the actual rainfall over a place is influence by topographical factors. It is the topography related difficulties in rainfall representation that translates to mean differences in percentage areas under drought on drought characterization with these products.

Similarly, the influence of gauge density and topographical variations on the mean differences in percentage of areas under different drought intensities (Fig. 4.11) follows the same logic as above.

The closer performance between FLDASN and FLDASV from temporal variability, higher correlations, lower mean differences in percent of areas under drought and different drought intensities, and explained amount of variabilities in crop production (Figs. 4.5, 4.9, 4.12, and 4.13, and Table 4.2) could be attributed to FLDASN and FLDASV being forced by CHIRPS rainfall. However, they are FLDAS versions driven by different models, Noah and VIC, respectively. Further, their lower mean differences compared to FLDASN and

GLDAS, and the higher percentage of variabilities in crop production explained by FLDASN over GLDAS implies that forcing precipitation plays a bigger role in the resulting soil moisture than model difference. This is supported by the fact that both FLDASN and GLDASN are products of same model, Noah, but of different precipitation forcings; FLDASN is forced by CHIRPS while GLDASN is forced by Princeton global meteorological forcing data (see, e.g., *Sheffield et al.*, 2006; *McNally et al.*, 2017). The role of forcing precipitation in determining the quality of resulting soil moisture has also been recognized in other studies (*Dirmeyer et al.*, 1999, 2004; *Entin et al.*, 1999). In addition, the different operating thresholds (due to different models) for soil wetness, i.e., different mean values, variances, and hydrologically critical thresholds, e.g., points where evaporation occurs at the potential rates or where surface run-off begins (*Dirmeyer et al.*, 2004), contribute to the differences. Therefore, the largest differences occurred when different models with difference forcing precipitations were considered, e.g., FLDAS and MERRA.

Like gauge density based mean differences, the spatial distribution of the moisture mean differences in percentage of areas under drought and different drought intensities were lower over Ethiopia and higher over Somalia (Figs. 4.9 and Fig. 4.12). However, for the soil moisture products, this could be linked more to the amount of rainfall and/or moisture levels and the individual model thresholds over the region but not directly on topography since Ethiopia has more topography related issues than Somalia (see section 4.2). The influence of topography on the percentage of area differences from soil moisture product is indirectly through the forcing precipitation.

The larger mean differences in areas under moderate and extreme droughts than severe droughts observed in all the differences (both rainfall and soil moisture; Figs. 4.11 and 4.12) across the region could be linked to differences in extreme drought conditions, i.e., lower (moderate) and higher (extreme) as captured by these products. For the soil moisture products, it could be related

to the drying thresholds implemented by different models.

Unlike Chapter 3 (over EA) where CHIRPS performed better than GPCC, here GPCC aided by a higher density of gauge distribution (and CHIRPS impeded by low and high varying number of incorporated in situ stations; Fig. 8.2) explained higher variabilities in national annual crop production. Similar to Chapter 3, FLDAS explained higher variabilities than GLDAS while MTWS and MERRA2 registered similar performances. The shorter duration regression results explain higher amount of variability in national annual crop production than the long duration probably due to the fact that under the short duration, the factors of production especially the areas under cultivation are constant. The influence of increase in areas under cultivation could be responsible for relatively lower percentage of variabilities explained, see e.g., *Taffesse et al.* (2012) who found a link between the increase in crop production and areas under cultivation over Ethiopia. The relationship between crop production (yields) and moisture availability (climate variables) holds subject to the area under cultivation and factors of production (e.g., fertilizers, crop cultivars, pesticides) being constant. In addition, production response to water at any stage of growth can be modified by various factors, e.g., diseases, weeds, insects, crop variety (*Steduto et al.*, 2012; *Hane and Pumphrey*, 1984), hence, results should not be generalized to other areas.

The information on the consistency of percentage of areas under drought and different drought intensities is critical in understanding and putting into perspective drought analysis results from different products over the region by various stakeholders. This is important to policy and decision makers as it will enable them to make decisions on the number of people affected and the extent to which they are affected without worrying about particular product, e.g., soil moisture used in any particular analysis. These particular decisions are essential for resource mobilization, aiding mitigation of drought impacts, improving drought response plans and early warning systems, and quantifying

drought impacts among others.

4.5 Concluding Remarks

This Chapter characterized agricultural drought over the upper GHA countries (Ethiopia, Sudan, South Sudan, and Somalia) using rainfall (CHIRPS, CHIRP, and GPCC), moisture (ERA-Interim, CPC, GLDAS, FLDAS Noah, FLDAS VIC, and MERRA2), and TWS (MERRA2 and GRACE) products with bias on the influence of topography. Further, the Chapter considered the consistency of differences in the percentage of areas under drought and different drought intensities from precipitation and selected moisture products. Finally, the Chapter assessed the effectiveness of various drought indicators in capturing agricultural drought over Ethiopia using national annual crop production. The following were the major results:

(i) The spatial-temporal drought patterns were found to be influenced by topography over the region. All the products were highly consistent over the low land low-medium rainfall regions of Eastern Ethiopian and Somalia while lowest consistency differed across products and regions.

(ii) The mean differences in percentages of areas under drought and different drought intensities from Precipitation products were determined by gauge density (distribution and availability) and topography. The mean differences attributed to gauge density were low in areas of high gauge density (Ethiopia) and higher in areas of low gauge density (Somalia) while the mean differences attributed to topography were low in low varying topographical areas (Somalia) and higher in rapid varying topographical areas (Ethiopia and South Sudan).

(iii) The mean differences in the percentage of areas under drought and different drought intensities over the region from precipitation products were on average 15.87% and 6.16%, respectively.

(iv) The mean differences in percentages of areas under drought and different drought intensities from soil moisture products was determined by the differences in the forcing precipitation, models pairs under consideration, and the regions.

(v) The mean differences in the percentage of areas under drought and different drought intensities over the region from soil moisture products were on average 12.65% and 5.20%, respectively.

(vi) Both rainfall and moisture products had larger mean differences in the percentage of areas under moderate and extreme droughts than severe droughts.

(vii) In assessing the utility of the various indicators in capturing agricultural drought over Ethiopia, the Chapter identified the following indicators as suited for agricultural drought monitoring during the study period; VCI, GPCC, ERA, CPC, and FLDAS (Noah and VIC).

(viii) Other than missing several drought episodes in characterization, GLDAS also explained the lowest variability in national annual crop production over Ethiopia.

As observed in Chapter 1, GHA region largely depends on subsistence rain-fed agriculture for its survival. This makes soil moisture crucial for agricultural drought analysis. However, the inconsistencies observed in drought characterization, the mean percentage of areas under drought and different drought intensities, and percentage of variabilities explained in national annual crop production from model and reanalysis soil moisture products (this Chapter and Chapter 3) calls for further analysis of the suitability of these products over the region. It is on this basis that the next Chapter analyses the uncertainties in the model and reanalysis soil moisture products and their characteristics over GHA.

5 Soil Moisture Variability in GHA, Uncertainties and the Influence of Climate Variability

5.1 Introductory Remarks

Soil moisture serve various critical roles in general e.g., controlling the interactions between land surface and atmosphere as it affects both energy and water cycle, determines the amount of run-off hence chances of droughts and floods occurring in a given area, and a direct indicator of water available for plants (crops) and agricultural drought (*Entin et al.*, 2000; *Legates et al.*, 2011; *Shukla et al.*, 2014). Its importance in agricultural drought monitoring is highlighted by the fact that it indicates plant water deficiencies earlier than other conventional products estimating vegetation status e.g., normalized difference vegetation index (NDVI; *Enenkel et al.*, 2015). In Greater Horn of Africa (GHA), lack of in-situ soil moisture monitoring networks has led to reliance on hydrological models and/or satellite remotely sensed soil moisture as the only sources of information to bridge the gap between rainfall deficit and vegetation response (e.g., *AghaKouchak et al.*, 2015). Such information is critical to agricultural drought monitoring, informing better water and agro-pastoral management decisions, and mitigation of socio-economic impacts of floods and droughts (*Shukla et al.*, 2014).

Observed soil moisture, e.g., satellite remotely sensed moisture, arguably provide the best representation of the actual amount of water contained in the soil (*Chen et al.*, 2014). However, majority of the currently available satellite remotely sensed soil moisture products suffer from; being too short (time series) to be useful for demonstration of their operational utility and/or provision of context for extreme wet and/or dry conditions, can only go up to a few centimetres in depth and are greatly influenced by vegetation water content, and potential shift in data due to sensor changes over time leading to inconsistent data quality (*Dirmeyer et al.*, 2004; *McNally et al.*, 2016). In comparison, land surface model (LSM)-based predictions of soil moisture offer

benefits of providing continuous estimates under all weather and surface condition (*Anderson et al.*, 2012), propagation of soil moisture to lower (deeper) depth (*Dirmeyer et al.*, 2004), and having a longer time series of data compared to satellite-derived soil moisture. However, lack of in-situ soil moisture to validate the LSM soil moisture products implies that the uncertainties in them and their characteristics (e.g., variabilities) are unknown. Consequently, the confidence in them is not as high, leading to their low uptake levels as reflected by lower number of soil moisture-based agricultural drought related studies compared to precipitation-based ones over GHA region. In addition, they lack demonstrable utility. Evaluation of uncertainties, characteristics (variabilities), and demonstration of utility, therefore, would increase confidence in these products and spur their uptake in agricultural drought monitoring related research that is critical to this food insecure region.

A number of studies and/or projects (e.g., *Anderson et al.*, 2012; *Sheffield et al.*, 2014; *Shukla et al.*, 2014; *McNally et al.*, 2016) utilizing LSM and/or LSM-derived soil moisture exist in GHA region. *Anderson et al.* (2012) applied triple collocation analysis (TCA, *Janssen et al.*, 2007) to three independent soil moisture products (soil moisture from; Advance Microwave Scanning Radiometer-Earth Observing System, Atmosphere Land Inverse surface energy balance algorithm, and Noah LSM) to characterize relative errors between the products and provide the basis for objective data merging. *Shukla et al.* (2014) developed agricultural drought forecast system to provide decision support for the Famine Early Warning System (FEWS NET) science team based on Variable Infiltration Capacity (VIC) LSM, while *Sheffield et al.* (2014) developed and implemented a drought monitoring and forecasting system for Sub-Sahara water resources and food security. Finally, *McNally et al.* (2016) evaluated the quality of merged active and passive soil moisture from European Space Agency climate change initiative and compared it to NDVI and LSM (Noah and VIC) soil moisture products. Of these major studies, only *Anderson*

et al. (2012) evaluated the uncertainties in the concerned products to provide objective for merging. *McNally et al.* (2016) considered the quality of the satellite-derived soil moisture but did not quantify the uncertainties involved. Other studies that have used LSM based soil moisture in addition to other products (e.g., precipitation and/or NDVI) to evaluate drought include *Dutra et al.* (2013); *Viste et al.* (2013); *Mwangi et al.* (2014); *Yilmaz et al.* (2014); *AghaKouchak* (2015); and *Agutu et al.* (2017). None of the aforementioned studies evaluated uncertainties in the LSM-derived soil moisture products and the variation of these uncertainties across the region and different LSMs.

The majority of the aforementioned studies and others over the region have used single soil moisture products in their drought analyses. But as was observed in Chapters 3 and 4, each soil moisture product had different areas under drought, drought intensity information, and drought cycle lags due to various factors e.g., different uncertainties in them (caused by different forcing precipitations, different model thresholds) and impacts of topography on the models (see Chapter 4). This calls for investigation and understanding of the magnitudes and characteristics of uncertainties in these products so as to aid in choosing the best products for the region. The characteristics of uncertainties on the long-term means, (annual and seasonal), is critical as the long term means plays a crucial role in defining climatological norms, the occurrence of extreme events, detection of climate change and projection of future climate variations as well as their impacts (*Giorgi et al.*, 1994; *Groisman et al.*, 2001). In addition, changes in hydrological fields and states e.g., precipitation and soil moisture are frequently measured relative to their climatological means (*Kim and Park*, 2016).

Due to the existence of various models and reanalyses soil moisture products of both regional and global spatial coverages with varied spatial resolutions (see e.g., *Bosilovich et al.*, 2016; *Rui and McNally*, 2016; *Dee et al.*, 2011; *Rodell et al.*, 2004; *van den Dool et al.*, 2003) this Chapter; (i) evaluated the uncertainties in the selected soil moisture products over the region using

generalized three-cornered hat (TCH) method (*Premoli and Tavella*, 1993; *Tavella and Premoli*, 1994), (ii) investigated the uncertainty characteristics, by considering the relationship between the selected individual soil moisture products and their ensemble mean in annual and seasonal means time laps, using Taylor diagrams (*Taylor*, 2001), (iii) investigated spatio-temporal analysis of the selected soil moisture products in relation to rainfall, and (iv) evaluated the relationship of the selected soil moisture products variabilities to global teleconnections. The generalized TCH method enables estimation of relative uncertainties in each product without using in-situ soil moisture, which the GHA region does not have. The findings of this Chapter are crucial for understanding the uncertainty characteristics of different soil moisture products over the region hence could serve as a guide for the best-suited soil moisture products for agricultural drought monitoring. In addition, the knowledge from the relationship between the soil moisture products and teleconnections could be used in building soil moisture forecast models based on the teleconnections.

The remainder of the Chapter is organized as follows. Section 5.2 provides a summary of the data set used and a discussion of the methodology. Results are presented and discussed in section 5.3 and the Chapter is concluded in section 5.4.

5.2 Data and Methods

The soil moisture products used in this Chapter are derived from the following models (and reanalysis) MERRA2, ERA-Interim, GLDAS, FLDAS, and CPC (see, e.g., Table 5.1). In addition, dominant climate variability indices (ENSO and IOD) were used. A detailed discussion of these products is presented in Chapter 2.

Due to lack of in-situ soil moisture over GHA, soil moisture from MERRA2, ERA-Interim, GLDAS, FLDAS, and CPC were evaluated for uncertainties using generalized TCH method. The uncertainties in spatial and interannual

Table 5.1: A summary of the soil moisture products used in this Chapter

Model	Soil moisture adopted name	Spatial resolution	Period
MERRA2	MERRA2	0.625° × 0.5°	1982-2010
ERA-Interim	ERA	0.25° × 0.25°	1982-2010
GLDAS NOAH	G_NOAH	1°× 1°	1982-2010
GLDAS VIC	G_VIC	1° × 1°	1982-2010
GLDAS CLM	G_CLM	1° × 1°	1982-2010
GLDAS MOSAIC	G_MOS	1° × 1°	1982-2010
FLDAS NOAH	F_NOAH	0.1° × 0.1°	1982-2010
FLDAS VIC	F_VIC	0.25° × 0.25°	1982-2010
CPC	CPC	0.5° × 0.5°	1982-2010

variability of annual and seasonal (MAM, JJAS, and OND) mean monthly soil moisture were further analyzed through Taylor diagrams. Each soil moisture product was compared to the ensemble mean of all the soil moisture products. In addition, the spatio-temporal variability of these soil moisture products were analysed through principal component analysis (PCA; see Chapter 2 for details and formulation). The PCA decomposed soil moisture were compared to PCA decomposed precipitation. Further, Pearson correlation (see Chapter 2 for details and formulation) was carried out between the dominant soil moisture temporal variability modes and climate indices (IOD and ENSO) to infer ths association between soil moisture variability and dominant global climate indices.

5.2.1 Generalized Three-cornered Hat (TCH) Method

Generalized TCH method (see Chapter 2 for details and formulation) was used to evaluate relative uncertainties on the above soil moisture products (Table 5.1). This was carried out on area (spatial) averages of soil moisture over GHA, EA, and Ethiopian highlands. The spatial extents of EA and Ethiopian highlands over which the averaging was done is shown in Figure 2.1. Finally, the uncertainties were analysed on pixel by pixel basis over the whole GHA region.

5.2.2 Uncertainty in Spatial and Interannual Variability

The climatological characteristics of the soil moisture products were studied in relation to their ensemble (ENS) mean. Much of the skill of soil moisture products comes from the precipitation forcing, and as such an objective weighting could be based on the quality of the precipitation. Many studies have done this in terms of streamflow evaluations, i.e., better streamflow simulations come from precipitation products that use more gauge data, (see e.g., *Xu et al.*, 2013; *Hansen et al.*, 1996; *Duncan et al.*, 1993). Due to the fact that the region lacks reliable and accessible ground-based data (precipitation and/or soil moisture), a simple averaging of all the observations (soil moisture products) was used to create ENS. Given N soil moisture time series $\{\mathbf{X}^i\}, i = 1..., N$, the ENS was derived as

$$ENS = \frac{1}{N}\sum_{i=1}^{N}\mathbf{X}^i, \tag{5.1}$$

where $\mathbf{X}$ is soil moisture time series. From the ENS and the respective soil moisture products, annual and seasonal (MAM, JJAS, and OND) mean soil moisture were computed. In addition, inter-data spread measured by standard deviation computed over the data sets in the ENS as (*Krzanowski*, 2000),

$$\sigma = \left[\frac{(k_1-1)S_1^2 + (k_2-1)S_2^2 + ... + (k_n-1)S_n^2}{k_1 + k_2 ... + k_n}\right]^{\frac{1}{2}}, \tag{5.2}$$

was used to analyze the spatial variability between the soil moisture products. Where σ is the inter-data standard deviation, n is the number of samples, k is sample sizes, and S_n is the standard deviation of the n^{th} sample. The spread (uncertainty) and magnitude of disagreement amongst the soil moisture products were measured using the signal to noise ratio (SNR) and Taylor diagrams (*Taylor*, 2001). SNR was computed as a ratio between the multi-data ENS mean (M) and standard deviation computed over all the datasets included in the ENS (*Kim*

et al., 2015).

$$SNR = \frac{M}{\sigma}. \tag{5.3}$$

Taylor diagram allows simultaneous evaluation of three properties; pattern correlation, standard deviations, and the centered root mean square errors between multiple data sets and reference data sets (*Kim and Park*, 2016). On this diagram, the correlation coefficient and the root mean square (RMS) difference between several fields and a reference field, along with the ratio of standard deviations are all indicated by a single point on a two-dimensional plot (*Taylor*, 2001). Together these statistics provide a quick summary of the degree of pattern correspondence, allowing one to judge the relationships (*Taylor*, 2001). Finally, area-averaged monthly time series were used to analyze the interannual variability of the annual and seasonal mean soil moisture over the 29 years considered using Taylor diagrams.

5.3 Results and Discussion

5.3.1 Soil Moisture Uncertainties

Preliminary analysis of spatially averaged soil moisture products over GHA, Ethiopian highlands, and EA (Fig. 5.1, see Fig. 2.1 for extents of Ethiopian highlands and EA over which averaging was done) shows over-estimation by CPC and underestimation by G_MOS (GLDAS MOSAIC) with the rest of the soil moisture products being within a general common range. Further, examination of the inter-quartile ranges shows all the soil moisture products having a larger inter-quartile range over Ethiopian highlands compared to EA (interquartile ranges over Ethiopian highlands is almost twice those over EA), due to impact of more complex topography and terrain leading to large variability in soil moisture hence larger interquartile range.

Generalized TCH analysis of uncertainties based on spatially averaged soil moisture products over GHA region (Fig. 2.1) showed MERRA2, F_NOAH

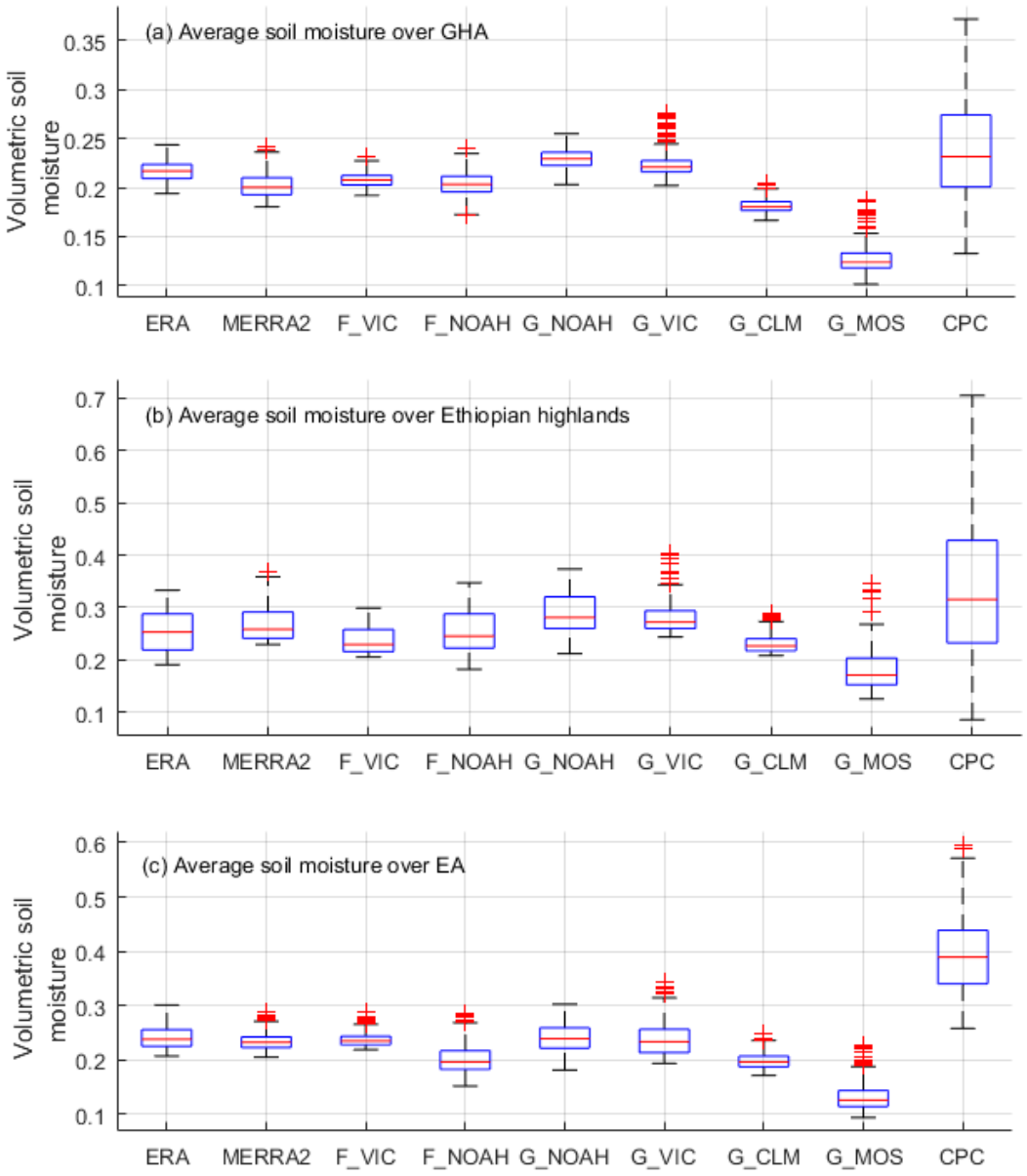

Figure 5.1: Box plot summaries of characteristics of spatially averaged soil moisture over (a) GHA, (b) Ethiopian highlands, and (c) EA. CPC consistently shows an over-estimation while G_MOS shows a high under-estimation. The whiskers indicate maximum and minimum range of soil moisture while the box shows the interquartile (first and third quartile) range of variation. The segment inside the box shows the median of the data and the red marks above or below the whiskers indicate the outliers. For Ethiopian highlands and EA, see Fig. 2.1.

(FLDAS NOAH), F_VIC (FLDAS VIC), and ERA with the lowest uncertainties in that order while CPC, G_VIC, and G_MOS had the highest uncertainties in

that order. Further, grid analysis of the uncertainties over GHA region revealed higher magnitudes of uncertainties over high rainfall regions and lower magnitudes of uncertainties over low rainfall (dry) regions (Fig. 5.3, in comparison with Fig. 2.2a and b for rainfall distribution). In addition, over the high rainfall regions and across all the soil moisture products, there is relatively higher uncertainty over Ethiopia highlands and eastern Sudan compared to Kenya, Uganda, and Tanzania.

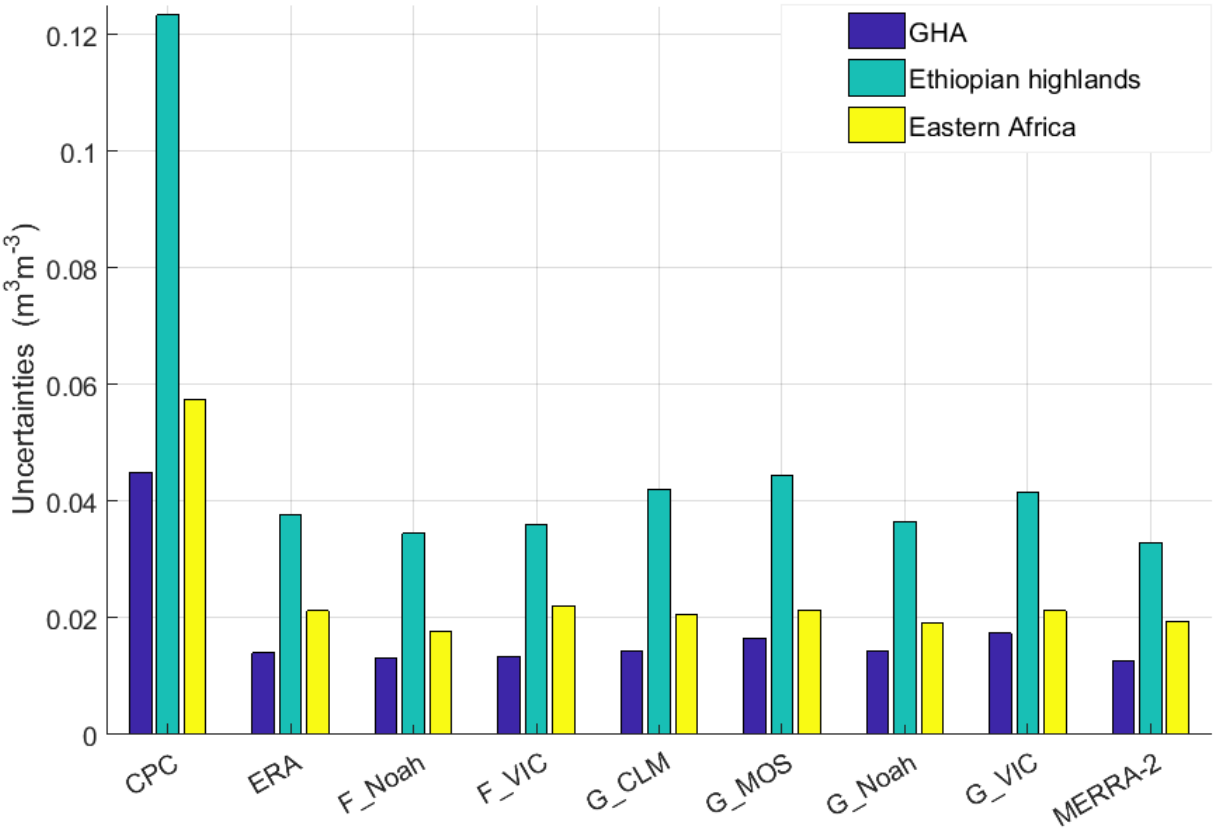

Figure 5.2: Magnitude of uncertainties of spatially averaged soil moisture products over GHA, Ethiopian highlands, and EA. F_NOAH and MERRA2 have consistently lower uncertainty ove the regions while CPC has the highest uncertainties across the three regions. The magnitude of uncertainties over Ethiopian highlands are almost twice those over EA. For Ethiopian highlands and EA, see Fig. 2.1. The uncertainties are in m^3m^{-3}.

Further, uncertainty analysis based on spatially averaged soil moisture products over Ethiopian highlands and EA (Fig. 2.1) showed Ethiopian highlands having almost twice the magnitude of uncertainties as EA, confirming

the spatial uncertainty distribution observed in Figure 5.3 and high variability (and/or high uncertainty) in the preliminary analysis (Fig. 5.1). MERRA2 and F_NOAH have consistently lower uncertainties over the two regions while CPC has the highest uncertainty across the regions.

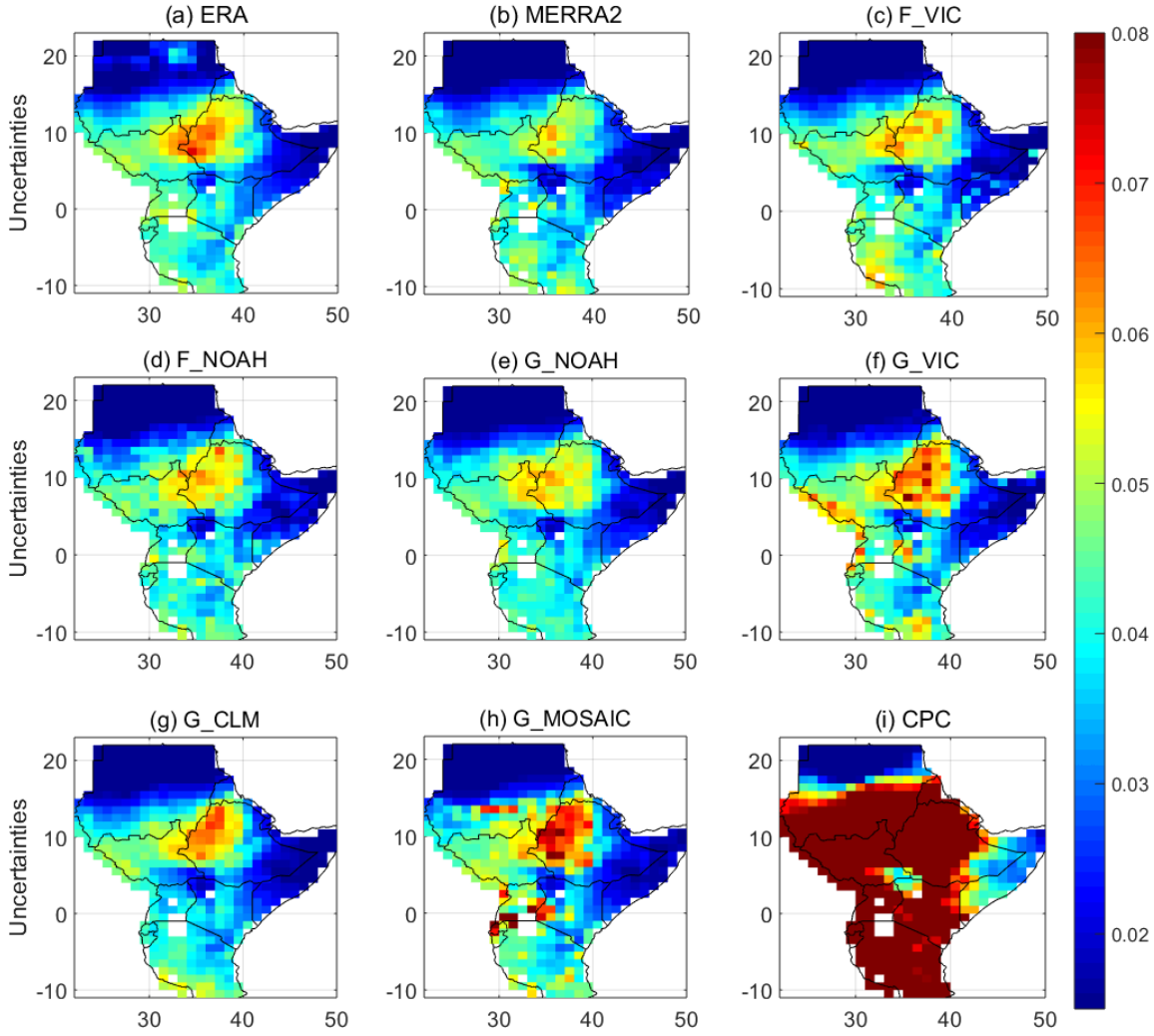

Figure 5.3: Spatial distribution of uncertainties of various soil moisture products over GHA. Higher magnitude of uncertainties are observed over high rainfall regions (e.g., Ethiopian highlands) while lower uncertainties are over low rainfall (dry/low moisture) regions (e.g., Sudan and Somalia). The uncertainties are in m^3m^{-3}.

The differences in the soil moisture products and the uncertainties captured in Figures 5.1, 2.1, and 5.3 are functions of different models' physics, different forcing precipitation, and variation of topography across the region. Each of the models

considered have different thresholds for soil wetness i.e., different mean values, variances, and hydrologically critical thresholds, e.g., points where evaporation occurs at the potential rates or where surface run-off begins (*Dirmeyer et al.*, 2004), which result in different soil moisture characteristics and also contributes to part of the uncertainties in those particular products.

The other important characteristic is the quality of the forcing precipitation as the errors in the precipitation are likely to be propagated into the resulting soil moisture. This is demonstrated by MERRA2 and F_NOAH with consistently low uncertainties over the region, resulting from model forcings with satellite-gauge merged precipitation products CMAP and CHIRPS, respectively, products that represent close to true rainfall for the region. Since F_NOAH and F_VIC are both forced by CHIRPS, their differences in uncertainties result from different model thresholds and based on the uncertainty magnitudes, F_NOAH is the better model (Fig. 2.1). Even though the GLDAS suite of G_VIC, G_CLM, and G_MOS were forced with the same precipitation products (see, e.g., *LDAS*, 2016), the inconsistency in their uncertainties (Fig. 2.1) is most likely due to model threshold differences and impacts of topography on different models (see Chapter 4). Finally, the importance of precipitation forcing is highlighted by comparing F_NOAH to G_NOAH and F_VIC to G_VIC; similar models but different precipitation forcing. Consistent with the foregoing discussion, F_NOAH and F_VIC forced by better quality precipitation for the region have lower uncertainties as compared to their counterparts G_NOAH and G_VIC, forced by global products.

The spatial variability of the uncertainties (Figs. 2.1 and 5.3) is a function of rainfall amounts and to a large extent topographical changes. The relatively high uncertainty over Ethiopian highlands is due to the complex rainfall - topography relationship over the region. The uncertainties in the forcing rainfall products do propagate into the resulting soil moisture. Ethiopian highlands has been known to be a challenge to both gauge and satellite derived rainfall due to

complex terrain-precipitation variability (*Dinku et al.*, 2007, 2008; *Romilly and Gebremichael*, 2011). Just like satellite and gauge-derived rainfall products, LSM derived soil moisture products are affected over Ethiopian highlands as evident by higher uncertainties even for products forced by regional precipitation. It's also important to note that gauge availability plays a role in the magnitude of the uncertainty as soil moisture products forced with in-situ gauge and satellite merged precipitation products registered relatively lower uncertainties even over the Ethiopian highlands.

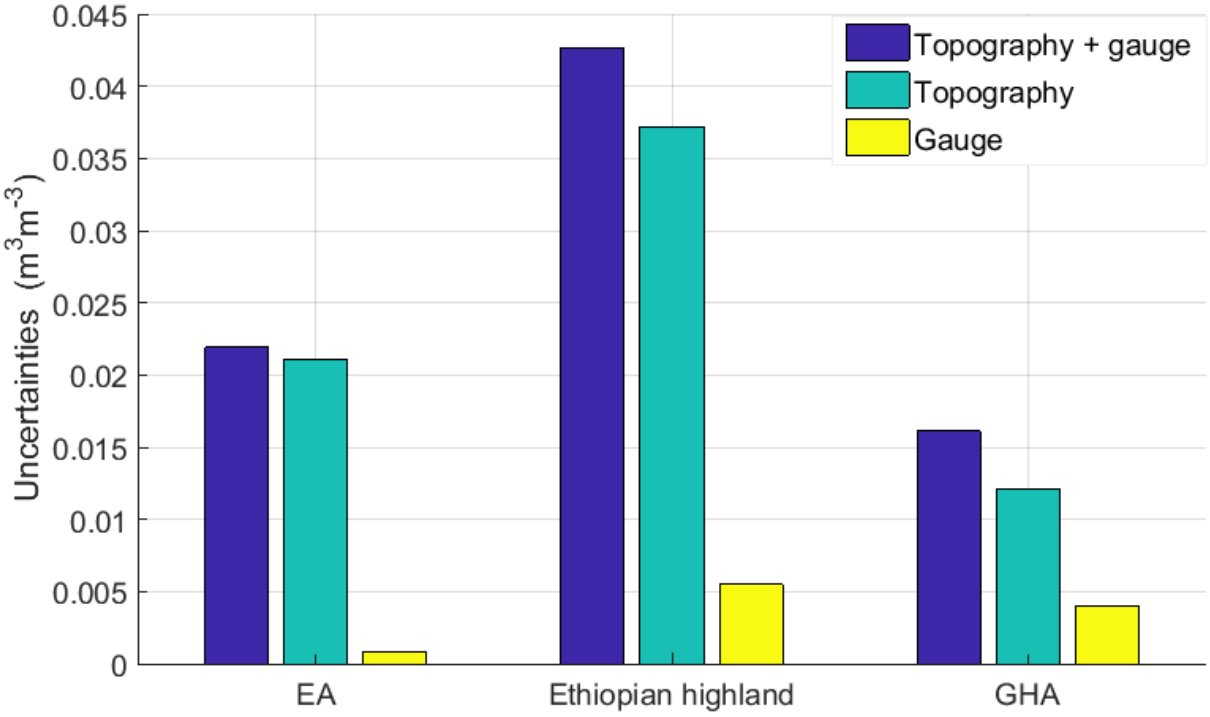

Figure 5.4: Topography and gauge uncertainty contributions. Topography has the highest contributions across the region with gauge being almost negligible. For Ethiopian highlands and EA, see Fig. 2.1. The uncertainties are in m^3m^{-3}.

Finally, the partitioning of the uncertainties into causes showed the forcing precipitation related (topography and gauge) to be the major source while the components due to the model physics were negligible. Further analysis of the forcing precipitation related uncertainties showed topography having the major contribution (Fig. 5.4). The level of uncertainties were highest when products forced with non-gauged precipitation products were considered (Fig. 5.4 -

topography and gauge) and they reduce when gauge-satellite forced products are considered. The reduction in uncertainties due to gauges were higher over Ethiopian highlands compared to EA (12.88% vis-a-vis 3.65%) due to the high gauge density (spatial distribution and availability) over Ethiopian highlands compared to EA (Fig. 5.4 - gauge; see Figs. 8.2 and 8.3). The rapid fluctuation in number of gauges available over EA coupled with low absolute numbers over Uganda could have contributed to the low reduction in the uncertainties when gauged precipitation products were considered. Topography related uncertainties were higher over Ethiopian highlands as compared to the EA due to the complex topographical variation over Ethiopian highlands.The spatial variation in magnitude of these uncertainties are consistent with those in Figs. 5.2 and 5.3.

5.3.2 Uncertainty in Spatial and Interannual Variability

5.3.2.1 Uncertainty in Spatial Variability

Climatology of the ENS annual, MAM, JJAS, and OND mean soil moisture and inter-product standard deviations are shown in Figure 5.5. The ENS comprised of all the soil moisture products (see Table 5.1) except CPC, which was excluded from this analysis due to its high un-usual uncertainty levels as observed in section 5.3.1. The annual climatology shows high moisture values over Ethiopian highlands, followed by South Sudan, the EA, and the least moisture over Sudan, especially north of latitude 15° (Fig. 5.5a-d). The high magnitudes in seasonal soil moisture means compared to the annual mean implies the annual climatology is controlled by seasonal soil moisture means (Fig. 5.5a-d); climatology over Ethiopian highland and South Sudan is determined by JJAS long term mean while soil moisture climatology over EA is chiefly determined by MAM. OND long term mean influences both regions (Ethiopian highlands and EA) though it has high values over Ethiopian highland. Even though Ethiopian highlands registers insignificant rainfall over OND, the high moisture levels are due to the carry over

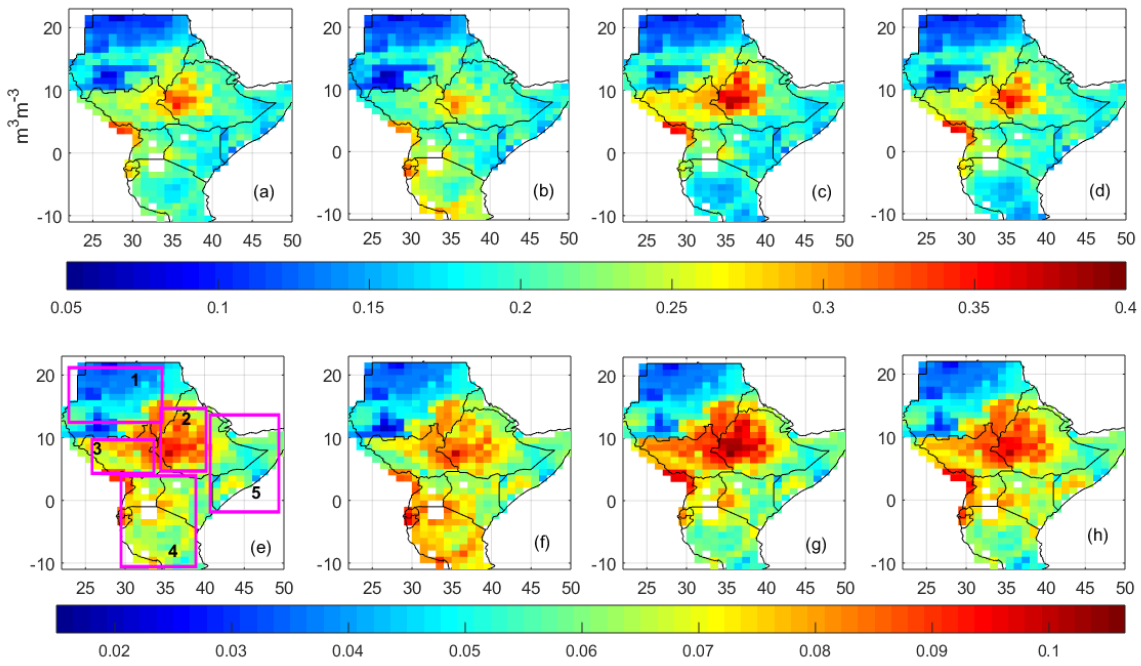

Figure 5.5: Climatology of the ensemble mean soil moisture for the duration 1980 - 2010; (a) annual, (b) MAM, (c) JJAS, and (d) OND. Inter-product soil moisture spread (measured by standard deviation) are also computed; (e) Annual, (f) MAM, (g) JJAS, and (h) OND. The standard deviation is computed over all the soil moisture products in the ensemble using eqn. 5.2. All the soil moisture products in Table 5.1, except CPC are in the ensemble. The inter-data spread have high values over high moisture areas. The rectangles in (e) denotes extents over which the area-averaged soil moisture has been derived for interannual variability analyses; 1 - Sudan, 2 - Ethiopian highlands, 3 - South Sudan, 4 - East Africa (EA), and 5 - Eastern Ethiopia and Somalia (EES).

effects of the JJAS moisture that are higher than OND moisture over EA. The inter-data spread measured by standard deviation among the data set in the ENS closely resemble the climatological mean values (Fig. 5.5e-h compared to a-d). The soil moisture products exhibited higher differences (large uncertainty ranges) in regions of high soil moisture and lowere differences (low uncertainty ranges) in areas of low soil moisture. This same pattern was shown by the uncertainties distributions in the TCH analysis (Fig. 5.3).

The range of uncertainties in the climatology of annual, MAM, JJAS, and OND soil moisture over the region measured in terms of SNR is shown in

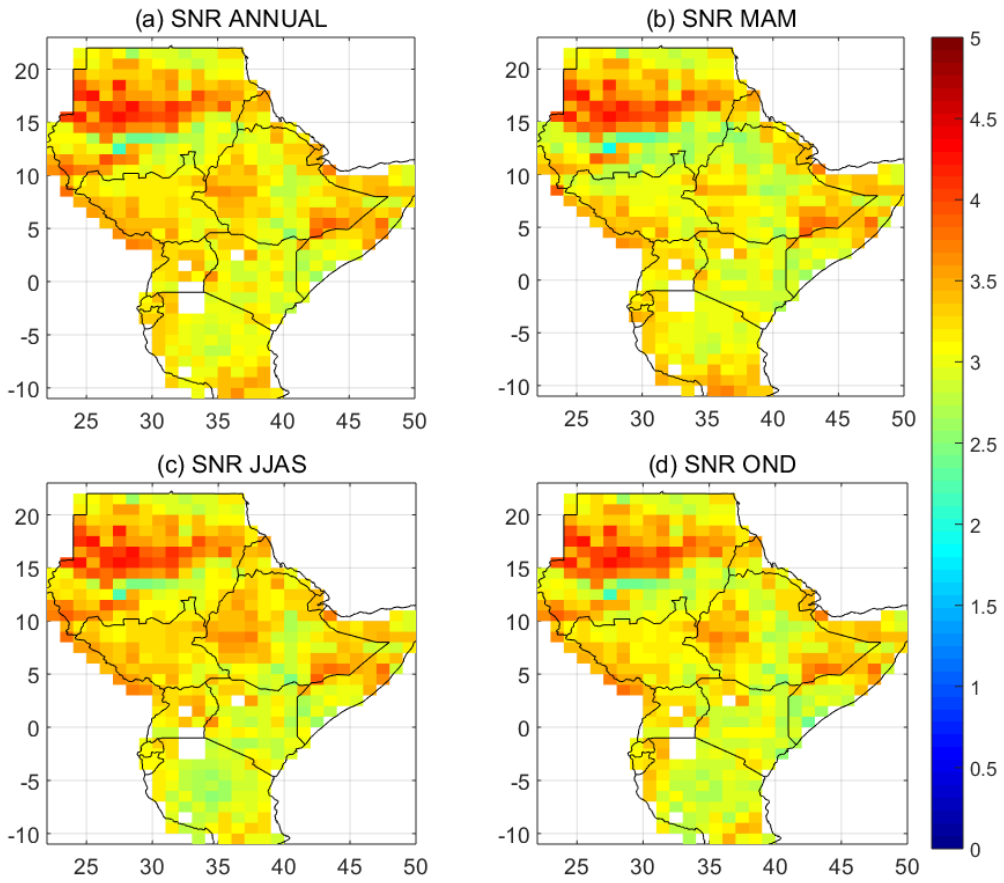

Figure 5.6: The signal-to-noise ratio (SNR) of the (a) annual, (b) MAM, (b) JJAS, and (c) OND ensemble soil moisture means (Fig. 5.5a-d). The $SNR > 1$ indicate a reliable representation of the original soil moisture products by the ensemble.

Figure 5.6. Since SNR was computed as a ratio between the ENS mean and the inter-data set variability, higher SNR ratio indicates good agreement between the soil moisture products and vice versa. As there is no established threshold for judging SNR, this Chapter will consider $SNR > 1$ (signal greater than noise) as an indication that the ENS is a good and/or reliable representation of the original datasets. The SNR for annual, MAM, JJAS, and OND show highest agreements between the soil moisture products over Sudan especially between latitudes 15° and 20° and varies geographically across the region (Fig. 5.6). In general, the lowest SNR is ≈ 2.5 indicating the ENS is a reliable representation of the original dataset over annual and seasonal time spans.

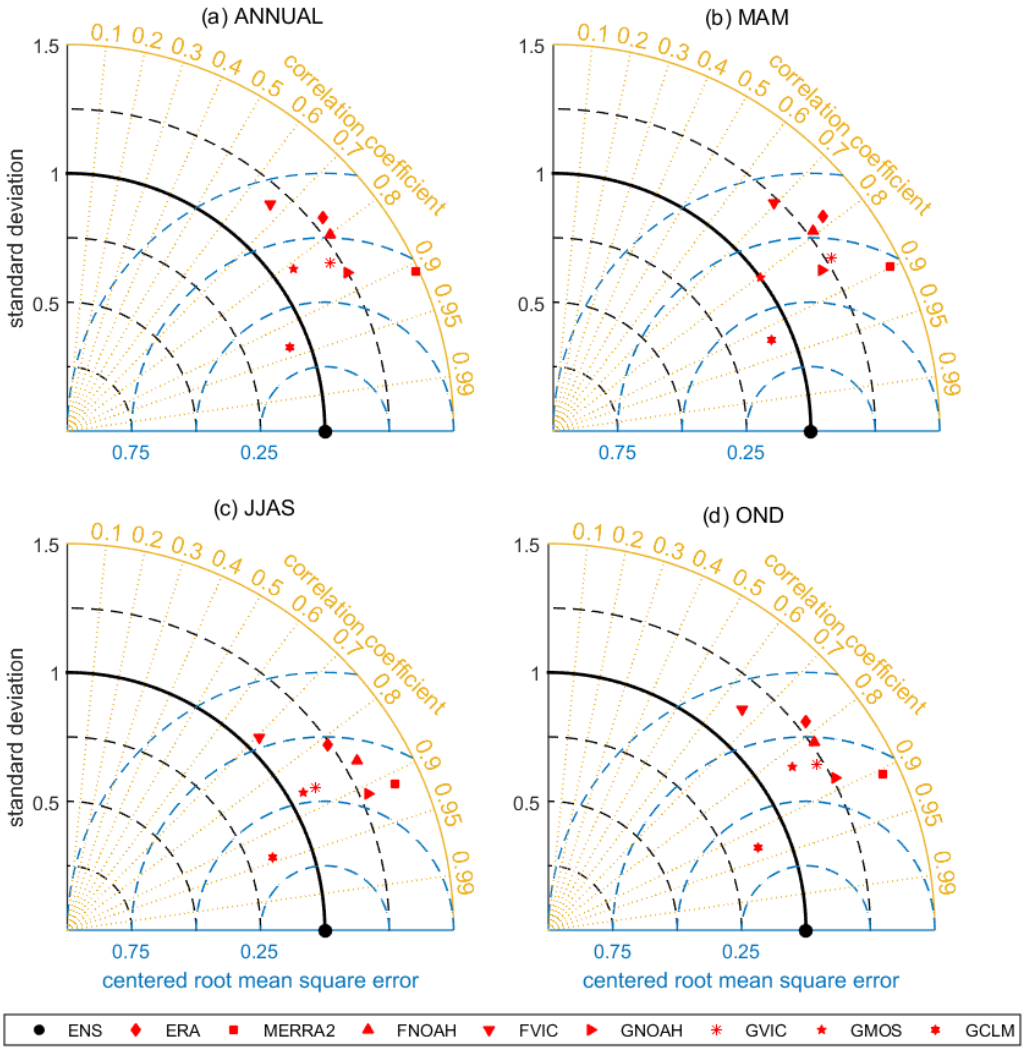

Figure 5.7: Spread amongst soil moisture products representing spatial variability of (a) annual, (b) MAM, (c) JJAS, and (d) OND individual soil moisture means in relation to the ensemble mean. They are represented in terms of spatial pattern correlations (azimuth direction), and magnitude of spatial variability (radial direction). The standard deviations of the individual soil moisture products are normalised using that of the reference data (ensemble; radial direction).

The agreement between the individual soil moisture product means and the ENS (reference) mean further analyzed in terms of spatial pattern correlation and the magnitude of spatial variability using Taylor diagrams is shown in Figure 5.7. The spread in radial and azimuthal directions indicate the spread in the magnitude of spatial variability and spatial patterns, respectively. The uncertainty ranges in spatial correlations (spatial patterns) are similar across

annual, MAM, JJAS, and OND means while the uncertainty range in magnitude of spatial variability was lower in OND and MAM (Fig. 5.7). This similarity in the spatial pattern (marked by equal correlation ranges $\approx 0.24 - 0.28$), could be a pointer to a common factor controlling the spatial variability. Both annual and JJAS means had almost similar uncertainty range reflecting the similarity noted between them in Figure 5.5a and c. Based on the centered root mean squared error (the distance of individual soil moisture products from the reference (ENS), G_CLM defined the lower range while F_VIC defined the upper range of uncertainty in spatial pattern variability across GHA. Finally, the uncertainties in spatial variabilities are not linked to the spatial resolutions of the individual soil moisture products, this follows from the fact that G_CLM with 1° x 1° spatial resolution show the smallest variability while F_VIC with 0.25° x 0.25° spatial resolution had the largest variability and F_NOAH with 0.1° x 0.1° spatial resolution falls somewhere in between across annual, MAM, JJAS, and OND (Fig. 5.7).

5.3.2.2 Uncertainty in Interannual Variability

The uncertainties (spread) in the interannual variability of the soil moisture products were examined using spatial averages of monthly soil moisture constructed for the 5 regions marked by boxes in Figure 5.5e. These regions were marked based on mean soil moisture amounts, the inter-data spreads, SNR, and the topography (Figs. 5.5, 5.6, and 2.1).

The interannual variability of the annual, MAM, JJAS, and OND mean soil moisture from each soil moisture product relative to the ENS over the 29 years considered were examined using Taylor diagrams (Figs. 5.8, 5.9, and 5.10). The spread in radial and azimuthal directions indicate the spread in the magnitude of interannual variability and phase (cycle), respectively.

For Sudan, EA, and EES (East Ethiopia and Somalia), the range of uncertainties in the interannual variability over annual, MAM, JJAS, and OND

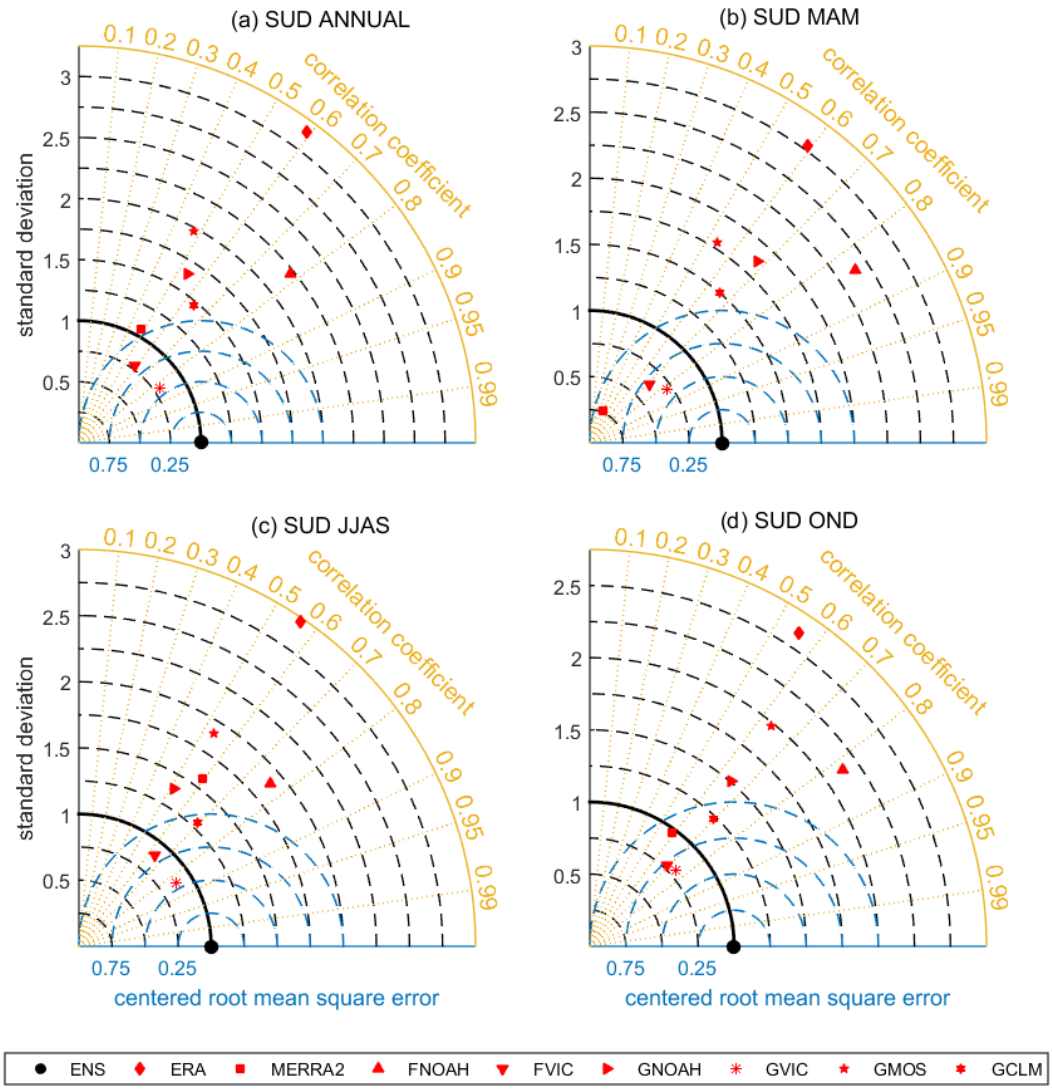

Figure 5.8: Spread in interannual variability of annual and seasonal area averaged soil moisture means, from 1982 - 2010, over Sudan. The radial direction represent uncertainty range (spread) in the magnitude of interannual variability (amplitudes) while azimuth direction represent uncertainty range in phase (interannual cycle).

monthly mean soil moisture were largely contributed by differences in magnitudes of interannual variabilities (amplitudes) as demonstrated by a rather large spread in radial direction (Figs. 5.8 and 5.9). Also, the ranges of uncertainties were higher during dry seasons than wet ones; MAM versus JJAS for Sudan (Fig. 5.8b compared to Fig. 5.8c), JJAS versus MAM and OND for EA (Fig. 5.9c compared to Fig. 5.9b and d), and JJAS versus MAM and OND

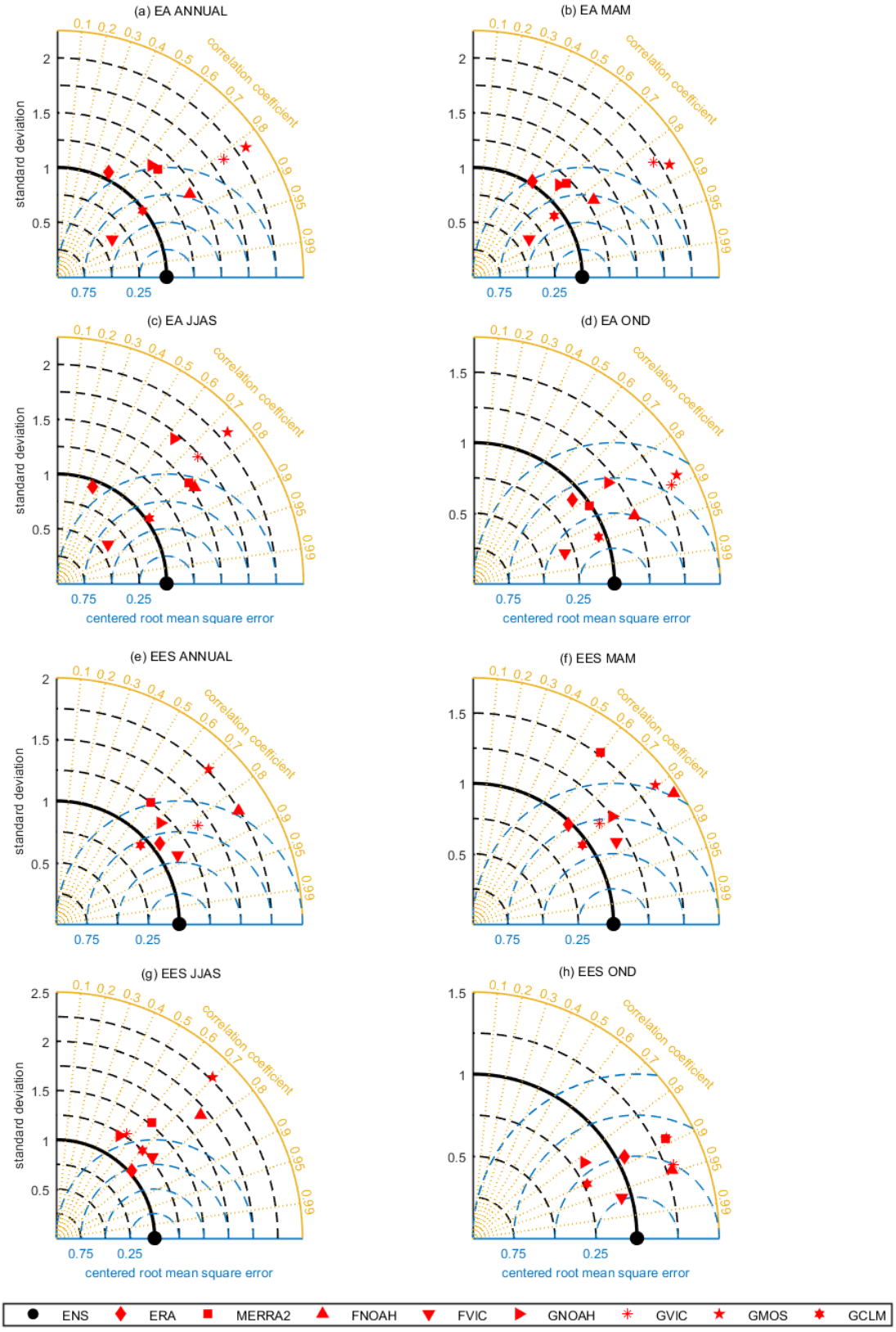

Figure 5.9: Same as Figure 5.8, but over EA (a-d) and East Ethiopia and Somalia (EES; e-h).

for EES (Fig. 5.9g compared to Fig. 5.9f and h). On the other hand, for Ethiopia and South Sudan, especially for annual and JJAS, the range of uncertainties are from both phase and magnitudes of spatial variability (Fig. 5.10). In addition, the ranges of uncertainties were higher during high soil moisture (wet) season than low soil moisture (dry) ones; JJAS versus MAM and OND for Ethiopia (Fig. 5.10c compared to Fig. 5.10b and d), and JJAS versus MAM and OND for South Sudan (Fig. 5.10g compared to Fig. 5.10f and h).

Since precipitation is one of the major factors determining the characteristics of the resulting soil moisture from model as was noted in Chapter 4 and in other studies (e.g., *Dirmeyer et al.*, 1999, 2004; *Entin et al.*, 1999), in EA (an area with very low topographical influence on precipitation if any) the uncertainties amongst rainfall product are low hence low uncertainties among resulting soil moisture products during rainfall seasons. On the contrary, during dry seasons when there is no much rainfall, the uncertainties are purely due to differences in model thresholds, which appears to be quite distinct for soil water (moisture) loss over EA, hence higher uncertainties. Unlike over EA, the topography over Ethiopian highlands and South Sudan have impact on rainfall leading to different precipitation values from different products hence higher uncertainty in precipitation (see, e.g., *Dinku et al.*, 2007, 2008; *Romilly and Gebremichael*, 2011). These uncertainties are translated into the resulting soil moisture when models are forced by these precipitation products and together with uncertainties from model threshold and direct impact of terrain on models leads to higher uncertainties during wet seasons. However, during dry seasons since there is no much precipitation the uncertainties are only due to model thresholds and influence of topography on the model hence lower uncertainties during dry seasons. The mixed performances of high spatial resolution (0.1° x 0.1° and 0.25° x 0.25°) versus low resolution (1° x 1°) in both the spatial pattern and interannual variability (Figs. 5.7, 5.8, 5.9 and 5.10) is an indication of lack of a link between spatial resolution and the performance of

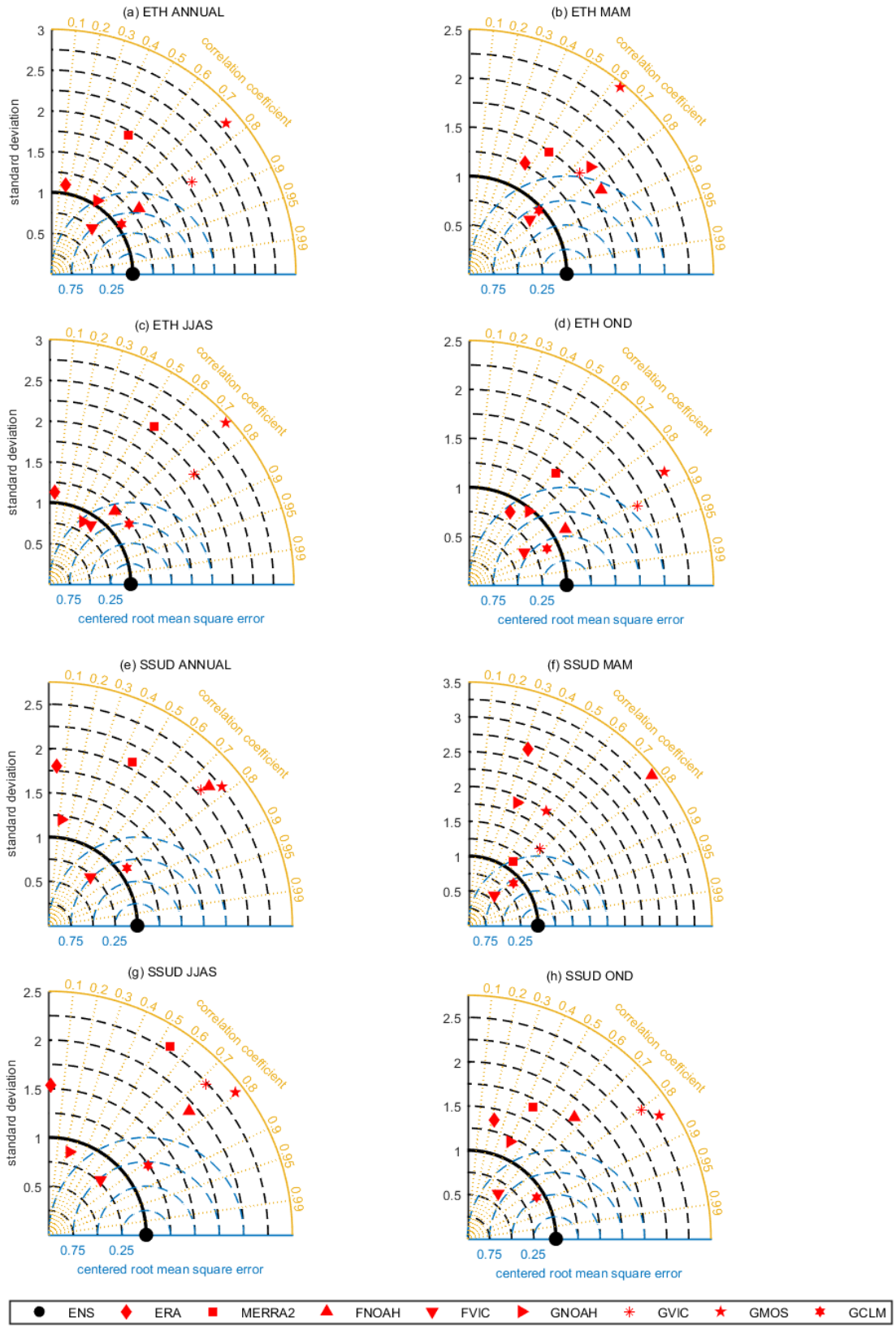

Figure 5.10: Same as Figure 5.8, but over Ethiopia highlands (a-d) and South Sudan (e-h).

the soil moisture products in the region. Finally, the range of uncertainties in interannual variability (annual and seasonal) over Ethiopian highland and South Sudan were higher than those over Sudan, EA, and EES (Fig. 5.10 vis-a-vis Figs. 5.8 and 5.9). This is consistent with uncertainty results from sections 5.3.1 and 5.3.2.1, and could be attributed to the impacts of topography, which is predominant over Ethiopian highlands and South Sudan (see, e.g., Chapter 4).

5.3.3 Spatio-temporal Soil Moisture Analysis

Other than the uncertainties in the model soil moisture products, it is important to understand how well they capture soil moisture spatio-temporal variability over the region. Since soil moisture is an integration of rainfall anomalies over time (*Sheffield and Wood*, 2008) and the fact that precipitation is the key model forcing parameter that determines the characteristics of the resulting soil moisture (*Crow et al.*, 2012; *Entin et al.*, 1999; *Dirmeyer et al.*, 2004), the spatio-temporal soil moisture variabilities are presented in relation to rainfall.

Principal component analysis of the soil moisture products resulted in two distinct dominant spatial patterns (modes) over GHA region across the products (Figs 5.11 and 5.12). The first mode is dominated by soil moisture variability over the high uni-modal rainfall regions of South Sudan and Ethiopian highlands (Fig. 5.11 compare with Fig. 2.2a, EOF1). From the percentage of variances explained by this mode across different products, three grouping of models emerges: ERA, MERRA2, and G_NOAH; F_NOAH, F_VIC, and CPC; and G_VIC, G_CLM, and G_MOS. Finally, all the GLDAS model variants except G_NOAH explained relatively lower percentage of variance in annual soil moisture variability under this mode. Like the uncertainties in sections 5.3.1 and **??**, the variabilities of the soil moisture modes are function of the forcing precipitation and the model thresholds as highlighted by different models with similar forcing precipitation (e.g., F_NOAH versus F_VIC), and similar models with different forcing precipitation (e.g., F_NOAH versus

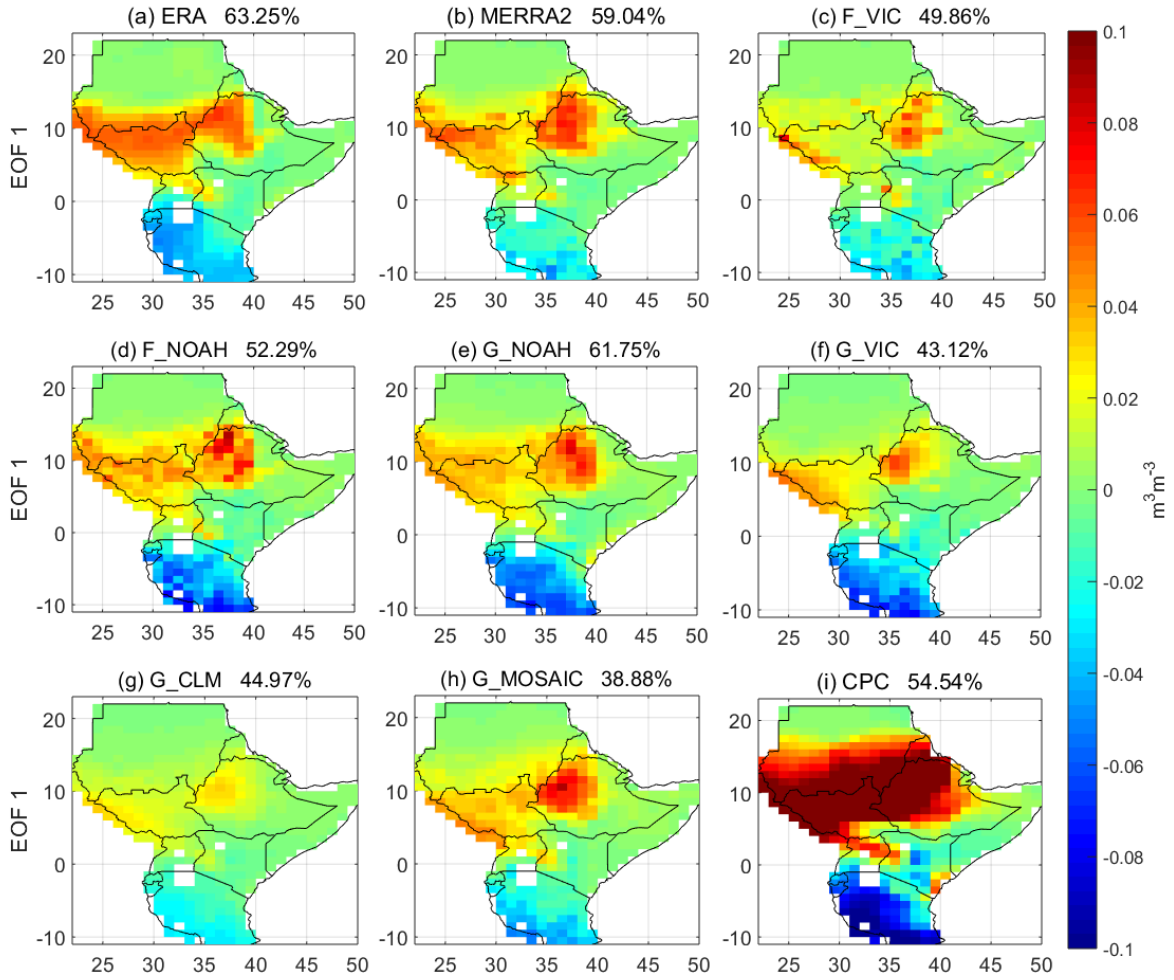

Figure 5.11: Soil moisture spatial patterns (principal component analysis mode 1). The spatial patterns are dominated by the uni-modal soil moisture variability over Sudan and Ethiopian highlands (compare with rainfall spatial viability, EOF 1, Fig. 2.2a)

G_NOAH) variability results (Figs. 5.11 and 5.12). Note the close percentages of variabilities explained by F_NOAH and F_VIC in relation to the relatively large difference in percentages of variabilities explained between F_NOAH and G_NOAH (Figs. 5.11c- e). This is consistent with the lower differences in percentage of areas under drought and different drought intensities between F_NOAH and F_VIC compared to the corresponding higher differences between F_NOAH and G_NOAH, that were observed in Chapter 4.

The second spatial pattern (mode) across most products is largely dominated by soil moisture variability in the bi-modal rainfall region of EA except for G_VIC,

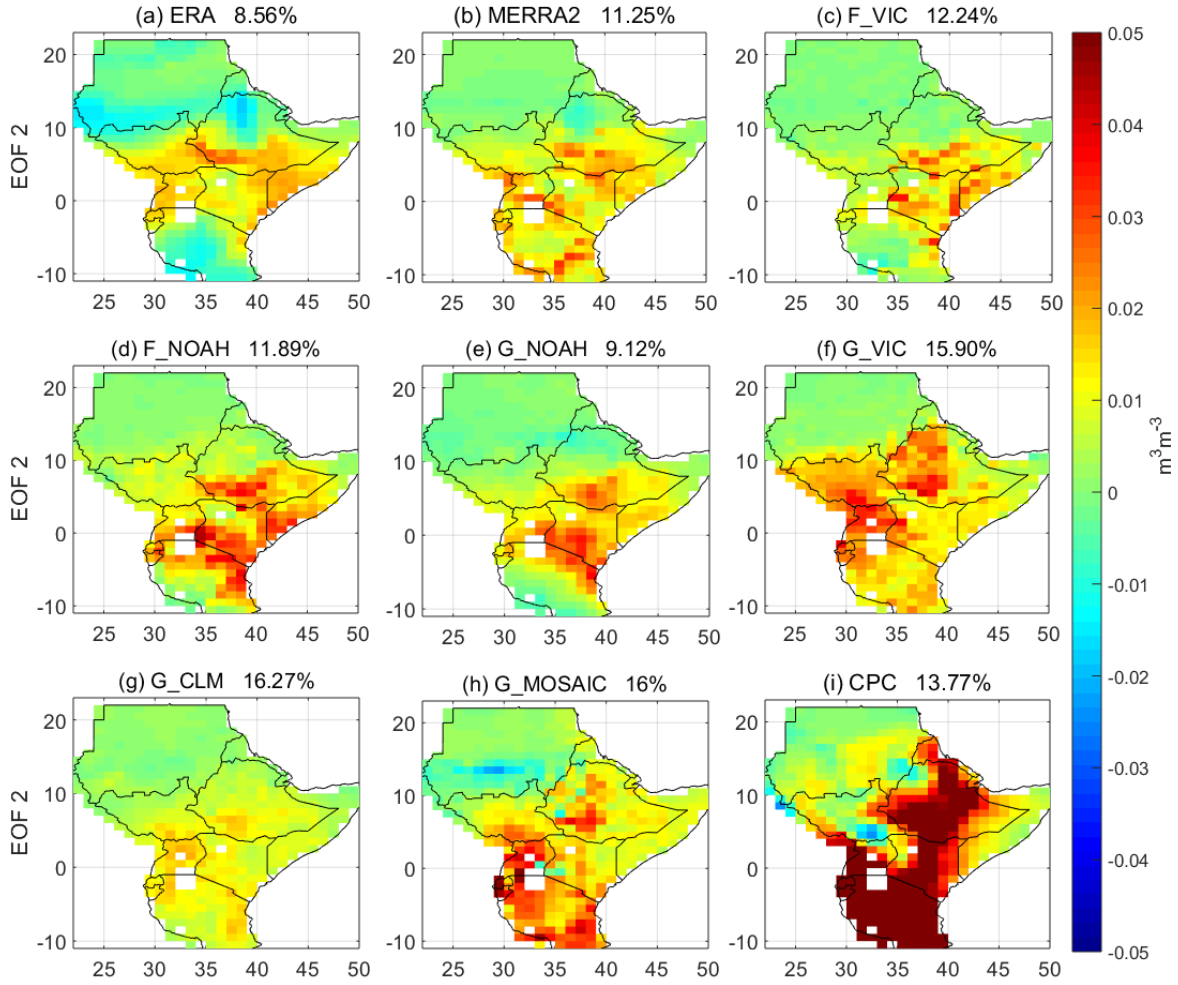

Figure 5.12: Soil moisture spatial patterns (principal component analysis mode 2). The spatial patterns are dominated by the bi-modal soil moisture variability over southern/eastern Ethiopia, Kenya, Uganda, and Tanzania (compare with rainfall spatial viability, EOF 2, Fig. 2.2b)

G_MOS, and CPC all of which have some overlap with the first mode (Fig. 5.12 compare with Fig. 2.2b, EOF2). Similar to the first mode, the role of forcing precipitation versus model differences and/or similarities stands out in the results (percentage of variabilities; Fig. 5.12c-e).

The temporal variabilities of the two dominant soil moisture modes are shown in Figures 5.13 and 5.15. The first mode of temporal variability is dominated by annual signals with a peak in August/September, one month after rainfall peak in July/August (Fig. 5.13 compared to Fig. 2.2c, PC1). The peak in

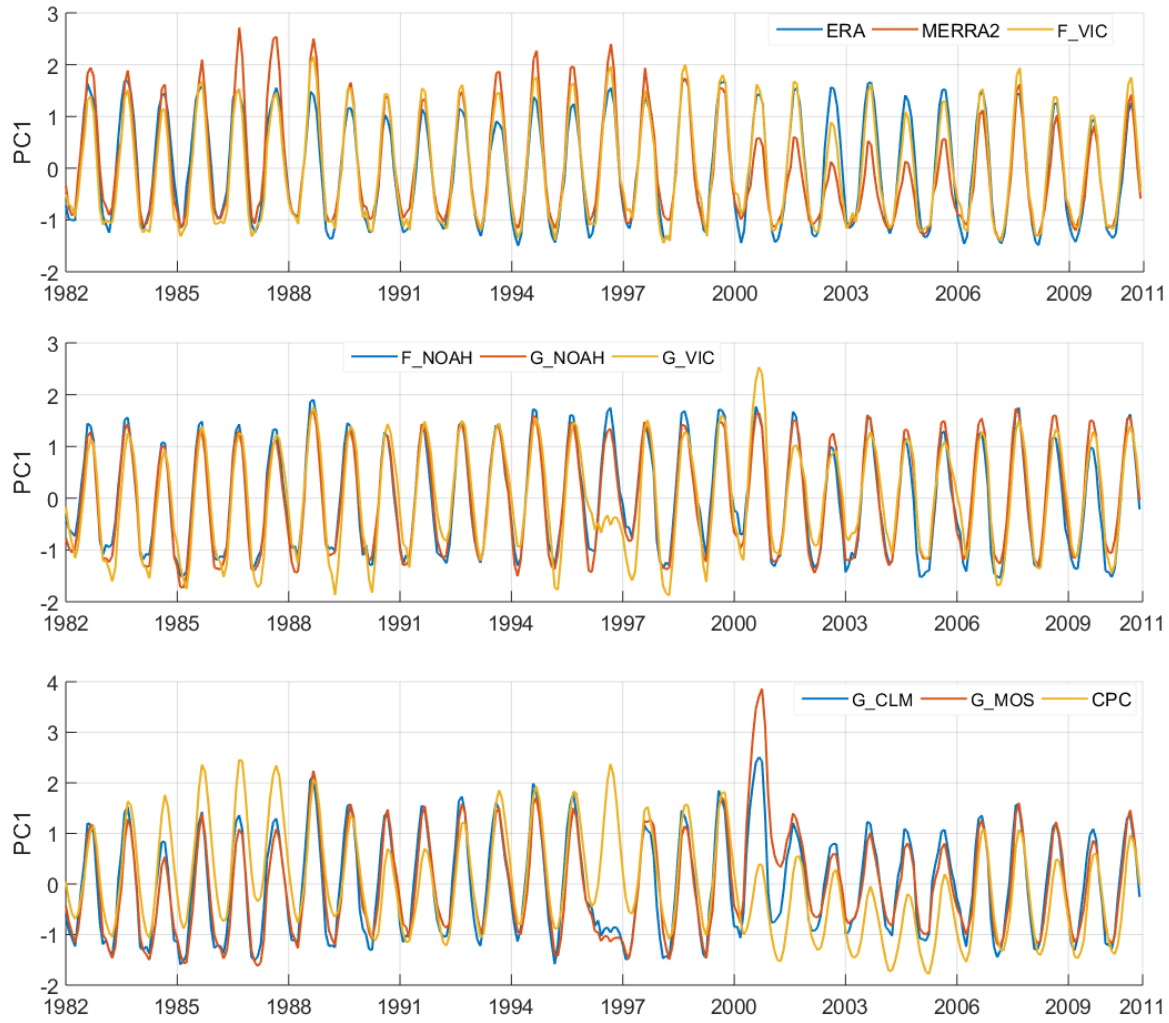

Figure 5.13: Temporal variability of soil moisture spatial patterns in Figure 5.11. Temporal variability dominated by annual soil moisture variability with peak being in August/September, a response to uni-modal rainfall with peaks in July/August, see Figure 2.2c, PC1.

August/September is further clearly depicted by the soil moisture seasonality (Fig. 5.14). G_VIC, G_CLM, and G_MOS failed to capture the annual peak in 1996 and over-estimated the annual peak in 2000. MERRA2 presents a relatively wet 1985 – 1988 and relatively drier 2000 – 2005, a pattern replicated by CPC though with shorter wet duration (1985 – 1987).

The second mode of temporal variability shows bi-modal moisture variability picked by MERRA2, ERA, F_VIC, F_NOAH, and G_NOAH with the first peak being in May and the second peak in November/December (Fig. 5.15). G_VIC,

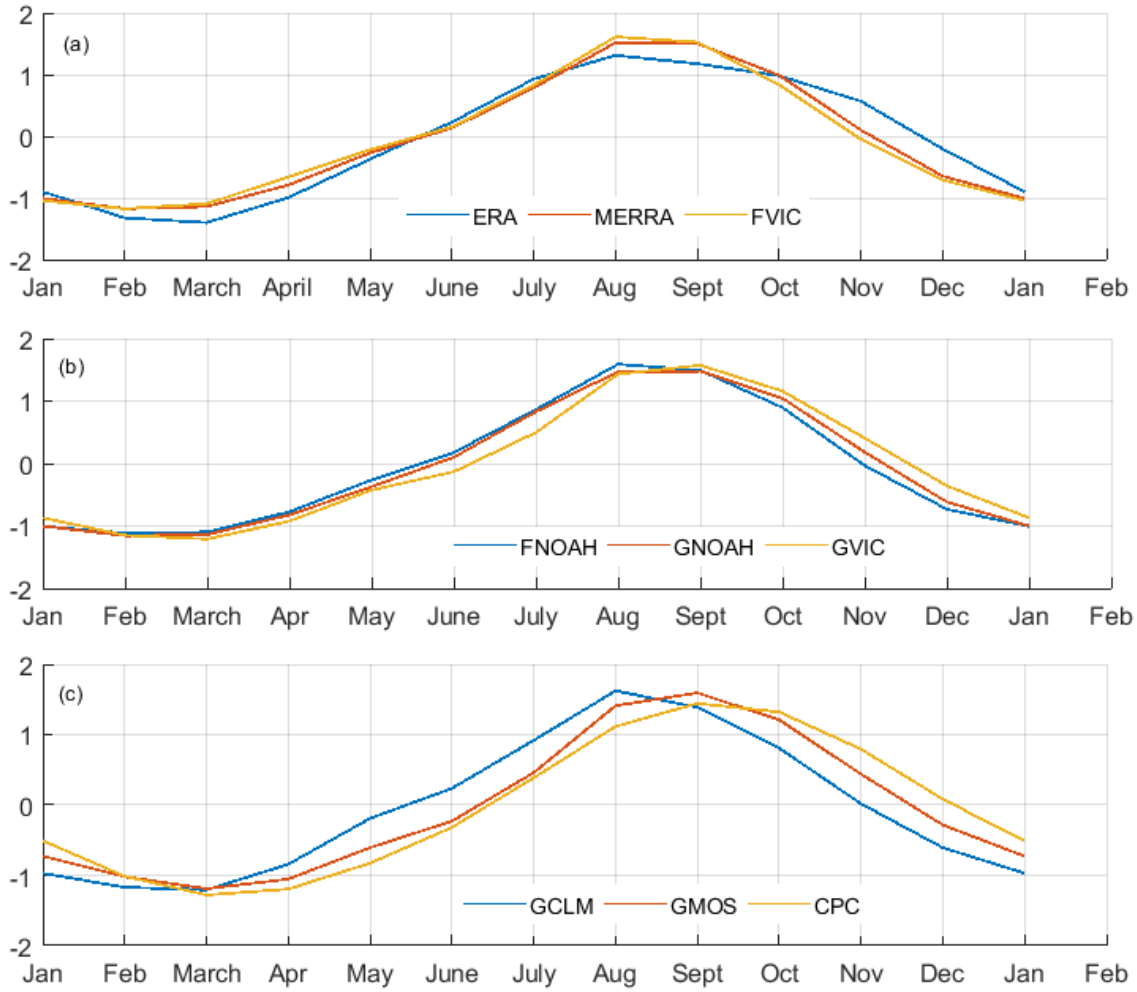

Figure 5.14: Soil moisture seasonality over the uni-modal rainfall regions of GHA (regions depicted by spatial patterns in Figure 5.11). The soil moisture values have been standardized.

CPC, G_CLM, and G_MOS seem to pick the first peak (May) a response to the main rainfall season while moisture variability in response to short rain (OND) is poorly captured. This is more clear when considering soil moisture seasonality over the bi-modal region (Fig. 5.16). Also, G_VIC, G_CLM, and G_MOS missed the May peak in 1996. The failure of G_VIC, G_CLM, and G_MOS in 1996 to pick both the modes could be attributed to the high uncertainties reported in the meteorological forcing data between 1995 and 1997 (see, e.g., *LDAS*, 2016). Most of the soil moisture products clearly showed high moisture years of 1985, 1990, 1997, and 2006 and low moisture years of 1983 – 1984, 1999 – 2002, 2005

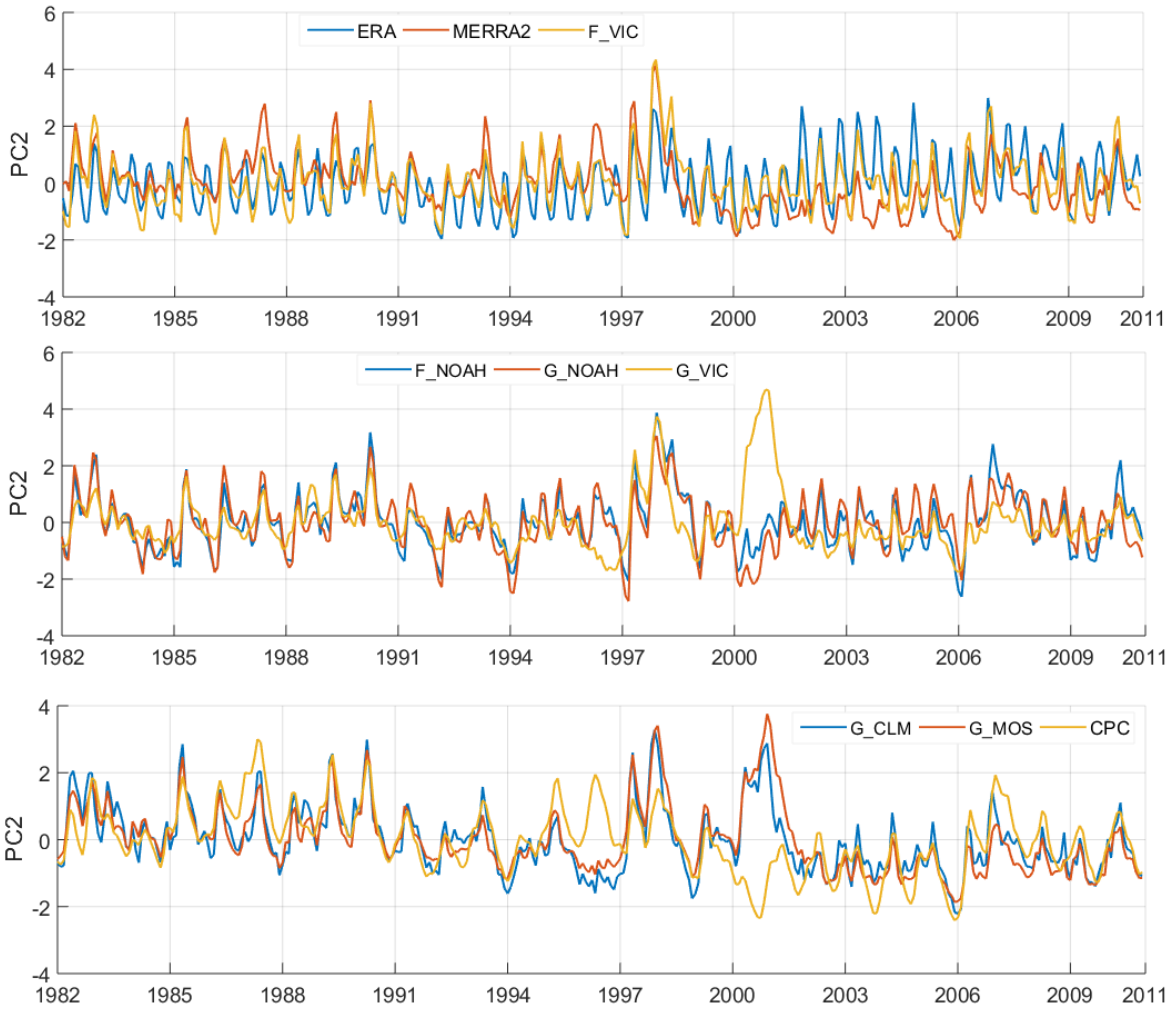

Figure 5.15: Temporal variability of soil moisture spatial patterns in Figure 5.12. Temporal variability dominated by bimodal soil moisture variability with peaks being in May and November/December, a response to bimodal rainfall with peaks in April and October/November, see Figure 2.2c, PC2.

and 2009 corresponding to high and low rainfall durations, respectively (compare with, Fig. 2.2c, PC1 and PC2). The moisture temporal variability following rainfall is expected since it is an integration of rainfall anomalies and also at the scales (meteorological) considered, the variability of soil moisture is governed by rainfall and evapotranspiration (*Entin et al.*, 2000).

To further analyze how best the products capture moisture conditions over the region, the amplitudes of the annual and bi-modal temporal variabilities were

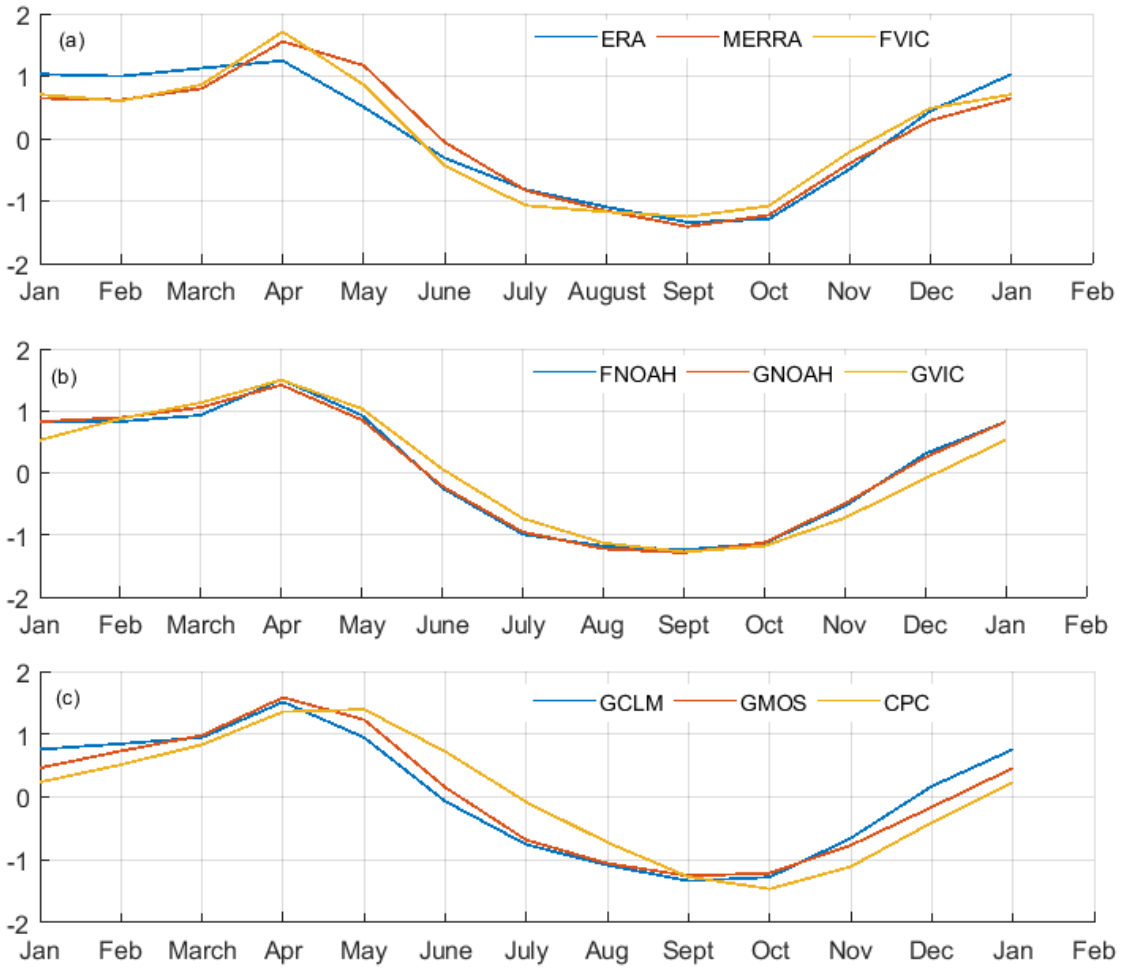

Figure 5.16: Soil moisture seasonality over the bi-modal rainfall regions of GHA (EA; regions depicted by spatial patterns in Figure 5.12). The soil moisture values have been standardized. G_VIC, CPC, G_CLM, and G_MOS poorly captures the second peak associated with OND rainfall.

compared to known drought events (see e.g., *IFRC* (2011); *Viste et al.* (2013); *Gebrehiwot et al.* (2011); *Elagib and Elhag* (2011); *Nicholson* (2014a); *Williams and Funk* (2011); *Masih et al.* (2014); *Agutu et al.* (2017); and Chapters 3 and 4 for drought events) to check the soil moisture response. It is expected that during a drought year, there will be low soil moisture and consequently the amplitudes for those particular years would be lower. The low amplitude and drought years had more matches over the bi-modal soil moisture variability region

Table 5.2: A comparison of soil moisture temporal variability over UGHA (Ethiopia highlands, Sudan, and South Sudan) with past drought episodes. Soil moisture (variability) amplitudes are matched against known drought episodes to evaluate how well the various soil moisture products fit the region. The amplitudes are expected to be low during drought episodes.

Drought year	ERA	MERRA2	F_VIC	F_NOAH	G_NOAH	G_VIC	G_CLM	G_MOS	CPC
1983/1984	0.5	0.5	1	1	1	1	1	1	0
1987	0	0	0	0.5	0.5	0.5	0.5	0.5	0
1989/1990/1991	1	0.5	0.5	0.5	0.5	0.5	0	0	1
1996	*0*	0	0	0	0	1	1	1	0
1997	0	0.5	0.5	0.5	0.5	0.5	0	0	0
1998	0	0	0	0	0	0	0	0	0
1999	0	0	0	0	0	0	0	0	0
2002/2003	0.5	1	1	1	1	1	1	1	1
2005	0	1	0.5	1	0	1	0	0.5	1
2008	0.5	0.5	0.5	1	0	0.5	0	0	1
2009	1	1	1	1	0	0	0.5	0.5	1
% captured full	18	27	27	45	9	36	27	27	45
% captured partially	27	36.5	36.5	27.5	27	36	18	27	0
% missed	55	36.5	36.5	27.5	64	28	55	46	55

Note: 0 - product missed that drought episode, 0.5 - product partially captured drought episode, and 1 - product captured drought episode.

than the uni-modal variability areas (Tables 5.2 and 5.3). This points to a better performance of the soil moisture products over EA compared to the Ethiopian highland regions, and could be attributed to better quality of soil moisture products over EA and the adverse impact of complex topographical changes on soil moisture variability over Ethiopian highland regions. This is consistent with results in sections 5.3.1 and **??**; low uncertainties implies better performance and vice versa. Also, F_NOAH, F_VIC, and MERRA2 showed consistently better performances across the two regions compared to the rest of the soil moisture products. As in section 5.3.1, their performance is attributed to superior quality of the forcing precipitation.

Table 5.3: Same as Table 5.2 but over East Africa (Kenya, Uganda,Tanzania, southern Ethiopia, and Somalia).

Drought years	ERA	MERRA2	F_VIC	F_NOAH	G_NOAH	G_VIC	G_CLM	G_MOS	CPC
1983-1984	1	1	1	1	1	1	1	1	1
1988	0.5	0.5	0.5	0.5	0.5	0	0.5	0.5	0.5
1991/1992	1	1	1	1	0.5	1	1	1	1
1993	1	1	1	1	1	1	1	1	1
1996	1	0.5	1	1	1	0	0	0	0
1998	0.5	1	0.5	0.5	0.5	1	0	0	0
2000-2001	1	1	1	1	1	0	0	0	0
2004	0.5	0.5	0.5	1	0	1	1	1	1
2005/2006	0	1	1	1	1	1	1	1	1
2009	0.5	1	1	1	1	1	0.5	0.5	0.5
2010	0.5	1	1	1	1	1	1	0.5	0.5
% captured full	45	73	73	82	64	73	55	45	45
% captured partially	45	27	27	18	27	0	18	27	27
% missed	10	0	0	0	9	27	27	28	28

Note: 0 - product missed that drought episode, 0.5 - product partially captured drought episode, and 1 - product captured drought episode.

5.3.4 Links to Global Tele-connection

Due to forecasted negative impacts of climate change and/or variability on rain-fed agriculture, which the population of the region depends on, the two dominant temporal modes of soil moisture variability were correlated with two climate indices (IOD and ENSO) known to impact on rainfall over the GHA region. On average, soil moisture temporal variability over East Africa (PC2) showed stronger associations with both IOD and ENSO compared to associations between PC1 (dominated by soil moisture variability over Ethiopian highlands and South Sudan) and the two climate indices (Table 5.4).

This follows from the fact that the uni-modal rainfall over Ethiopian highlands and South Sudan (which dominates PC1) originates from rainforest over Congo Basin in response to westerly winds and low pressure created by ITCZ (*Williams et al.*, 2012). This rainfall has no direct association with IOD or ENSO hence the moisture variability associated with it is not expected to have meaningful relationships with either IOD or ENSO. On the other hand, the bi-modal rainfall over EA is associated with IOD and ENSO, which do occur independently and

Table 5.4: Relationship between temporal soil moisture variability modes and global climate indices. Bimodal soil moisture variability (PC2) have stronger association with both IOD and ENSO. Non-significant correlations are in italics ($p < 0.05$).

PC	ERA	MERRA2	F_VIC	F_NOAH	G_NOAH	G_VIC	G_CLM	G_MOS	CPC	Climate index
PC1	*0.0856*	*0.1047*	*0.0839*	*0.0907*	0.1252	0.1503	0.1752	0.2103	*0.0543*	IOD
PC2	0.1255	0.1679	0.2667	0.2203	0.1547	0.2661	0.1827	0.1150	*-0.0361*	IOD
PC1	*-0.0101*	*0.0325*	*-0.0908*	*-0.0986*	*-0.0562*	*-0.1040*	*-0.0591*	*-0.0984*	*-0.0515*	ENSO
PC2	*0.0769*	0.3184	0.2717	0.2428	0.2897	0.1321	0.2423	0.1963	0.2483	ENSO

concurrently (*Bowden and Semazzi*, 2007; *Saji et al.*, 1999). It then follows that the soil moisture associated with it has relationships with both ENSO and IOD.

5.4 Concluding Remarks

The Chapter applied generalized TCH method to evaluate the uncertainties of the following soil moisture products over GHA; MERRA2, ERA, F_NOAH, F_VIC, G_NOAH, G_VIC, G_CLM, G_MOS, and CPC. The Chapter further analyzed the uncertainty ranges/characteristics in spatial patterns and interannual variabilities of individual soil moisture products in relation to their ensemble mean using Taylor diagrams. In addition, the Chapter employed PCA to analyze the spatio-temporal variabilities of the soil moisture products and compared it to rainfall variability and drought years. Finally, the temporal variabilities were correlated with IOD and ENSO.

The major findings of this Chapter were:

(i) From generalized TCH analyses, the spatial distribution of uncertainties showed high magnitudes of uncertainties associated with high rainfall areas and low magnitudes of uncertainties associated with low rainfall areas. This was supported by inter-data spread which also showed larger differences (uncertainties) between individual soil moisture products over high soil moisture areas and low uncertainties over dry areas, for annual, MAM, JJAS, and OND.

(ii) The magnitude of uncertainties over complex topographical changing regions of Ethiopian highlands were almost twice the magnitudes of uncertainties over relatively flat EA region.

(iii) The uncertainties were attributed to quality of forcing precipitation, different model physics, and topographical changes.

(iv) MERRA2 and F_NOAH had consistently low uncertainties across the region while CPC had the highest uncertainty.

(v) Visual analysis of spatial variabilities using Taylor diagram indicated the high range of uncertainties in spatial variabilities between the soil moisture products to come from the magnitude of spatial variability than uncertainty in spatial patterns.

(vi) Interannual variability analysis of spatial averages of monthly annual, MAM, JJAS, and OND soil moisture means showed higher magnitude of uncertainties across soil moisture products on the wet season (rainfall months) than dry ones over Ethiopia highlands and South Sudan while Sudan, East Africa, and Eastern Ethiopia and Somalia had higher uncertainties during dry seasons than wet ones.

(vii) Higher magnitude of uncertainties over Sudan, East Africa, and Eastern Ethiopia and Somalia were from differences in magnitude of interannual variabilities (interannual amplitudes) while over Ethiopia and South Sudan the uncertainties were from differences in both magnitude of interannual variabilities and phase.

(viii) The range and magnitude of uncertainties were independent of individual soil moisture spatial resolution.

(ix) PCA resulted in two dominant distinct modes; the first mode was dominated by unimodal moisture variability over Sudan, South Sudan, and Ethiopian

highlands while the second mode was dominated by bi-modal moisture variability over EA, Eastern Ethiopia, and Somalia.

(x) The temporal variabilities of both modes were consistent with rainfall variabilities over the two regions with G_VIC, CPC, G_CLM, and G_MOS missing the variability associated with OND rainfall over EA.

(xi) The comparison of the magnitude of amplitudes of temporal variabilities with known drought years had all the products performing better over EA compared to Ethiopian highland, South Sudan, and Sudan regions. These results mirrored those of uncertainty distributions. MERRA2 and F_NOAH were again more consistent across the whole region.

(xii) Overal, the following moisture products were found to be the most suitable over GHA region; MERRA2, ERA, F_NOAH, and F_VIC.

(xiii) The correlation analysis showed soil moisture temporal variability over EA having relationships with both ENSO and IOD while soil moisture temporal variability over Sudan, South Sudan, and Ethiopia highland regions did not show any meaningful relationship with both ENSO and IOD.

The results of this Chapter are important as they contribute to the knowledge of uncertainties and variabilities of the major LSM-derived soil moisture products over GHA and help build more confidence in the products hence more LSM-derived soil-moisture based agricultural drought research. Soil moisture being the most accurate indicator of available plant water is very critical to agricultural drought research and yield prediction. This together with results from Chapters 3 and 4 contribute to further understanding of agricultural drought for a region that plunges into food insecurity whenever droughts occur (see section 1.2). Effective understanding of agricultural drought for such a region could contribute to improvements in mitigation measures and responses to drought impacts hence enhancement of food security. Other than

drought, other factors noted to contribute to food insecurity included lower crop yields due to poor water control, negative impacts of climate change on rain-fed agriculture and surface water sources, and increase in food demand due to population growth (see section 1.2). In an attempt to address these additional factors, the next Chapter explores the use of GRACE for large scale groundwater monitoring and the potential for irrigated agriculture in the groundwater regions. Groundwater is likely to be critical in bridging the food needs through groundwater irrigated agriculture and therefore its sustainable utilization would be extremely important to policy and decision makers. The sustainable exploitation of groundwater can only be achieved through continuous monitoring.

6 GRACE-derived Groundwater Changes over GHA: Temporal Variability and the Potential for Irrigated Agriculture

6.1 Introductory Remarks

Groundwater is a critical source of freshwater for human-related uses (*Taylor et al.*, 2013). Globally, it contributes 42%, 36%, and 27% of water used for irrigation, households, and manufacturing, respectively (*Döll et al.*, 2012), and is the third largest water storage after oceans (salty water) and cryosphere (water in its solid state of snow and ice), but by far the largest available reservoir of fresh water (*Kundzewicz and Döll*, 2009). In Africa, groundwater is estimated to be about 0.66 *million* km^3 (*MacDonald et al.*, 2012), compared to annual average rainfall of about 0.02 *million* km^3 (*New et al.*, 2000), while freshwater stored in lakes is estimated to be 0.03 *million* km^3 (*Shiklomanov and Rodda*, 2004). Groundwater holds numerous advantages over surface water sources, e.g., reliable availability during drought periods due to slow response to climate changes (*Calow et al.*, 1997, 2010), less vulnerability to pollution (*Kundzewicz and Döll*, 2009), and a reliable source of safe and clean drinking water in arid and semi-arid regions (*Döll*, 2009). In addition, groundwater offers better accessibility as surface water sources are normally far and widely spaced, seasonal, or are not available in arid and semi-arid areas (*Döll et al.*, 2012). Despite the significant role played by groundwater in irrigation globally and its numerous advantages listed above (see also *Wichelns*, 2014), its use in irrigated agriculture in Africa has remained rather low.

The level of irrigation in Africa is generally low and agriculture is mainly rain-fed. On average, 5.5% of the cultivated land over the continent is equipped for irrigated agriculture while for East Africa within the Greater Horn of Africa (GHA), this is only 1.5%. Of this 1.5%, only 3.4% is equipped for irrigation using groundwater (*Siebert et al.*, 2010). The limited use of groundwater for

irrigated agriculture in the wider GHA region could be attributed to various factors such as; lack of detailed analysis of countrywide groundwater irrigation potential, existence of large swathes of land with high potential for surface water irrigated agriculture, limited information on aquifer potentials and yields of individual boreholes, inadequate groundwater resource management plans, and inadequate groundwater related knowledge by majority of the population leading to inappropriate groundwater development (see, e.g., *Kashaigili*, 2010; *Mumma et al.*, 2011). However, with a high population growth rate (see, e.g., *Ashton and Turton*, 2009) and impact of climate change on rain-fed agriculture and surface water sources, further development and utilization of groundwater may becomes essential for increased food production (*Moore and Williams*, 2014; *MacDonald et al.*, 2012; *Kundzewicz and Döll*, 2009; *Funk and Brown*, 2009). Indeed, *Alley and Konikow* (2015) have pointed to the fact that for Sub-Sahara Africa, increased groundwater use could significantly improve the wellbeing of its inhabitants. Further, *Xie et al.* (2014) have shown the potential for profitable small holder irrigation expansion in sub-Sahara Africa.

Furthermore, the GHA region has limited long-term groundwater monitoring infrastructure, resulting in little or no long-term groundwater monitoring data. In cases where they are available, often inconsistencies exist due to different methodologies used at different times making comparisons rather difficult, and the resulting trends unclear (*Comte et al.*, 2016). This infrastructural limitation has led to sparse in-situ measurements contributing to lack of or limited knowledge on groundwater level changes. The lack of long term groundwater level changes has contributed to decision makers not having a better understanding of the long term sustainability of the aquifers as sources of water supply. In addition, without the long term groundwater level changes, the impact of climate change (and/or variability) on groundwater levels over the region remains largely unknown (see, e.g., *Becker et al.*, 2010; *Alley*, 2007). This situation calls for additional and/or further studies on groundwater variability (level changes) and its relation to

climate change (and/or variability).

Groundwater level changes have been determined using various methods, e.g., groundwater well level observations in combination with estimated storage capacities, using models, e.g., WaterGap Hydrological Model (WGHM; *Döll et al.*, 2014) and satellite based approaches, e.g., Gravity Recovery and Climate Change Experiment (GRACE; *Tapley et al.*, 2004). The potentials and limitations of using GRACE satellites to assess groundwater depletion and dynamics have been presented in, e.g., *Castellazzi et al.* (2016). Furthermore, its ability to provide a wider picture that could benefit the setting of broader regional and national policies has earned it consideration as one of the hydrologists' toolbox (see, e.g., *Alley and Konikow*, 2015). Over Africa, its application to investigate trends and seasonality cycles of groundwater is reported, e.g, in *Moore and Williams* (2014). Other studies in the region that present groundwater related information include, e.g., *MacDonald et al.* (2012), *Altchenko and Villholth* (2013), *Abiye* (2010), *Gossel et al.* (2004), *Taylor et al.* (2012), *Comte et al.* (2016).

For GHA, a region experiencing groundwater data deficiency (*Comte et al.*, 2016), use of GRACE products to provide a broader picture on changes in groundwater at a regional scale could be useful in; better understanding of the long term sustainability of groundwater (aquifers) as sources of water supply, making appropriate policy formulation and/or choices, and assessing the impact of climate change (and/or variability) on groundwater by decision makers and/or regional bodies e.g., Intergovernmental Authority on Development (IGAD) and the East African Community (EAC) secretariat. To this end, this Chapter exploits the advantages of GRACE to study groundwater changes over the entire GHA region and the associated impacts of climate variabilities. The study exploits the advantage of Independent Component Analysis (ICA, *Comon*, 1994; *Cardoso*, 1999; *Forootan and Kusche*, 2013), a fourth-order statistical method, to localize the GRACE-derived groundwater changes into smaller locations associated with aquifers. This enables a more localized

analysis of groundwater temporal variability and their association to climate variability, a feat currently not possible due to scarce groundwater change monitoring information in the region. Specifically, this Chapter aims at (i) employing ICA method to localize GRACE-derived groundwater changes into their respective groundwater locations and analyse the corresponding temporal variabilities and their links to climate variability, and (ii), exploring the irrigation potentials of the localized groundwater regions in (i) above.

6.2 Hydrogeology of Greater Horn of Africa

Greater Horn of Africa (Fig. 6.1) is prone to impacts of climate change extremes (droughts and floods), which is projected to impact negatively on per capita food production (see, e.g., *Boko et al.*, 2007; *Funk and Brown*, 2009; *Niang et al.*, 2014). Groundwater, if sustainably exploited could help increase food production through groundwater irrigated agriculture.

Groundwater occurrence depends on geology, history of weathering, and the recharge of groundwater (i.e., dependent on rainfall, rock types, and land use and/or land cover over the recharge region; *MacDonald et al.*, 2008). Over Africa, most (high quantities) of groundwater occur in large sedimentary aquifers in Northern Africa and were recharged more than 5000 years ago when the climate over the Sahel was wet (*Scanlon et al.*, 2006). Over GHA and the wider African continent, groundwater can be categorised to occur in four major rock types namely; crystalline basement rocks, consolidated sedimentary rocks, volcanic rocks, and unconsolidated sediments (Fig. 6.1a). These blocks have the following average groundwater potentials; crystalline (low to moderate), consolidated (moderate to high), volcanic (low to high), and unconsolidated (low to high), with the potentials being dependent on level of fracturing and/or weathering, and individual composition/rock elements (*MacDonald et al.*, 2008). The quality of groundwater is inherently dependent on the chemical composition of the aquifer rocks. Some of the major aquifers over GHA are

shown in Fig. 6.1b, with their regional characteristics summarised in Table 6.1 (see *Altchenko and Villholth*, 2013, for additional information).

6.3 Data and Methods

The dataset used in this Chapter is summarised in Table 6.2, while their detailed descriptions are given in Chapter 2.

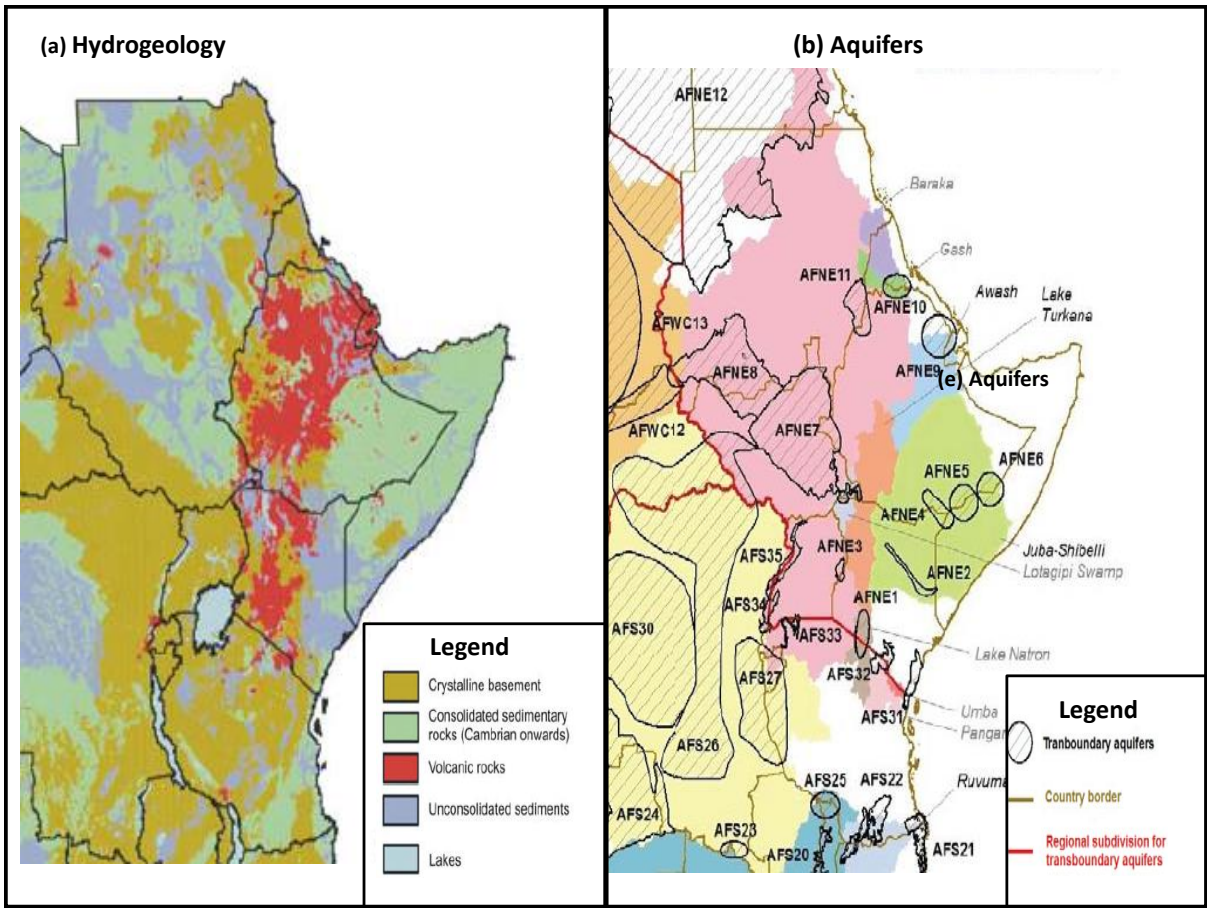

Figure 6.1: Greater Horn of Africa (a) Hydrogeological characteristics (adapted from *MacDonald et al.*, 2008), and (b) Selected aquifers (adapted from *Altchenko and Villholth*, 2013). The aquifers characteristics are presented in Table 6.1 .

Table 6.1: Summary of GHA aquifers' regional characteristics. Table adapted from *Altchenko and Villholth* (2013). Aquifer locations are showed in Fig. 6.1b.

ID	NAME	POPULATION	AREA (km^2)	ID	NAME	POPULATION	AREA (km^2)
AFNE1	Rift aquifer	279 000	21 150	AFNE12	Nubian Sandstone	67 320 500	2 608 000
AFNE2	Merti aquifer	129 000	13 500	AFS21	Coastal sedimentary basin 3	794 000	23 000
AFNE3	Mount Elgon	806 550	5 400	AFS22	Karoo Sandstone	214 500	40 000
AFNE4	Dawa	223 150	24 000	AFS25	Weathered basement	852 000	25 842
AFNE5	Juba aquifer	197 600	34 600	AFS26	Karoo Carbonate	9 400 000	941 100
AFNE6	Shebelle aquifer	334 400	31 000	AFS27	Tanganyika aquifer	11 940 000	222 300
AFNE7	Sudd basin	2 926 500	331 600	AFS31	Coastal sedimentary basin 1	2 150 000	16 800
AFNE8	Baggara basin	2 433 500	239 300	AFS32	Kilimanjaro aquifer	1 396 000	14 600
AFNE9	Awash valley basin	627 400	50 700	AFS33	Kagere aquifer	493 500	5 800
AFNE10	Maerb aquifer	1 827 900	22 800	AFS34	Mgahinga	1 151 000	4 400
AFNE11	Gedaref	732 000	38 700	AFS35	Western Rift Valley sediment	1 151 000	29 500

Table 6.2: A summary of the dataset employed in this Chapter

Data	Period	Spatial resolution
GRACE	2003 - 2014	1° by 1°
GLDAS(TWS, soil moisture, and canopy water content)	2003 - 2014	1° by 1°
Satellite Altimetry	2003 - 2014	N/A
WGHM groundwater changes	2003 - 2009	0.5° by 0.5°
Climate indices (IOD and ENSO)	2003 - 2014	N/A
TRMM	2003 - 2014	0.25° by 0.25°

6.3.1 Spatio-temporal GRACE-derived Groundwater Changes Analysis

6.3.1.1 GRACE-derived Groundwater

GRACE provides monthly global mass changes, which over the continents have been equated to changes in terrestrial water storage (TWS). These changes are quantified as combinations of different components i.e., changes in biomass/canopy water content, accumulated soil moisture, changes in surface water storage, and changes in groundwater (see, e.g., *Longuevergne et al.*, 2010; *Moore and Williams*, 2014, and the references therein). Over GHA, changes in groundwater (after removal of the undesired components of TWS) can be

quantified as (e.g., *Castellazzi et al.*, 2016)

$$\Delta GW = \Delta TWS - (\Delta SW + \Delta CW + \Delta SM), \tag{6.1}$$

with ΔGW being changes in groundwater, ΔTWS changes in terrestrial water storage, ΔSW changes in surface water storage, ΔCW changes in canopy water content, and ΔSM changes in soil moisture. Changes in surface water (ΔSW) was derived through defining lake Kernel function using lakes' geodetic boundary coordinates with 1 (one) unit of water over the respective lake and 0 (zero) elsewhere over the region as

$$\partial_{lake}(\phi, \lambda) = \left\{ \begin{array}{c} 1, over\ lake \\ 0, elsewhere \end{array} \right\}, \tag{6.2}$$

where ϕ and λ are the geodetic latitude and longitude, respectively. Since GRACE fields are represented in terms of spherical harmonics, the lake kernel function (equation 6.2) is then expressed as (*Moore and Williams*, 2014)

$$\partial_{lake}(\phi, \lambda) = \frac{1}{4\pi} \sum_{l=0}^{l_{max}} \sum_{m=0}^{l} (C_{l,m}^{lake} \cos m\lambda + S_{l,m}^{lake} \sin m\lambda) P_{l,m}(\sin \phi), \tag{6.3}$$

where $P_{l,m}$ is the normalised associated Legendre function of degree l and order m, and $C_{l,m}^{lake}$ and $S_{l,m}^{lake}$ the dimensionless lakes' spherical harmonic coefficients. The summation in equation 6.3 was restricted to $l_{max} = 60$ in line with CSR RL05 monthly spherical harmonic coefficients used herein. Figure 6.2 shows the kernel functions of the considered lakes as per equation 6.3, whose coefficients were scaled with respective altimetry level changes to give changes in surface water, ΔSW.

Following the accounting of ΔSW using satellite altimetry scaled lake kernel functions, and ΔCW and ΔSM using GLDAS hydrological model, the derived groundwater changes (ΔGW) still contain some uncertainties (δGW). These

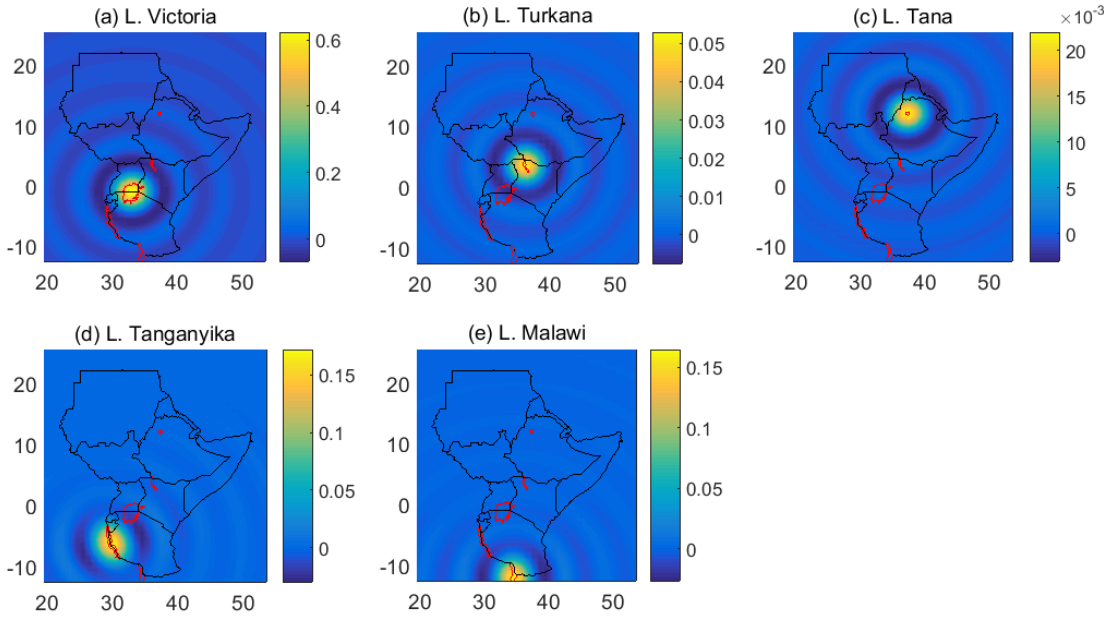

Figure 6.2: Greater Horn of Africa Lakes' kernel (coefficient) functions. The areas and minimum/maximum values for the kernel functions are (a) lake Victoria ($68,800km^2$, min/max $-0.0674/0.6235$), (b) lake Turkana ($6,405km^2$, min/max $-0.0074/0.0529$), (c) lake Tana ($2,156km^2$, min/max $-0.003/0.0220$), (d) lake Tanganyika ($39,200km^2$, min/max $-0.0298/0.1722$), (e) lake Malawi ($29,600km^2$, min/max $-0.0264/0.1647$). Lake coefficient function depends on the area and shape of the lake. Circular/spherical shapes results in higher lake coefficients compared to narrow elongated ones.

uncertainties arise from GLDAS-derived components, surface water variability corrections, and other unaccounted for smaller surface water bodies, e.g., Lakes Edward and Kyoga, the Sudd-wetlands, etc. Assuming that ΔGW is sufficiently larger than δGW (i.e., $\Delta GW >>> \delta GW$, see more details in section 6.3.1.2), the estimated ΔGW can sufficiently be assumed to represent groundwater changes over the GHA region, which following *Döll et al.* (2014) can be expressed as

$$\Delta GW = R - Q - B + L, \tag{6.4}$$

where R is diffuse recharge (largely soil moisture percolating into groundwater), Q is net abstraction (groundwater withdrawals minus return flow from irrigation with both surface water and groundwater), B is base-flow from groundwater to

surface water bodies, and L recharge from underground streams/runoff.

6.3.1.2 Evaluation of GRACE-derived Groundwater Changes Using WGHM Model

Due to lack of in-situ groundwater data over GHA, the GRACE-derived groundwater changes (ΔGW) were compared to those obtained from WGHM model as the model has been found to adequately capture groundwater changes (see, *Döll et al.*, 2014). In *Döll et al.* (2014), WGHM groundwater changes were compared with independent estimates (observations, local scale modelling, and GRACE-derived estimates) across various locations globally that included North Western Sahara Aquifer and Nubian Sandstone Aquifer, which falls within the study region of the current work. Although WGHM model has been found to adequately capture groundwater changes over various locations globally, being a model it suffers from various uncertainties (see Chapters 4 and 5, for model uncertainties) thus does not represent in-situ groundwater changes 100%. Nevertheless, such comparison is standard and has been applied, e.g., in *Döll et al.* (2014); *Rajner and Liwosz* (2017); *Zhang et al.* (2017); *Hu et al.* (2017). The results of GRACE-derived groundwater changes captured similar temporal variability over the region as those derived from WGHM variants (WGHM IRR_70_S (limited irrigation) and WGHM_NOUSE), albeit with stronger amplitudes (Fig. 6.3a). The correlation between GRACE-derived groundwater changes and those of WGHM IRR_70_S and WGHM_NOUSE were 0.7147 and 0.7173, respectively (significant at 95% confidence level). Such strong correlation validates the assumption of relatively small δGW ($i.e., \Delta GW >>> \delta GW$), taken in section 6.3.1.1. In addition, the close relationship between GRACE-derived groundwater changes and WGHM IRR_70_S, and WGHM_NOUSE points to low groundwater extraction in the region as already reported in other studies (e.g., *Siebert et al.*, 2010; *Villholth*, 2013). The spatial correlation between GRACE-derived groundwater and

WGHM variants are similar except for areas north of latitude 15° where the WGHM NOUSE model variant had (almost) constant values hence no

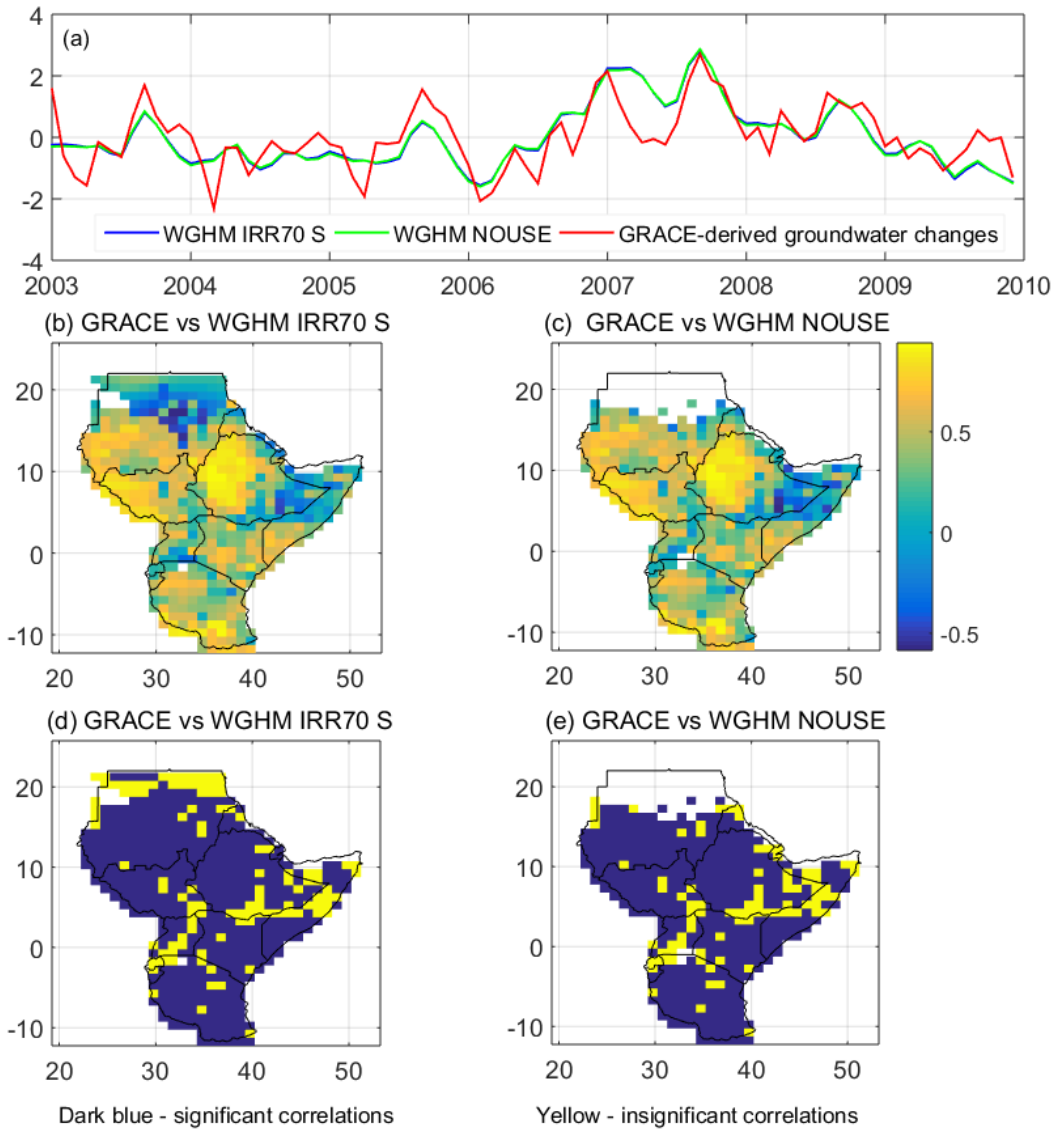

Figure 6.3: A comparison between GRACE-derived groundwater changes and those of WaterGap Hydrological Model (WGHM). (a) Temporal variability of standardized (spatially averaged) groundwater changes from 2003 to 2009, (b) and (c) are correlation coefficients between GRACE derives groundwater changes and those of WGHM variants, (d) and (e) are significance of the correlations. GRACE-derived groundwater changes sufficiently captures groundwater changes over GHA. The similarity in variability of the two WGHM variants indicates limited groundwater exploitation in the region. The correlations are significant at $p < 0.05$.

correlation coefficients (Figs. 6.3b and c). The correlation are fairly strong and significant in most areas within the GHA region (Figs. 6.3d and e). The low and/or strong anti-correlation in isolated areas (e.g., North of latitude 15° eastern Ethiopia, and northern Somalia) could be caused by (phase) shifts due to depth differences between GRACE and WGHM since GRACE sense greater depths. Based on the largely close relationship between GRACE-derived groundwater and WGHM variant WGHM IRR_70_S, and the fact that WGHM variant WGHM IRR_70_S has been found to adequately capture groundwater changes in various location globally, see, e.g., *Döll et al.* (2014), it is sufficient to imply that GRACE-derived groundwater captures groundwater changes over GHA sufficiently well.

Further, the GRACE-derived groundwater changes were analyzed as follows;

(i) Localization of GRACE-derived Groundwater

ICA (see Chapter 2 for formulation and description) was used to decompose and localize GRACE-derived groundwater changes (ΔGW) into spatio-temporal components as

$$\Delta GW = PQ, \tag{6.5}$$

where P is the temporal groundwater changes and Q the corresponding groundwater change patterns (spatial patterns).

(ii) Temporal Groundwater Change Trend Analysis

Temporal groundwater change linear trends (see Chapter 2 for formulation and description) were evaluated and analysed in the context of rainfall changes in the vicinity of the spatial groundwater changes.

(iii) Correlation Analysis

Pearson correlation analysis (see Chapter 2 for formulation and description) was used to determined the relationship between rainfall and temporal

groundwater changes taking lag into consideration. In addition, the impacts of climate variability on groundwater level changes was evaluated through correlation of temporal groundwater variabilities with dominant climate variability indices (ENSO and IOD) at various lags.

6.3.2 Groundwater Sustainability

Due to lack of recharge (both in-situ and from WGHM), this section compares GRACE TWS and model derived water flux in a bid to understand the sustainability of groundwater for irrigation;

$$\frac{d(TWS)}{dt} = P - R - E^{1}$$

Where time (dt) is per month, P is precipitation, R runoff, and E – evapotranspiration.

On average GRACE TWS showed similar temporal variability with model derived water flux albeit with larger amplitudes (Fig. 6.4a). The overall average correlation stood at 0.5508 at zero lag while with water flux proceeding GRACE TWS with one month, the correlation improved to 0.8390. Fig. 6.4b shows the spatial variation in the correlation at zero lag while Fig. 6.5a shows maximum correlation at various lags shown in Fig. 6.5b. The high correlation over Ethiopian highlands, South Sudan, Lower Sudan, Tanzania and Western Uganda points to GRACE TWS accurately representing water flux and could by extension imply the dependent of groundwater (since TWS has groundwater as one of the components) on rainfall. The areas with low and/or negative correlations e.g., Upper Sudan (North of latitude 15°), Somalia, Eastern Ethiopia and Eastern Kenya have relatively high evapotranspiration coupled with groundwater recharge from outside the local areas hence GRACE TWS and model-derived flux have weak relationships. With climate studies (see, e.g., *Niang et al.*, 2014, and the references therein) pointing towards possible future increase in extreme events,

[1] P from CHIRPS while R and E are from GLDAS 2

the close relationship between GRACE TWS and model derived water flux over several areas points to sustainability of groundwater based on rainfall.

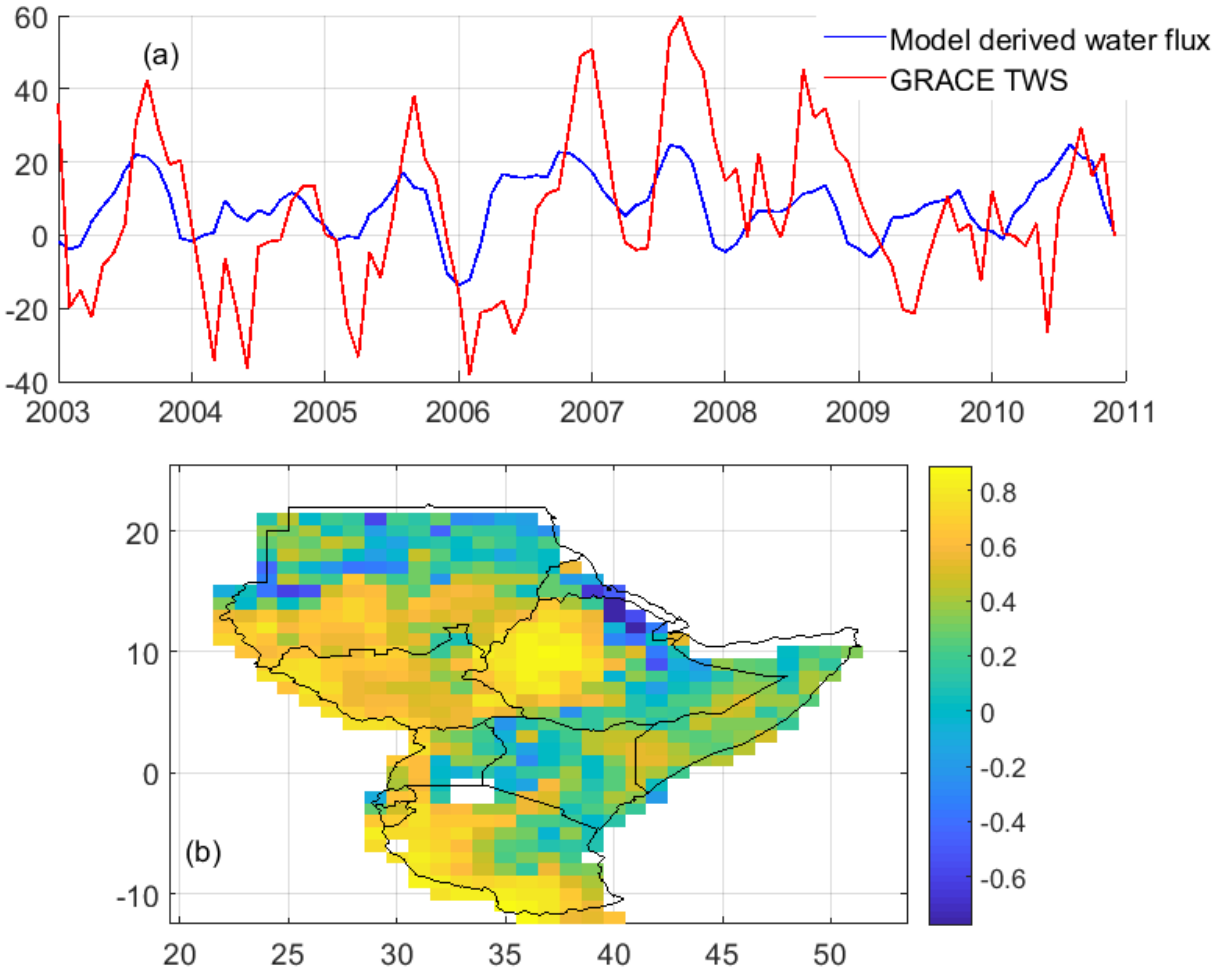

Figure 6.4: Relationship between GRACE-TWS and Model-derived water flux; (a) time series plot (b) Correlation.The water flux is derived from rainfall (CHIRPS), runoff (GLDAS 2) and evapotranspiration(GLDAS 2).

6.3.3 Potential for Groundwater Irrigated Agriculture

Preliminary analysis of potential for groundwater irrigated agriculture was carried out on groundwater localized regions. The potential for groundwater irrigated agriculture was based on groundwater quantity (provided by combination of GRACE-derived groundwater level changes and groundwater hydrogeology), quality (measured by total dissolved substance; from secondary

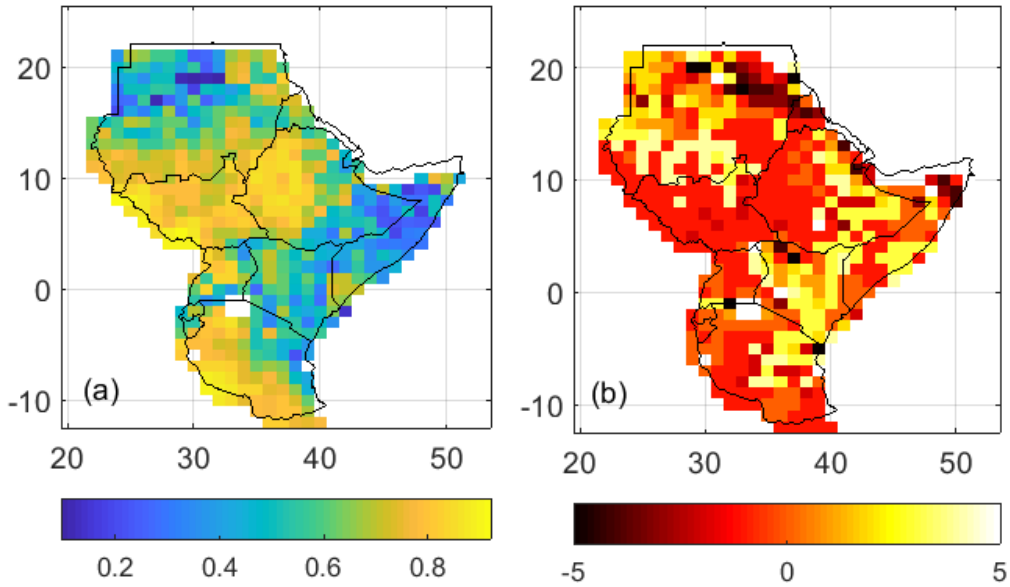

Figure 6.5: Lag cross correlation; (a) maximum correlation (b) Lag at maximum correlation. Negative lag values indicate water flux leading while positive indicate water flux lagging GRACE TWS.

information), and soil characteristics of the region. Each site was then rated based on all the aforementioned factors.

6.4 Results and Discussion

6.4.1 Spatio-temporal Variability of GRACE-derived Groundwater Changes

The decomposition of GRACE-derived groundwater changes using ICA resulted in spatio-temporal groundwater changes. Cross comparison of the locations of spatial groundwater change patterns with aquifer (and/or groundwater) location maps of the region (see, e.g., Fig. 6.1b; *Altchenko and Villholth*, 2013; *Abiye*, 2010; *Kebede*, 2013) revealed several spatial groundwater change patterns in regions belonging to various aquifers. These spatial groundwater change patterns are thereafter referred to by names of the aquifer (and/or basins) in whose regions they occur (Fig. 6.6).

Majority of the identified spatial groundwater change patterns (aquifers) are

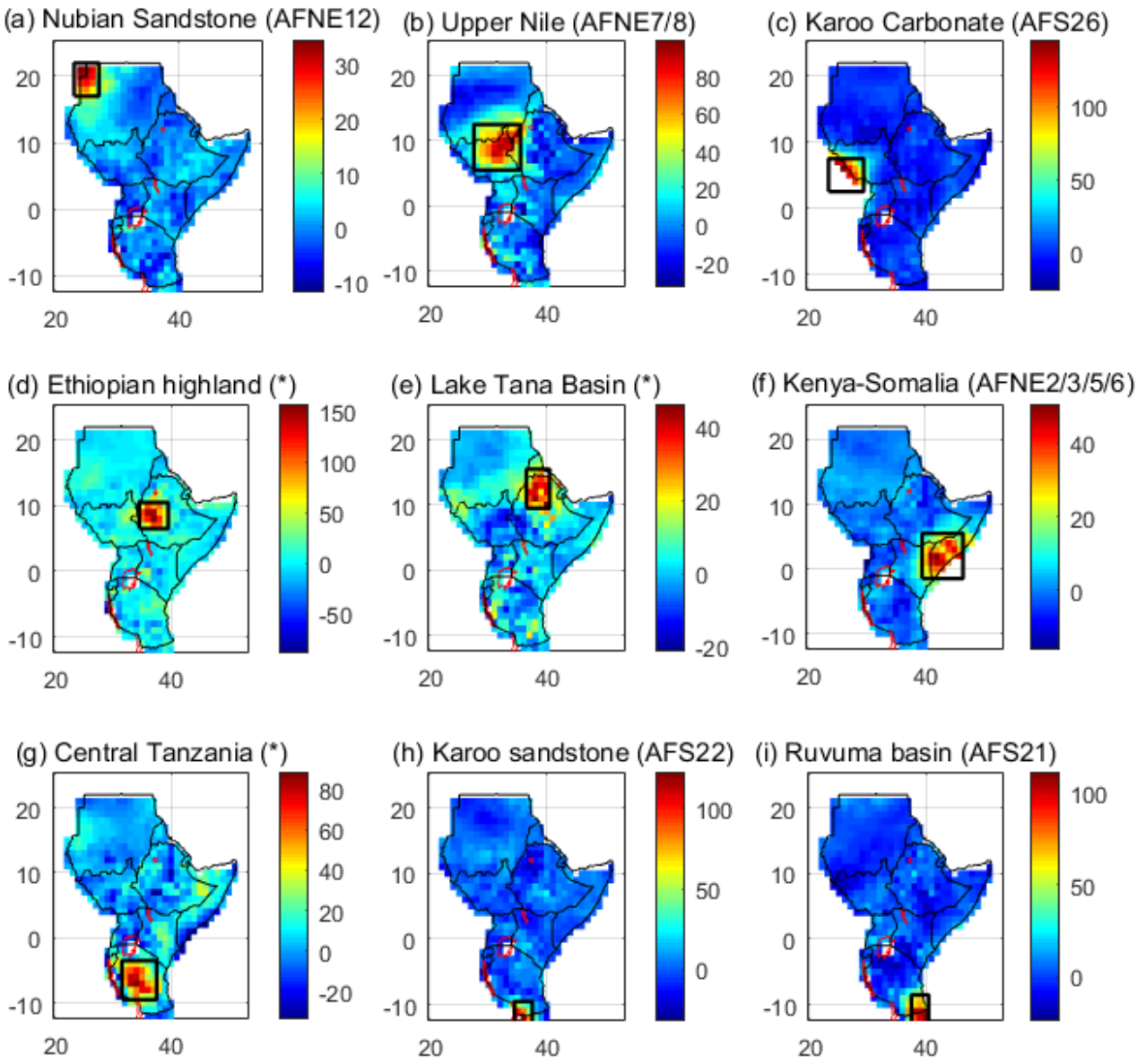

Figure 6.6: Selected spatial groundwater change patterns over GHA. The spatial patterns result from regionalization/localization of GRACE-derived groundwater changes (2003 - 2014) using Independent Component Analysis (ICA). The names in brackets correspond to aquifers' names as referred in Figure 6.1, while * denotes those aquifers not in Figure 6.1 and are only found entirely within a country. The rectangles (black) within each figure indicate areas over which precipitation and WGHM-derived groundwater have been spatially averaged.

transboundary i.e., their extent transverse 2 or more countries. Only two in Ethiopia (Fig. 6.6d and e) and one in Tanzania (Fig. 6.6g) are within countries. Due to the limited resources, political will, and the cross-country boundary

location of most of these aquifers, very limited resources are allocated if any for their monitoring (e.g., *Altchenko and Villholth*, 2013). GRACE thus provides an efficient and affordable way for large-scale monitoring (i.e., several aquifers at the same time) of these aquifers. The general characteristics of these aquifers (spatial groundwater change patterns) are summarised in Table 6.3.

Table 6.3: Groundwater characteristics and usage.

Groundwater changes	Recharge rate mm/annum	Recharge source or mode	Aquifer type (characteristic)	Current water Usage	Source
Nubian Sandstone (Sahara Nubian Basin)	0 - 2	Occasional rainfall	Consolidated sedimentary	Domestic Watering livestock	*Altchenko and Villholth* (2013) *Salama* (1988); *Omer* (2002)
Upper Nile (Sudd basin, Baggara basin, and other small aquifers)	2 - 100	Rivers Wadies Direct rainfall	Aquifers in precambrian and volcanic rocks. Umm Rawaba formation Confined, unconfined, and semi confined.	Domestic Agricultural (Subsistence) Watering livestock	*Abiye* (2010) *Selley* (1997) *Altchenko and Villholth* (2013)
Karoo Carbonate	100 − > 300	Rainfall River Congo	Limestone and sandstone	Domestic Watering livestock Irrigation (limited)	*Altchenko and Villholth* (2013)
Ethiopia highlands	150 - 250	Direct deffuse recharge through soil (rainfall)	Precambrian metamorphic Crystalline basement	Urban and rural Watering livestock Irrigation	*Kebede* (2013)
Lake Tana region	20 - 300	Summer rains Losing streams	Deep and shallow volcanic aquifers. Shallow basement aquifers.	Irrigation (both large and small scales). Domestic. Watering livestock.	*Kebede* (2013)
Kenya-Somalia	2 - 100	Underground run-off. River Ewaso Ngiro. Dera drainage (river and swamp). Limited direct recharge from rainfall.	Semi-consolidated sedimentary	Refugee camps. Domestic Public water supply Watering livestock	*Altchenko and Villholth* (2013) *Mwango et al.* (2004) *Oord et al.* (2014); *Krhoda* (1989) *Mumma et al.* (2011) *Swarzenski and Mundorff* (1973)
Central Tanzania	2 - 20 (periodic)	Direct rainfall infiltration, preferential flow, and through fractures	Crystalline basement aquifers.	Domestic Irrigation Watering livestock	*Kashaigili* (2010) *Pavelic et al.* (2012)
Karoo Sandstone	20 − > 300 (periodic)	Rivers Rainfall	Consolidated sedimentary	Domestic	*Altchenko and Villholth* (2013) *Wellfield and British* (2011)
Ruvuma	20 - 300	River Ruvuma rainfall	un/semi-confined Quaternary consolidated sedimentary rocks	Domestic Watering livestock	*Altchenko and Villholth* (2013) *Wellfield and British* (2011)

The temporal evolutions of the groundwater changes are presented in Figure 6.7. Other than Nubian Sandstone and Kenya-Somalia (Fig. 6.7a and f), the temporal evolutions of groundwater changes of the rest of the aquifers showed an annual pattern which could be due to the fact that recharge takes place once every year during main rainfall seasons. Also, the groundwater temporal evolutions seemed to peak 2-3 months, on average, after rainfall (Figs. 6.7b-e and g-i). The

temporal evolution of the groundwater changes in UGHA (Nubian Sandstone, Upper Nile, Karoo Carbonate, Ethiopian highland, and Lake Tana Basin) had low maximum (peak) values in 2005, 2010, 2012, and 2014 (Fig. 6.7a-e), which could be attributed to low rainfall hence reduced recharge and/or relatively more usage of groundwater on those years. These years were preceded by low maximum (peak) rainfall in 2004, 2009, and 2010 (see, Fig. 6.7a-e for rainfall) hence drought as has been reported in other studies (e.g., *Viste et al.*, 2013; *Elagib*, 2013; *Masih et al.*, 2014, and the references therein).

In EA, the temporal evolutions (Kenya-Somalia, Central Tanzania, Karoo

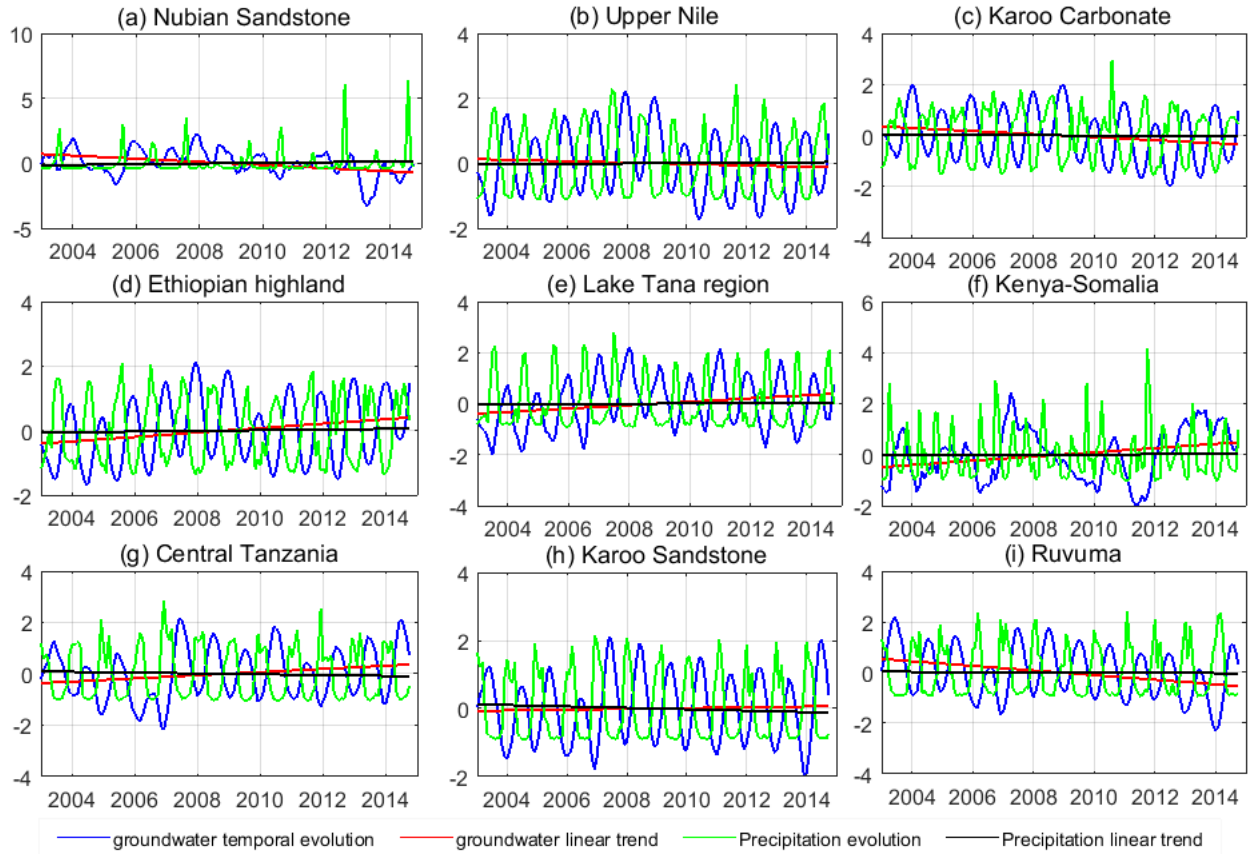

Figure 6.7: Temporal variability of spatial groundwater change patterns (in Figure 6.6) and precipitation spatial averages (2003-2014), fitted with linear trends. The groundwater temporal evolutions are the independent components from ICA localization of GRACE-derived groundwater changes while precipitation spatial averages (standardized) are done over the rectangles in Figure 6.6. The magnitude of the trends are tabulated in Table 6.4. The groundwater temporal evolutions largely reflects the average rainfall.

sandstone, and Ruvuma basin) recorded relatively higher maximum (peak) values due to high recharge from the impact of El Niño induced rain that occurred in the region in 2006/2007 (Figs. 6.7f-i; *Kijazi and Reason*, 2009; *Becker et al.*, 2010; *Taylor et al.*, 2012). In addition, the temporal evolutions had low maximum (peak) values in 2004, 2006, 2011, and 2013 (Figs. 6.7f-i), years that were preceded by relatively lower rainfall (Fig. 6.7f-i) and were reported as having been drought years (see, e.g., *IFRC*, 2011; *Loewenberg*, 2011; *Nicholson*, 2014a; *Masih et al.*, 2014, and the references therein).

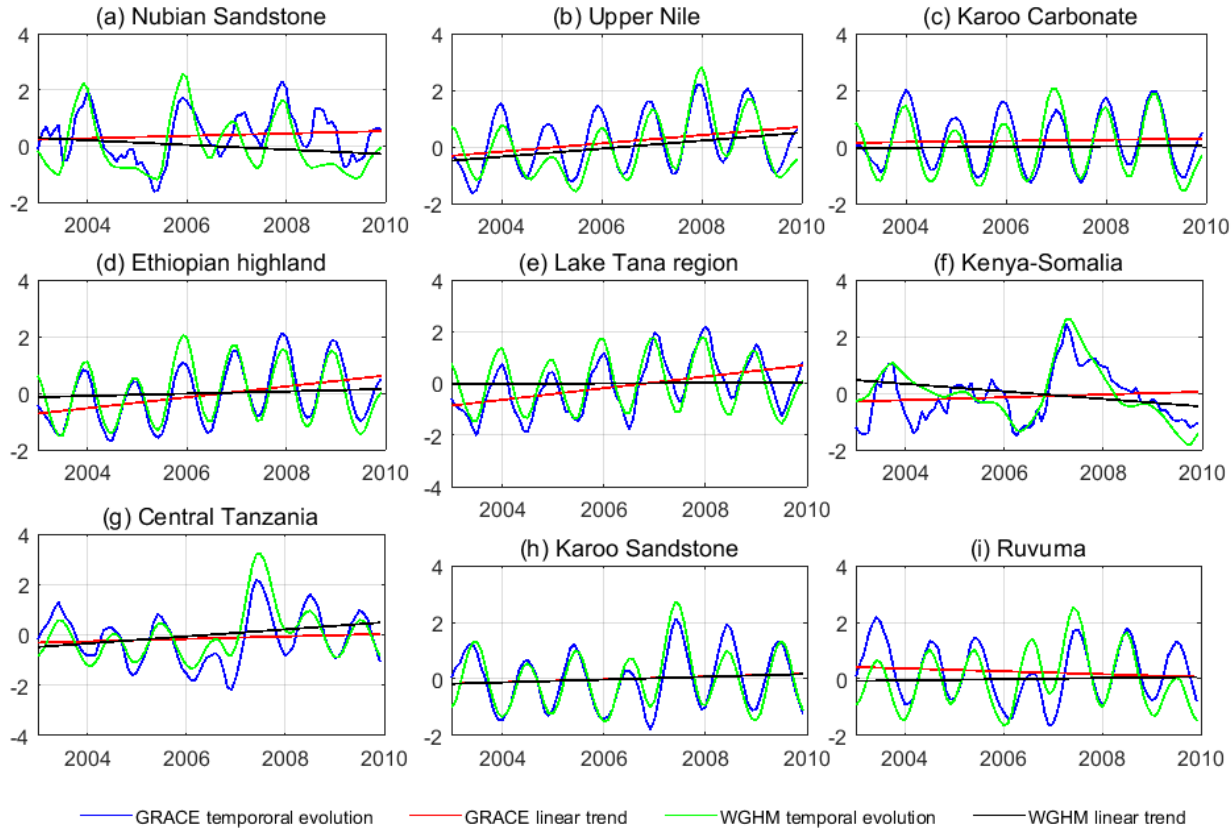

Figure 6.8: Temporal variability of spatial groundwater change patterns (in Figure 6.6) and WGHMIRR_70_S groundwater change spatial averages (2003-2010), fitted with linear trends. The groundwater temporal evolutions are the independent components from ICA localization of GRACE-derived groundwater changes while WGHMIRR_70_S groundwater change spatial averages (standardized) are done over the rectangles in Figure 6.6. The magnitude of the trends are tabulated in Table 6.4. The WGHM temporal evolutions are consistent with those of GRACE-derived groundwater changes.

Table 6.4: Trend magnitudes and lag relationships. Ethiopia highlands, Lake Tana region, and Kenya-Somalia have increasing groundwater trends, Nubian Sandstone and Ruvuma have reducing groundwater trends, while the rest have stable groundwater levels over the considered duration (2003 - 2014). The relationships between temporal groundwater changes and average rainfall are weak. Maximum correlations were found when rainfall preceded groundwater changes by the tabulated months. Significant trends are in bold ($p < 0.05$).

Groundwater	Groundwater trend mm/month	WGHMIRR_70_S trend mm/month	Rainfall trend mm/month	maximum correlation with groundwater	Lag at maximum correlation (months)	Average annual rainfall (mm)
Nubian sandstone	**-1.328**	-0.001	0.016	0.1540	80	35
Upper Nile	0.963	**0.069**	0.034	0.4542	2	907
Karoo Carbonate	-2.362	-0.013	-0.044	0.3299	3	1480
Ethiopia highlands	**3.134**	0.022	0.071	0.3974	27	1385
Lake Tana region	**1.228**	0.002	0.041	0.4560	27	887
Kenya-Somalia	**1.582**	-0.025	0.015	0.2047	105	432
Central Tanzania	2.163	**0.125**	-0.095	0.3734	3	916
Karoo sandstone	0.283	0.073	-0.191	0.4778	2	1230
Ruvuma	**-2.753**	0.026	-0.040	0.4181	9	1050

The close relationship between groundwater change temporal evolution and rainfall as observed above could be attributed to the fact that due to limited groundwater exploitation in the region (see, e.g., *Siebert et al.*, 2010; *Villholth*, 2013), the temporal evolution is to a large extent influenced by recharge (equation 6.4). Recharge in itself is dependent on rainfall (intensity, duration, and volume), hydrogeological characteristics of the groundwater region (e.g., geomorphology, geology, and pedology), and vegetation cover and/or land use in the recharge regions (*Siebert et al.*, 2010; *Comte et al.*, 2016). Land use land cover changes e.g., deforestation (afforestation) leads to increased (reduced) run-off and/or evapotranspiration and has a site-specific influence on recharge while continued urbanization leads to lower long-term average groundwater recharge (*Kundzewicz and Döll*, 2009; *Comte et al.*, 2016).

Further, the temporal evolutions of GRACE-derived groundwater changes were found to be largely similar with spatially averaged WGHM IRR_70_S (averaged over the boxed areas in Figure 6.6) though with relatively larger amplitudes (Fig. 6.8). Over EA, both GRACE-derived groundwater changes

and WGHM IRR_70_S temporal evolutions clearly depict the high 2007 and low 2006 maximum (peak) values corresponding to the El Niño induced rains of 2007 and the droughts of 2005-2006, respectively. Over UGHA, distinctive feature like the low maximum (peak) value in 2005 is clearly visible in all the figures.

The relationships between the temporal groundwater changes and spatially average rainfall (averaged over extents shown in Fig. 6.6) showed weak relationships with varied lags (Table 6.4). The weak relationships could be attributed to the fact that most of the aquifers considered are recharged by additional means, e.g., losing streams, preferential flows and through fractures, and underground rivers, other than direct rainfall infiltration (see, Table 6.3 and the references therein). Probably a stronger relationship would be between rainfall and recharge as opposed to the relationship between rainfall and groundwater level changes. This follows from the evidence of episodic recharge link to extreme rainfall events in an aquifer in Central Tanzania (see, e.g., *Taylor et al.*, 2012). Other than the Nubian Sandstone and Kenya-Somalia with lags of 80 and 105 months, respectively, the rest of the aquifers had lags in the range of 2 to 27 months (Table 6.4). These lags are largely dependent on among other things; the depth and characteristics of the associated aquifers (e.g., confined vs unconfined, volcanic vs Precambrian etc.), the source and mode of the recharge (Table 6.3), and the land use land cover in the recharge region. The reflection of rainfall in groundwater level changes after durations of time (lag) forms one of the major advantages of groundwater as a source of water due to the fact that it can be used without worry even during longer drought events, see e.g., *Calow et al.* (1997, 2010).

Least squares trend analysis results of GRACE-derived temporal groundwater changes, and spatially average rainfall and WGHM IRR_70_S are shown in Table 6.4 (also see, Figures 6.7, and 6.8). GRACE-derived temporal groundwater changes had: significant positive trends over Ethiopian highlands, Lake Tana region, and Kenya-Somalia; significant negative trends over Nubian

Sandstone and Ruvuma; and stable temporal groundwater changes over the remaining aquifers i.e., recharge balanced base flow and usage over the considered duration of time.

The trends in averaged WGHM IRR_70_S were all insignificant except for Upper Nile and Central Tanzania, while average rainfall had insignificant trends over all the groundwater localized areas. The lack of significance in these trends especially for WGHM IRR_70_S could be attributed to the short duration of time under consideration (7 years), while the rainfall appears to be stable over the considered duration (2003 – 2014).

Table 6.5: Relationship between temporal groundwater changes and climate indices. All the correlations are statistically significant ($p < 0.05$) but largely weak. Both Nubian Sandstone and Kenya-Somalia do not show any meaningful relationship with ENSO while Nubian Sandstone, Kenya-Somalia, Ethiopia highlands, and Lake Tana region do not show any meaningful relationship with IOD.

Groundwater	Maximum correlation with IOD	Maximum correlation with ENSO	Lag at maximum correlation with IOD	Lag at maximum correlation with ENSO
Nubian Sandstone	0.5652	0.5404	19	29
Upper Nile	0.3176	0.3052	19	16
Karoo Carbonate	0.2822	0.2427	61	16
Ethiopia highlands	0.2373	0.1658	19	51
Lake Tana region	0.3026	0.1928	19	52
Kenya-Somalia	0.4387	0.3974	95	5
Central Tanzania	0.3525	0.3132	37	17
Karoo Sandstone	0.2537	0.2234	37	15
Ruvuma	0.2655	0.3503	37	23

Considering equation 6.4, the insignificant rainfall trends, and the average annual rainfall (Table 6.4), the positive trends in GRACE-derived temporal groundwater changes over Ethiopian highlands and Lake Tana region could be attributed to a combination of steady recharge (evidenced by stable average annual rainfall), limited abstraction (see, e.g., *Siebert et al.*, 2010; *Kebede*, 2013), and very low based flow in comparison to recharge amounts. The case for Kenya-Somalia is special due to low annual rainfall coupled with high

evapotranspiration over the region (e.g., 432 mm/annum of average annual rainfall (Table 6.4) vis-a-vis $\simeq$ 2330 mm/annum of evapotranspiration; *Mwango et al.*, 2004). The recharge for groundwater in this region is from River Ewaso Ng'iro (originating from Mount Kenya region) and underground runoff from other regions e.g., Ethiopian highlands (e.g., *Mumma et al.*, 2011; *Oord et al.*, 2014; *Abiye*, 2010). The Nubian Sandstone is characterized by very limited active recharge as indicated by low correlation, long lags, and very low annual average rainfall (Table 6.4) hence its significant negative trend (depletion; as there is no recharge) could be driven by base flow and abstraction. This is in line with other studies (see, e.g., *Gossel et al.*, 2004; *Scanlon et al.*, 2006; *Döll et al.*, 2014), which have documented the negative trend in the aquifer as being driven by abstraction without a recharge. The negative trend for Ruvuma is driven by higher base flow as water flows back into the river tributaries in several locations in the region (*Wellfield and British*, 2011), coupled with low net abstraction.

Finally, in exploring the impact of climate variability on temporal groundwater changes, the correlation between temporal groundwater changes and the dominant climate variability indices (ENSO and IOD) showed weak relationships (Table 6.5). Since climate variability impact on groundwater through its influence on rainfall, the study considered only the correlations when groundwater was lagging climate indices. Due to the short duration considered, approximately 10 years, these results should be analyzed with caution as longer duration datasets may be necessary to give concrete results. The association of groundwater temporal evolution with IOD was relatively higher than that with ENSO, which could be attributed to the relatively stronger influence of IOD on the regions rainfall (see, e.g., *Saji et al.*, 1999; *Williams and Funk*, 2011; *Ashok et al.*, 2003). Both Nubian Sandstone and Kenya-Somalia did not show any meaningful relationship with ENSO, while the following temporal groundwater changes did not show any meaningful relationship with IOD; Nubian Sandstone,

Ethiopian highlands, Lake Tana region, and Kenya-Somalia. The lack of meaningful relationships follows from the fact that climate variability impacts on groundwater change through rainfall, thus the lag at maximum correlation are expected to be higher in the correlation of temporal groundwater changes with climate variability indices than with rainfall (Table 6.5 vis-a-vis Table 6.4). For Nubian Sandstone and Kenya-Somalia, their lack of meaningful relationships could be attributed to low or no recharge from rainfall while for Ethiopian highlands and Lake Tana region, their lack of meaningful relationships could be attributed to the fact that IOD does not have much influence on rainfall in those regions. The rainfall over these regions (Ethiopian highland and northern Ethiopia) results from moisture migration from rain forest regions over Congo Basin as a result of westerly winds and thermal low pressure of ITCZ (*Williams et al.*, 2012). Longer duration of temporal groundwater changes (groundwater level changes) would be necessary in order to understand with certainty the impact of climate variability (and/or change) on groundwater changes hence long term resource sustainability.

6.4.2 Potential of Groundwater Irrigated Agriculture

The GRACE-derived groundwater changes characteristics from section 6.4.1 were combined with existing secondary information (literature) e.g., groundwater potential, groundwater quality, and soil types, with a view to examining the potential for groundwater irrigated agriculture, which was explored based on water availability (quantity and quality) and dominant soil types (Table 6.6). An indication of water availability for sustainable exploitation was provided by temporal groundwater changes, trends (section 6.4.1) and yield information (Table 6.7), while quality was based on either physicochemical properties of total dissolved solids (TDS) or electrical conductivity (EC); both measures of dissolved minerals content in water. The study assumed the TDS/EC values to cover the entire spatial groundwater

change areas. For a comprehensive suitability analysis, a more detailed investigation will have to be carried out at a larger scale considering specific nutrients, well-specific yields, and finer soil classification.

Table 6.6: Soil characteristics (adopted from *Driessen and Deckers*, 2001; *Eswaran and Cook*, 1987)

Soil type	Characteristics (summary)
Acrisols	Suitable for production of rain-fed and irrigated crops only after liming and application of fertilizer. Its limitations include; poor chemical properties, low levels of plant nutrients, and aluminium toxicity and P-sorption.
Solonetz	Characterized by high concentration of sodium which impacts negatively on plants. Its use for agriculture is dependent on its depth and property of surface soil. Reclamation is possible but expensive.
Vertisols	They have high natural fertility and positive response to management, however, their moisture control problem imposes critical constraints to low input agriculture. Under rain-fed conditions and depending on temperature, they have been used to produce wheat, maize, sorghum, soya-beans, cassava e.t.c.
Ferrisols	They have great soil depth, good permeability, and stable micro-structure. They are well drained but have low water holding capacity. They have poor chemical properties hence careful selection of fertilizer and liming would be necessary for better returns.
Plinthosols	Their potential for agriculture depends on how deep they are. Requires management intervention due to poor natural soil fertility and water logging issues.
Nitisols	Are among the most productive soils of the humid tropics. They are of good work-ability, good internal drainage, fair water holding properties, and of good fertility. They contain high concentration of weathered materials and are suitable for a wide range of crops.
Cambisols	They have natural to weakly acid retention, satisfactory chemical fertility, and active soil fauna. They make good agricultural lands and are intensively used.
Leptosols	Are common in mountainous regions. Their shallowness and/or stoniness and implicit low water holding capacity are some of their limitations. Erosion is the greatest threat to steep slope soil areas. Hill slopes are normally fertile.
Alisols	Strongly acidic soils with accumulated high activity of clay at sub-soils. They have toxic levels of aluminium at shallow depths and poor natural soil fertility. Use restricted to acid tolerant plants/crops and low volume grazing. Productivity for subsistence agriculture is low as these soils do not recover easily from chemical exhaustion. Crop production is possible if fully limed and fertilized.
Lixisols	Agricultural use is subject to use of fertilizer and/or lime addition due to low level of plant nutrient and low cation retention.
Calciols	Have substantial secondary lime accumulation. Suitable for lime tolerant crops. They reach their full potential when carefully irrigated; furrow irrigation performs better.
Luvisols	Most Luvisols are fertile soils and are suitable for a wide range of agricultural activities.

TDS of $< 450mg/l, 450-2000mg/l$, and $> 2000mg/l$ are considered suitable, slight to moderately suitable, and severe, respectively, in degrees of restriction of

use for irrigated agriculture while EC of $< 700\mu S/cm, 700 - 3000\mu S/cm, and > 3000\mu S/cm$ are considered excellent, good, and fair (would greatly affect yield), respectively (see, e.g., *Ayers, R. S and Westcot, D. W. and Food and Agriculture Organization of the United Nations* , 1976; *Kumar et al.*, 2007; *Salifu et al.*, 2015). Based on water availability (Fig. 6.7 and Table 6.4), water quality (TDS) and dominant soil types (Tables 6.6 and 6.7), the potential for groundwater irrigated agriculture for various groundwater localized areas is presented in Table 6.7.

Table 6.7: Potential for groundwater irrigated agriculture based on groundwater characteristics and dominant soil types. Potential for groundwater irrigated agriculture varies from low to high across the groundwater availability regions. The hydrogeology information has been sourced from *MacDonald et al.* (2008), the soil type from *Dewitte et al.* (2013) and the water quality from the references in Table 6.3.

Groundwater region	Materials/ properties	Groundwater potential	Average yield (l/s)	Water quality	Dominant soil type	Agricultural potential
Nubian	Sandstone	Moderate to high	1 - 20	Dissolved particles in the ranges of 500 - 800 p.p.m. Patches of areas with high sodium and bicarbonate concentration.	Alisols	Low
Upper Nile	Precambrian basement. Volcanic rocks. Unconsolidated and semi-consolidated sediments (gravel, sane, clay, etc.)	Moderate to high	1 - 40	Varied with dissolved particles reaching 500 - 800 p.p.m over the Umm Rawaba formation	Vertisols	Moderate to High
Karoo Carbonate	Limestone Sandstone	Moderate to high	1 - 100	Good quality	Plinthosols Lixisols	Low to Moderate
Ethiopia highlands	Precambrian - metaomorphic Tertiary volacanic	Moderate	1 - 40	Dissolved particles approximately 500 - 800 p.p.m. dominated by calcium bicarbonate ions.	Nitisols	High
Lake Tana region	Deep and shallow volcanic rocks. Crystalline basement	Low to high	0.1 - 100	Low level of dissolved solids suitable for drinking and irrigatioon	Leptosols Luvisols Vertisols	Low to Moderate
Kenya-Somalia	Semi-consolidated sedimentary	Low to moderate	1 - 10	Fresh water along the aqui-fer center (limited area) and brackish water in the remaining sections.	Solonetz Calciols	Low
Central Tanzania	Crystalline basement precambrian formation (Granite and/or Gneiss)	Moderate	0.1 - 40	TDS in the range 1000 - 3000 p.p.m. Varied with high alkalinity in some areas.	Cambisols Solonetz Acrisols Vertisols	Low to Moderate
Karoo Sandstone	Sandstone (consolidated)	Moderate to high	1 - 20	Generally good. Dissolved particles in the range of 400 - 800 p.p.m.	Loamy sandy soils	Moderate to High
Ruvuma	Aluvium Sedimentary	High	1 - 40	Water with good quality though some locations are brackish or saline.	Cambisols Acrisols	Low to Moderate

Kenya-Somalia has good water availability (quantity) considering the temporal groundwater changes (Fig. 6.7d), trends (Table 6.4), and average yield (Table 6.7) that can easily support subsistence agriculture. The freshwater within the center of Merti aquifer has TDS of less than 1000 mg/l with a PH of between 7.2 to 7.8 with the rest of the area overlain by Precambrian crystalline or consolidated sedimentary having TDS of 2000 – 4000 mg/l (Fig. 6.1d; *Swarzenski and Mundorff*, 1973). The dominant soil types over the region are Solonetz and Calciols (Table 6.7), poor soils that requires expensive agricultural management, e.g., leaching with fresh water, liming, fertilization, and construction of engineering drainage systems in order to be suitable for crop production, hence low potential for groundwater irrigated agriculture (Table 6.7). However, the area could be used for sodium and calcium tolerant crops. The limited fresh water at the center is under pressure from the community and the refugee centers, and could run the risk of saline intrusion if subjected to an additional pressure of supporting irrigated agriculture in areas of suitable soils.

Although Nubian Sandstone (Nubian Sahara) has falling (groundwater) trends (Fig. 6.7b and Table 6.4) due to limited recharge, it has a good yield (Table 6.7) with one of the largest deposits of fossil water in Africa (see, e.g., *MacDonald et al.*, 2008). The fall is due to water use by other states sharing the aquifer as the Sudanese side comprises only of pastoralist communities (*Alker*, 2007). It has a fair quality of water with TDS values of between 500 – 800 mg/l (*Salama*, 1988) and a dominant soil type of Alisols (Table 6.7), which like Solonetz and Calciols found in Kenya-Somalia has poor agricultural potential. Alisols requires liming and addition of fertilizer for productive use though they do not easily recover from chemical exhaustion (Table 6.6), hence low potential for groundwater irrigated agriculture (Table 6.7).

Upper Nile, comprising of several aquifers, has good water availability (Fig. 6.7a and Tables 6.4 and 6.7) with varying TDS in the ranges of 200 – 500 mg/l and 100 – 400 mg/l over Sudd and Baggara basins, respectively (*Salama*,

1988). The dominant soil type is Vertisols (Table 6.7), which despite containing a high level of plant nutrients, may require additional management practice due to its high clay content. The high clay content presents a moisture control challenge that may impose a critical constraint on low input agriculture, hence moderate to high potential for groundwater irrigated agriculture (Table 6.7).

Ethiopian highland is characterized by good water availability (Fig. 6.7a and Tables 6.4) of suitable quality with high agricultural potential soil hence high potential for groundwater irrigated agriculture (Table 6.7).

Lake Tana has both good water availability and soils of good agricultural potential. Considering Figure 6.7c and Tables 6.4 and 6.7, coupled with TDS of less than 500 mg/l (*Kebede*, 2013) the region has low to high agricultural potential. On areas of the crystalline basement with low groundwater potential, the agricultural potential is likewise low while over areas of volcanic hydrogeology, the agricultural potential is moderate (Table 6.7).

Karoo Carbonate is characterized by large volumes of good quality water (Fig. 6.7c and Tables 6.4 and 6.7) with poor quality soils (Plinthosols and Lixisols) requiring additional management practices e.g., the addition of fertilizer and/or lime, water logging issues etc. Its irrigated agricultural potential is thus low to moderate (Table 6.7).

Central Tanzania has a stable quantity of groundwater (Fig. 6.7c and Tables 6.4) though with relatively high TDS of 1000 – 3000 mg/l (*Kashaigili*, 2010) and varying groundwater potential and yield depending on the hydrogeology (Table 6.7). Due to varied dominant soils e.g., Cambisols, Solonetz, Acrisols, and Vertisols its groundwater irrigated potential ranges from low to moderate as additional intervention measures could be necessary for good agricultural returns (Table 6.7).

Karoo Sandstone is dominated by good agricultural soil which coupled with groundwater availability (Tables 6.4 and 6.7) with TDS of 400 – 800 mg/l (*Wellfield and British*, 2011) make the region to have moderate to high

potential for groundwater irrigated agriculture (Table 6.7).

Finally, Ruvuma though characterized by high potential of groundwater with good quality (Table 6.7), the falling trend (Tables 6.4) coupled with average soils (Cambisols and Acrisols) qualifies it for low to moderate potential for groundwater irrigated agriculture. The regions dominated with Acrisols, soils with low levels of plant nutrients and poor chemical properties, have low potentials for agriculture (Table 6.7).

Based on the yield, groundwater potential, and recharge rates (Table 6.7), large-scale groundwater irrigated agriculture may not be possible but subsistence, medium to small-scale groundwater irrigated agriculture would be sufficiently supported in these areas. Groundwater with high TDS or EC levels results in plants being unable to absorb sufficient water from the salty solution despite the presence of sufficient moisture hence reduced yield/productivity (*Fipps*, 2003). On the same note, soils with high concentration of salts result in the salts leaching into the ground during rainfall events. This leads to increase in concentration of salts in the soil, thus impeding plants from absorbing water and nutrients. Finally, in the case of salty water, as it is used up (some evaporates) the salt remains deposited in the soil and is washed back and the cycle continues making the soil unsuitable for agricultural activities. Also, salt resistant crops could be tried in regions of salty water and/or soils with excess salts.

6.5 Concluding Remarks

The Chapter derived groundwater changes from GRACE TWS and subsequently used ICA method to localize the resulting groundwater changes into aquifer regions and corresponding temporal variabilities. The temporal groundwater changes were then analyzed and correlated with dominant climate variability indices (ENSO and IOD) in order to explore the impact of climate variability. Finally, the potential for groundwater irrigated agriculture in the aquifer regions were explored. The major findings of the Chapter include:

(i) GRACE-derived groundwater changes showed similar temporal variability to WGHM variants IRR_70_S and WGHM_NOUSE with Pearson correlation coefficients of 0.7147 and 0.7173 (significant at 95% confidence level), respectively. This indicates the potential of using GRACE satellites to study groundwater changes in this data deficient region.

(ii) Based on the aquifer (and/or groundwater) location maps of the region, the study identified the following aquifers (and/or groundwater areas); Nubian sandstone, Karoo Carbonate, Upper Nile, Ethiopian highlands, Lake Tana region, Kenya-Somalia, Central Tanzania, Karoo sandstone, and Ruvuma.

(iii) The temporal evolution of the identified GRACE-derived groundwater changes showed largely similar variability to those of spatially averaged WGHM variants IRR_70_S and reflected changes in annual average rainfall. All the temporal groundwater changes, except Nubian sandstone and Kenya-Somalia, showed an annual (cyclic) pattern indicating an annual (yearly) recharge cycle.

(iv) Least squares trend analysis of the temporal groundwater changes had; increasing groundwater levels for Ethiopian highlands, Lake Tana region, and Kenya-Somalia; stable groundwater levels for Upper Nile, Karoo Carbonate, and Central Tanzania; and decreasing groundwater levels for Nubian Sandstone and Ruvuma.

(v) Correlation analysis showed weak associations/relationships between the temporal groundwater changes and the dominant climate indices (IOD and ENSO), an indication of the limited impact of climate variability and/or change on the groundwater level changes. Both Nubian Sandstone and Kenya-Somalia did not show any meaningful relationship with ENSO, while Nubian Sandstone, Ethiopian highlands, Lake Tana region, and Kenya-Somalia did not show any meaningful relationship with IOD. Due to the short duration of the groundwater changes considered, longer

duration of groundwater changes would be required for certainty of the observed (and/or lack of) association.

(vi) Based on water availability (from GRACE), water quality (indicated by the total dissolved substance) and dominant soil types, potential for groundwater irrigated agriculture results showed: low potentials for Nubian Sandstone and Kenya-Somalia areas; low to moderate potentials for Karoo Carbonate, Lake Tana region, central Tanzania, and Ruvuma; moderate to high potentials for Upper Nile and Karoo Sandstone; and high potential for Ethiopian highland.

7 Enhancement of Food Security and Future Outlook

7.1 Introductory Remarks

This thesis has looked into issues of agricultural drought, the possibility of using GRACE to monitor large-scale groundwater level changes, and the potential for groundwater irrigated agriculture over GHA. This is in response to drought induced food insecurity over the region (see section 1.2). Droughts are permanent features of the region's climate system and will continue to recur with studies suggesting an increase in their frequency and intensity (see, e.g., *Ibrahim*, 1988; *Olsson*, 1993; *Gebrehiwot et al.*, 2011; *Edossa et al.*, 2010; *Williams and Funk*, 2011; *Lyon*, 2014; *Nicholson*, 2014a; *Niang et al.*, 2014). By investigating agricultural drought-related issues that have not been given prominence by other studies over the region, this thesis contributes to enhancement of food security. Further, the problem of low per capita food production driven by climate change and/or variability, high population growth rate, and low yield is indirectly addressed by the thesis through large-scale groundwater monitoring and evaluation of potential for groundwater irrigated agriculture. Groundwater can only be sustainably exploited if there is continuous monitoring. This Chapter highlights the links of the major findings of the thesis to food security enhancement and possible areas for future research.

7.2 Thesis Major Findings Linked to Food Security Enhancement

In general, the results from agricultural drought and soil moisture analyses (Chapters 3, 4, and 5) are important to the region as they extend the current understanding of agricultural drought since at present only a few studies exist. Additional understanding of agricultural drought is important for the region

since droughts are permanent and recurring features and every time they occur, the region plunges into food insecurity. Soil moisture being the only reliable indicator of available plant water between rainfall deficit and crop response, is therefore very critical for yield monitoring. Knowing the characteristics of these soil moisture products would be important to researchers and other decision makers in the region as it could aid in their choice of which products to use. In addition, it could spur more soil moisture based research in for example agricultural drought monitoring as currently very few studies are using these (soil moisture) products.

Specifically, the results of this thesis contribute to enhancement of food security in the following areas/manner (see summary in Figure 7.1):

(i) Drought monitoring framework

In order to improve food security, there is need to shift from crises management to risk management of drought-induced food insecurity. An effective proactive risk management strategy requires that the best available information from operations and reliable drought monitoring tools for the region be collectively analyzed to provide objective information for near real-time food security assessment (*Tadesse et al.*, 2008). As the region currently lacks a clear drought monitoring approach, the drought characterization framework employed in this thesis (Chapters 3 and 4) can be used to provide effective, clear, and concise drought information to aid risk management approach. This drought characterization framework is suited for effective drought monitoring as it involves a spectrum of indicators from precipitation, soil moisture, NDVI, and terrestrial water storage. Effective drought monitoring calls for use of a combination of indicators as precipitation alone may not tell the whole story, although drought stems from precipitation deficit, due to the complex nature of drought phenomenon (*Naumann et al.*, 2014; *Damberg and AghaKouchak*, 2014). Finally, the assessment of the effectiveness of

drought indicators in this framework (sections 3.2.2 and 4.3.3) serve to enhance the credibility and importance of the indicators with a wide range of decision makers.

(ii) Development of food security early warning systems (EWS)

For a region with frequent drought-induced food insecurity incidents (section 1.2), GHA needs a reliable and effective food security early warning system to enable stakeholders, decision and policy makers respond in time. Currently, situation and outlook reports produced by Famine Early Warning System (FEWS-NET) serves this purpose. The situation and outlook reports are produced by integrating precipitation percentiles and normalized difference vegetation index (see, e.g., *Verdin et al.*, 2005; *Tadesse et al.*, 2008). These situation and outlook reports can benefit a lot by incorporating the rainfall, moisture, and VCI based indicators that did explain very high variability in national annual crop production over the region (sections 3.3.2 and 4.4.1.4). Regression models developed from these indicators and used with seasonal forecasts would give a clear picture of the expected food situation 3 – 6 months before harvest as the seasonal forecast are produced 3 – 6 months in advance. Also, these indicators can be used to drive crop models for yield/production prediction. Such production predictions can then be combined with socio-economic data (information on how the communities make living and poverty levels), and drought spatial patterns to estimate the food security situation and the likely extent of impact 3 – 6 months beforehand hence an effective EWS (*Brown et al.*, 2007; *Tadesse et al.*, 2008).

(iii) Enhance the mobilization, management, and distribution of relief food

Mobilization of relief food for any disaster, e.g., drought, takes up to 6 months from the time assistance is sought from the donors for the food to begin arriving in affected areas. This implies that the budgeting process

preceding the humanitarian action has to be done way before the harvest is known and official production figures for the region in question available (*Brown et al.*, 2007). With rainfall, moisture, and VCI based indicators explaining very high variability in national annual crop production over the region (sections 3.3.2 and 4.4.1.4), they can be used with forecast information to predict yield/production as outlined above to serve the budgeting process. It would also help in improving the response time from governments and other relief agencies as their current responses do come way too late when the impacts of drought have costed lives. In addition, the drought intensity information (sections 3.3.1.3 and 4.4.1.3) would be applicable in delineating the level of impacts expected when combined with poverty information thereby guiding the distribution of relief assistance hence reducing political patronage in the process. The consistency in the percentage of areas under drought and different drought intensities from various products (sections 4.4.1.2 and 4.4.1.3) should serve as a control for other derived drought-related statistics that depend on areas. Such information include the number of people affected and the extents, which various players in the sector (e.g., governments and aid agencies) have had different figures leading to lack of (or low) accountability in the process. By having ideas on the percentage differences in areas under different products, it is possible to propagate acceptable differences on the derived quantities thereby enforcing accountability.

(iv) Improve the effectiveness of monitoring and predictive systems

For drought monitoring framework, food security early warning systems, and mobilization management and distribution of relief foods to be effective, relevant, and reliable, they require the best possible drought indicators as inputs. Given that soil moisture is the best agricultural drought indicator coupled with the fact that GHA lacks in-situ soil moisture monitoring network, soil moisture suitability analyses (Chapter

5) provide the means of selecting the most suitable soil moisture product for the region. This is critical for the region as rain-fed agriculture become under increasing pressure from frequent droughts, rainfall variability, climate variability and/or change, and high population growth, thus making the region food insecurity vulnerable.

(v) Sustained groundwater exploitation

Given that the region lacks groundwater monitoring infrastructure, the potential shown by GRACE in monitoring groundwater (section 6.4.1) points to its importance as groundwater sustainability aiding tool. The fact that most of the aquifers fall within marginalized/border and arid/semi-arid regions makes it even more important as policy and decision makers can now formulate groundwater exploitation policies and provide incentives for the residence to utilize the water for food production. By providing continuous groundwater level changes over such large region (cross country boundary), the policies and/or uses could be formulated region-wide in order to minimize chances of conflict when pressure on the aquifers becomes greater due to increased demand driven by population growth and/or climate variability. With suitable incentives, policies, and given the importance and success of groundwater irrigated agriculture in other semi-arid/arid regions of Sub-Sahara Africa (see, e.g., *Foster and Shah*, 2012; *Villholth*, 2013), improvement in food security situation of the residents should be expected.

(vi) Enhancement of groundwater irrigated agriculture

The potentials for groundwater irrigated agriculture around the groundwater localized areas (section 6.4.2) contributes to the enhancements of food production as it provides a rough indication of the suitability of each area. The policy makers and stakeholders could use this information to suggest suitable crops for the respective areas thereby

helping the inhabitants make informed choices on what to grow. For areas with low potential, salt resistant crops could be suggested since their low potential was due to high salt levels either in the water or in the soil. The availability of a reliable water source (groundwater) is likely to encourage the inhabitants of these areas to invest more into farming (fertilizers, better quality seeds etc.) as they are assured of good returns hence enhanced household food security over the region.

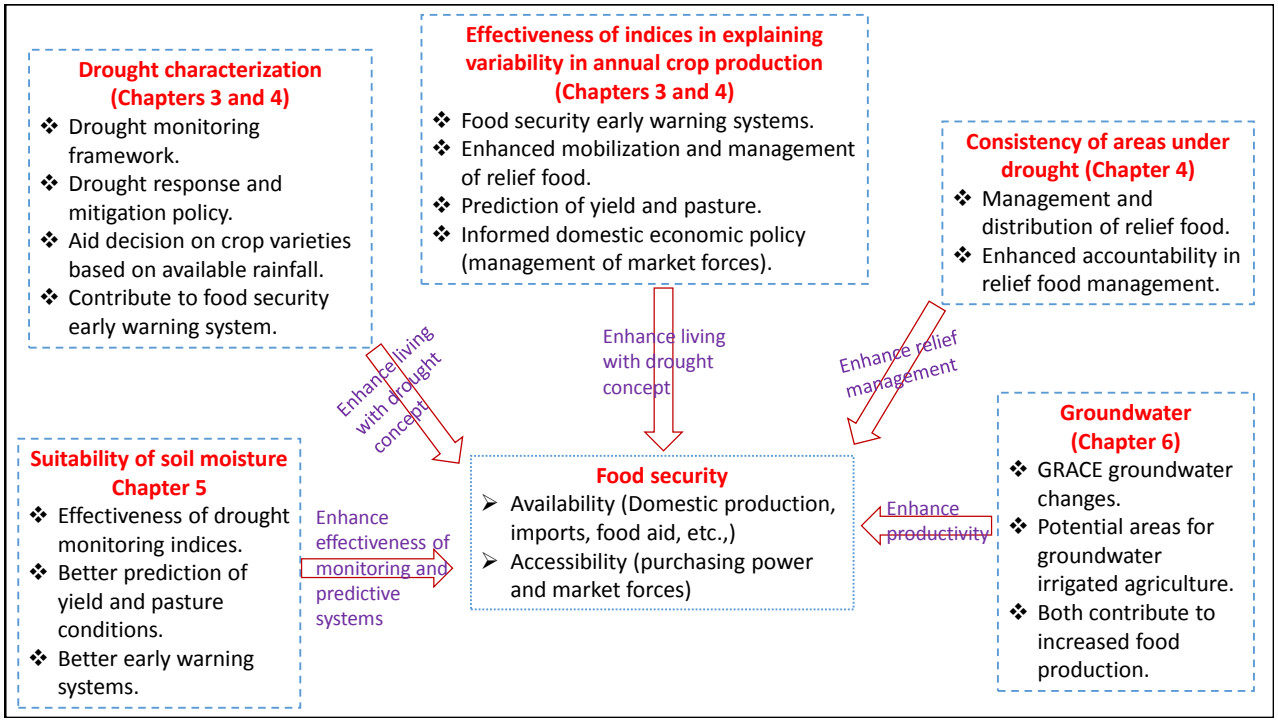

Figure 7.1: Relationship between thesis major findings and food security (availability and accessibility) enhancement.

7.3 Future Outlook

In the course of this research, the following issues were identified as possible areas requiring further research:

(i) Since droughts are permanent features of a climate system and studies indicate they will increase in intensity and frequency (see, e.g., *Ibrahim*,

1988; *Olsson*, 1993; *Gebrehiwot et al.*, 2011; *Edossa et al.*, 2010; *Williams and Funk*, 2011; *Lyon*, 2014; *Nicholson*, 2014a; *Niang et al.*, 2014), there is a need for more research on agricultural drought to contribute to better understanding and living with it (see, e.g., *Awange et al.*, 2016c). More studies need to be done to ascertain the probability of occurrence of various magnitudes of agricultural droughts and their links to climate change and/or variability indices e.g., ENSO and IOD, which research has shown to tightly influence the rainfall patterns over GHA. Such studies would contribute to the early warning systems of the region and would enhance the response of governments and other aid providers when droughts eventually occur.

(ii) In evaluating the impact of climate variability on soil moisture and groundwater changes over the region, this study concentrated only on the dominant climate variability indices (IOD and ENSO). Future studies could extend to other indices e.g., Inter-decadal Pacific Oscillation (IPO) and Northern Atlantic Oscillation (NAO), in order to make our understanding of climate variability impacts on soil moisture and groundwater changes comprehensive.

(iii) Further studies should also be done at large scales i.e., crop areas and/or sub country. This will add more value and relevance as it will translate the work (and or results) in to a practical platform and inform decision making at local levels.

(iv) Also, as modelling and climatic studies have indicated that the regional yield will remain low while productive land areas shift into low productive status, there is need to use available satellite and observation data to analyse, demarcate, and monitor the changes in the suitability of various crops grown in the region. The results of such analyses could inform change of seed varieties and/or development of groundwater irrigation facilities to

compensate for the loss of crop water due to rainfall variability.

(v) The differences observed in the soil moisture products coupled with their inconsistencies in both drought characterization and percentage of areas under drought calls for more regional based and improved soil moisture products. Other than using regional rainfall products for model forcing, further improvements could be made on the models themselves for consistency in handling wet and drying events.

(vi) Finally, the uncertainties observed in the soil moisture products need to be further studied with aim of extending understanding of the uncertainty spatial drivers (e.g., from topography and land cover etc.). This would be crucial in reducing the uncertainties before the soil moisture products can be used to improve food security.

As mentioned in Chapters 3 - 6, inadequate and/or lack of in-situ measurements is one of the major sources of uncertainties in the precipitation, soil moisture, and TWS products applied in this thesis. The uncertainties in the precipitation products are majorly caused by sparse and irregular distribution of rain-gauge stations coupled with influence of topography on precipitation interpolation. For the soil moisture products, lack of in-situ monitoring network has prompted the use of model-derived soil moisture whose uncertainties are chiefly driven by precipitation uncertainties. In addition, lack of in-situ soil moisture implies the uncertainties in the model-derived soil moisture products could not be evaluated. Even though GRACE TWS represents direct observations, lack of in-situ groundwater observation for validating the GRACE-derived groundwater implies that the level of uncertainties were not quantified. Also the uncertainties in GRACE measurements were contributed by its low spatial resolution of GRACE as dominant (and regional) signals obscure the local (and minor) ones. Lack of in-situ measurements was therefore one of the major sources of uncertainties in the product used and in the final results.

Other than lack of in-situ measurements, the other major shortcoming of the thesis approach and results was the scale of the study. Even though at this scale (regional) the approach and results are suitable for policy formulation, the results cannot be directly utilized in local decision making in aid of drought mitigation and/or food security decisions since each country in the region make country level decisions. The thesis attempted to address these shortcomings and above uncertainties through innovative mathematical approaches though to a limited success. To overcome these shortcomings, future studies should consider local (country or less) level studies and if possible incorporate in-situ measurements as this would make the analysis more robust and results solid. In addition, it would make the results more relevant to the local decision making teams in each country.

In regards to GRACE-derived measurements, even though the thesis applied ICA to localize the signals, there is still need for higher resolution measurements in order to aid detailed local scale groundwater changes.

8 Appendix

Table 8.1: Three Corner-Hat (TCH) method and Triple collocation analysis (TCA) derived uncertainties of selected products over Greater Horn of Africa (GHA), Eastern Africa (EA), and Upper Greater Horn of Africa (UGHA). The two methods show similar trends of uncertainties but different magnitudes.

Product	TCH_EA	TCA_EA	TCH_UGHA	TCA_UGHA	TCH_GHA	TCA_GHA
MERRA-2	0.0202	0.2048	0.0248	0.2019	0.0134	0.6151
F_NOAH	0.0166	0.0749	0.0261	-0.0043	0.0103	-0.4634
G_VIC	0.0222	0.2678	0.0336	0.5180	0.0158	0.8276

Note: Negative values indicate violation of one of the assumptions of TCA (e.g., linear relationship between the measurement and true value, uncorrelated errors between measurements and/or with the truth).

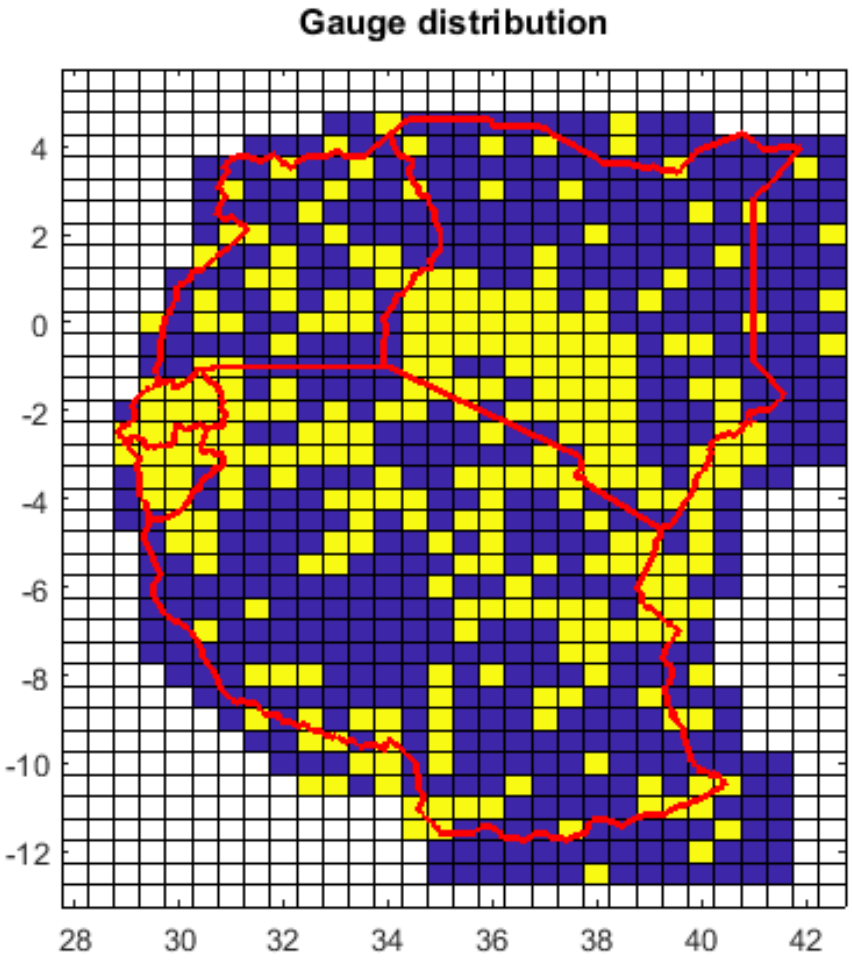

Figure 8.1: GPCC gauge distribution over East Africa. The yellow grids have rain gauge(s) while blue have none. Each grid is 0.5° by 0.5°.

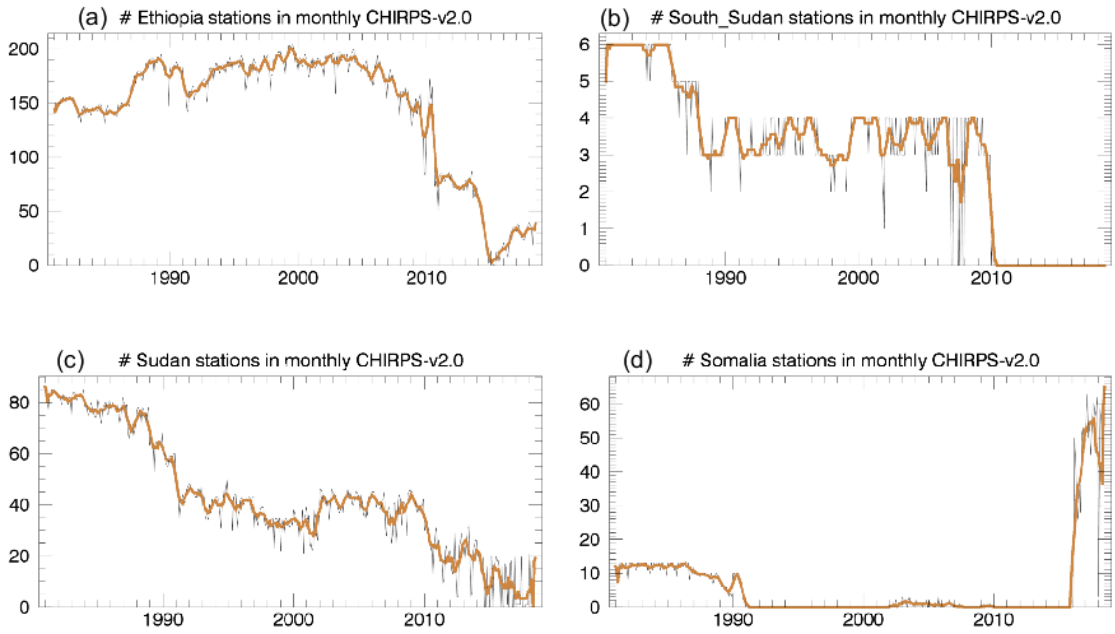

Figure 8.2: CHIRPS in-situ station numbers per country per month over UGHA. Ethiopia has relatively high number of stations while Somalia has the lowest. There is fluctuation in the station numbers across all the countries. (Source:http://chg.geog.ucsb.edu/data/chirps/#plus7).

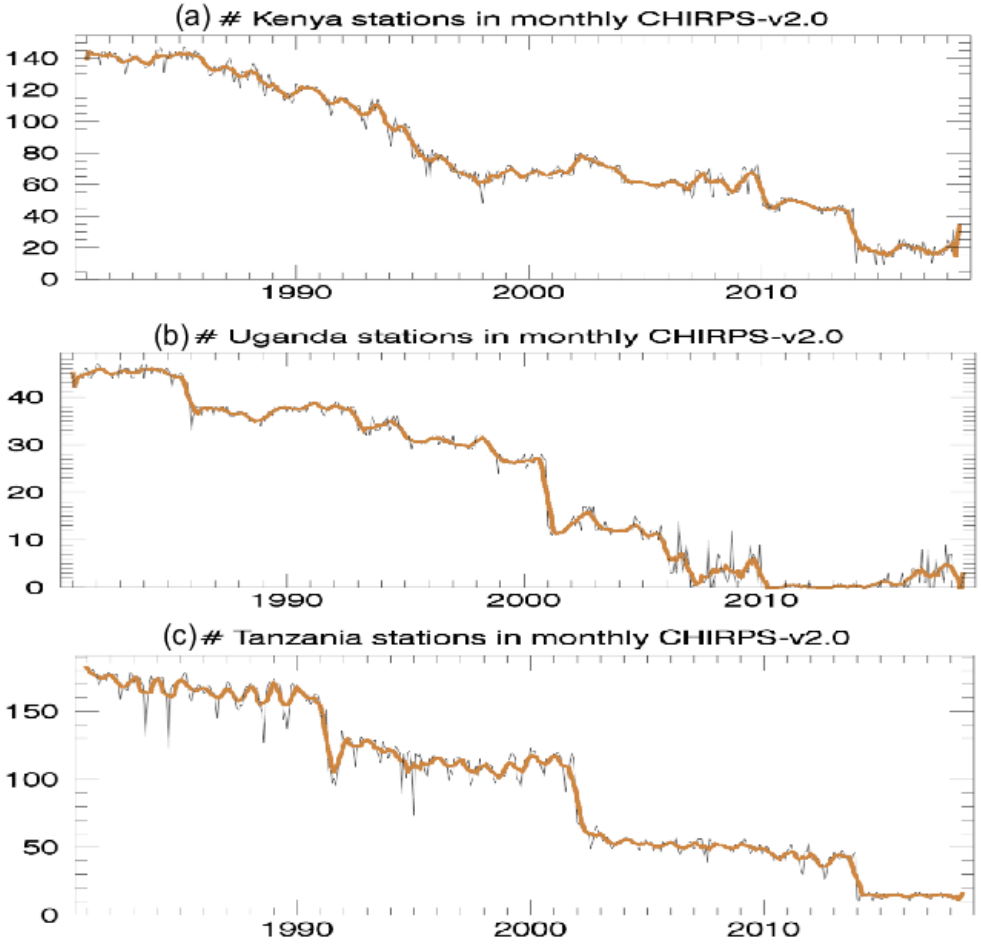

Figure 8.3: CHIRPS in-situ station numbers per country per month over East Africa. Kenya and Tanzania have relatively high number of stations while Uganda has low numbers. There is rapid fluctuation in the station numbers across all the countries as compared to Ethiopia (Fig. 8.2). (Source:http://chg.geog.ucsb.edu/data/chirps/#plus7).

Remote Sensing of Environment 194 (2017) 287–302

Contents lists available at ScienceDirect

Remote Sensing of Environment

journal homepage: www.elsevier.com/locate/rse

Assessing multi-satellite remote sensing, reanalysis, and land surface models' products in characterizing agricultural drought in East Africa

N.O. Agutu[a,b,*], J.L. Awange[a,c], A. Zerihun[d], C.E. Ndehedehe[a], M. Kuhn[a], Y. Fukuda[c]

[a] Department of Spatial Sciences, Curtin University Perth, Australia
[b] Department of Geomatic Engineering and Geospatial Information Systems, JKUAT, Nairobi, Kenya
[c] Department of Geophysics, Kyoto University, Japan
[d] Centre for Crop and Disease Management, Department of Environment and Agriculture, Curtin University, Perth, Australia

ARTICLE INFO

Article history:
Received 4 July 2016
Received in revised form 15 March 2017
Accepted 30 March 2017
Available online xxxx

Keywords:
Agricultural drought
East Africa
Partial least squares regression
Rotated principal component analysis
Rainfall
Standardized anomalies
Standardized index
SPI
Soil moisture
TWS
VCI

ABSTRACT

Heavy reliance of East Africa (EA) on rain-fed agriculture makes it vulnerable to drought-induced famine. Yet, most research on EA drought focuses on meteorological aspects with little attention paid on agricultural drought impacts. The inadequacy of in-situ rainfall data across EA has also hampered detailed agricultural drought impact analysis. Recently, however, there has been increased data availability from remote sensing (rainfall, vegetation condition index – VCI, terrestrial water storage – TWS), reanalysis (soil moisture and TWS), and land surface models (soil moisture). Here, these products were employed to characterise EA droughts between 1983 and 2013 in terms of severity, duration, and spatial extent. Furthermore, the capability of these products to capture agricultural drought impacts was assessed using maize and wheat production data. Our results show that while all products were similar in drought characterisation in dry areas, the similarity of CHIRPS and GPCC extended over the whole EA. CHIRPS and GPCC also identified the highest proportion of areas under drought followed closely by soil moisture products whereas VCI had the least coverage. Drought onset was marked first by a decline/lack of rainfall, followed by VCI/soil moisture, and then TWS. VCI indicated drought lag at 0–4 months following rainfall while soil moisture and TWS products had variable lags vis-à-vis rainfall. GLDAS mischaracterized the 2005–2006 drought vis-à-vis other soil moisture products. Based on the annual crop production variabilities explained, we identified CHIRPS, GPCC, FLDAS, and VCI as suitable for agricultural drought monitoring/characterization in the region for the study period. Finally, GLDAS explained the lowest percentages of the Kenyan and Ugandan annual crop production variances. These findings are important for the gauge data deficient EA region as they provide alternatives for monitoring agricultural drought.

© 2017 Elsevier Inc. All rights reserved.

1. Introduction

East Africa (EA, defined as Kenya, Uganda, Tanzania, Rwanda, and Burundi) relies heavily on rain-fed subsistence agriculture, which is increasingly becoming vulnerable to frequent drought events (see, e.g., Loewenberg, 2011; Rojas et al., 2011; Stampoulis et al., 2016). Furthermore, the impacts of drought are compounded by high levels of poverty, conflicts, population migration, and lack of social infrastructure across the region, triggering famine cycles every time an episode occurs (IFRC, 2011; Kurnik et al., 2011; Loewenberg, 2011; Nicholson, 2014; OEA, 2011a,b). As drought is in part a naturally recurrent feature in EA, there is a need for comprehensive and reliable monitoring in order to aid planning and mitigation of drought impacts. Since frequency and severity of droughts are likely to intensify with climate change (e.g., Williams and Funk, 2011), the need to characterize droughts in terms of duration, severity, frequency and spatial extent is critical.

Comprehensive characterization of drought in EA, like in many other places around the world, faces a number of challenges with respect to use of in-situ precipitation data. For instance, often spatial variability in precipitation cannot be adequately captured due to sparse and uneven spatial distribution of rain gauges. Furthermore, gaps in individual rainfall records, and at times lack of consistency due to poor handling complicate the use of precipitation data (Naumann et al., 2014; Nicholson, 2014; Rojas et al., 2011). In many studies, this led to the replacement or augmentation of in-situ rainfall data with remotely sensed precipitation, reanalysis, and model outputs, providing consistent and homogeneous data with global

* Corresponding author.
E-mail address: nathanagutu01@gmail.com (N.O. Agutu).

http://dx.doi.org/10.1016/j.rse.2017.03.041
0034-4257/© 2017 Elsevier Inc. All rights reserved.

coverage at various spatial scales that are suitable for drought monitoring (Damberg and AghaKouchak, 2014). However, these products can have considerable discrepancies and limitations in representing rainfall at local and regional scales (AghaKouchak et al., 2009; Damberg and AghaKouchak, 2014; Hong et al., 2006; Naumann et al., 2014; Rojas et al., 2011).

In addition to satellite and model-based precipitation products, normalised difference vegetation index (NDVI, Rousel et al., 1974; Tucker, 1979) and Gravity Recovery and Climate Experiment (GRACE) total water storage (TWS, Tapley et al., 2004) have been used to monitor drought. NDVI has been used directly or in its derivative form to monitor impacts of drought on vegetation health (e.g., Bayarjargal et al., 2006; Kogan, 1995; Rhee et al., 2010). In EA, it has been used by Anyamba and Tucker (2005), Anderson et al. (2012), and Nicholson (2014), while the use of GRACE satellite temporal gravity measurements (see, e.g., Tapley et al., 2004; Wouters et al., 2014) in EA has been limited to monitoring changes in TWS (e.g., Awange et al., 2008, 2013; Becker et al., 2010; Swenson and Wahr, 2009), and recently drought analysis (Awange et al., 2016).

Currently, drought studies carried out in the EA region range from purely precipitation based (e.g., Clark et al., 2003; Kurnik et al., 2011; Naumann et al., 2014), a combination of precipitation and climate models (e.g., Dutra et al., 2013; Yang et al., 2014a), to precipitation in combination with soil moisture and/or NDVI (e.g., AghaKouchak, 2015; Anderson et al., 2012; Nicholson, 2014). Some of the aforementioned studies and few others (see, e.g., Anderson et al., 2012; Mwangi et al., 2014; Rojas et al., 2011; Shukla et al., 2014) have examined agricultural drought using standardised precipitation index (SPI), NDVI, and/or soil moisture. However, for a region like EA, where the majority of the population depends on subsistence rain-fed agriculture, additional studies focusing on agricultural drought impacts, e.g., related to crop production, would be more relevant and beneficial to the population. Therefore, this study focuses on both the characterization of drought behavior in general and agricultural drought in particular using various indicators (precipitation, soil moisture, and total water storage) derived from multi-satellite remote sensing, reanalysis, and model products. Further, this study evaluates the utility of these products using annual crop production, which has so far not been done by the aforementioned studies.

To support agricultural drought monitoring from diverse indicators, it is imperative to identify and provide information on the most effective agricultural drought indicator or a combination of indicators for the EA region. Therefore, the objectives of this study are: (i) to characterise agricultural drought in terms of severity, duration, and spatial (areal) extent using satellite remote sensing, reanalysis, and modelled soil moisture data, and (ii) evaluate how well these products capture agricultural drought in the region as reflected by national crop production data (wheat and maize) during the study period.

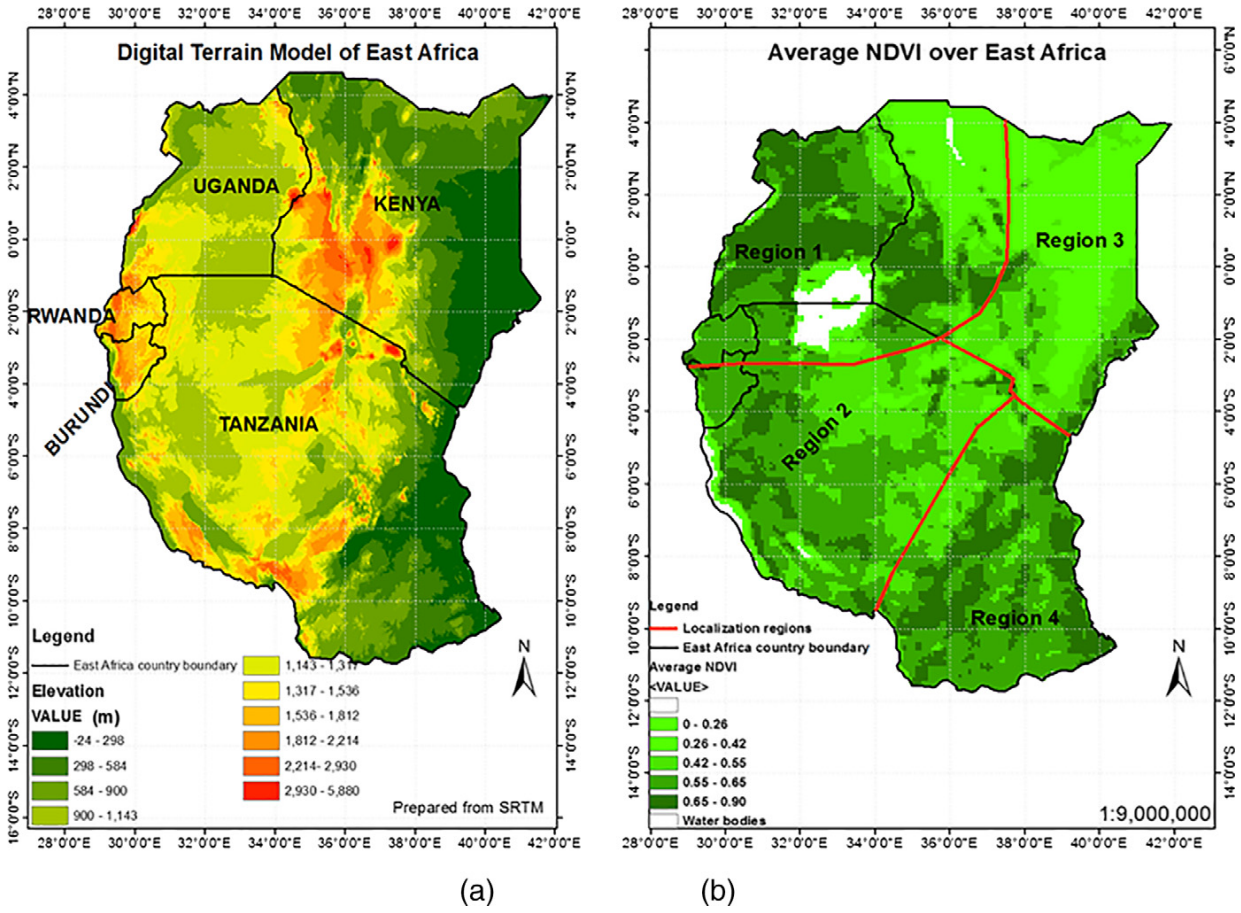

Fig. 1. East Africa (EA) region; (a) Elevation variation from Shuttle Radar Topographical Mission (SRTM, source: http://www.cgiar-csi.org/data/srtm-90m-digital-elevation-database), (b) Temporal NDVI average (1983–2014) with standardised indices localization regions (see Fig. 2 and Table 3 for region details).

To the best of our knowledge, this is the first comprehensive study to assess the potential of these remotely sensed products, reanalysis data, and land surface model outputs to monitor agricultural drought in the EA region. Moreover, this contribution proposes for the first time the possibility of using GRACE satellite products for agricultural drought monitoring in EA thus providing a link between TWS and crop production.

2. Study area and data

2.1. Study area

The EA region (Fig. 1) has a bimodal rainfall regime, the March-April-May (MAM; long rains) and the October-November-December (OND; short rains) with the MAM contributing over 70% of the annual rainfall while the OND contributing less than 20% (Michael, 2006). The rainfall regime is controlled by the inter-tropical convergence zone, effects of El Niño Southern Oscillation (ENSO), and sea surface temperature variations in the Indian and Pacific oceans (Clark et al., 2003; EACS, 2014; Lyon and DeWitt, 2012; Pricope et al., 2013; Tierney et al., 2013; Williams et al., 2012).

The amount of the MAM rainfall has been declining in the region since 1999, with the recent (1990's to 2000's) mean being below the 1980's mean (Lyon and DeWitt, 2012; Williams et al., 2012), while the frequency and duration of drought episodes have increased since 1998 (Lyon, 2014; Nicholson, 2014). Drought events have been observed in 2000–2001, 2005–2006, 2008–2009, and 2010–2011, with the latter being the worst in 60 years due to failure of short rains in 2010 and long rains in 2011. This particular drought affected over 12 million people bringing untold sufferings to the region (IFRC, 2011; Loewenberg, 2011).

2.2. Data

The following data sets were used (see Table 1 for a summary): precipitation products from the Global Precipitation Climatology Centre (GPCC) and Climate Hazard Group (Climate Hazard Group InfraRed Precipitation with Stations (CHIRPS)); soil moisture products from the Global Land Data Assimilation System (GLDAS), Climate Prediction Center (CPC), the European Centre for Medium-Range Weather Forecasts Interim Re-Analysis (ERA-Interim), the second Modern-Era Retrospective analysis for Research and Applications (MERRA-2), and Famine Early Warning System Network (FEWS NET) Land Data Assimilation System (FLDAS); Global Inventory Monitoring and Modelling Studies (GIMMS) NDVI; and terrestrial water storage (TWS) from MERRA-2 and GRACE.

2.2.1. Precipitation

1. CHIRPS is a quasi-global (50° S — 50° N) high resolution, 0.05°, daily, pentad, and monthly precipitation data set produced from a combination of in-situ station observations and satellite precipitation estimates based on Cold Cloud Duration (CCD) observations to represent sparsely gauged regions. It has been developed to primarily support agricultural drought monitoring (see Funk et al. (2015) for a detailed description). Monthly precipitation data, version 2.0, from 1982 to 2013 was downloaded from ftp://ftp.chg.ucsb.edu/pub/org/chg/products/CHIRPS-2.0/. CHIRPS precipitation was found to have correlation of greater than 0.75 with GPCC over EA region (see, e.g., Funk et al., 2015) and has subsequently been used in a number of drought and hydrology related studies in the region (see, e.g., McNally et al., 2016; Pricope et al., 2013; Shukla et al., 2014).
2. GPCC (Schneider et al., 2014) full data reanalysis version 7, 0.5° spatial resolution, monthly land surface precipitation from 1982 to 2013 downloaded from ftp://ftp.dwd.de/pub/data/gpcc/html/fulldata_v7_doi_download.html was used in addition to CHIRPS for drought analysis. It is a purely gauge gridded product based on 75,000 rain gauge stations worldwide, that feature record durations of 10 years or longer (see, Schneider et al., 2014). It has been used in several drought related studies both globally and in EA region (see, e.g., Dutra et al., 2014; Funk et al., 2014; Kurnik et al., 2011; Ziese et al., 2014).

2.2.2. Soil moisture

Soil moisture nominal depths considered in the study were root zone for MERRA-2; aggregation of 0–1 m depth layers for ERA-Interim, GLDAS, and FLDAS; and whole column depth (≈0.76 m) for CPC since its a single bucket layer product.

1. MERRA-2 is a NASA atmospheric re-analysis from 1980 that replaces the original MERRA reanalysis (Decker et al., 2012; Rienecker et al., 2011) using upgraded version of the Goddard Earth Observing System Model, version 5.12.4 (GEOS 5.12.4)

Table 1
A summary of the dataset used in this study.

	Data	Temporal resolution	Spatial resolution	Period used	Primary references/studies where used
Precipitation	GPCC	Monthly	0.5° × 0.5°	1982–2013	Dutra et al. (2014), Funk et al. (2014), Kurnik et al. (2011), Schneider et al. (2014), Ziese et al. (2014).
	CHIRPS	Monthly	0.05° × 0.05°	1982–2013	Funk et al. (2015), McNally et al. (2016), Pricope et al. (2013), Shukla et al. (2014).
Soil moisture	MERRA-2	Monthly	0.625° × 0.5°	1982–2013	Bosilovich et al. (2016, 2015).
	ERA-Interim	Monthly	0.25° × 0.25°	1982–2013	Albergel et al. (2012), Balsamo et al. (2009), Decker et al. (2012), Dee et al. (2011), Dutra et al. (2013), Mwangi et al. (2014), Viste et al. (2013).
	GLDAS	Monthly	1° × 1°	1982–2013	Anderson et al. (2012), Rodell et al. (2004), Yilmaz et al. (2014).
	FLDAS	Monthly	0.1° × 0.1°	1982–2013	Anderson et al. (2012), McNally et al. (2016), Rui and McNally (2016), Yilmaz et al. (2014).
	CPC	Monthly	0.5° × 0.5°	1982–2013	Dirmeyer et al. (2004), Fan and van den Dool (2004), van den Dool et al. (2003).
TWS	GRACE	Monthly	1° × 1°	2003–2013	Awange et al. (2016), Chen et al. (2004, 2009), Long et al. (2013), Tapley et al. (2004), Wouters et al. (2014).
	MERRA-2	Monthly	0.625° × 0.5°	1982–2013	Bosilovich et al. (2016, 2015).
VCI	NDVI	15 days	0.083° × 0.083°	1982–2013	Chen et al. (2014), Dorigo et al. (2012), Guan et al. (2012), Pinzon and Tucker (2014), Rojas et al. (2011), Tucker et al. (2005), Verdin et al. (2005).
Crop production	Crop production	Annual	National	1982–2013	http://www.fao.org/faostat/en/#data/QC

data assimilation system (Bosilovich et al., 2016). Monthly 0.625° by 0.5° root zone soil moisture from 1982 to 2013 was downloaded from https://gmao.gsfc.nasa.gov/reanalysis/MERRA-2/data_access/. Because of the improved assimilation system (updates to the treatment of canopy interception) and better forcing data (use of observation-corrected precipitation), MERRA-2 has improved soil moisture estimates over MERRA (Bosilovich et al., 2015).

2. ERA-Interim (Decker et al., 2012; Dee et al., 2011) monthly (monthly means of daily means) soil moisture, from 1982 to 2013, at 0.25° spatial resolution was downloaded from http://apps.ecmwf.int/datasets/data/interim-full-moda/levtype=sfc/. The three layers of soil moisture from 0 to 1 m were aggregated into one soil moisture product before application to drought analysis. ERA-Interim has been found to have a good skill in capturing surface soil moisture variability, though it tends to overestimate soil moisture, especially over dry lands (Albergel et al., 2012). In addition, it has been used in a number of studies globally and in EA region (see, e.g., Balsamo et al., 2009; Decker et al., 2012; Dee et al., 2011; Dutra et al., 2013; Mwangi et al., 2014; Viste et al., 2013).
3. GLDAS (Rodell et al., 2004) version 2, Noah, monthly 1° spatial resolution soil moisture product from 1982 to 2010 was downloaded from http://disc.sci.gsfc.nasa.gov/services/grads-gds/gldas. Like ERA-Interim, the three layers of soil moisture from 0 to 1 m depth were aggregated into one soil moisture product before further processing.
4. FLDAS is a custom instance of NASA Land information System (LIS), adapted to work with domains, data streams and monitoring, and forecast systems associated with food security assessment in data sparse, developing country settings (Rui and McNally, 2016). FLDAS is driven by Noah and VIC land surface models. FLDAS Noah 0.1° spatial resolution, monthly soil moisture from 1982 to 2013 downloaded from ftp://hydro1.sci.gsfc.nasa.gov/data/s4pa/FLDAS/FLDAS_NOAH01_C_EA_M.001/ was used. This soil moisture resulted from simulation run forced by a combination of MERRA-2 and CHIRPS dataset. Noah model (GLDAS and FLDAS) was chosen due to its wide use by atmospheric and land modelling communities hence model parameters are well tested (McNally et al., 2016). In addition, various studies have used it (Noah) over EA region e.g., Anderson et al. (2012), McNally et al. (2016), Yilmaz et al. (2014).
5. CPC (Fan and van den Dool, 2004; van den Dool et al., 2003) global monthly mean 0.5° spatial resolution soil moisture, version 2, for the duration 1982–2013 downloaded from the National Oceanic & Atmospheric Administration's (NOAA) Earth System Research Laboratory database (http://www.esrl.noaa.gov/psd/data/gridded/data.cpcsoil.html) was used. It is used in the present study because it incorporates in-situ rainfall as one of its inputs, hence likely to be closer to real soil moisture. CPC soil moisture simulates the seasonal and interseasonal annual variability reasonably well over EA region (see, Dirmeyer et al., 2004).

2.2.3. Terrestrial water storage (TWS)

1. GRACE satellite mission has been in operation from 2002 providing global monthly temporal gravity variations (see, e.g., Tapley et al., 2004; Wouters et al., 2014). These gravity variations are provided in terms of spherical harmonic coefficients. The Centre for Space Research's (CSR) release five (RL05) monthly spherical harmonic coefficients for the duration 2003–2013 downloaded from International Centre for Global Earth Models (ICGEM, http://icgem.gfz-potsdam.de/ICGEM/shms/monthly/csr-rl05/) were processed following the approach of Wahr et al. (1998) and used in this study. During the processing, the coefficients were filtered using a decorrelation and non-isotropic filter (see, e.g., Kusche, 2007; Kusche et al., 2009) in order to remove stripes and spurious patterns. This was followed by the application of a scaling factor, derived using GLDAS TWS following the approach of Landerer and Swenson (2012), onto the synthesised GRACE TWS to remove the leakage effect due to filtering. The synthesised GRACE-derived TWS over EA comprises changes from accumulated soil moisture, groundwater, surface water, and biomass/canopy water content. It is referred to as GTWS in the remainder of the manuscript. GRACE measurements agree with Earth rotation-derived changes and geophysical model estimates (Chen et al., 2004), and have a global root mean square error of 2 cm to degree and order 70, uniformly over land and ocean (Tapley et al., 2004). It has been used in a number of drought related studies both globally and in EA region (see, e.g., Awange et al., 2016; Chen et al., 2009; Long et al., 2013).
2. MERRA-2 total land water storage from 1982 to 2013, at 0.5° latitude by 0.625° longitude downloaded from https://gmao.gsfc.nasa.gov/reanalysis/MERRA-2/data_access/ was used in addition to GTWS. It does not include canopy water content and groundwater. It is referred to as MTWS in the remainder of the manuscript.

2.2.4. Vegetation condition index (VCI)

Long term series of NOAA Advanced Very High Resolution Radiometer (AVHRR) NDVI dataset 1982–2013, from NASA's Global Inventory and Modelling Systems (GIMMS) downloaded from http://ecocast.arc.nasa.gov/data/pub/gimms/3g.v0/ was used to compute VCI (Kogan, 1995). The data is comprised of 15 days maximum composites at 5-arc-minute spatial resolution (for a detailed description see Pinzon and Tucker (2014), Tucker et al. (2005)). VCI is advantageous as it is able to isolate weather related vegetation stress (Kogan, 1995; Quiring and Ganesh, 2010; Rojas et al., 2011), which within the study area, would correspond to water availability. It is computed as (Kogan, 1995)

$$VCI_i = 100 * \frac{NDVI_i - NDVI_{min}}{NDVI_{max} - NDVI_{min}}, \quad (1)$$

where $NDVI_i$ is the monthly NDVI, $NDVI_{max}$ and $NDVI_{min}$ are multi-year maximum and minimum NDVI, respectively.

AVHRR NDVI has been used extensively globally and over Africa for drought and other related studies (see, e.g., Chen et al., 2014; Dorigo et al., 2012; Guan et al., 2012; Rojas et al., 2011; Verdin et al., 2005).

2.2.5. National annual crop production

National annual maize and wheat production data for Kenya, Uganda, and Tanzania downloaded from Food and Agriculture Organization (FAO) data portal (http://www.fao.org/faostat/en/#data/QC) was used to evaluate the effectiveness of various satellite/model drought indices in capturing agricultural droughts. Even though this data set undergoes several quality checks along the processing chain (see, e.g., Kasnakoglu and Mayo, 2004), lack of direct production/yield reporting from farmers to government agencies in developing countries (e.g., EA region) means there is some level of uncertainty in the production data used. Even with the uncertainties, this data is still the most credible, readily available production data.

3. Methodology

Due to the existence of a link between agricultural drought and 1 to 6 months precipitation anomalies (e.g., Elagib, 2013; Kurnik et al., 2011; Rouault and Richard, 2003; Svoboda et al., 2012), Standardized

Table 2
Drought categories according to SPI values (Agnew, 2000).

SPI	Drought category
>1.65	Extremely wet
>1.28	Severely wet
>0.84	Moderately wet
> −0.84 and <0.84	Normal
< −0.84	Moderate drought
< −1.28	Severe drought
< −1.65	Extreme drought

Indices (SI) (e.g., SPI, McKee et al. (1993)) were derived to characterize agricultural drought using precipitation, VCI, TWS, and soil moisture products. Similarly, Standardized Anomalies (SA)/Z-scores (Wu et al., 2001) were computed to characterize drought from GTWS due to its short duration. The resulting SI and SA indices were then subjected to rotated principal component analysis to obtain their most dominant spatial and temporal drought variabilities. Finally, the temporal variabilities were subjected to partial least-squares regression analysis to determine how well they captured drought variability. Other than GRACE and GLDAS, all the other data sets were spatially aggregated to 1° by 1° before standardization for consistency. For all products, the unstandardized data were tested using w-statistics (Shapiro et al., 1968) and found to be normally distributed.

Given the differences in the variables used in this study, comparison of drought information was primarily carried out between various products of the same variables, e.g., between precipitation products, or soil moisture products, or TWS. Notwithstanding the differences between the variables, links/relations in drought information across the various products were explored since drought progresses from deficiencies in rainfall followed by moisture through to TWS.

3.1. Standardized precipitation index (SPI)

SPI (McKee et al., 1993), one of the most commonly used drought indices due to its numerous advantages (Svoboda et al., 2012), expresses precipitation anomalies with respect to its long term average. Its computation involves fitting a gamma probability distribution function to precipitation time series followed by the transformation of the accumulated gamma probability distribution to the cumulative distribution function of the standard normal distribution (see, e.g., Farahmand and AghaKouchak, 2015; Naresh Kumar et al., 2009). Due to the sensitivity of the computed SPI values to the fitted parametric distributions, especially at the tail ends of the distribution (see, Quiring, 2009), a non-parametric SPI fitting method was adopted in this study (see, e.g., Farahmand and AghaKouchak (2015) and the references therein for the formulation). This approach was implemented using the Standardized Drought Analysis Toolbox (SDAT, Farahmand and AghaKouchak (2015)) and the SPI drought limit categories (intensities) proposed by Agnew (2000) (Table 2) were used. For this study, a drought episode begins any time SPI is continuously less than −0.84 for a period of at least three months, and ends when SPI value exceeds −0.84. The various drought intensities (moderate, severe, and extreme) are then said to occur when the values in Table 2 are attained. The resulting standardized indices in this study were SPI, standardized soil moisture index (SSI), standardized vegetation condition index (SVCI), and standardized terrestrial water storage index (STWSI).

3.2. Standardized anomalies (SA)

As already pointed out, due to the short time frame of the GRACE products, SA instead of SI was computed for characterizing agricultural drought. Here, the 3 and 6-month GTWS time series cumulations were obtained in a manner similar to those of the Standardized Precipitation Index (McKee et al., 1993). Due to seasonality in precipitation, soil moisture, TWS, and NDVI dataset (Yang et al., 2014b), GTWS anomalies were calculated by removing the monthly mean from the 1, 3, and 6-month time series. The anomalies were then divided by the standard deviation for the duration of the data (e.g., Peters et al., 2002), i.e.,

$$XS_{ijk} = \frac{X_{ijk} - \frac{1}{n}\sum_{k=1}^{n} X_{ijk}}{\sigma_{ij}}, \quad (2)$$

where XS_{ijk} is the monthly standardized GTWS anomaly for location i, month j, and year k; X_{ijk} is the monthly GTWS for location i, month j, and year k; n is the length of GTWS in years; and σ_{ij} is the multi-year standard deviation for location i, month j. The resulting standardized anomalies (z-scores), express the deviation of the GTWS above or below the mean value and has been used to monitor drought in various studies (e.g., Agnew and Chappell, 1999; Katz and Glantz, 1986; Lough, 1997; Wu et al., 2001). Positive values indicate wet conditions, 0 indicate normal (average) conditions while negative values indicate drought conditions (Wu et al., 2001).

In order to demonstrate the consistency between SPI and SA in characterizing drought over the region, the study compared the spatio-temporal decompositions of CHIRPS-derived SPI and CHIRPS-derived SA over the study region. This comparison showed similar spatio-temporal drought patterns (See Figs. 2 and 4 for CHIRP-derived SPI spatio-temporal drought patterns). Further, Pearson correlations between the SI and SA temporal patterns were greater than 0.95 over the region. Due to the close association between SA and SI (see, Wu et al., 2001), the SPI drought limit categories (Table 2) were used to differentiate the various SA drought intensities.

3.3. Principal component analysis

Principal component analysis (PCA, Hannachi et al., 2007; Jolliffe, 2002; Lorenz, 1956; Preisendorfer, 1988; Wilks, 2006) is one of the most widely used methods in atmospheric sciences for pattern extraction and dimensionality reduction. It has been used in drought studies (e.g., Raziei et al., 2009; Santos et al., 2010; Sigdel and Ikeda, 2010) to decompose spatial-temporal fields such as SPI, SSI, SVCI, and STWSI, into spatial patterns and their corresponding temporal evolutions.

In this contribution, PCA was applied to the 1, 3, 6-month time scales of SI and SA. Log-eigenvalue (LEV) diagrams (Jolliffe, 2002) were used to determine and retain the significant components that were then rotated through Varimax rotation (Forina et al., 1988; Jolliffe, 1995; Kaiser, 1958) for better localization (for more information on rotated PCA, see, e.g., Hannachi et al. (2007), Richman (1986), Schönemann (1958), von Storch and Zwiers (1999)). The resulting spatial patterns, normalised by multiplying with the standard deviation of their corresponding rotated principal components (RPC) series, represent the correlation between the original data (in our case 1, 3, 6-month SI or SA at single grid point) and the corresponding RPC. Normalised RPC (divided by its standard deviation) represent SI/SA in each case (see Bordi et al. (2006)).

3.4. Partial least squares regression (PLSR)

PLSR is a regression technique in which the response variables are regressed on the predictor scores. The scores (few new variables) are

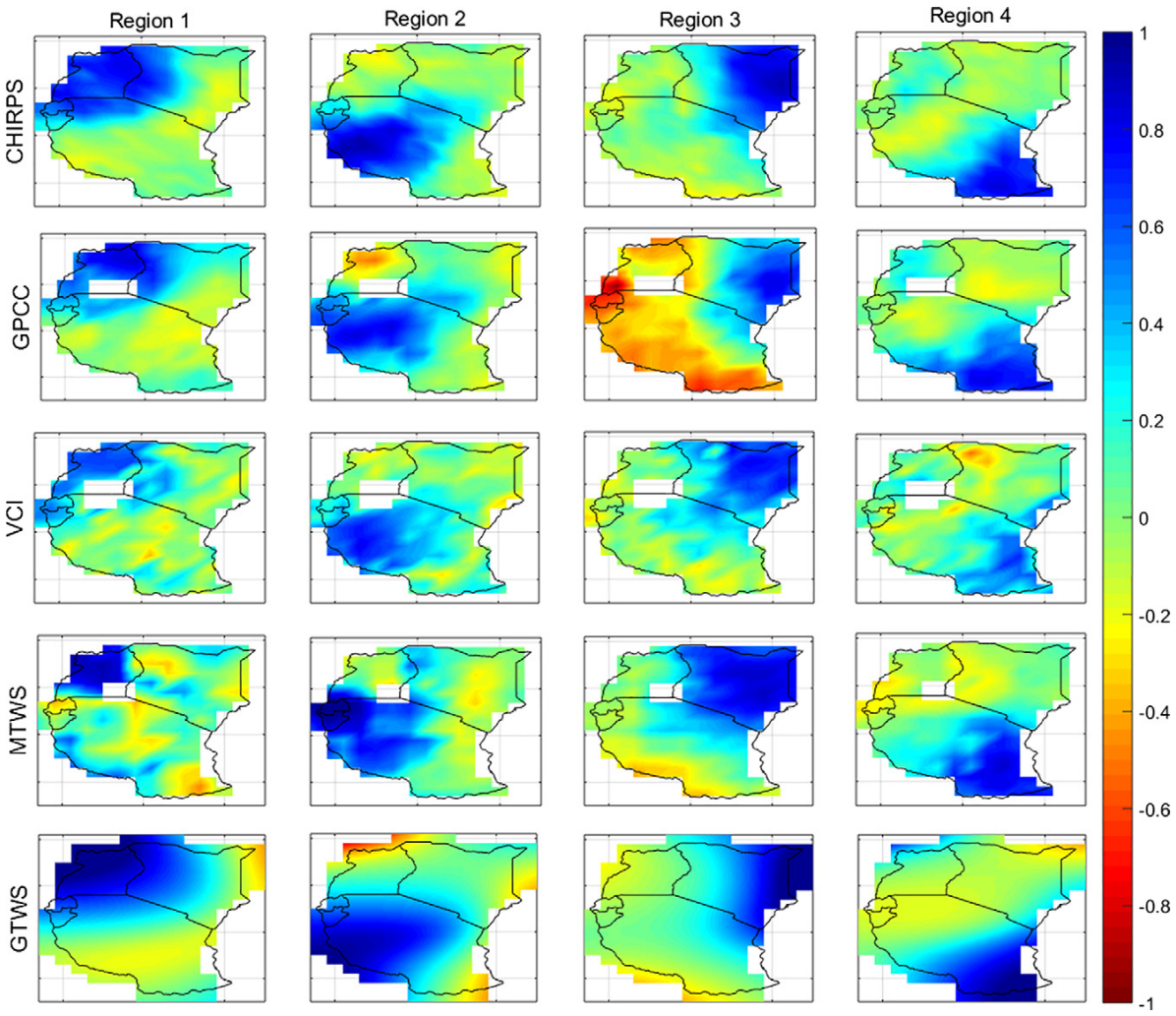

Fig. 2. Rotated principal component spatial patterns of standardized index/anomalies (SI/SA). Rows denote products while columns denote regions (also see Table 3). The spatial patterns have been scaled to ±1, thus the temporal evolutions shown in Fig. 4 indicate the actual magnitude of SA/SA for regions where the spatial patterns have values close to ±1. The spatial patterns are interpreted in conjunction with temporal evolutions in Fig. 4 and represent drought spatial patterns any time the temporal evolutions falls below −0.84, as in Table 2. The white rectangular area in all the images except CHIRPS and GTWS is Lake Victoria.

linear combinations of the original predictor variables (Geladi and Kowalski, 1986; Wold et al., 2001). The generation of the scores takes into account the variability in the dependent variable ensuring that only those components of the independent variables that are related to the dependent variables are used in the regression (Geladi and Kowalski, 1986). It is a generalization of the multiple linear regression (MLR), but unlike MLR, it can analyze data with collinearity (correlated), noisy, and with numerous predictor variables (Wold et al., 2001) hence its use in the current study. Detailed description and formulation can be found in Helland (2004) and van Huffel (1997).

For each country, SI/SA values for each month of the year over the entire duration were extracted from the rotated principal components. For example, considering Kenya with four GRACE SA rotated principal components, each component comprising 120 values/months (2004 to 2013), corresponding to January, February, ..., December were extracted resulting in four 10 by 12 matrices, i.e., 10 years of data for every month of the year. The resulting four matrices were concatenated to a 10 by 48 matrix, which served as the predictor variable in the PLSR against national annual production data (maize/wheat) as the response variable. This was done for 1, 3, and 6-month SA time scales for all the variables across Kenya, Uganda, and Tanzania.

4. Results and discussion

4.1. Spatio-temporal drought patterns

The PCA decomposition of SI/SA showed spatial and temporal patterns, which became very distinct upon applying varimax rotation as compared to unrotated components (data not shown). Integrating the spatial and temporal patterns of the SIs/SAs, and using the drought category definitions in Table 2, percentages of areas under various drought intensities were evaluated. The results presented and discussed here are for the 3-month time scale only, as this was representative of the results for the 1 and 6-month time scales.

4.1.1. Spatial variability

The four most significant components in terms of explaining the total variability from RPCA of SI/SA revealed four distinct spatial

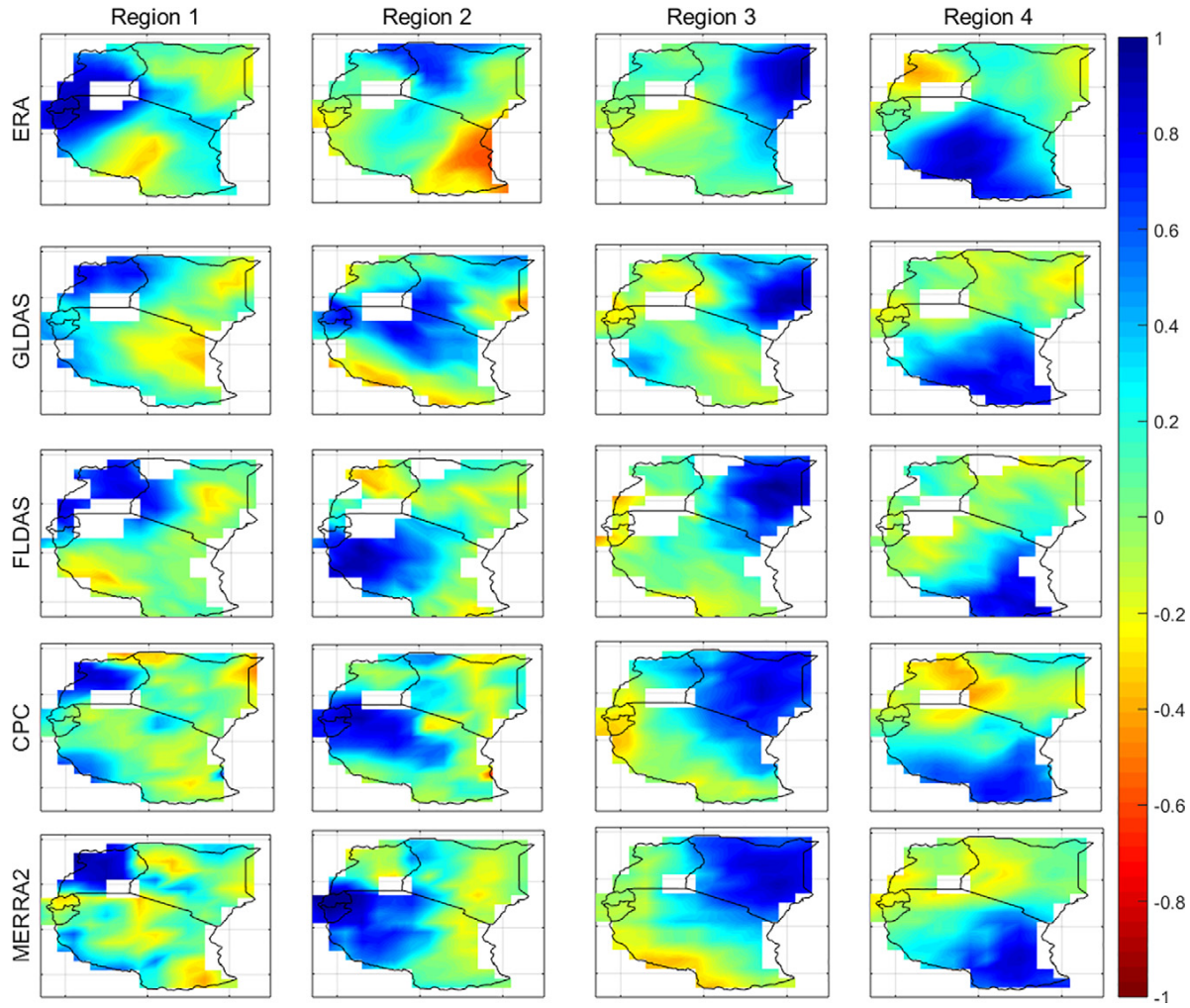

Fig. 3. Rotated principal component spatial patterns of standardized soil moisture indices (SSI). Rows denote products while columns denote regions (also see Table 3). The spatial patterns have been scaled to ±1, thus the temporal evolutions shown in Fig. 5 indicate the actual magnitude of SSI for regions where the spatial patterns have values close to ±1. The spatial patterns are interpreted in conjunction with temporal evolutions in Fig. 5 and represent drought spatial patterns any time the temporal evolutions falls below −0.84, as in Table 2. Patterns are consistent with those in Fig. 2 except for ERA-interim and to some extent GLDAS in region 2. The white rectangular area in all the images is Lake Victoria.

patterns across all products (Figs. 2 and 3). The geographical coverage of these spatial patterns is summarized in Table 3. The spatial patterns of ERA-Interim and to some extent of GLDAS in region 2 were different from those of other products.

The four RPCs explained between 38% (SVCI) and 96% (GTWS SA) of the total variance of the respective original SI/SA variables (Table 4). Most of the products had the highest and the lowest variabilities explained in regions 3 and 4, respectively (Table 4). This could be attributed to the fact that region 3 covering almost the entire region of Kenya (in those indicators showing it highest) is wet and dry on the western and eastern parts of the country, respectively, hence has high variability due to the presence of wet and dry extremes. On the other hand, region 4 is relatively wet and receives consistent rainfall resulting in a smaller variation in SI/SA.

4.1.2. Temporal patterns

The temporal evolutions of the spatial patterns in regions 1 to 4 (Figs. 2 and 3) from the rotated PCA are shown in Figs. 4 and 5. In general, the temporal evolutions (interpreted in conjunction with Figs. 2, 3, and Table 2) show most of the regions suffering from severe to extreme drought in 1984/1985, 1999, 2000, 2005/2006, and 2010/2011. These and other drought episodes captured in these figures are consistent with documented drought episodes in the EA region (e.g., IFRC, 2011; Masih et al., 2014; Nicholson, 2014).

All products had similar performance in region 3 (Figs. 4c and 5c), which may be attributed to the relatively flat terrain (Fig. 1a) coupled with relatively less rainfall hence good performance by the models and rainfall products. The performance of the rainfall products (CHIRPS and GPCC) were almost identical over the entire study region as a result of both containing in-situ rainfall (CHIRPS has satellite-derived precipitation estimates in addition to in-situ data while GPCC is purely gridded in-situ product, see e.g., Funk et al., 2015; Schneider et al., 2014). In relation to the rainfall products, the remaining products (VCI, soil moisture, and TWS) showed delayed (lagged) response in the temporal evolution. This is clearly visible in Fig. 4a in which MTWS appears like a low pass filtered version of the CHIRPS/GPCC signals. This behavior could be due to a delayed response of terrestrial water storage changes to rainfall and

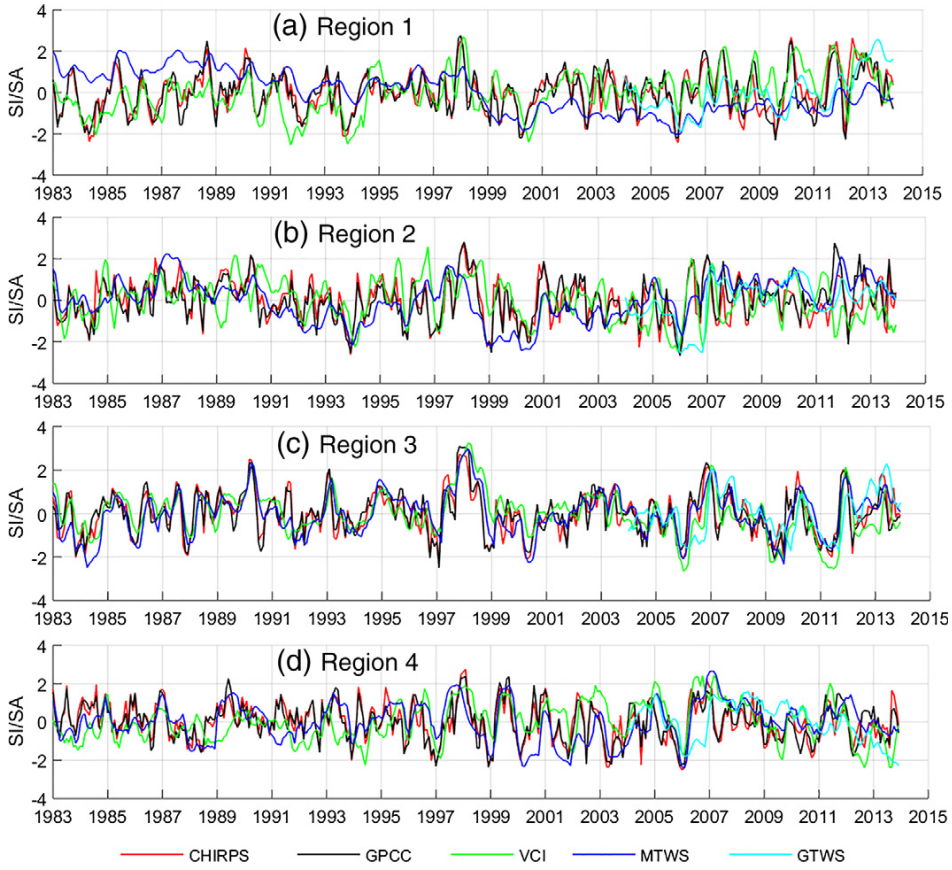

Fig. 4. Temporal evolutions of SA/SI spatial patterns in Fig. 2. The temporal evolutions are interpreted in conjunction with Table 2, to classify drought and/or wet conditions. Rainfall products (CHIRPS and GPCC) exhibit similar consistent performance across the region. Also, all the products exhibit consistent performance in region 3, while VCI and GTWS show some lag in relation to rainfall.

soil moisture changes. Finally, the soil moisture products seemed to be from largely two classes/categories of models with ERA-Interim, FLDAS, and GLDAS in one category and CPC and MERRA-2 on the other, especially considering region 1 (Fig. 5).

Further, correlation analysis between the drought indices revealed close relationships between various products e.g., CHIRPS and GPCC, MERRA-2, MTWS, and CPC, across the regions (Table 5). The close relationship between MTWS and MERRA-2 is similar to that between CHIRPS and GPCC, since MTWS include aspects of soil moisture captured by MERRA-2 in addition to greater depth of soil water content. Furthermore, the significant and high correlations between the drought indices in region 3 support the similar performance observed in Figs. 4c and 5c. VCI had weak negative correlation trends with the following products: MTWS, MERRA-2 and CPC in region 1 due to these products showing a pre-dominantly wet pre-1993 and dry post-1999 that was opposite to the general VCI trend.

Table 3
Geographical coverage of SI/SA spatial patterns.

Region	Countries/areas
1	Lake Victoria, Uganda, and western Kenya
2	Western Tanzania, Rwanda, and Burundi
3	Eastern Kenya
4	Eastern and southern Tanzania

4.1.3. Drought intensity area analyses

In order to gain further insight into the spatial extent of the drought events and their intensities, the spatial and temporal patterns (Figs. 2, 3, 4, and 5) were integrated and using drought limit (intensity) categories in Table 2, percentages of areas under drought (by intensity) were evaluated and results presented in Fig. 6. Rainfall, soil moisture and VIC products produced significantly different estimates of percentage of area under drought ($F_{2,2212} = 19.7$, $p < 0.0001$). In particular, the estimates from the rainfall (CHIRPS and GPCC at 13.09%) and soil moisture (11.90%) products were more than twice those of VCI (5.5%). One reason for the rainfall products showing more areas as being under drought may be that meteorological drought is a binary event (present or absent) which is not affected by modulating factors unlike the other drought indicators e.g., VCI. VCI-based drought, unlike meteorological drought, is modulated by soil characteristics (water holding capacity) and/or plant (vegetation) type. Thus, for example, there could be meteorological drought over an area but due to soil water retention capacity and/or vegetation with deep roots capable of drawing water from deep soils (underground), VCI indicates no drought condition, hence the smaller area under drought. Since the soil moisture products and MTWS are modelled from rainfall and other additional inputs, their estimates of percentage areas under drought are likely to follow closely those of rainfall. However, the soil moisture products had statistically significantly different percent of areas under drought among themselves as was determined by one way ANOVA ($F_{4,1250} = 3.5410$, $p = 0.0070$).

Table 4
Proportion of variances explained by various spatial patterns across the four regions (see, Figs. 2 and 3, and Table 3 for the regions). Many of the products explain highest and lowest variabilities in regions 3 and 4, respectively. In addition, MERRA-2 and MTWS appear very close.

Region	CHIRPS	GPCC	VCI	MTWS	GTWS	ERA-interim	GLDAS	CPC	MERRA-2	FLDAS
Region 1	15.26	12.07	8.24	13.86	29.88	18.91	11.79	10.29	13.61	14.86
Region 2	14.62	13.15	10.01	18.13	24.58	10.78	15.75	16.46	17.72	15.77
Region 3	15.26	13.67	12.57	21.44	21.58	14.32	14.22	21.80	21.98	18.21
Region 4	10.60	11.64	6.94	13.67	19.77	20.05	16.72	13.27	14.64	12.64
Total	55.53	50.53	37.77	67.10	95.81	64.06	58.48	61.83	67.95	61.48

The observed differences in percentage of drought areas between the various soil moisture products arise from differences in; (i) forcing precipitation, (ii) the ways in which the individual hydrological models partition precipitation into run-off and evapotranspiration, and (iii) water holding capacities, the last two of which impact on the modelled soil moisture sensitivities to precipitation variability (Shukla et al., 2014). The contribution of forcing precipitation on the differences in percentage of areas is highlighted by the differences in areas presented by GLDAS and FLDAS, products of the same model (Noah) but different forcing precipitation, hence different drought spatial extents and cycles. Of all the model forcing parameters, precipitation is the key factor determining the characteristics of the resulting soil moisture (see, e.g., Dirmeyer et al., 1999, 2004; Entin et al., 1999; Mo et al., 2012), hence the areal extents under drought.

The MERRA-2 products show similar patterns and are closer to CPC (Fig. 6d, e, and h) while GLDAS is closer to ERA-interim as had been observed from the correlations (Table 5) and in the temporal evolutions (Figs. 4 and 5). FLDAS appear to be in between the two groups. Also, the lag in drought detection (already noted in Figs. 4 and 5) becomes more evident with the rainfall products detecting drought onset and duration first, followed by VCI/soil moisture products, and finally the TWS products. This would be attributed to time delayed response in moisture accumulation from rainfall through soil moisture, vegetation, and finally to changes in TWS during both the start and cessation of rainfall. Generally, the results also indicate the post-1999 period as having more drought events with higher intensity than the pre-1999 period except for ERA-Interim and GLDAS indicators. This is in line with other drought and climate studies that observed a decline in rainfall since 1999 and increased drought frequencies (see, Lyon, 2014; Lyon and DeWitt, 2012; Yang et al., 2014a). Also, GLDAS seems to have underestimated the 2005–2006 drought in terms of both duration and intensity as compared to the rest of the soil moisture products.

Further, GTWS returned higher percentage of areas under drought on average than MTWS as confirmed by one way ANOVA (25.307 *vs* 9.8147 *at* $F_{1,138} = 16.1064, p = 0.0001$) though with

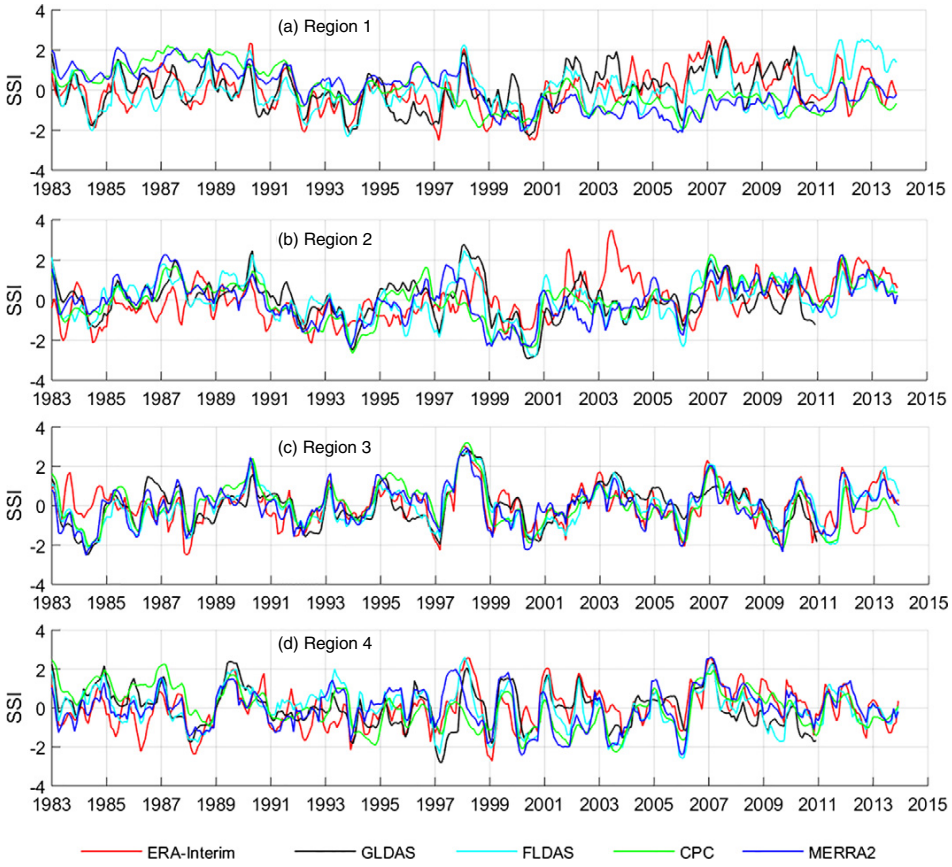

Fig. 5. Temporal evolutions of SSI spatial patterns in Fig. 3. The temporal evolutions are interpreted in conjunction with Table 2, to classify drought and/or wet conditions. All the moisture products have consistent performance in region 3 while in the rest of the regions, CPC is similar to MERRA-2 and similarly, ERA-Interim is closer to GLDAS.

Table 5
Relationship between the drought indices by regions: (i) Region-1 upper table, upper triangle (red), (ii) Region-2 upper table, lower triangle (blue), (iii) Region-3 lower table, upper triangle (green), and (iv) Region-4 lower table, lower triangle (brown). Regions are as in Fig. 2. Non-significant correlations are in italics ($p < 0.05$). Region 3 has the strongest relationships with all values being significant. Also, note the high correlations between the following products across the regions: GPCC and CHIRPS; and MTWS, MERRA-2, and CPC. (MTWS - MERRA-2 TWS, GTWS - GRACE TWS).

	CHIRPS	GPCC	VCI	MTWS	ERA	CPC	MERRA2	FLDAS	GLDAS	GTWS
CHIRPS	1	0.8991	0.4907	0.1203	0.4255	0.1073	0.2052	0.7300	0.5106	0.3196
GPCC	0.8619	1	0.4250	0.1288	0.4505	0.1266	0.2161	0.6120	0.5454	0.2433
VCI	0.2832	0.1918	1	–0.1082	0.4366	–0.1091	–0.0690	0.6737	0.527	0.3658
MTWS	0.3922	0.4683	0.2152	1	0.0526	0.8437	0.9910	0.1888	0.0359	0.7939
ERA	0.0947	0.2525	–0.1041	0.3628	1	0.1788	0.1138	0.5229	0.6664	–0.1708
CPC	0.2970	0.3962	0.2410	0.8714	0.4240	1	0.8482	0.1370	0.0976	0.5036
MERRA2	0.4546	0.5310	0.1889	0.9864	0.3791	0.8513	1	0.2431	0.0810	0.7352
FLDAS	0.6324	0.6352	0.4079	0.7372	0.2704	0.6844	0.7212	1	0.6365	0.7047
GLDAS	0.4141	0.4499	0.4494	0.5911	0.3352	0.6274	0.5583	0.6940	1	0.0643
GTWS	0.1101	0.0776	0.1863	0.7310	0.5553	0.6465	0.6651	0.4429	0.4505	1
CHIRPS	1	0.9267	0.5771	0.7388	0.6827	0.5622	0.7921	0.5914	0.4727	0.3796
GPCC	0.8959	1	0.5733	0.7023	0.6797	0.5583	0.7589	0.5377	0.4782	0.2643
VCI	0.2740	0.2788	1	0.7895	0.6614	0.8072	0.7636	0.7144	0.6837	0.6688
MTWS	0.4808	0.4919	0.4735	1	0.7195	0.8676	0.9912	0.8604	0.7316	0.6209
ERA	0.4095	0.3615	0.5310	0.5082	1	0.6686	0.7307	0.6937	0.6083	0.5950
CPC	0.4003	0.3978	0.2787	0.6799	0.3201	1	0.8267	0.8335	0.7513	0.6861
MERRA2	0.5482	0.5534	0.4569	0.9837	0.5250	0.6692	1	0.8256	0.6903	0.5743
FLDAS	0.6516	0.6312	0.4592	0.7627	0.5595	0.6161	0.7465	1	0.8302	0.7693
GLDAS	0.5047	0.5016	0.4130	0.4736	0.5432	0.5496	0.4578	0.7438	1	0.5598
GTWS	0.0196	0.0609	0.4195	0.4637	0.4334	0.4860	0.4200	0.2699	–0.0189	1

almost equal percentage of areas at drought peaks, at which GTWS lagged MTWS by 0–3 months in the detection of drought onset and cessation (Fig. 7a and b). Since MTWS is modelled on precipitation and other input without groundwater while GTWS is observed, the lack of groundwater in MTWS probably explains why it does not properly account for the buffer effect, hence possible lag by GRACE in detecting the onset and cessation of drought. In addition, GTWS shows drought episodes in the post 2012 period while MTWS does not (see, Fig. 7).

The drought severity is well captured by all the products as evidenced by the majority of the areas being under moderate drought followed by severe drought and then extreme according to the definition of SPI (see, e.g., Figs. 6 and 7; McKee et al., 1993). All the products captured different severity levels except MTWS and MERRA-2, which had similar severity levels as a result of overlapping formulation. The differences in severity levels among the other products could be attributed to the different formulation of the products and to the fact that they represent droughts in different environments with different impacting factors, e.g., soil properties influence the severity of drought as captured by the soil moisture products while rainfall characteristics (amount, intensity and duration) influence the drought severity as captured by rainfall products.

Finally, from the knowledge gained in the analyses above, the droughts of 1983–1984, 2005–2006, and 2010–2011 were examined closely using selected indicators in order to quantify the above-observed lags in drought cycles (Fig. 8, Table 6). These drought years have been selected for further analysis because they had more severe impacts in the region (see, e.g., Masih et al., 2014; Shukla et al., 2014; Spinage, 2012). From this analysis, VCI had a lag of 0–4 months in relation to CHIRPS in picking drought stages (onset, peak, and cessation) while the soil moisture products (CPC, ERA-Interim, GLDAS, FLDAS, and MERRA-2) had inconsistent lags among themselves, and in relation to CHIRPS for the considered drought episodes (e.g., Fig. 8, Table 6). Soil moisture, being an integration of rainfall anomalies over time (Dutra et al., 2008; Sheffield and Wood, 2008), is expected to have a lag in response to rainfall behavior throughout the hydrological cycle hence the soil moisture products and VCI (an indicator of moisture availability to vegetation) lag rainfall in the analysis. The inconsistency in the lags by the soil moisture products, similar to observed inconsistency in the percentage of areas under drought (Fig. 6), could be due to the different model forcing parameters used in generating various products in addition to different model thresholds as discussed above. Finally, the TWS products had different lags with GTWS having longer lag (Fig. 7). This longest lag from GTWS could be due to the fact that it is the last in the transition from rain event to moisture accumulation, and eventually groundwater change over time. Also, the under-characterization of the 2005–2006 drought by GLDAS already observed in Fig. 6g is clearer in Fig. 8b.

4.2. Assessing the effectiveness of drought indicators using crop production

In order to assess the effectiveness of the indicators in capturing agricultural drought, partial least square regression (PLSR) models were fitted with indices as the predictors and annual crop production data as the responses. The model with the lowest estimated mean

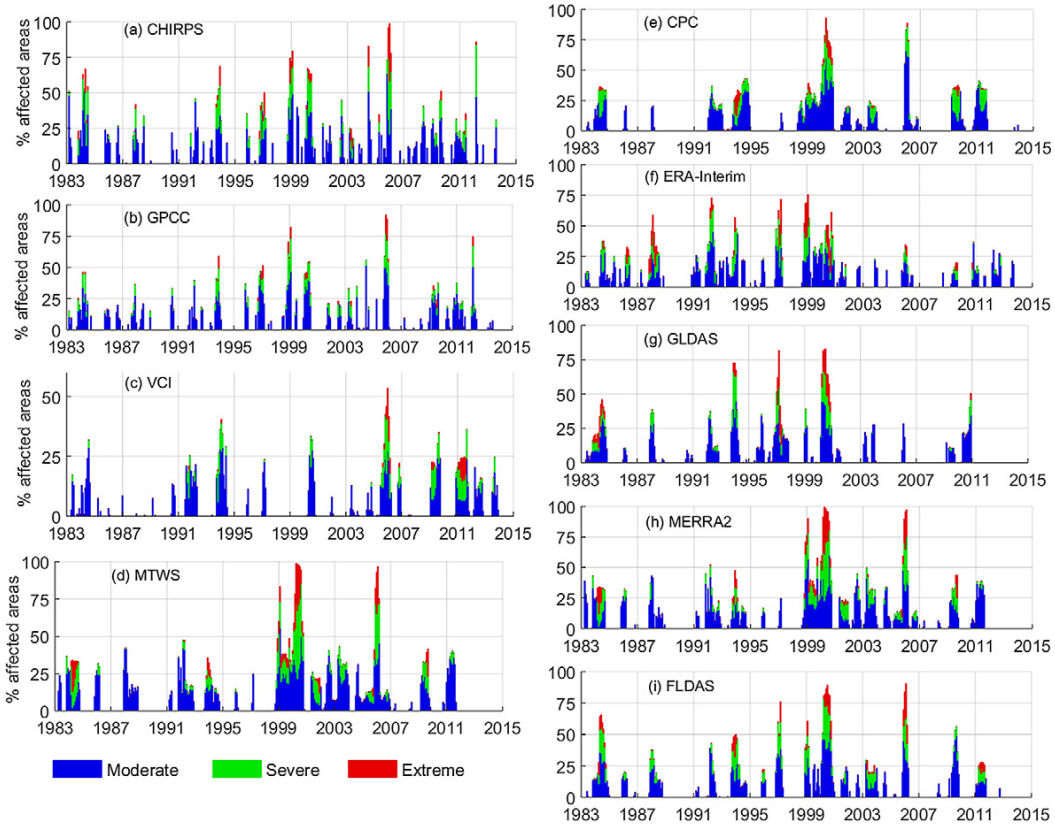

Fig. 6. Percentage of area affected by various drought intensities during the period 1983–2013. Percentage areas are computed by integrating the regional spatial and temporal patterns (Figs. 2, 3, 4, and 5) then determining percentage of pixels under each drought category as per Table 2. The rainfall products have the highest percentage areas under drought followed closely by soil moisture products and finally the lowest percentage areas are by VCI. In addition to the soil moisture products having different percentage areas under drought, CPC is consistent with MERRA-2, GLDAS is consistent with ERA-interim while FLDAS is in between.

squared prediction error was adopted in each case and the proportion of variability explained (R^2) used for comparison. As production is known to be related to water availability at various stages of crops growth (Hane and Pumphrey, 1984; Steduto et al., 2012), and water being a major growth determinant in the EA region (Barron et al., 2003), a good relationship is expected between drought indices that capture (characterize) drought well and crop production over the considered duration of time.

Because crop production data is reported at country level (national) while the generalization in Section 4.1 (Figs. 2 and 3) had signals across countries, SIs/SAs were re-computed for each country and the resulting rotated principal components reconstructed and used in PLSR with country level crop production data. The SIs were computed for the long term duration (1983–2013) and SAs for the short term (2004–2013). The latter duration though shorter, was necessitated by the need to compare the performance of GRACE SA against the other products. The proportions of variabilities explained (R^2) from the regression using the short duration (SAs) should be interpreted with care due to the short length of the data used.

For Kenya, other than GLDAS and ERA, the rest of the products performed fairly well for the period 1983–2013 with CHIPS, GPCC, and VCI explaining up to 94%, 73%, and 89%, respectively of the total annual variability in crop (wheat and maize) production (Fig. 9a). Similarly for Tanzania, CHIRPS, GPCC, and VCI explained up to 96%, 85%, and 89%, respectively of the total annual variability in crop (wheat and maize) production (Fig. 9b). Finally in Uganda, other than GLDAS, all the other products performed well with CHIRPS, ERA, FLDAS, and MTWS explaining up to 88%, 92%, 84%, and 77%, respectively of the total annual variability in crop (wheat and maize) production (Fig. 9c). The poor performance of GLDAS in Kenya and Uganda compared to other soil moisture products could be linked to poor performance in drought characterization as was observed in Section 4.1.3 and Figs. 6g and 8b. Most of the products explained higher proportions of annual variability in crop production (R^2) in 1-month standardized anomalies followed by 3 then 6-months. Also, the close performance of MERRA-2 and MTWS witnessed in drought characterization (Section 4.1.2 and Table 5) is evident in the amount of variabilities explained by these products across the region.

CHIRPS performed generally better than GPCC across the region (Fig. 9a–c). This could be attributed to the fact that in addition to rain gauge input, CHIRPS has satellite-derived rainfall estimates for areas with less or no rain gauge information unlike GPCC with only rain gauge measured rainfall hence its performance is dependent on gauge density and terrain changes (see, e.g., Funk et al., 2015; Schneider et al., 2014). In relation to the rainfall products (CHIRPS and GPCC), the soil moisture products explained less variability in annual crop production over EA region except in Uganda where the performance of ERA-Interim was almost as good as rainfall-derived indicators. Since soil moisture products represent the rainfall that remains after run-off and evaporation, the effective water available to the plants (crops), they are expected to explain higher variabilities in the annual crop production than rainfall thus their poor performance could be linked to how well they fit the region. In addition, the inconsistent performance of the soil moisture products

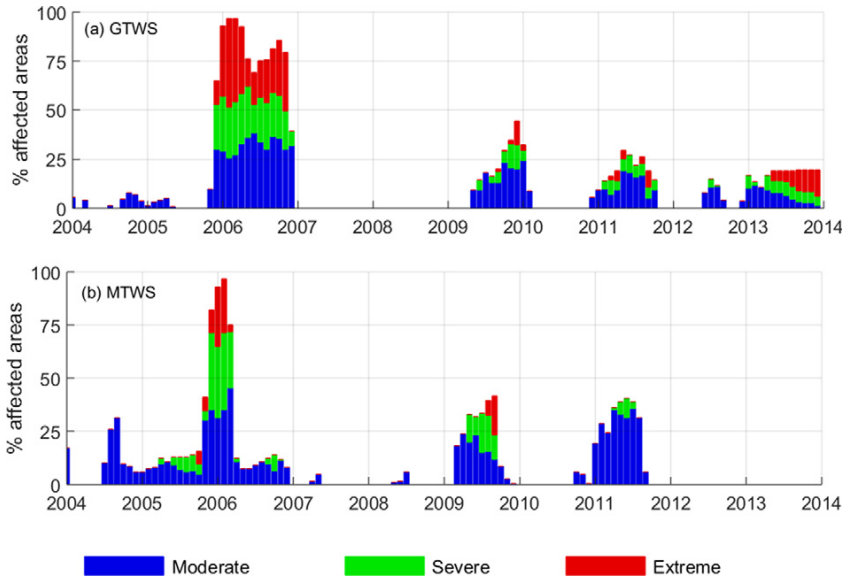

Fig. 7. Comparison of performance between GTWS and MTWS in terms of percentage of areas affected by various drought categories. Percentage areas are computed as in Fig. 6. They have consistent performance, with GTWS having a lag in drought detection probably due to groundwater that is lacking in MTWS.

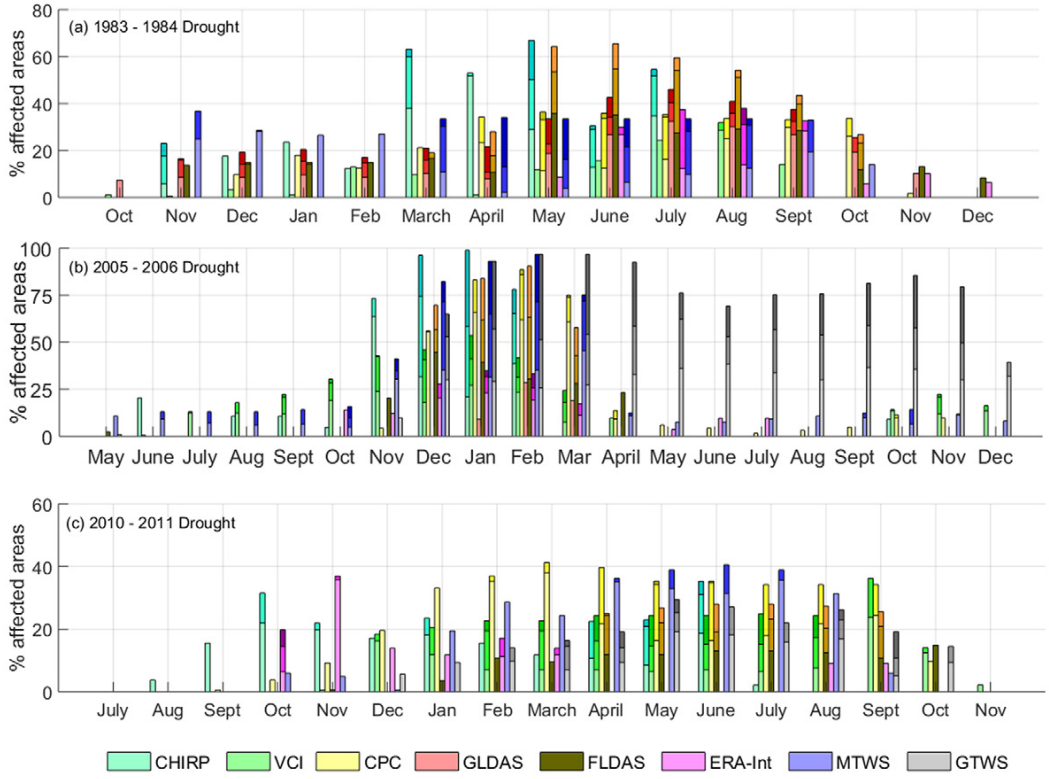

Fig. 8. Percentage of areas affected by various drought intensites during the 1983–1984, 2005–2006, and 2010–2011 drought episodes. Each bar has up to 3 colour grades (gradients) representing from bottom moderate, severe, and extreme droughts at the top. Percentage areas are computed as in Fig. 6 but only for the duration of drought. VCI has a lag of about 2–3 months in identifying the drought cycle in relation to CHIRPS. The rest of the products have inconsistent lags in relation to rainfall across the three drought episodes.

Table 6
Drought lags (in months) by various products in relation to CHIRPS drought cycle (onset, peak, and cessation). Negative values indicate the respective product had drought cycle before CHIRPS while dash indicate products not available during that particular drought. the lags were quantified from selected droughts of 1983–1984, 2005–2006, and 2010–2011, see Fig. 8.

Year/drought cycle	VCI	CPC	ERA	GLDAS	FLDAS	MTWS/MERRA2	GTWS
1983–1984/ Onset	1	1	6	−1	0	0	–
1983–1984/ Peak	3	0	3	2	1	−6	–
1983–1984/ Cessation	2	4	5	4	5	3	–
2005–2006/ Onset	1	5	4	7	5	−1	6
2005–2006/ Peak	0	1	0	1	1	1	1
2005–2006/ Cessation	2	>5	5	1	2	>5	>5
2010–2011/ Onset	3	1	2	–	3	2	4
2010–2011/ Peak	3	−3	−7	–	0	0	−1
2010–2011/ Cessation	4	3	−4	–	3	2	3

(CPC, ERA-Interim, GLDAS, FLDAS, and MERRA-2) and MTWS across the EA region in explaining the annual variability in crop production could be linked to the inconsistencies observed in the drought characterization as discussed in Section 4.1.2.

Overall, the good performance of FLDAS over GLDAS across the study region despite both being products of the same model (Noah) is due to the fact that for FLDAS, the Noah model was forced by CHIRPS, a precipitation product designed for the region. The magnitudes of the annual variabilities in crop production explained by FLDAS could be a pointer to difficulties faced by Noah in correctly partitioning precipitation into moisture, run-off, and evapotranspiration as per natural occurrence in the EA region.

Though based on a short duration data set (10 years), GRACE SA has mixed performance between wheat and maize across the countries but does better than or equals to soil moisture products across the region (Fig. 9d–f). The performance could be attributed to

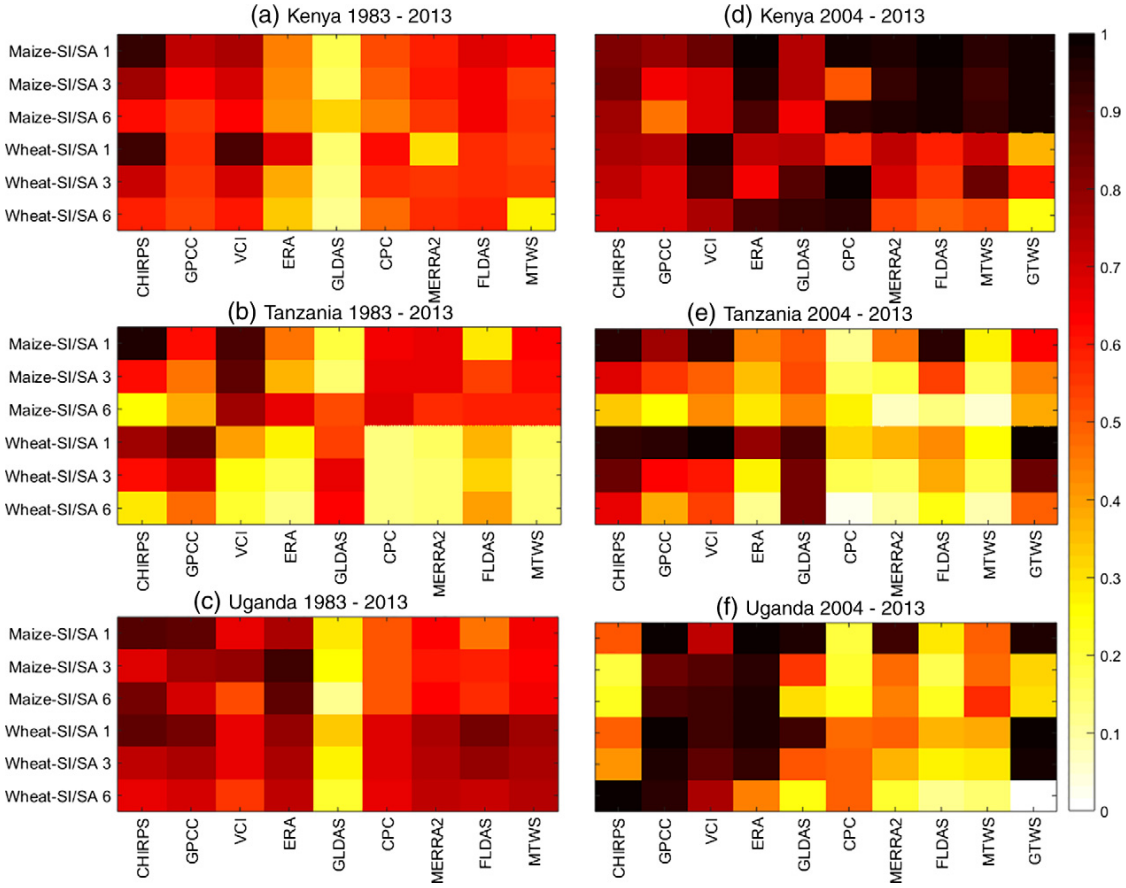

Fig. 9. Proportions of variability in national annual crop (maize and wheat) production (R^2) explained by various drought indices for Kenya, Tanzania, and Uganda. CHIRPS, GPCC, and VCI consistently explains relatively higher variability in crop production, while the soil moisture products have inconsistent performance (a, b, and c). The figures d, e, and f should be interpreted with care as the datasets used to fit the models are only 10 years long. Both SI and SA are computed at annual scales. (The y axis indicates the crop (maize/wheat), SI (for a, b, and c), and SA (for d, e and f) while 1,3 and 6 indicate the standardization time scales for the indicators on the x axis).

the fact that over a shorter duration of time such as the one considered (i.e., 1-, 3-, and 6-month anomalies), the bulk of the variation in the GRACE TWS occurs in the soil moisture compartment, which is more sensitive to climate variability than groundwater change (e.g., Yang et al., 2014b). This shows the potential of GRACE product to monitor agricultural drought although longer duration of dataset is essential.

Results from regression analysis should be interpreted with caution though, as the relationship between production and climate conditions (water availability) only hold if other factors in the production chain are held constant, e.g., areas under cultivation over the period considered and technical factors of production (e.g., fertilizers, crop cultivars, pesticides). In addition, production response to water at any stage of growth can be modified by various factors e.g., diseases, weeds, insects, crop variety (Hane and Pumphrey, 1984; Steduto et al., 2012), hence, results should not be generalized to other areas.

5. Conclusions

This study characterized agricultural drought over EA region using precipitation products (CHIRPS and GPCC), soil moisture products (CPC, ERA-Interim, MERRA-2, FLDAS, and GLDAS), and TWS products (MERRA-2 and GRACE). This was accomplished through standardized index/standardized anomaly and rotated principal component analyses. In addition, the study carried out partial least squares regression (PLSR) analysis over Kenya, Uganda, and Tanzania to assess the utility of these products in capturing agricultural drought in these countries.

Drought characterization results showed CHIRPS and GPCC as being similar and consistent over the entire region, while all the other products were consistent for region 3 (dry lowland eastern Kenya). In terms of percentage of areas under drought, the rainfall products (CHIRPS and GPCC) covered the highest areas followed closely by the soil moisture products, while VCI covered the least percentage areas under drought. Results further indicated drought cycle detection in the order; rainfall, VCI/soil moisture, and TWS. VCI had 0–4 months of lag in detecting drought cycle (onset, peak, and cessation) in relation to rainfall products while the soil moisture and TWS products had inconsistent lag varying from one drought to the next. Soil moisture products had different results (both lag and areas under drought), with ERA-Interim being closer to GLDAS, MERRA-2 being close to CPC while FLDAS was in between. GLDAS under-characterized the 2005–2006 drought to under 2 months in comparison to over 7 months of ERA and CPC. Finally, the TWS products were consistent with GTWS having few months' lag probably due to groundwater that is missing in MTWS.

From the PLSR analysis, consistent performances by CHIRPS, GPCC, and VCI in explaining relatively high proportions of variabilities in annual crop production in Kenya, Tanzania, and Uganda over the duration of the study was noted. In addition, the lack of consistency observed from the soil moisture products in drought characterization also was evident in the amount of annual crop production variability explained by them (soil moisture products) across the region. The study identified the following indicators as suitable for agricultural drought monitoring/characterization for the region during the study period; (a) for Kenya: CHIRPS, GPCC, VCI, MERRA-2, FLDAS and MTWS; (b) for Uganda: CHIRPS, GPCC, VCI, FLDAS, ERA, MERRA-2, and MTWS; and (c) for Tanzania: CHIRPS, GPCC, VCI, FLDAS, GLDAS and ERA. Also, GTWS showed potential in explaining the annual variability in crop production, albeit a longer period of dataset is required to evaluate its potential.

Further studies need to be undertaken to determine how well the model soil moisture products (CPC, ERA-Interim, MERRA-2, FLDAS, and GLDAS) and MTWS fit the region. Also, care should be taken in generalizing these results as production response to water at any different stages of crop growth can be modified by several factors.

Acknowledgements

N. O. Agutu and C. E. Ndehedehe are grateful to Curtin University for their PhD funding through the CSIRS programme. J.L. Awange is grateful for the financial support of the Japan Society of Promotion of Science for supporting his stay at Kyoto University (Japan) and the conducive working atmosphere provided by his host Prof Yoichi Fukuda (Department of Geophysics, Kyoto University, Japan). The authors are grateful to the following organizations for providing the data sets used in this study; CSR, FAO, ICGM, NASA, ECMWF, and USGS.

References

AghaKouchak, A., 2015. A multivariate approach for persistence-based drought prediction: application to the 2010–2011 East African Drought. J. Hydrol. 526, 127–135. http://dx.doi.org/10.1016/j.jhydrol.2014.09.063.

AghaKouchak, A., Nasrollahi, N., Habib, E., 2009. Accounting for uncertainties of the TRMM satellite estimates. Remote Sens. 1, 606–619. http://dx.doi.org/10.3390/rs1030606.

Agnew, C., Chappell, A., 1999. Drought in the Sahel. GeoJournal 48 (4), 299–311. http://dx.doi.org/10.1023/A:1007059403077.

Agnew, C.T., 2000. Using the SPI to identify drought. Drought Netw. News 12, 6–12.

Albergel, C., de Rosnay, P., Balsamo, G., Isaksen, L., Muñoz-Sabater, J., 2012. Soil moisture analyses at ECMWF: evaluation using global ground-based in situ observations. J. Hydrometeorol. 13 (5), 1442–1460. http://dx.doi.org/10.1175/JHM-D-11-0107.1.

Anderson, W.B., Zaitchik, B.F., hain, C.R., Anderson, M.C., Yilmaz, M.T., Mecikalski, J., Schultz, L., 2012. Towards an integrated soil moisture drought monitor for East Africa. Hydrol. Earth Syst. Sci. 16, 2893–2913. http://dx.doi.org/10.5194/hess-16-2893-2012.

Anyamba, A., Tucker, C.J., 2005. Analysis of Sahelian vegetation dynamics using NOAA-AVHRR NDVI data from 1981–2003. J. Arid Environ. 63 (3), 596–614. http://dx.doi.org/10.1016/j.jaridenv.2005.03.007.

Awange, J., Khandu, Schumacher, M., Forootan, E., Heck, B., 2016. Exploring hydrometeorological drought patterns over the Greater Horn of Africa (1979–2014) using remote sensing and reanalysis products. Adv. Water Resour. 94, 45–59. http://dx.doi.org/10.1016/j.advwatres.2016.04.005.

Awange, J.L., Sharifi, M.A., Ogonda, G., Wickert, J., Grafarend, E.W., Omulo, M.A., 2008. The falling lake Victoria water level: GRACE, TRIMM and CHAMP satellite analysis of the lake basin Water Resour. Manag. 22 (7), 775–796. http://dx.doi.org/10.1007/s11269-007-9191-y.

Awange, J.L., Anyah, R., Agola, N., Forootan, E., Omondi, P., 2013. Potential impacts of climate change and environmental change on the stored water of Lake Victoria Basin and economic implications. Water Resour. Res. 49, 8160–8173. http://dx.doi.org/10.1002/2013WR014350.

Balsamo, G., Beljaars, A., Scipal, K., Viterbo, P., van den Hurk, B., Hirschi, M., Betts, A.K., 2009. A revised hydrology for the ECMWF model: verification from field site to terrestrial water storage and impact in the integrated forecast system. J. Hydrometeorol. 10 (3), 623–643. http://dx.doi.org/10.1175/2008JHM1068.1.

Barron, J., Rockström, J., Gichuki, F., Hatibu, N., 2003. Dry spell analysis and maize yields for two semi-arid locations in east Africa. Agric. For. Meteorol. 117, 23–37. http://dx.doi.org/10.1016/S0168-1923(03)00037-6.

Bayarjargal, Y.A.K., Bayasgalan, M., Khudulmur, S., Gandush, C., Tucker, C.J., 2006. Comparative study of NOAA AVHRR derived vegetation indices using change vector analysis. Remote Sens. Environ. 105, 9–22. http://dx.doi.org/10.1016/j.rse.2006.06.003.

Becker, M., LLovel, W., Cazenave, A., Güntner, A., Crétaux, J., 2010. Recent hydrological behaviour of the East African great lakes region inferred from GRACE, satellite altimetry and rainfall observations. C. R. Geoscience 342, 223–233. http://dx.doi.org/10.1016/j.crte.2009.12.010.

Bordi, I., Fraedrich, K., Petitta, M., Sutera, A., 2006. Large-scale assessment of drought variability based on NCEP/NCAR and ERA-40 re-analyses. Water Resour. Manag. 20 (6), 899–915. http://dx.doi.org/10.1007/s11269-005-9013-z.

Bosilovich, M., Lucchesi, G., Suarez, M., 2016. MERRA-2: File Specification. GMAO Office Note No. 9 (Version 1.1). (73 pp, Available form: http://gmao.gsfc.nasa.gov/pubs/office_notes).

Bosilovich, M.G., Akella, S., Coy, L., Cullather, R., Draper, C., Gelaro, R., Kovach, R., Liu, Q., Molod, A., Norris, P., Chao, W., Reichle, R., Takacs, L., Todling, R., Vikhliaev, Y., Bloom, S., Collow, A., Partyka, G., Firth, S., Labow, G., Pawson, S., Reale, O., Schubert, S., Suarez, M., 2015. Merra-2: Initial evaluation of the climate. Technical Report Series on Global Modeling and Data Assimilation NASA/TM2015-104606/Vol. 43. NASA:GSFCG., available online at.

Chen, J.L., Wilson, C.R., Tapley, B.D., Ries, J.C., 2004. Low degree gravitational changes from GRACE: validation and interpretation. Geophys. Res. Lett. 31 (22). http://dx.doi.org/10.1029/2004GL021670. (n/a–n/a, l22607).

Chen, J.L., Wilson, C.R., Tapley, B.D., Yang, Z.L., Niu, G.Y., 2009. 2005 drought event in the Amazon River basin as measured by GRACE and estimated by climate models. J. Geophys. Res. Solid Earth 114 (B5). http://dx.doi.org/10.1029/2008JB006056. (n/a–n/a, B05404).

Chen, T., de Jeu, R., Liu, Y., van der Werf, G., Dolman, A., 2014. Using satellite based soil moisture to quantify the water driven variability in NDVI: a case study over mainland Australia. Remote Sens. Environ. 140, 330–338. http://dx.doi.org/10.1016/j.rse.2013.08.022.

Clark, C.O., Webster, P.J., Cole, J.E., 2003. Interdecadal variability of the relationship between the Indian Ocean Zonal Mode and East African Coastal Rainfall Anomalies. J. Clim. 16, 548–554. http://dx.doi.org/10.1175/1520-0442(2003)016¡0548:IVOTRB¿2.0.CO;2.

Damberg, L., AghaKouchak, A., 2014. Global trends and patterns of drought from space. Theor. Appl. Climatol. 117, 441–448. http://dx.doi.org/10.1007/s00704-013-1019-5.

Decker, M., Brunke, M.A., Wang, Z., Sakaguchi, K., Zeng, X., Bosilovich, M.G., 2012. Evaluation of the reanalysis products from GSFC, NCEP, and ECMWF using flux tower observations. J. Clim. 25, 1916–1944. http://dx.doi.org/10.1175/JCLI-D-11-00004.1.

Dee, D.P., Uppala, S.M., Simmons, A.J., Berrisford, P., Poli, P., Kobayashi, S., Andrae, U., Balmaseda, M.A., Balsamo, G., Bauer, P., Bechtold, P., Beljaars, A.C.M., van de Berg, L., Bidlot, J., Bormann, N., Delsol, C., Dragani, R., Fuentes, M., Geer, A.J., Haimberger, L., Healy, S.B., Hersbach, H., Hólm, E.V., Isaksen, L., Kållberg, P., Köhler, M., Matricardi, M., McNally, A.P., Monge-Sanz, B.M., Morcrette, J.-J., Park, B.-K, 2011. The ERA-Interim reanalysis: configuration and performance of the data assimilation system. Q. J. R. Meteorol. Soc. 137 (656), 553–597. http://dx.doi.org/10.1002/qj.828.

Dirmeyer, P.A., Dolman, A.J., Sato, N., 1999. The pilot phase of the global soil wetness project. Bull. Am. Meteorol. Soc. 80 (5), 851–878. http://dx.doi.org/10.1175/1520-0477(1999)080¡0851:TPPOTG¿2.0.CO;2.

Dirmeyer, P.A., Guo, Z., Gao, X., 2004. Comparison, validation, and transferability of eight multiyear global soil wetness products. J. Hydrometeorol. 5 (6), 1011–1033. http://dx.doi.org/10.1175/JHM-388.1.

Dorigo, W., de Jeu, R., Chung, D., Parinussa, R., Liu, Y., Wagner, W., Fernández-Prieto, D., 2012. Evaluating global trends (1988–2010) in harmonized multi-satellite surface soil moisture. Geophys. Res. Lett. 39 (18). http://dx.doi.org/10.1029/2012GL052988. (l18405).

Dutra, E., Viterbo, P., Miranda, P.M.A., 2008. ERA-40 reanalysis hydrological applications in the characterization of regional drought. Geophys. Res. Lett. 35 (19), 1–5. http://dx.doi.org/10.1029/2008GL035381. (l19402).

Dutra, E., Magnusson, L., Wetterhall, F., Cloke, H.L., Balsamo, G., Boussetta, S., Pappenberger, F., 2013. The 2010–2011 drought in the Horn of Africa in ECMWF reanalysis and seasonal forecast products. Int. J. Climatol. 33, 1720–1729. http://dx.doi.org/10.1002/joc.3545.

Dutra, E., Wetterhall, F., Di Giuseppe, F., Naumann, G., Barbosa, P., Vogt, J., Pozzi, W., Pappenberger, F., 2014. Global meteorological drought part 1: probabilistic monitoring. Hydrol. Earth Syst. Sci. 18 (7), 2657–2667. http://dx.doi.org/10.5194/hess-18-2657-2014.

EACS, 2014. East African Community Facts and Figures-2014. Report. East African Community Secretariat., (Retreaved on March 15, 2015).

Elagib, N.A., 2013. Meteorological drought and crop yield in Sub-Sahara Sudan. Int. J. Water Resour. Arid Environ. 2 (3), 164–171.

Entin, J.K., Robock, A., Vinnikov, K.Y., Zabelin, V., Liu, S., Namkhai, A., Adyasuren, T., 1999. Evaluation of global soil wetness project soil moisture simulations. J. Meteorol. Soc. Jpn. Ser. II 77 (1B), 183–198.

Fan, Y., van den Dool, H., 2004. Climate prediction center global monthly soil moisture data set at 0.5° resolution for 1948 to present. J. Geophys. Res. 109, D10102. http://dx.doi.org/10.1029/2003JD004345.

Farahmand, A., AghaKouchak, A., 2015. A generalized framework for deriving nonparametric standardized drought indicators. Adv. Water Resour. 76, 140–145. http://dx.doi.org/10.1016/j.advwatres.2014.11.012.

Forina, M., Armanino, C., Lanteri, S., Leardi, R., 1988. Methods of varimax rotation in factor analysis with applications in clinical and food chemistry. J. Chemom. 3, 115–125. http://dx.doi.org/10.1002/cem.1180030504.

Funk, C., Hoell, A., Shukla, S., Blade, I., Liebmann, B., Roberts, J.B., Robertson, F.R., Husak, G., 2014. Predicting East African spring droughts using Pacific and Indian Ocean sea surface temperature indices. Hydrol. Earth Syst. Sci. 18, 4965–4978. http://dx.doi.org/10.5194/hess-18-4965-2014.

Funk, C., Peterson, P., Landsfeld, M., Pedreros, D., Verdin, J., Shukla, S., Husak, G., Rowland, J., Harrison, L., Hoell, A., Michaelsen, J., 2015. The climate hazards infrared precipitation with stations - a new environmental record for monitoring extremes. Scientific Data 2 (150066), 1–21. http://dx.doi.org/10.1038/sdata.2015.66.

Geladi, P., Kowalski, B.R., 1986. Partial least-squares regression: a tutorial. Anal. Chem. Acta 185, 1–17.

Guan, K., Wood, E., Caylor, K., 2012. Multi-sensor derivation of regional vegetation fractional cover in Africa. Remote Sens. Environ. 124, 653–665. http://dx.doi.org/10.1016/j.rse.2012.06.005.

Hane, D.C., Pumphrey, F.V., 1984. Crop water use curves for irrigation scheduling. Special Report 706. Agricultural Experiment Station Oregon State University, Corvallis. (Retreaved on March 15, 2015).

Hannachi, A., Jolliffe, I.T., Stephenson, D.B., 2007. Empirical orthogonal functions and related techniques in atmospheric science: a review. Int. J. Climatol. 27, 1119–1152. http://dx.doi.org/10.1002/joc.1499.

Helland, I., 2004. Partial Least Squares Regression. John Wiley and Sons, Inc.. http://dx.doi.org/10.1002/0471667196.ess6004.pub2.

Hong, Y., Hsu, K.-l., Moradkhani, H., Sorooshian, S., 2006. Uncertainty quantification of satellite precipitation estimation and Monte Carlo assessment of the error propagation into hydrologic response. Water Resour. Res. 42 (8). http://dx.doi.org/10.1029/2005WR004398. (n/a–n/a, w08421).

IFRC, 2011. Drought in the Horn of Africa: preventing the next disaster. . International Federation of Red Cross and Red Crescent Societies, Geneva. Retreaved on March 15, 2015.

Jolliffe, I.T., 1995. Rotation of principal components: choice of normalization constraints. J. Appl. Stat. 22 (1), 29–35. http://dx.doi.org/10.1080/757584395.

Jolliffe, I.T., 2002. Principal Component Analysis. second ed., Springer Series in Statistics, Springer.

Kaiser, H.F., 1958. The Varimax Criterion for analytic rotation in factor analysis. Psychometrika 23 (3), 187–200. http://dx.doi.org/10.1007/BF02289233.

Kasnakoglu, H., Mayo, R., 2004. FAO statistical data quality framework: a multilayered approach to monitoring and assessment. Conference on Data Quality for International Organizations, Wiesbaden, Germany, 27 and 28 May 2004. (Accessed on 4/10/2016).

Katz, R.W., Glantz, M.H., 1986. Anatomy of a rainfall index. Mon. Weather Rev. 114, 764–771. http://dx.doi.org/10.1175/1520-0493(1986)114¡0764:AOARI¿2.0.CO;2.

Kogan, F., 1995. Application of vegetation index and brightness temperature for drought detection. Adv. Space Res. 15, 91–100. http://dx.doi.org/10.1016/0273-1177(95)00079-T.

Kurnik, B., Barbosa, P., Vogt, J., 2011. Testing two different precipitation datasets to compute the standardized precipitation index over the Horn of Africa. Int. J. Remote Sens. 32 (21), 5947–5964. http://dx.doi.org/10.1080/01431161.2010.499380.

Kusche, J., 2007. Approximate decorrelation and non-isotropic smoothing of time-variable GRACE-type gravity field models. J. Geod. 81, 733–749. http://dx.doi.org/10.1007/s00190-007-0143-3.

Kusche, J., Schmidt, R., Petrovic, S., Rietbroek, R., 2009. Decorrelated GRACE time-variable gravity solution by GFZ, and their validation using a hydrological model. J. Geod. 83, 903–913. http://dx.doi.org/10.1007/s00190-009-0308-3.

Landerer, F.W., Swenson, S.C., 2012. Accuracy of scaled GRACE terrestrial water storage estimates. Water Resour. Res. 48, http://dx.doi.org/10.1029/2011WR011453. (n/a–n/a, w04531).

Loewenberg, S., 2011. Humanitarian response inadequate in Horn of Africa crisis. The Lancet 378 (9791), 555–558. http://dx.doi.org/10.1016/S0140-6736(11)61276-2.

Long, D., Scanlon, B.R., Longuevergne, L., Sun, A.Y., Fernando, D.N., Save, H., 2013. GRACE satellite monitoring of large depletion in water storage in response to the 2011 drought in Texas. Geophys. Res. Lett. 40, 3395–3401. http://dx.doi.org/10.1002/grl.50655.

Lorenz, E.N., 1956. Empirical orthogonal function and statistical weather prediction. Statistical forecasting project: Scientific Report No. 1. Department of Meteorology, MIT., (Retrieved on March 15, 2015).

Lough, J.M., 1997. Regional indices of climate variation: temperature and precipitation in Queensland, Australia. Int. J. Climatol. 17, 55–66. http://dx.doi.org/10.1002/(SICI)1097-0088(199701)17:1¡55::AID-JOC109¿3.0.CO\ignorespaces;2-Z.

Lyon, B., 2014. Seasonal drought in the Greater Horn of Africa and its recent increase during the March-May long rains. J. Clim. 27, 7953–7975. http://dx.doi.org/10.1175/JCLI-D-13-00459.1.

Lyon, B., DeWitt, D.G., 2012. A recent and abrupt decline in the East African long rains. Geophys. Res. Lett. 39, L02702. http://dx.doi.org/10.1029/2011GL050337.

Masih, I., Maskey, S., Mussá, F.E.F., Trambauer, P., 2014. A review of droughts on the African continent: a geospatial and long-term perspective. Hydrol. Earth Syst. Sci. 18 (9), 3635–3649. http://dx.doi.org/10.5194/hess-18-3635-2014.

McKee, T.B., Doesken, N.J., Kleist, J., 1993. The relationship of drought frequency and duration to time scale. Conference Proceedings. (eighth Conference of Applied Climatology, Anaheim, California).

McNally, A., Shukla, S., Arsenault, K.R., Wang, S., Peters-Lidard, C.D., Verdin, J.P., 2016. Evaluating ESA CCI soil moisture in East Africa. Int. J. Appl. Earth Obs. Geoinf. 48, 96–109. http://dx.doi.org/10.1016/j.jag.2016.01.001.

Michael, C., 2006. Climate change impacts on East Africa. A review of the scientific literature. WFF-World Wide Fund For Nature, Gland, Switzerland. (Retrieved on March 15, 2015).

Mo, K.C., Chen, L.-C., Shukla, S., Bohn, T.J., Lettenmaier, D.P., 2012. Uncertainties in North American land data assimilation systems over the contiguous United States. J. Hydrometeorol. 13 (3), 996–1009. http://dx.doi.org/10.1175/JHM-D-11-0132.1.

Mwangi, E., Wetterhall, F., Dutra, E., Di Giuseppe, F., Pappenberger, F., 2014. Forecasting droughts in East Africa. Hydrol. Earth Syst. Sci. 18 (2), 611–620. http://dx.doi.org/10.5194/hess-18-611-2014.

Naresh Kumar, M., Murthy, C.S., Sesha Sai, M.V.R., Roy, P.S., 2009. On the use of Standardized Precipitation Index (SPI) for drought intensity assessment. Meteorol. Appl. 16 (3), 381–389. http://dx.doi.org/10.1002/met.136.

Naumann, G., Dutra, E., Pappenberger, F., Wetterhall, F., Vogt, J.V., 2014. Comparison of drought indicators derived from multiple data sets over Africa. Hydrol. Earth Syst. Sci. 18, 1625–1640. http://dx.doi.org/10.5194/hess-18-1625-2014.

Nicholson, S.E., 2014. A detailed look at the recent drought situation in the Greater Horn of Africa. J. Arid Environ. 103, 71–79. http://dx.doi.org/10.1016/j.jaridenv.2013.12.003.

OEA, 2011. Eastern Africa Drought humanitarian report. OCHA Eastern Africa, number 3, 01-31 May 2011. (Retrieved on March 17, 2015).

OEA, 2011. Eastern Africa Drought humanitarian report. . OCHA Eastern Africa, number 4, 01 June–15 July 2011., (Retrieved on March 17, 2015).

Peters, A.J., Waletr-Shea, E.A., Ji, L., Vin-a, A., Hayes, M., Svoboda, M.V., 2002. Drought monitoring with NDVI-Based Standardized Vegetation Index. Photogramm. Eng. Remote Sens. 68, 71–75.
Pinzon, J.E., Tucker, C.J., 2014. A non-stationary 1981–2012 AVHRR NDVI3g Time Series. Remote Sens. 6 (8), 6929. http://dx.doi.org/10.3390/rs6086929.
Preisendorfer, R.W., 1988. Principal component analysis in meteorology and oceanography. Development in Atmospheric Science 17. Elsevier, Elsevier, Amsterdam.
Pricope, N.G., Husak, G., Lopez-Carr, D., Funk, C., Michaelsen, J., 2013. The climate-population nexus in the East African Horn: emerging degradation trends in rangeland and pastoral livelihood zones. Glob. Environ. Chang. 23 (6), 1525–1541. http://dx.doi.org/10.1016/j.gloenvcha.2013.10.002.
Quiring, S.M., 2009. Developing objective operational definitions for monitoring drought. J. Appl. Meteorol. Climatol. 48 (6), 1217–1229. http://dx.doi.org/10.1175/2009JAMC2088.1.
Quiring, S.M., Ganesh, S., 2010. Evaluation of utility of Vegetation Condition Index (VCI) for monitoring meteorological drought in Texas. Agric. For. Meteorol. 150, 330–339. http://dx.doi.org/10.1016/j.agrformet.2009.11.015.
Raziei, T., saghafian, B., Paulo, A.A., Pereira, L.S., Bordi, I., 2009. Spatial patterns and temporal variability of drought in Western Iran. Water Resour. Manag. 23, 439–455. http://dx.doi.org/10.1007/s11269-008-9282-4.
Rhee, J., Im, J., Carbone, G.J., 2010. Monitoring agricultural drought for arid and humid regions using multi-sensor remote sensing data. Remote Sens. Environ. 114, 2875–2885. http://dx.doi.org/10.1016/j.rse.2010.07.005.
Richman, M.B., 1986. Rotation of Principal Components. J. Climatol. 6 (2), 293–335.
Rienecker, M.M., Suarez, M.J., Gelaro, R., Todling, R., Bacmeister, J., Liu, E., Bosilovich, M.G., Schubert, S.D., Takacs, L., Kim, G.-K., Bloom, S., Chen, J., Collins, D., Conaty, A., da Silva, A., Gu, W., Joiner, J., Koster, R.D., Lucchesi, R., Molod, A., Owens, T., Pawson, S., Pegion, P., Redder, C.R., Reichle, R., Robertson, F.R., Ruddick, A.G., Sienkiewicz, M., Woollen, J., 2011. MERRA: NASA's Modern-Era Retrospective Analysis for Research and Applications. J. Clim. 24 (14), 3624–3648. http://dx.doi.org/10.1175/JCLI-D-11-00015.1.
Rodell, M., Houser, P.R., Jambor, U., Gottschalck, J., Mitchell, K., Meng, C.J., Arsenault, K., Cosgrove, B., Radakovich, J., Bosilovich, M., Entin, J.K., Walker, J.P., Lohmann, D., Toll, D., 2004. The global land data assimilation system. Bull. Am. Meteorol. Soc. 85 (3), 381–394. http://dx.doi.org/10.1175/BAMS-85-3-381.
Rojas, O., Vrieling, A., Rembold, F., 2011. Assessing the drought probability for agricultural areas in Africa with coarse resolution remote sensing imagery. Remote Sens. Environ. 115, 343–352. http://dx.doi.org/10.1016/j.rse.2010.09.006.
Rouault, M., Richard, Y., 2003. Intensity and spatial extension of drought in South Africa at different time scales. Water SA 29 (4), 489–500. http://dx.doi.org/10.4314/wsa.v29i4.5057.
Rousel, J.W., Haas, R.H., Schell, J.A., Deering, D.W., Harlan, J.C., 1974. Monitoring the vernal advancement and retrogradation (green wave effect) of natural vegetation. NASA/GSFC Type III Final Report. (Greenbelt, MD).
Rui, H., McNally, A., 2016. FEWS NET land data assimilation system Version 1 (FLDAS-1) Products README. NASA/GSFC/HSL 1–18. (Retreaved from:ftp://hydro1.sci.gsfc.nasa.gov/data/s4pa/FLDAS/FLDAS_NOAH01_A_EA_M.001/doc/, on September 23 2016).
Santos, J.F., Pulido-Calvo, I., Portela, M.M., 2010. Spatial and temporal variability of drought in Portugal. Water Resour. Res. 46 (3). http://dx.doi.org/10.1029/2009WR008071. (n/a–n/a, w03503).
Schneider, U., Becker, A., Finger, P., Meyer-Christoffer, A., Ziese, M., Rudolf, B., 2014. GPCC's new land surface precipitation climatology based on quality-controlled in situ data and its role in quantifying the global water cycle. Theor. Appl. Climatol. 115 (1), 15–40. http://dx.doi.org/10.1007/s00704-013-0860-x.
Schönemann, P.H., 1958. Varisim: a new machine method for orthogonal rotation. Psychometrika 31 (2), 235–248. http://dx.doi.org/10.1007/BF02289510.
Shapiro, S.S., Wilk, M.B., Chen, H.J., 1968. A comparative study of various tests for normality. J. Am. Stat. Assoc. 63 (324), 1343–1372.
Sheffield, J., Wood, E.F., 2008. Global trends and variability in soil moisture and drought characteristics, 1950–2000, from observation-driven simulations of the terrestrial hydrologic cycle. J. Clim. 21 (3), 432–458.
Shukla, S., McNally, A., Husak, G., Funk, C., 2014. A seasonal agricultural drought forecast system for food-insecure regions of East Africa. Hydrol. Earth Syst. Sci. 18 (10), 3907–3921. http://dx.doi.org/10.5194/hess-18-3907-2014.
Sigdel, M., Ikeda, M., 2010. Spatial and temporal analysis of drought in Nepal using standardised precipitation index and its relationship with climate indices. J. Hydrol. and Meteorology 7 (1), 59–74. http://dx.doi.org/10.3126/jhm.v7i1.5617.
Spinage, C., 2012. African Ecology: Benchmarks and Historical Perspectives. Springer Geography, Springer Berlin Heidelberg.
Stampoulis, D., Andreadis, K.M., Granger, S.L., Fisher, J.B., Turk, F.J., Behrangi, A., Ines, A.V., Das, N.N., 2016. Assessing hydro-ecological vulnerability using microwave radiometric measurements from WindSat. Remote Sens. Environ. 184, 58–72. http://dx.doi.org/10.1016/j.rse.2016.06.007.
Steduto, P., Hsiao, T.C., Fereres, E., Raes, D., 2012. Crop yield response to water. FAO Irrigation and Drainage paper No. 66. FAO, Rome. (Retreaved on March 15, 2015).
Svoboda, M., Hayes, M., Wood, D., 2012. Standardized precipitation index user guide. World meteorological organization, WMO - No. 1090. (Retreaved on March 15, 2015).
Swenson, S., Wahr, J., 2009. Monitoring the water balance of Lake Victoria, East Africa, from space. J. Hydrol. 370, 163–176. http://dx.doi.org/10.1016/j.jhydrol.2009.03.008.
Tapley, B., Belabour, S., Watkins, M., Reigber, C., 2004. The gravity recovery and climate experiment: mission overview and early results. Geophys. Res. Lett. 31, 1–4. http://dx.doi.org/10.1029/2004GL019920.
Tierney, J.E., Smerdon, J.E., Anchukaitis, K.V., Seager, R., 2013. Multidecadal variability in East African hydroclimate controlled by the Indian Ocean. Nature 493, 389–392. http://dx.doi.org/10.1038/nature11785.
Tucker, C., Pinzon, J., Brown, M., Slayback, D., Pak, E., Mahoney, R., Vermote, E., El Saleous, N., 2005. An extended AVHRR 8-km NDVI dataset compatible with MODIS and SPOT vegetation NDVI data. Int. J. Remote Sens. 26 (20), 4485–4498. http://dx.doi.org/10.1080/01431160500168686.
Tucker, C.J., 1979. Red and photographic infra-red linear combinations for monitoring vegetation. Remote Sens. Environ. 8, 127–150. http://dx.doi.org/10.1016/0034-4257(79)90013-0.
van den Dool, H., Huang, J., Fan, Y., 2003. Performance and analysis of the constructed analogue method applied to U.S. soil moisture over 1981–2001. J. Clim. 108(D16), 8617. http://dx.doi.org/10.1029/2002JD003114.
van Huffel, S., 1997. Recent advances in total least squares techniques and errors-in–variables modeling. SIAM Proceedings in Applied Mathematics Series. Society for Industrial and Applied Mathematics.,
Verdin, J., Funk, C., Senay, G., Choularton, R., 2005. Climate science and famine early warning. Philos. Trans. R. Soc. Lond. B: Biol. Sci. 360 (1463), 2155–2168. http://dx.doi.org/10.1098/rstb.2005.1754.
Viste, E., Korecha, D., Sorteberg, A., 2013. Recent drought and precipitation tendencies in Ethiopia. Theor. Appl. Climatol. 112, 535–551. http://dx.doi.org/10.1007/s00704-012-0746-3.
von Storch, H., Zwiers, F.W., 1999. Statistical Analysis in Climate Research. Cambridge University Press, Cambridge.
Wahr, J., Molenaar, M., Bryan, F., 1998. Time variability of the Earth's gravity field: hydrological and oceanic effects and their possible detection using GRACE. J. Geophys. Res. Solid Earth 103(B12), 30205–30229. http://dx.doi.org/10.1029/98JB02844.
Wilks, D.S., 2006. Statistical methods in atmospheric sciences. second ed., Academic press, Amsterdam.
Williams, A.P., Funk, C., 2011. A westward extension of the warm pool leads to a westward extension of the Walker circulation, drying eastern Africa. Clim. Dyn. 37 (11), 2417–2435. http://dx.doi.org/10.1007/s00382-010-0984-y.
Williams, A.P., Funk, C., Michaelsen, J., Rauscher, S.A., Robertson, I., Wils, T.H.G., Koprowski, M., Eshetu, Z., Loader, N.J., 2012. Recent summer precipitation trends in the Greater Horn of Africa and the emerging role of Indian Ocean Sea surface temperature. J. Clim. Dynamics 39, 2307–2328. http://dx.doi.org/10.1007/s00382-011-1222-y.
Wold, S., Sjstrm, M., Eriksson, L., 2001. Pls-regression: a basic tool of chemometrics. Chemom. Intell. Lab. Syst. 58 (2), 109–130. http://dx.doi.org/10.1016/S0169-7439(01)00155-1.
Wouters, B., Bonin, J.A., Chambers, D.P., Riva, R.E.M., Sasgen, I., Wahr, J., 2014. GRACE, time-varying gravity, earth system dynamics and climate change. Rep. Prog. Phys. 77, http://dx.doi.org/10.1088/0034-4885/77/11/116801. (41pp).
Wu, H., Hayes, M.J., Weiss, A., Hu, Q., 2001. An evaluation of the standardized precipitation index, the China-Z index and the statistical Z-Score. Int. J. Climatol. 21, 745–758. http://dx.doi.org/10.1002/joc.658.
Yang, W., Seager, R., Cane, M.A., 2014. The East African long rains in observations and models. J. Clim. 27, 7185–7202. http://dx.doi.org/10.1175/JCLI-D-13-00447.1.
Yang, Y., Long, D., Guan, H., Scanlon, B.R., Simmons, C.T., Jiang, L., Xu, X., 2014. GRACE satellite observed hydrological controls on interannual and seasonal variability in surface greenness over mainland Australia. J. Geophys. Res. Biogeo. 119, 2245–2260. http://dx.doi.org/10.1002/2014JG002670.
Yilmaz, M.T., Anderson, M.C., Zaitchik, B., Hain, C.R., Crow, W.T., Ozdogan, M., Chun, J.A., Evans, J., 2014. Comparison of prognostic and diagnostic surface flux modeling approaches over the Nile River basin. Water Resour. Res. 50 (1), 386–408. http://dx.doi.org/10.1002/2013WR014194.
Ziese, M., Schneider, U., Meyer-Christoffer, A., Schamm, K., Vido, J., Finger, P., Bissolli, P., Pietzsch, S., Becker, A., 2014. The GPCC drought index a new, combined and gridded global drought index. Earth Syst. Sci. Data 6 (2), 285–295. http://dx.doi.org/10.5194/essd-6-285-2014.

ELSEVIER LICENSE
TERMS AND CONDITIONS

Aug 02, 2017

This Agreement between Mr. NATHAN AGUTU ("You") and Elsevier ("Elsevier") consists of your license details and the terms and conditions provided by Elsevier and Copyright Clearance Center.

License Number	4160731477840
License date	Aug 02, 2017
Licensed Content Publisher	Elsevier
Licensed Content Publication	Remote Sensing of Environment
Licensed Content Title	Assessing multi-satellite remote sensing, reanalysis, and land surface models' products in characterizing agricultural drought in East Africa
Licensed Content Author	N.O. Agutu,J.L. Awange,A. Zerihun,C.E. Ndehedehe,M. Kuhn,Y. Fukuda
Licensed Content Date	Jun 1, 2017
Licensed Content Volume	194
Licensed Content Issue	n/a
Licensed Content Pages	16
Start Page	287
End Page	302
Type of Use	reuse in a thesis/dissertation
Portion	full article
Format	both print and electronic
Are you the author of this Elsevier article?	Yes
Will you be translating?	No
Title of your thesis/dissertation	A REMOTE SENSING BASED APPROACH TO ENHANCE FOOD SECURITY IN THE GREATER HORN OF AFRICA
Expected completion date	Aug 2017
Estimated size (number of pages)	225
Requestor Location	Mr. NATHAN AGUTU FLAT 6, UNIT 2 63 JACKSON ROAD PERTH, KARAWARA 6152 Australia Attn: Mr. NATHAN AGUTU
Total	0.00 AUD
Terms and Conditions	

INTRODUCTION

1. The publisher for this copyrighted material is Elsevier. By clicking "accept" in connection with completing this licensing transaction, you agree that the following terms and conditions

apply to this transaction (along with the Billing and Payment terms and conditions established by Copyright Clearance Center, Inc. ("CCC"), at the time that you opened your Rightslink account and that are available at any time at http://myaccount.copyright.com).

GENERAL TERMS

2. Elsevier hereby grants you permission to reproduce the aforementioned material subject to the terms and conditions indicated.

3. Acknowledgement: If any part of the material to be used (for example, figures) has appeared in our publication with credit or acknowledgement to another source, permission must also be sought from that source. If such permission is not obtained then that material may not be included in your publication/copies. Suitable acknowledgement to the source must be made, either as a footnote or in a reference list at the end of your publication, as follows:

"Reprinted from Publication title, Vol /edition number, Author(s), Title of article / title of chapter, Pages No., Copyright (Year), with permission from Elsevier [OR APPLICABLE SOCIETY COPYRIGHT OWNER]." Also Lancet special credit - "Reprinted from The Lancet, Vol. number, Author(s), Title of article, Pages No., Copyright (Year), with permission from Elsevier."

4. Reproduction of this material is confined to the purpose and/or media for which permission is hereby given.

5. Altering/Modifying Material: Not Permitted. However figures and illustrations may be altered/adapted minimally to serve your work. Any other abbreviations, additions, deletions and/or any other alterations shall be made only with prior written authorization of Elsevier Ltd. (Please contact Elsevier at permissions@elsevier.com). No modifications can be made to any Lancet figures/tables and they must be reproduced in full.

6. If the permission fee for the requested use of our material is waived in this instance, please be advised that your future requests for Elsevier materials may attract a fee.

7. Reservation of Rights: Publisher reserves all rights not specifically granted in the combination of (i) the license details provided by you and accepted in the course of this licensing transaction, (ii) these terms and conditions and (iii) CCC's Billing and Payment terms and conditions.

8. License Contingent Upon Payment: While you may exercise the rights licensed immediately upon issuance of the license at the end of the licensing process for the transaction, provided that you have disclosed complete and accurate details of your proposed use, no license is finally effective unless and until full payment is received from you (either by publisher or by CCC) as provided in CCC's Billing and Payment terms and conditions. If full payment is not received on a timely basis, then any license preliminarily granted shall be deemed automatically revoked and shall be void as if never granted. Further, in the event that you breach any of these terms and conditions or any of CCC's Billing and Payment terms and conditions, the license is automatically revoked and shall be void as if never granted. Use of materials as described in a revoked license, as well as any use of the materials beyond the scope of an unrevoked license, may constitute copyright infringement and publisher reserves the right to take any and all action to protect its copyright in the materials.

9. Warranties: Publisher makes no representations or warranties with respect to the licensed material.

10. Indemnity: You hereby indemnify and agree to hold harmless publisher and CCC, and their respective officers, directors, employees and agents, from and against any and all claims arising out of your use of the licensed material other than as specifically authorized pursuant to this license.

11. No Transfer of License: This license is personal to you and may not be sublicensed, assigned, or transferred by you to any other person without publisher's written permission.

12. No Amendment Except in Writing: This license may not be amended except in a writing signed by both parties (or, in the case of publisher, by CCC on publisher's behalf).

13. Objection to Contrary Terms: Publisher hereby objects to any terms contained in any purchase order, acknowledgment, check endorsement or other writing prepared by you, which terms are inconsistent with these terms and conditions or CCC's Billing and Payment terms and conditions. These terms and conditions, together with CCC's Billing and Payment terms and conditions (which are incorporated herein), comprise the entire agreement between you and publisher (and CCC) concerning this licensing transaction. In the event of any conflict between your obligations established by these terms and conditions and those established by CCC's Billing and Payment terms and conditions, these terms and conditions shall control.
14. Revocation: Elsevier or Copyright Clearance Center may deny the permissions described in this License at their sole discretion, for any reason or no reason, with a full refund payable to you. Notice of such denial will be made using the contact information provided by you. Failure to receive such notice will not alter or invalidate the denial. In no event will Elsevier or Copyright Clearance Center be responsible or liable for any costs, expenses or damage incurred by you as a result of a denial of your permission request, other than a refund of the amount(s) paid by you to Elsevier and/or Copyright Clearance Center for denied permissions.

LIMITED LICENSE

The following terms and conditions apply only to specific license types:
15. **Translation**: This permission is granted for non-exclusive world **English** rights only unless your license was granted for translation rights. If you licensed translation rights you may only translate this content into the languages you requested. A professional translator must perform all translations and reproduce the content word for word preserving the integrity of the article.
16. **Posting licensed content on any Website**: The following terms and conditions apply as follows: Licensing material from an Elsevier journal: All content posted to the web site must maintain the copyright information line on the bottom of each image; A hyper-text must be included to the Homepage of the journal from which you are licensing at http://www.sciencedirect.com/science/journal/xxxxx or the Elsevier homepage for books at http://www.elsevier.com; Central Storage: This license does not include permission for a scanned version of the material to be stored in a central repository such as that provided by Heron/XanEdu.
Licensing material from an Elsevier book: A hyper-text link must be included to the Elsevier homepage at http://www.elsevier.com . All content posted to the web site must maintain the copyright information line on the bottom of each image.

Posting licensed content on Electronic reserve: In addition to the above the following clauses are applicable: The web site must be password-protected and made available only to bona fide students registered on a relevant course. This permission is granted for 1 year only. You may obtain a new license for future website posting.
17. **For journal authors:** the following clauses are applicable in addition to the above:
Preprints:
A preprint is an author's own write-up of research results and analysis, it has not been peer-reviewed, nor has it had any other value added to it by a publisher (such as formatting, copyright, technical enhancement etc.).
Authors can share their preprints anywhere at any time. Preprints should not be added to or enhanced in any way in order to appear more like, or to substitute for, the final versions of articles however authors can update their preprints on arXiv or RePEc with their Accepted Author Manuscript (see below).
If accepted for publication, we encourage authors to link from the preprint to their formal publication via its DOI. Millions of researchers have access to the formal publications on ScienceDirect, and so links will help users to find, access, cite and use the best available version. Please note that Cell Press, The Lancet and some society-owned have different preprint policies. Information on these policies is available on the journal homepage.

Accepted Author Manuscripts: An accepted author manuscript is the manuscript of an article that has been accepted for publication and which typically includes author-incorporated changes suggested during submission, peer review and editor-author communications.
Authors can share their accepted author manuscript:

- immediately
  - via their non-commercial person homepage or blog
  - by updating a preprint in arXiv or RePEc with the accepted manuscript
  - via their research institute or institutional repository for internal institutional uses or as part of an invitation-only research collaboration work-group
  - directly by providing copies to their students or to research collaborators for their personal use
  - for private scholarly sharing as part of an invitation-only work group on commercial sites with which Elsevier has an agreement
- After the embargo period
  - via non-commercial hosting platforms such as their institutional repository
  - via commercial sites with which Elsevier has an agreement

In all cases accepted manuscripts should:

- link to the formal publication via its DOI
- bear a CC-BY-NC-ND license - this is easy to do
- if aggregated with other manuscripts, for example in a repository or other site, be shared in alignment with our hosting policy not be added to or enhanced in any way to appear more like, or to substitute for, the published journal article.

Published journal article (JPA): A published journal article (PJA) is the definitive final record of published research that appears or will appear in the journal and embodies all value-adding publishing activities including peer review co-ordination, copy-editing, formatting, (if relevant) pagination and online enrichment.
Policies for sharing publishing journal articles differ for subscription and gold open access articles:
Subscription Articles: If you are an author, please share a link to your article rather than the full-text. Millions of researchers have access to the formal publications on ScienceDirect, and so links will help your users to find, access, cite, and use the best available version.
Theses and dissertations which contain embedded PJAs as part of the formal submission can be posted publicly by the awarding institution with DOI links back to the formal publications on ScienceDirect.
If you are affiliated with a library that subscribes to ScienceDirect you have additional private sharing rights for others' research accessed under that agreement. This includes use for classroom teaching and internal training at the institution (including use in course packs and courseware programs), and inclusion of the article for grant funding purposes.
Gold Open Access Articles: May be shared according to the author-selected end-user license and should contain a CrossMark logo, the end user license, and a DOI link to the formal publication on ScienceDirect.
Please refer to Elsevier's posting policy for further information.
18. **For book authors** the following clauses are applicable in addition to the above:
Authors are permitted to place a brief summary of their work online only. You are not allowed to download and post the published electronic version of your chapter, nor may you scan the printed edition to create an electronic version. **Posting to a repository:** Authors are permitted to post a summary of their chapter only in their institution's repository.
19. **Thesis/Dissertation**: If your license is for use in a thesis/dissertation your thesis may be submitted to your institution in either print or electronic form. Should your thesis be

published commercially, please reapply for permission. These requirements include permission for the Library and Archives of Canada to supply single copies, on demand, of the complete thesis and include permission for Proquest/UMI to supply single copies, on demand, of the complete thesis. Should your thesis be published commercially, please reapply for permission. Theses and dissertations which contain embedded PJAs as part of the formal submission can be posted publicly by the awarding institution with DOI links back to the formal publications on ScienceDirect.

Elsevier Open Access Terms and Conditions

You can publish open access with Elsevier in hundreds of open access journals or in nearly 2000 established subscription journals that support open access publishing. Permitted third party re-use of these open access articles is defined by the author's choice of Creative Commons user license. See our open access license policy for more information.

Terms & Conditions applicable to all Open Access articles published with Elsevier:

Any reuse of the article must not represent the author as endorsing the adaptation of the article nor should the article be modified in such a way as to damage the author's honour or reputation. If any changes have been made, such changes must be clearly indicated.

The author(s) must be appropriately credited and we ask that you include the end user license and a DOI link to the formal publication on ScienceDirect.

If any part of the material to be used (for example, figures) has appeared in our publication with credit or acknowledgement to another source it is the responsibility of the user to ensure their reuse complies with the terms and conditions determined by the rights holder.

Additional Terms & Conditions applicable to each Creative Commons user license:

CC BY: The CC-BY license allows users to copy, to create extracts, abstracts and new works from the Article, to alter and revise the Article and to make commercial use of the Article (including reuse and/or resale of the Article by commercial entities), provided the user gives appropriate credit (with a link to the formal publication through the relevant DOI), provides a link to the license, indicates if changes were made and the licensor is not represented as endorsing the use made of the work. The full details of the license are available at http://creativecommons.org/licenses/by/4.0.

CC BY NC SA: The CC BY-NC-SA license allows users to copy, to create extracts, abstracts and new works from the Article, to alter and revise the Article, provided this is not done for commercial purposes, and that the user gives appropriate credit (with a link to the formal publication through the relevant DOI), provides a link to the license, indicates if changes were made and the licensor is not represented as endorsing the use made of the work. Further, any new works must be made available on the same conditions. The full details of the license are available at http://creativecommons.org/licenses/by-nc-sa/4.0.

CC BY NC ND: The CC BY-NC-ND license allows users to copy and distribute the Article, provided this is not done for commercial purposes and further does not permit distribution of the Article if it is changed or edited in any way, and provided the user gives appropriate credit (with a link to the formal publication through the relevant DOI), provides a link to the license, and that the licensor is not represented as endorsing the use made of the work. The full details of the license are available at http://creativecommons.org/licenses/by-nc-nd/4.0.

Any commercial reuse of Open Access articles published with a CC BY NC SA or CC BY NC ND license requires permission from Elsevier and will be subject to a fee.

Commercial reuse includes:

- Associating advertising with the full text of the Article
- Charging fees for document delivery or access
- Article aggregation
- Systematic distribution via e-mail lists or share buttons

Posting or linking by commercial companies for use by customers of those companies.

20. **Other Conditions**:

v1.9

Questions? customercare@copyright.com or +1-855-239-3415 (toll free in the US) or +1-978-646-2777.

Bibliography

Abdi, H., W. Chin, V. Vinzi, G. Russolillo, and L. Trinchera (2013), *New Perspectives in Partial Least Squares and Related Methods*, Springer Proceedings in Mathematics & Statistics, Springer New York.

Abiye, T. A. (2010), An overview of the transboundary aquifers in East Africa, *Journal of African Earth Sciences*, *58*(4), 684 – 691, doi:http://dx.doi.org/10.1016/j.jafrearsci.2009.10.003.

Adhikari, U., A. P. Nejadhashemi, and S. A. Woznicki (2015), Climate change and Eastern Africa: a review of impact on major crops, *Food and Energy Security*, *4*(2), 110–132, doi:10.1002/fes3.61.

AghaKouchak, A. (2015), A multivariate approach for persistence-based drought prediction: Application to the 2010–2011 East African Drought, *Journal of Hydrology*, *526*, 127–135, doi:10.1016/j.jhydrol.2014.09.063.

AghaKouchak, A., N. Nasrollahi, and E. Habib (2009), Accounting for Uncertainties of the TRMM Satellite Estimates, *Remote Sensing*, *1*, 606–619, doi:10.3390/rs1030606.

AghaKouchak, A., A. Farahmand, F. S. Melton, J. Teixeira, M. C. Anderson, B. D. Wardlow, and C. R. Hain (2015), Remote sensing of drought: Progress, challenges and opportunities, *Reviews of Geophysics*, *53*(2), 452–480, doi:10.1002/2014RG000456, 2014RG000456.

Agnew, C., and A. Chappell (1999), Drought in the Sahel, *GeoJournal*, *48*(4), 299–311, doi:10.1023/A:1007059403077.

Agnew, C. T. (2000), Using the SPI to identify drought, *Drought Network News*, *12*, 6 – 12.

Agola, N. O., and J. L. Awange (2014), *Globalized Poverty and Environment*, 1 ed., Springer Berlin Heidelberg, doi:10.1007/978-3-642-39733-2.

Agutu, N., J. Awange, A. Zerihun, C. Ndehedehe, M. Kuhn, and Y. Fukuda (2017), Assessing multi-satellite remote sensing, reanalysis, and land surface models' products in characterizing agricultural drought in East Africa, *Remote Sensing of Environment*, *194*, 287 – 302, doi:http://doi.org/10.1016/j.rse.2017.03.041.

Albergel, C., P. de Rosnay, G. Balsamo, L. Isaksen, and J. Muñoz-Sabater (2012), Soil Moisture Analyses at ECMWF: Evaluation Using Global Ground-Based In Situ Observations, *Journal of Hydrometeorology*, *13*(5), 1442–1460, doi:10.1175/JHM-D-11-0107.1.

Alker, M. (2007), The Nubian Sandstone Aquifer System: A case study for the research project – Transboundary groundwater management in Africa, *German Development Institute*, pp. 233–273, Accessed from: http://mercury.ethz.ch/serviceengine/Files/ISN/103367/ichaptersection_singledocument/86a7e72a-f661-4151-a978-11727d7e45ac/en/8.pdf, On August 29, 2016.

Alley, W. M. (2007), *Sustainable Management of Groundwater in Mexico: Proceedings of a Workshop (Series: Strengthening Science-Based Decision Making in Developing Countries)*, chap. The Importance of Monitoring To Groundwater Management, pp. 76–85, The National Academies Press,Washington, DC, doi:10.17226/11875.

Alley, W. M., and L. F. Konikow (2015), Bringing GRACE down to earth, *Groundwater*, *53*(6), 826–829, doi:10.1111/gwat.12379.

Altchenko, Y., and K. G. Villholth (2013), Transboundary aquifer mapping and management in Africa: a harmonised approach, *Hydrogeology Journal*, *21*(7), 1497–1517, doi:10.1007/s10040-013-1002-3.

Anderson, W. B., B. F. Zaitchik, C. R. hain, M. C. Anderson, M. T. Yilmaz, J. Mecikalski, and L. Schultz (2012), Towards an integrated soil moisture

drought monitor for East Africa, *Hydrology and Earth System Sciences*, *16*, 2893–2913, doi:10.5194/hess-16-2893-2012.

Anyamba, A., and C. J. Tucker (2005), Analysis of Sahelian vegetation dynamics using NOAA-AVHRR NDVI data from 1981-2003, *Journal of Arid Environments*, *63*(3), 596 – 614, doi:10.1016/j.jaridenv.2005.03.007.

Ashok, K., Z. Guan, and T. Yamagata (2003), A look at the Relationship between the ENSO and the Indian Ocean Dipole, *Journal of the Meteorological Society of Japan. Ser. II*, *81*(1), 41–56, doi:10.2151/jmsj.81.41.

Ashton, P., and A. Turton (2009), *Facing Global Environmental Change: Environmental, Human, Energy, Food, Health and Water Security Concepts*, chap. Water and Security in Sub-Saharan Africa: Emerging Concepts and their Implications for Effective Water Resource Management in the Southern African Region, pp. 661–674, Springer Berlin Heidelberg, Berlin, Heidelberg, doi:10.1007/978-3-540-68488-6_50.

Awange, J., V. Ferreira, E. Forootan, Khandu, S. Andam-Akorful, N. Agutu, and X. He (2016a), Uncertainties in remotely sensed precipitation data over Africa, *International Journal of Climatology*, *36*(1), 303–323, doi:10.1002/joc.4346.

Awange, J., Khandu, M. Schumacher, E. Forootan, and B. Heck (2016b), Exploring hydro-meteorological drought patterns over the Greater Horn of Africa (1979–2014) using remote sensing and reanalysis products, *Advances in Water Resources*, *94*, 45 – 59, doi:http://dx.doi.org/10.1016/j.advwatres.2016.04.005.

Awange, J. L., M. A. Sharifi, G. Ogonda, J. Wickert, E. W. Grafarend, and M. A. Omulo (2008), The falling Lake Victoria water level: GRACE, TRIMM and CHAMP satellite analysis of the Lake Basin, *Water Resources Management*, *22*(7), 775–796, doi:10.1007/s11269-007-9191-y.

Awange, J. L., R. Anyah, N. Agola, E. Forootan, and P. Omondi (2013), Potential impacts of climate change and environmental change on the stored water of Lake Victoria Basin and economic implications, *Water Resources Research*, *49*, 8160–8173, doi:10.1002/2013WR014350.

Awange, J. L., E. Forootan, M. Kuhn, J. Kusche, and B. Heck (2014), Water storage changes and climate variability within the Nile Basin between 2002 and 2011, *Advances in Water Resources*, *73*, 1 – 15, doi:10.1016/j.advwatres.2014.06.010.

Awange, J. L., F. Mpelasoka, and R. M. Goncalves (2016c), When every drop counts: Analysis of droughts in Brazil for the 1901-2013 period, *Science of The Total Environment*, *566*, 1472 – 1488, doi:http://dx.doi.org/10.1016/j.scitotenv.2016.06.031.

Ayers, R. S and Westcot, D. W. and Food and Agriculture Organization of the United Nations (1976), *Water quality for agriculture*, Rome : Food and Agriculture Organization of the United Nations.

Balsamo, G., A. Beljaars, K. Scipal, P. Viterbo, B. van den Hurk, M. Hirschi, and A. K. Betts (2009), A revised hydrology for the ECMWF model: Verification from field site to terrestrial water storage and impact in the integrated forecast system, *Journal of Hydrometeorology*, *10*(3), 623–643, doi:10.1175/2008JHM1068.1.

Barletta, V. R., L. S. Sørensen, and R. Forsberg (2013), Scatter of mass changes estimates at basin scale for Greenland and Antarctica, *The Cryosphere*, *7*(5), 1411–1432, doi:10.5194/tc-7-1411-2013.

Barron, J., J. Rockström, F. Gichuki, and N. Hatibu (2003), Dry spell analysis and maize yields for two semi-arid locations in East Africa, *Agriculture and Forest Meteorology*, *117*, 23–37, doi:10.1016/S0168-1923(03)00037-6.

Bayarjargal, Y. A. K., M. Bayasgalan, S. Khudulmur, C. Gandush, and C. J. Tucker (2006), Comparative study of NOAA - AVHRR derived vegetation indices using change vector analysis, *Remote Sensing of Environment*, *105*, 9 – 22, doi:10.1016/j.rse.2006.06.003.

Becker, M., W. LLovel, A. Cazenave, A. Güntner, and J. Crétaux (2010), Recent hydrological behaviour of the East African great lakes region inferred from GRACE, satellite altimetry and rainfall observations, *C. R. Geoscience*, *342*, 223–233, doi:10.1016/j.crte.2009.12.010.

Bewket, W. (2009), Rainfall variability and crop production in Ethiopia: Case study in the Amhara region, in *Proceedings of the 16th International Conference of Ethiopian Studies*, vol. 3, edited by S. Ege, H. Aspen, B. Teferra, and S. Bekele, pp. 823–836, Department of Social Anthropology, Norwegian University of Science and Technology, Trondheim.

Bi, H., J. Ma, W. Zheng, and J. Zeng (2016), Comparison of soil moisture in GLDAS model simulations and in situ observations over the Tibetan Plateau, *Journal of Geophysical Research: Atmospheres*, *121*(6), 2658–2678, doi:10.1002/2015JD024131, 2015JD024131.

Bingham, N., and J. Fry (2010), *Regression: Linear Models in Statistics*, Springer Undergraduate Mathematics Series, Springer London.

Boergens, E., E. Rangelova, M. G. Sideris, and J. Kusche (2014), Assessment of the capabilities of the temporal and spatiotemporal ICA method for geophysical signal separation in GRACE data, *Journal of Geophysical Research: Solid Earth*, *119*(5), 4429–4447, doi:10.1002/2013JB010452.

Boko, M., I. Niang, A. Nyong, C. Vogel, A. Githeko, M. Medany, B. Osman-Elasha, R. Tabo, and P. Yanda (2007), *Climate Change 2007: Impacts, Adaptation and Vulnerability. Contribution of Working Group II to the Fourth Assessment Report of the Intergovernmental Panel on Climate*

Change, chap. Africa, pp. 433–467, Cambridge University Press, Cambridge, United Kingdom.

Bosilovich, M., G. Lucchesi, and M. Suarez (2016), MERRA-2: File Specification, *GMAO Office Note No. 9 (Version 1.1)*, *73 pp*, available form:http://gmao.gsfc.nasa.gov/pubs/office_notes.

Bosilovich, M. G., S. Akella, L. Coy, R. Cullather, C. Draper, R. Gelaro, R. Kovach, Q. Liu, A. Molod, P. Norris, W. Chao, R. Reichle, L. Takacs, R. Todling, Y. Vikhliaev, S. Bloom, A. Collow, G. Partyka, S. Firth, G. Labow, S. Pawson, O. Reale, S. Schubert, and M. Suarez (2015), Merra-2: Initial evaluation of the climate, *Technical Report Series on Global Modeling and Data Assimilation NASA/TM–2015-104606/Vol. 43*, NASA:GSFCG, Available online at https://gmao.gsfc.nasa.gov/reanalysis/MERRA-2/docs/.

Bowden, J. H., and F. H. M. Semazzi (2007), Empirical analysis of intraseasonal climate variability over the Greater Horn of Africa, *Journal of Climate*, *20*(23), 5715–5731, doi:10.1175/2007JCLI1587.1.

Brown, M. E., C. C. Funk, G. Galu, and R. Choularton (2007), Earlier famine warning possible using remote sensing and models, *Eos, Transactions American Geophysical Union*, *88*(39), 381–382, doi:10.1029/2007EO390001.

Caires, S., and A. Sterl (2003), Validation of ocean wind and wave data using triple collocation, *Journal of Geophysical Research: Oceans*, *108*(C3), n/a–n/a, doi:10.1029/2002JC001491, 3098.

Calow, R. C., N. S. Robins, A. M. Macdonald, D. M. J. Macdonald, B. R. Gibbs, W. R. G. Orpen, P. Mtembezeka, A. J. Andrews, and S. O. Appiah (1997), Groundwater Management in Drought-prone Areas of Africa, *International Journal of Water Resources Development*, *13*(2), 241–262, doi:10.1080/07900629749863.

Calow, R. C., A. M. MacDonald, A. L. Nicol, and N. S. Robins (2010), Ground Water Security and Drought in Africa: Linking Availability, Access, and Demand, *Ground Water*, *48*(2), 246–256, doi:10.1111/j.1745-6584.2009.00558.x.

Cardoso, J. F. (1998), Blind signal separation: Statistical principles, *Proceedings of the IEEE*, *86*(10), 2009 – 2025.

Cardoso, J. F. (1999), High-Order Contrast for Independent Component Analysis, *Neural Computations*, (11), 157 – 192.

Cardoso, J. F., and A. Souloumian (1993), Blind beamforming for non-gaussian signals, *IEEE Proceedings*, *140*(6), 362 – 370.

Castellazzi, P., R. Martel, D. L. Galloway, L. Longuevergne, and A. Rivera (2016), Assessing groundwater depletion and dynamics using GRACE and InSAR: Potential and limitations, *Groundwater*, pp. n/a–n/a, doi:10.1111/gwat.12453.

Chen, J. L., C. R. Wilson, B. D. Tapley, Z. L. Yang, and G. Y. Niu (2009), 2005 drought event in the Amazon River basin as measured by GRACE and estimated by climate models, *Journal of Geophysical Research: Solid Earth*, *114*(B5), n/a–n/a, doi:10.1029/2008JB006056, b05404.

Chen, T., R. de Jeu, Y. Liu, G. van der Werf, and A. Dolman (2014), Using satellite based soil moisture to quantify the water driven variability in NDVI: A case study over mainland Australia, *Remote Sensing of Environment*, *140*, 330 – 338, doi:http://dx.doi.org/10.1016/j.rse.2013.08.022.

Cheng, M., B. D. Tapley, and J. C. Ries (2013), Deceleration in the Earth's oblateness, *Journal of Geophysical Research: Solid Earth*, *118*(2), 740–747, doi:10.1002/jgrb.50058.

Clark, C. O., P. J. Webster, and J. E. Cole (2003), Interdecadal variability of the relationship between the Indian Ocean Zonal Mode and East

African Coastal Rainfall Anomalies, *Journal of Climate*, *16*, 548–554, doi:10.1175/1520-0442(2003)016 < 0548 : $IVOTRB$ > 2.0.CO;2.

Comon, P. (1994), Higher order statistics independent component analysis, a new concept?, *Signal Processing*, *36*(3), 287 – 314, doi:http://dx.doi.org/10.1016/0165-1684(94)90029-9.

Comte, J. C., R. Cassidy, J. Obando, N. Robins, K. Ibrahim, S. Melchioly, I. Mjemah, H. Shauri, A. Bourhane, I. Mohamed, C. Noe, B. Mwega, M. Makokha, J. L. Join, O. Banton, and J. Davies (2016), Challenges in groundwater resource management in coastal aquifers of East Africa: Investigations and lessons learnt in the Comoros Islands, Kenya and Tanzania, *Journal of Hydrology: Regional Studies*, *5*, 179 – 199, doi:http://dx.doi.org/10.1016/j.ejrh.2015.12.065.

Crow, W. T., S. V. Kumar, and J. D. Bolten (2012), On the utility of land surface models for agricultural drought monitoring, *Hydrology and Earth System Sciences*, *16*(9), 3451–3460, doi:10.5194/hess-16-3451-2012.

Damberg, L., and A. AghaKouchak (2014), Global trends and patterns of drought from space, *Theoretical and Applied climatology*, *117*, 441–448, doi:10.1007/s00704-013-1019-5.

Decker, M., M. A. Brunke, Z. Wang, K. Sakaguchi, X. Zeng, and M. G. Bosilovich (2012), Evaluation of the Reanalysis Products from GSFC, NCEP, and ECMWF Using Flux Tower Observations, *Journal of Climate*, *25*, 1916–1944, doi:10.1175/JCLI-D-11-00004.1.

Dee, D. P., S. M. Uppala, A. J. Simmons, P. Berrisford, P. Poli, S. Kobayashi, U. Andrae, M. A. Balmaseda, G. Balsamo, P. Bauer, P. Bechtold, A. C. M. Beljaars, L. van de Berg, J. Bidlot, N. Bormann, C. Delsol, R. Dragani, M. Fuentes, A. J. Geer, L. Haimberger, S. B. Healy, H. Hersbach, E. V. Hólm, L. Isaksen, P. Kållberg, M. Köhler, M. Matricardi, A. P. McNally,

B. M. Monge-Sanz, J.-J. Morcrette, B.-K. Park, C. Peubey, P. de Rosnay, C. Tavolato, J.-N. Thépaut, and F. Vitart (2011), The ERA-Interim reanalysis: configuration and performance of the data assimilation system, *Quarterly Journal of the Royal Meteorological Society*, *137*(656), 553–597, doi:10.1002/qj.828.

Demombynes, G., and J. Kiringai (2011), The drought and food crisis in the Horn of Africa: Impacts and proposed policy responses for Kenya, *Poverty Reduction and Economic Management (PREM) Network*, (71), 1–4, Accessed from: http://siteresources.worldbank.org/INTPREMNET/Resources/EP71.pdf, On 27/04/2017.

Dewitte, O., A. Jones, O. Spaargaren, H. Breuning-Madsen, M. Brossard, A. Dampha, J. Deckers, T. Gallali, S. Hallett, R. Jones, M. Kilasara, P. L. Roux, E. Michéli, L. Montanarella, L. Thiombiano, E. V. Ranst, M. Yemefack, and R. Zougmore (2013), Harmonisation of the soil map of Africa at the continental scale, *Geoderma*, *211-212*, 138 – 153, doi:http://dx.doi.org/10.1016/j.geoderma.2013.07.007.

Dinku, T., P. Ceccato, E. Grover-Kopec, M. Lemma, S. J. Connor, and C. F. Ropelewski (2007), Validation of satellite rainfall products over East Africa's complex topography, *International Journal of Remote Sensing*, *28*(7), 1503–1526, doi:10.1080/01431160600954688.

Dinku, T., S. Chidzambwa, P. Ceccato, S. J. Connor, and C. F. Ropelewski (2008), Validation of high resolution satellite rainfall products over complex terrain, *International Journal of Remote Sensing*, *29*(14), 4097–4110, doi:10.1080/01431160701772526.

Dirmeyer, P. A., A. J. Dolman, and N. Sato (1999), The pilot phase of the global soil wetness project, *Bulletin of the American Meteorological Society*, *80*(5), 851–878, doi:10.1175/1520-0477(1999)080⟨0851:TPPOTG⟩2.0.CO;2.

Dirmeyer, P. A., Z. Guo, and X. Gao (2004), Comparison, validation, and transferability of eight multiyear global soil wetness products, *Journal of Hydrometeorology*, *5*(6), 1011–1033, doi:10.1175/JHM-388.1.

Döll, P. (2009), Vulnerability to the impact of climate change on renewable groundwater resources: a global-scale assessment, *Environmental Research Letters*, *4*(3), 035,006, doi:10.1088/1748-9326/4/3/035006.

Döll, P., H. Hoffmann-Dobrev, F. Portmann, S. Siebert, A. Eicker, M. Rodell, G. Strassberg, and B. Scanlon (2012), Impact of water withdrawals from groundwater and surface water on continental water storage variations, *Journal of Geodynamics*, *59–60*, 143 – 156, doi:http://dx.doi.org/10.1016/j.jog.2011.05.001.

Döll, P., H. Müller Schmied, C. Schuh, F. T. Portmann, and A. Eicker (2014), Global-scale assessment of groundwater depletion and related groundwater abstractions: Combining hydrological modeling with information from well observations and GRACE satellites, *Water Resources Research*, *50*(7), 5698–5720, doi:10.1002/2014WR015595.

Dong, J., and W. T. Crow (2017), An improved triple collocation analysis algorithm for decomposing autocorrelated and white soil moisture retrieval errors, *Journal of Geophysical Research: Atmospheres*, *122*(24), 13,081–13,094, doi:10.1002/2017JD027387, 2017JD027387.

Dorigo, W., R. de Jeu, D. Chung, R. Parinussa, Y. Liu, W. Wagner, and D. Fernández-Prieto (2012), Evaluating global trends (1988–2010) in harmonized multi-satellite surface soil moisture, *Geophysical Research Letters*, *39*(18), doi:10.1029/2012GL052988, l18405.

Driessen, P., and O. Deckers (2001), Lecture notes on the major soils of the World, *FAO Corporate Document Repository*, Accessed from: http://www.fao.org/docrep/003/y1899e/y1899e00.htm#toc, On 24/02/2017.

Duncan, M., B. Austin, F. Fabry, and G. Austin (1993), The effect of gauge sampling density on the accuracy of streamflow prediction for rural catchments, *Journal of Hydrology*, *142*(1), 445 – 476, doi:https://doi.org/10.1016/0022-1694(93)90023-3.

Dutra, E., P. Viterbo, and P. M. A. Miranda (2008), ERA-40 reanalysis hydrological applications in the characterization of regional drought, *Geophysical Research Letters*, *35*(19), 1–5, doi:10.1029/2008GL035381, l19402.

Dutra, E., L. Magnusson, F. Wetterhall, H. L. Cloke, G. Balsamo, S. Boussetta, and F. Pappenberger (2013), The 2010–2011 drought in the Horn of Africa in ECMWF reanalysis and seasonal forecast products, *International Journal of Climatology*, *33*, 1720–1729, doi:10.1002/joc.3545.

Dutra, E., F. Wetterhall, F. Di Giuseppe, G. Naumann, P. Barbosa, J. Vogt, W. Pozzi, and F. Pappenberger (2014), Global meteorological drought - part 1: Probabilistic monitoring, *Hydrology and Earth System Sciences*, *18*(7), 2657–2667, doi:10.5194/hess-18-2657-2014.

EACS (2014), East African Community Facts and Figures–2014, *Report*, East African Community Secretariat, Accessed from:http://www.eac.int on March 15, 2015.

Edossa, D. C., M. S. Babel, and A. S. Gupta (2010), Drought analysis in the Awash River Basin, Ethiopia, *Water Resources Management*, *24*, 1441–1460, doi:10.1007/s11269-009-9508-0.

Elagib, N. A. (2013), Meteorological Drought and Crop Yield in Sub-Sahara Sudan, *International Journal of Water Resources and Arid Environments*, *2*(3), 164–171.

Elagib, N. A., and M. M. Elhag (2011), Major climate indicators of ongoing drought in Sudan, *Journal of Hydrology*, *409*, 612–625, doi:10.1016/j.jhydrol.2011.08.047.

Enenkel, M., L. See, R. Bonifacio, V. Boken, N. Chaney, P. Vinck, L. You, E. Dutra, and M. Anderson (2015), Drought and food security – improving decision-support via new technologies and innovative collaboration, *Global Food Security*, *4*, 51 – 55, doi:http://dx.doi.org/10.1016/j.gfs.2014.08.005.

Entin, J. K., A. Robock, K. Y. Vinnikov, V. Zabelin, S. Liu, A. Namkhai, and T. Adyasuren (1999), Evaluation of global soil wetness project soil moisture simulations, *Journal of the Meteorological Society of Japan. Ser. II*, *77*(1B), 183–198.

Entin, J. K., A. Robock, K. Y. Vinnikov, S. E. Hollinger, S. Liu, and A. Namkhai (2000), Temporal and spatial scales of observed soil moisture variations in the extratropics, *Journal of Geophysical Research: Atmospheres*, *105*(D9), 11,865–11,877, doi:10.1029/2000JD900051.

Enyew, B. D., and G. J. Steeneveld (2014), Analysing the impact of topography on precipitation and flooding on the Ethiopian Highlands, *Journal of Geology & Geosciences*, *3*(6), 1–6, doi:10.4172/2329-6755.1000173.

Eswaran, H., and T. Cook (1987), Classification and management-related properties of Vertisols, in *Management of Vertisols in Sub-Saharan Africa*, edited by S. C. Jutzi, I. Haque, J. McIntire, and J. E. S. Stares, Proceedings of a conference held at ILCA, Addis Ababa, Ethiopia, 31 August-4 September 1987. ILCA, Addis Ababa.

Fan, Y., and H. van den Dool (2004), Climate Prediction Center global monthly soil moisture data set at 0.5° resolution for 1948 to present, *Journal of Geophysical Research*, *109*, D10,102, doi:10.1029/2003JD004345.

FAO (2011), Drought related food insecurity: A focuss on the Horn of Africa, *Emergency Ministerial Level Meeting, FAO, Rome*, pp. 1–7, Accessed from: http://www.fao.org/crisis/28402-0f9dad42f33c6ad6ebda108ddc1009adf.pdf, on 27/04/2017.

Farahmand, A., and A. AghaKouchak (2015), A generalized framework for deriving nonparametric standardized drought indicators, *Advances in Water Resources*, *76*, 140 – 145, doi:10.1016/j.advwatres.2014.11.012.

Fipps, G. (2003), Irrigation water quality standards and salinity management strategies, *Texas Agricultural Extension Services, Texas A&M University System, College Station, TX (USA)*, *B–1667*(4–03), 1–19, Accessed from: http://oaktrust.library.tamu.edu/bitstream/handle/1969.1/87829/pdf_94.pdf ?sequence=1 on August 29, 2016.

Fisher, R. (1944), *Statistical methods for research workers*, Oliver and Boyd.

Forina, M., C. Armanino, S. Lanteri, and R. Leardi (1988), Methods of Varimax Rotation in Factor Analysis with Applications in Clinical and Food Chemistry, *Journal of Chemometrics*, *3*, 115–125, doi:10.1002/cem.1180030504.

Forootan, E., and J. Kusche (2013), Separation of deterministic signals using independent component analysis (ICA), *Studia Geophysica et Geodaetica*, *57*(1), 17–26, doi:10.1007/s11200-012-0718-1.

Foster, S., and T. Shah (2012), Groundwater Resources and Irrigated Agriculture-making a beneficial relation more sustainable, *International Association of Hydrogeologists-Strategic Overview Series*, (4), Accessed from: http://www.gwp.org/en/ToolBox/PUBLICATIONS/Perspectives-Papers/, on 01/03/2017.

Frappart, F., G. Ramillien, M. Leblanc, S. O. Tweed, M.-P. Bonnet, and P. Maisongrande (2011), An independent component analysis filtering approach for estimating continental hydrology in the GRACE gravity data, *Remote Sensing of Environment*, *115*(1), 187 – 204, doi:http://dx.doi.org/10.1016/j.rse.2010.08.017.

Funk, C., P. Steffen, G. B. Senay, J. Rowland, and J. Verdin (2003), Estimating Meher crop production using rainfall in the 'long cycle' region of

Ethiopia, *Special report*, FEWS-NET, USGS/FEWS/USAID. Accessed from: http://reliefweb.int/sites/reliefweb.int/files/resources on March 15, 2015.

Funk, C., A. Hoell, S. Shukla, I. Blade, B. Liebmann, J. B. Roberts, F. R. Robertson, and G. Husak (2014), Predicting East African spring droughts using Pacific and Indian Ocean sea surface temperature indices, *Hydrology and Earth System Sciences*, *18*, 4965–4978, doi:10.5194/hess-18-4965-2014.

Funk, C., P. Peterson, M. Landsfeld, D. Pedreros, J. Verdin, S. Shukla, G. Husak, J. Rowland, L. Harrison, A. Hoell, and J. Michaelsen (2015), The climate hazards infrared precipitation with stations - a new environmental record for monitoring extremes, *Scientific Data*, *2*(150066), 1–21, doi:10.1038/sdata.2015.66.

Funk, C. C., and M. E. Brown (2009), Declining global per capita agricultural production and warming oceans threaten food security, *Food Security*, *1*(3), 271–289, doi:10.1007/s12571-009-0026-y.

Galindo, J. F., J. J. Ruiz, E. Giachino, A. Premoli, and P. Tavella (2001), *Advanced Mathematical and Computational Tools in Metrology 5*, *Series on Advances in Mathematics for Applied Sciences*, vol. 57, chap. Estimation of the Covariance Matrix of Individual Standards by Means of Comparison Measurement, pp. 179–183, World Scientific, Singapore.

Gebrehiwot, T., A. van der Veen, and B. Maathuis (2011), Spatial and temporal assessment of drought in the Northern highlands of Ethiopia, *International Journal of Applied Earth Observation and Geoinformation*, *13*(3), 309 – 321, doi:10.1016/j.jag.2010.12.002.

Gedif, B., L. Hadish, S. Addisu, and K. V. Suryabhagavan (2014), Drought risk assessment using remote sensing and gis: the case of southern zone, Tigray Region, Ethiopia, *Journal of natural Science Research*, *4*(23), 87–94, ISSN 2225-0921.

Geladi, P., and B. R. Kowalski (1986), Partial least-squares regression:a tutorial, *Analytica Chemica Acta*, *185*, 1 – 17.

Giorgi, F., C. S. Brodeur, and G. T. Bates (1994), Regional Climate Change Scenarios over the United States Produced with a Nested Regional Climate Model, *Journal of Climate*, *7*(3), 375–399, doi:10.1175/1520-0442(1994)007⟨0375:RCCSOT⟩2.0.CO;2.

Gossel, W., A. M. Ebraheem, and P. Wycisk (2004), A very large scale GIS-based groundwater flow model for the Nubian sandstone aquifer in Eastern Sahara (Egypt, northern Sudan and eastern Libya), *Hydrogeology Journal*, *12*(6), 698–713, doi:10.1007/s10040-004-0379-4.

Gringorten, I. I. (1963), A plotting rule for extreme probability paper, *Journal of Geophysical Research*, *68*(3), 813–814, doi:10.1029/JZ068i003p00813.

Groisman, P. Y., R. W. Knight, and T. R. Karl (2001), Heavy Precipitation and High Streamflow in the Contiguous United States: Trends in the Twentieth Century, *Bulletin of the American Meteorological Society*, *82*(2), 219–246, doi:10.1175/1520-0477(2001)082⟨0219:HPAHSI⟩2.3.CO;2.

Gruber, A., C.-H. Su, S. Zwieback, W. Crow, W. Dorigo, and W. Wagner (2016), Recent advances in (soil moisture) triple collocation analysis, *International Journal of Applied Earth Observation and Geoinformation*, *45*, 200 – 211, doi:https://doi.org/10.1016/j.jag.2015.09.002, advances in the Validation and Application of Remotely Sensed Soil Moisture - Part 1.

Guan, K., E. Wood, and K. Caylor (2012), Multi-sensor derivation of regional vegetation fractional cover in Africa, *Remote Sensing of Environment*, *124*, 653 – 665, doi:http://dx.doi.org/10.1016/j.rse.2012.06.005.

Hane, D. C., and F. V. Pumphrey (1984), Crop Water Use Curves for Irrigation Scheduling, *Special Report 706*, Agricultural Experiment Station Oregon

State University, Corvallis, Accessed from: http://ir.library.oregonstate.edu on March 15, 2015.

Hannachi, A., I. T. Jolliffe, and D. B. Stephenson (2007), Empirical orthogonal functions and related techniques in atmospheric science: A review, *International Journal of Climatology*, *27*, 1119 – 1152, doi:10.1002/joc.1499.

Hansen, D., W. Ye, A. Jakeman, R. Cooke, and P. Sharma (1996), Analysis of the effect of rainfall and streamflow data quality and catchment dynamics on streamflow prediction using the rainfall-runoff model IHACRES, *Environmental Software*, *11*(1), 193 – 202, doi:https://doi.org/10.1016/S0266-9838(96)00048-2, modelling and Simulation Theme: Regional Development and Environmental Change.

Hastenrath, S., D. Polzin, and C. Mutai (2007), Diagnosing the 2005 Drought in Equatorial East Africa, *Journal of Climate*, *20*(18), 4628–4637, doi:10.1175/JCLI4238.1.

Hastenrath, S., D. Polzin, and C. Mutai (2010), Diagnosing the Droughts and Floods in Equatorial East Africa during Boreal Autumn 2005–08, *Journal of Climate*, *23*(3), 813–817, doi:10.1175/2009JCLI3094.1.

Helland, I. (2004), *Partial Least Squares Regression*, John Wiley and Sons, Inc., doi:10.1002/0471667196.ess6004.pub2.

Hochberg, Y., and A. Tamhane (1987), *Multiple comparison procedures*, Wiley series in probability and mathematical statistics: Applied probability and statistics, Wiley.

Hong, Y., K.-l. Hsu, H. Moradkhani, and S. Sorooshian (2006), Uncertainty quantification of satellite precipitation estimation and monte carlo assessment of the error propagation into hydrologic response, *Water Resources Research*, *42*(8), n/a–n/a, doi:10.1029/2005WR004398, w08421.

Hu, K., J. L. Awange, Khandu, E. Forootan, R. M. Goncalves, and K. Fleming (2017), Hydrogeological characterisation of groundwater over Brazil using remotely sensed and model products, *Science of The Total Environment*, *599*, 372 – 386, doi:http://dx.doi.org/10.1016/j.scitotenv.2017.04.188.

Huang, Y., L. Chen, B. Fu, Z. Huang, J. Gong, and X. Lu (2012), Effect of land use and topography on spatial variability of soil moisture in a gully catchment of the Loess Plateau, China, *Ecohydrology*, *5*(6), 826–833, doi:10.1002/eco.273.

Huffman, G. J., R. F. Adler, D. T. Bolvin, G. Gu, E. J. Nelkin, K. P. Bowman, Y. Hong, E. F. Stocker, and D. B. Wolff (2007), The TRMM Multi-Satellite Precipitation Analysis (TMPA): Quasi-Global, Multi Year, Combined-Sensor Precipitation Estimates at Fine Scales, *Journal of Hydrometeorology*, *8*, 38 – 55, doi:10.1175/JHM560.1.

Ibrahim, F. (1988), Causes of the famine among the rural population of the Sahelian zone of the Sudan, *GeoJournal*, *17*(1), 133–141, doi:10.1007/BF00209083.

IFRC (2011), Drought in the Horn of Africa: Preventing the next disaster, *International Federation of Red Cross and Red Crescent Societies, Geneva*, Accessed from: http://www.ifrc.org on March 15, 2015.

Janssen, P. A. E. M., S. Abdalla, H. Hersbach, and J.-R. Bidlot (2007), Error estimation of buoy, satellite, and model wave height data, *Journal of Atmospheric and Oceanic Technology*, *24*(9), 1665–1677, doi:10.1175/JTECH2069.1.

Jolliffe, I. T. (1995), Rotation of Principal Components: Choice of normalization constraints, *Journal of Applied Statistics*, *22*(1), 29–35, doi:10.1080/757584395.

Jolliffe, I. T. (2002), *Principal Component Analysis*, Springer Series in Statistics, second ed., Springer.

Kaiser, H. F. (1958), The Varimax Criterion for analytic rotation in Factor analysis, *Psychometrika*, *23*(3), 187–200, doi:10.1007/BF02289233.

Kashaigili, J. J. (2010), Assessment of groundwater availability and its current and potential use and impact in Tanzania, *Final report*, International Water Management Institute (IWMI), Accessed from: http://gw-africa.iwmi.org/Data/Sites/24/media/pdf/Country_Report-Tanzania .pdf on May 15, 2016.

Kasnakoglu, H., and R. Mayo (2004), FAO Statistical Data Quality Framework: A multilayered approach to monitoring and assessment, *Conference on Data Quality for International Organizations, Wiesbaden, Germany, 27 and 28 May 2004*, Accessed from: http://unstats.un.org/unsd/accsub/2004docs-CDQIO/1-FAO.pdf on 4/10/2016.

Katz, R. W., and M. H. Glantz (1986), Anatomy of a rainfall index, *Monthly Weather Review*, *114*, 764–771, doi:10.1175/1520-0493(1986)114< 0764 : *AOARI* >2.0.CO;2.

Kebede, S. (2013), *Groundwater in Ethiopia*, Springer Hydrogeology, 1 ed., Springer-Verlag Berlin Heidelberg.

Kendall, M., and A. Stuart (1963), *The advanced theory of statistics*, no. 2 in The Advanced Theory of Statistics, Griffin.

Kijazi, A. L., and C. J. C. Reason (2009), Analysis of the 2006 floods over northern Tanzania, *International Journal of Climatology*, *29*(7), 955–970, doi:10.1002/joc.1846.

Kim, J., and S. K. Park (2016), Uncertainties in calculating precipitation climatology in East Asia, *Hydrology and Earth System Sciences*, *20*(2), 651–658, doi:10.5194/hess-20-651-2016.

Kim, J., J. Sanjay, C. Mattmann, M. Boustani, M. V. S. Ramarao, R. Krishnan, and D. Waliser (2015), Uncertainties in estimating spatial and interannual variations in precipitation climatology in the India-Tibet region from multiple gridded precipitation datasets, *International Journal of Climatology*, *35*(15), 4557–4573, doi:10.1002/joc.4306.

King, B. (2010), Analysis of variance, in *International Encyclopedia of Education*, edited by P. Peterson, E. Baker, and B. McGaw, third edition ed., pp. 32 – 36, Elsevier, Oxford, doi:https://doi.org/10.1016/B978-0-08-044894-7.01306-3.

Kogan, F. (1995), Application of vegetation index and brightness temperature for drought detection, *Advances in Space research*, *15*, 91 – 100, doi:10.1016/0273-1177(95)00079-T.

Konikow, L. F., and E. Kendy (2005), Groundwater depletion: A global problem, *Hydrogeology Journal*, *13*(1), 317–320, doi:10.1007/s10040-004-0411-8.

Koot, L., O. d. Viron, and V. Dehant (2006), Atmospheric angular momentum time-series: Characterization of their internal noise and creation of a combined series, *Journal of Geodesy*, *79*(12), 663, doi:10.1007/s00190-005-0019-3.

Krhoda, G. O. (1989), Groundwater assessment in sedimentary basins of Eastern Kenya, Africa, *Proceedings of the Baltimore Symposium, May 1989*, *IAHS Pub. no. 182*, Accessed from: http://www.oceandocs.org/bitstream/handle/1834/7780/ktf0465.pdf?sequence=2 on May 15, 2016.

Krzanowski, W. (2000), *Principles of Multivariate Analysis*, Oxford Statistical Science Series, OUP Oxford.

Kumar, M., K. Kumari, A. Ramanathan, and R. Saxena (2007), A comparative evaluation of groundwater suitability for irrigation and drinking purposes in two intensively cultivated districts of Punjab, India, *Environmental Geology*, *53*(3), 553–574, doi:10.1007/s00254-007-0672-3.

Kummerow, C., J. Simpson, O. Thiele, W. Bernes, A. T. C. Chang, E. Stocker, R. F. Adler, A. Hou, R. Kakar, F. Wentz, P. Ashcroft, T. Kozu, Y. Hong, K. Okamoto, T. Iguchi, F. Kuroiwa, E. Im, Z. Haddad, G. Huffman, B. Ferrier, W. S. Olson, E. Zipser, E. A. Smith, T. T. Wilheit, G. North, T. Krishnamurti, and K. Nakamura (2000), The Status of the Tropical Rainfall Measuring Mission (TRMM) after Two Years in Orbit, *Journal of Applied Meteorology*, *39*, 1965 – 1982, doi:10.1175/1520-0450(2001)040 < 1965 : $TSOTTR$ > 2.0.CO;2.

Kundzewicz, Z. W., and P. Döll (2009), Will groundwater ease freshwater stress under climate change?, *Hydrological Sciences Journal*, *54*(4), 665–675, doi:10.1623/hysj.54.4.665.

Kurnik, B., P. Barbosa, and J. Vogt (2011), Testing two different precipitation datasets to compute the standardized precipitation index over the Horn of Africa, *International Journal of Remote Sensing*, *32*(21), 5947–5964, doi:10.1080/01431161.2010.499380.

Kusche, J. (2007), Approximate decorrelation and non-isotropic smoothing of time-variable GRACE-type gravity field models, *Journal of Geodesy*, *81*, 733–749, doi:10.1007/s00190-007-0143-3.

Kusche, J., R. Schmidt, S. Petrovic, and R. Rietbroek (2009), Decorrelated GRACE time-variable gravity solution by GFZ, and their validation using a hydrological model, *Journal of Geodesy*, *83*, 903 – 913, doi:10.1007/s00190-009-0308-3.

Kutner, M. (2005), *Applied Linear Statistical Models*, McGrwa-Hill international edition, McGraw-Hill Irwin.

Landerer, F. W., and S. C. Swenson (2012), Accuracy of scaled GRACE terrestrial water storage estimates, *Water Resources Research*, *48*(4), n/a–n/a, doi:10.1029/2011WR011453, w04531.

Larsson, H. (1996), Relationship between rainfall and sorghum, millet and sesame in the Kassala Province, Eastern Sudan, *Journal of Arid Environment*, *32*(2), 211–223, doi:10.1006/jare.1996.0018.

LDAS (2016), Land Data Assimilation Systems FAQ, [ONLINE] Available at: http://ldas.gsfc.nasa.gov/faq/. [Accessed 6 January 2017].

Lee, H. R. (2007), The geology of Somalia: a selected bibliography of Somalian geology, geography and earth sciences, *Engineering Research and development Center*, pp. 1–431, Retreaved from:http://www.dtic.mil/dtic/tr/fulltext/u2/a464006.pdf, On 22/06/2017.

Legates, D. R., R. Mahmood, D. F. Levia, T. L. DeLiberty, S. M. Quiring, C. Houser, and F. E. Nelson (2011), Soil moisture: A central and unifying theme in physical geography, *Progress in Physical Geography*, *35*(1), 65–86, doi:10.1177/0309133310386514.

Li, H. (2007), *Understanding Soil Moisture Dynamics Using Observations and Climate Models*, Rutgers, The State University of New Jersey - New Brunswick.

Liang, X., D. P. Lettenmaier, E. F. Wood, and S. J. Burges (1994), A simple hydrologically based model of land surface water and energy fluxes for general circulation models, *Journal of Geophysical Research: Atmospheres*, *99*(D7), 14,415–14,428, doi:10.1029/94JD00483.

Loewenberg, S. (2011), Humanitarian response inadequate in Horn of Africa crisis, *The Lancet*, *378*(9791), 555–558, doi:10.1016/S0140-6736(11)61276-2.

Long, D., B. R. Scanlon, L. Longuevergne, A. Y. Sun, D. N. Fernando, and H. Save (2013), GRACE satellite monitoring of large depletion in water storage in response to the 2011 drought in Texas, *Geophysical Research Letters*, *40*, 3395 – 3401, doi:10.1002/grl.50655.

Longley, C., R. Jones, M. H. Ahmed, and P. Audi (2001), Supporting local seed systems in southern Somalia: a developmental approach to agricultural rehabilitation in emergency situations, *Network paper 115*, Agricultural Research and Extension Network, 20 pp.

Longuevergne, L., B. R. Scanlon, and C. R. Wilson (2010), GRACE hydrological estimates for small basins: Evaluating processing approaches on the High Plains Aquifer, USA, *Water Resources Research*, *46*(11), n/a–n/a, doi:10.1029/2009WR008564, w11517.

Lorenz, E. N. (1956), Empirical Orthogonal Function and Statistical Weather Prediction, *Statistical forecasting project: Scientific report no. 1*, Department of Meteorology, MIT, Retreaved from:http://eaps4.mit.edu/research/Lorenz, on March 15, 2015.

Lough, J. M. (1997), Regional indices of climate variation: temperature and precipitation in Queensland, Australia, *International Journal of Climatology*, *17*, 55–66, doi:10.1002/(SICI)1097-0088(199701)17:1< 55 :: $AID - JOC109 >$3.0.CO;2-Z.

Lyon, B. (2004), The strength of El Niño and the spatial extent of tropical drought, *Geophysical Research Letters*, *31*(21), doi:10.1029/2004GL020901.

Lyon, B. (2014), Seasonal Drought in the Greater Horn of Africa and Its Recent Increase during the March–May Long Rains, *Journal of Climate*, *27*, 7953–7975, doi:10.1175/JCLI-D-13-00459.1.

Lyon, B., and D. G. DeWitt (2012), A recent and abrupt decline in the East African long rains , *Geophysical Research Letters*, *39*, L02,702, doi:10.1029/2011GL050337.

MacDonald, A. M., J. Davies, and R. C. Calow (2008), *Applied Groundwater Studies in Africa: IAH Selected Papers on Hydrogeology*, *IAH - Selected Papers*

on Hydrogeology, vol. 13, chap. African hydrogeology and rural water supply, CRC Press.

MacDonald, A. M., H. C. Bonsor, B. E. O. Dochartaigh, and R. G. Taylor (2012), Quantitative maps of groundwater resources in Africa, *Environmental Research Letters*, *7*(2), 024,009, doi:10.1088/1748-9326/7/2/024009.

Martín-Clemente, R., J. I. Acha, and C. G. Puntonet (2004), Eigen decomposition of self-tuned cumulant-matrices for blind source separation, *Signal Processing*, *84*(7), 1201 – 1211, doi:http://dx.doi.org/10.1016/j.sigpro.2004.04.002.

Masih, I., S. Maskey, F. E. F. Mussá, and P. Trambauer (2014), A review of droughts on the African continent: a geospatial and long-term perspective, *Hydrology and Earth System Sciences*, *18*(9), 3635–3649, doi:10.5194/hess-18-3635-2014.

McCalla, A. F. (1999), Prospects for food security in the 21st Century:1Developed from a speech given at the World Food Prize Symposium, Des Moines, Iowa, 16 October 1997.1 with special emphasis on Africa, *Agricultural Economics*, *20*(2), 95 – 103, doi:http://dx.doi.org/10.1016/S0169-5150(98)00080-2.

McColl, A. K., V. Jur, K. A. G., E. Dara, P. María, and S. Ad (2014), Extended triple collocation: Estimating errors and correlation coefficients with respect to an unknown target, *Geophysical Research Letters*, *41*(17), 6229–6236, doi:10.1002/2014GL061322.

McKee, T. B., N. J. Doesken, and J. Kleist (1993), The Relationship of drought frequency and duration to time scale, in *Conference Proceedings*, eighth Conference of Applied Climatology, Anaheim, California.

McNally, A., S. Shukla, K. R. Arsenault, S. Wang, C. D. Peters-Lidard, and J. P. Verdin (2016), Evaluating ESA CCI soil moisture in East Africa, *International Journal of Applied Earth Observation and Geoinformation*, *48*, 96 – 109, doi:http://dx.doi.org/10.1016/j.jag.2016.01.001.

McNally, A., K. Arsenault, S. Kumar, S. Shukla, P. Peterson, S. Wang, C. Funk, C. D. Peters-Lidard, and J. P. Verdin (2017), A land data assimilation system for sub-Saharan Africa food and water security applications, *Scientific Data*, *4*(170012), 1–21, doi:10.1038/sdata.2017.12.

Milliken, G., and D. Johnson (1993), *Analysis of Messy Data: Designed Experiments*, v. 1, Taylor & Francis.

Miyaoka, K., A. Gruber, F. Ticconi, S. Hahn, W. Wagner, J. Figa-Saldaña, and C. Anderson (2017), Triple collocation analysis of soil moisture from metop-a ascat and smos against jra-55 and era-interim, *IEEE Journal of Selected Topics in Applied Earth Observations and Remote Sensing*, *10*(5), 2274–2284, doi:10.1109/JSTARS.2016.2632306.

Mo, K. C., L.-C. Chen, S. Shukla, T. J. Bohn, and D. P. Lettenmaier (2012), Uncertainties in North American Land Data Assimilation Systems over the Contiguous United States, *Journal of Hydrometeorology*, *13*(3), 996–1009, doi:10.1175/JHM-D-11-0132.1.

Moench, M., J. Burke, and Y. Moench (2003), Rethinking the approach to groundwater and food security, *Rome: Food and Agriculture Organization of the United Nations*, Accessed from: ftp://ftp.fao.org/agl/aglw/docs/wr24e.pdf, on 01/03/2017.

Moore, P., and S. D. P. Williams (2014), Integration of altimetric lake levels and GRACE gravimetry over Africa: Inferences for terrestrial water storage change 2003 – 2011, *Water Resource Research*, *50*, 9696–9720, doi:10.1002/2014WR015506.

Morton, J. F. (2007), The impact of climate change on smallholder and subsistence agriculture, *Proceedings of the National Academy of Sciences*, *104*(50), 19,680–19,685, doi:10.1073/pnas.0701855104.

Mpelasoka, F., J. L. Awange, and A. Zerihun (2018), Influence of coupled ocean-atmosphere phenomena on the Greater Horn of Africa droughts and their implications, *Science of The Total Environment*, *610–611*, 691 – 702, doi:https://doi.org/10.1016/j.scitotenv.2017.08.109.

Mumma, A., M. Lane, E. Kairu, A. Tuinhof, and R. Hirji (2011), Kenya groundwater governance case study, *Water papers: World Bank*, Accessed from: www.worldbank.org/water on May 15, 2016.

Mutasim, B. N., and I. A. Elgizouli (n.d), Climate change adaptation and decision making in the Sudan, *World Resources Report*, Retreaved from:http://www.wri.org/our-work/project/world-resources-report, On 22/06/2017.

Mwangi, E., F. Wetterhall, E. Dutra, F. Di Giuseppe, and F. Pappenberger (2014), Forecasting droughts in East Africa, *Hydrology and Earth System Sciences*, *18*(2), 611–620, doi:10.5194/hess-18-611-2014.

Mwango, F. K., B. C. Muhangú, C. O. Juma, and I. T. Githae (2004), Groundwater resources in Kenya, in *Managing shared aquifer resources in Africa*, edited by G. Appelgren, p. 216, United Nations educational, Scientific and Cultural Organization., Accessed from: http://unesdoc.unesco.org/images/0013/001385/138581m.pdf on May 15, 2016.

Naresh Kumar, M., C. S. Murthy, M. V. R. Sesha Sai, and P. S. Roy (2009), On the use of Standardized Precipitation Index (SPI) for drought intensity assessment, *Meteorological Applications*, *16*(3), 381–389, doi:10.1002/met.136.

Naumann, G., E. Dutra, F. Pappenberger, F. Wetterhall, and J. V. Vogt (2014), Comparison of drought indicators derived from multiple data sets over Africa, *Hydrology and Earth System Sciences*, *18*, 1625–1640, doi:10.5194/hess-18-1625-2014.

Ndehedehe, C. E., J. L. Awange, R. J. Corner, M. Kuhn, and O. Okwuashi (2016), On the potentials of multiple climate variables in assessing the spatio-temporal characteristics of hydrological droughts over the Volta Basin, *Science of The Total Environment*, *557–558*, 819 – 837, doi:http://dx.doi.org/10.1016/j.scitotenv.2016.03.004.

New, M., M. Hulme, and P. Jones (2000), Representing Twentieth-Century Space–Time Climate Variability. Part II: Development of 1901–96 Monthly Grids of Terrestrial Surface Climate, *Journal of Climate*, *13*(13), 2217–2238, doi:10.1175/1520-0442(2000)013⟨2217:RTCSTC⟩2.0.CO;2.

Niang, I., O. C. Ruppel, M. A. Abdrabo, A. Essel, C. Lennard, J. Padgham, and P. Urquhart (2014), *Climate Change 2014: Impacts, Adaptation, and Vulnerability. Part B: Regional Aspects. Contribution of Working Group II to the Fifth Assessment Report of the Intergovernmental Panel on Climate Change*, chap. Africa, pp. 1199–1265, Cambridge University Press, Cambridge, United Kingdom and New York, NY, USA.

Nicholson, S. E. (2014a), A detailed look at the recent drought situation in the Greater Horn of Africa, *Journal of Arid Environments*, *103*, 71–79, doi:10.1016/j.jaridenv.2013.12.003.

Nicholson, S. E. (2014b), The Predictability of Rainfall over the Greater Horn of Africa. Part I: Prediction of Seasonal Rainfall, *Journal of Hydrometeorology*, *15*(3), 1011–1027, doi:10.1175/JHM-D-13-062.1.

Nicholson, S. E. (2015), Long-term variability of the East African 'short rains' and its links to large-scale factors, *International Journal of Climatology*, *35*(13), 3979–3990, doi:10.1002/joc.4259.

Nicholson, S. E. (2016), Climate and climatic variability of rainfall over eastern Africa, *Reviews of Geophysics*, *55*(3), 590–635, doi:10.1002/2016RG000544.

OEA (2011a), *Eastern Africa Drought humanitarian report*, OCHA Eastern Africa, number 3, 01–31 May 2011. Accessed from: http://reliefweb.int/report/burundi/eastern-africa-drought-humanitarian-report-no-3 on March 17,2015.

OEA (2011b), *Eastern Africa Drought humanitarian report*, OCHA Eastern Africa, number 4, 01 June – 15 July 2011. Accessed from: http://reliefweb.int/report/burundi/eastern-africa-drought-humanitarian-report-no-4 on March 17,2015.

Olsson, L. (1993), On the causes of famine: drought, desertification and market failure in the Sudan, *Ambio*, *22*(6), 395–403, url:http://www.jstor.org/stable/4314110.

Omer, A. (2002), Focus on groundwater in Sudan, *Environmental Geology*, *41*(8), 972–976, doi:10.1007/s00254-001-0476-9.

Oord, A., R. Collenteur, and L. Tolk (2014), Hydrological assessment of the Merti aquifer, Kenya, *Draft Report 01*, NERC – UPGRO, Accessed from:http://www.worldagroforestry.org, On May 15, 2016.

Pavelic, P., M. Keraita, V. Ramesh, and T. Rao (Eds.) (2012), *Groundwater availability and use in Sub-Sahara Africa: A review of 15 countries*, Colombo, Sri Lanka: International Water Management Institute (IWMI), doi: 10.5337/2012.213.

Peace Bulletin (2003), Conflicts impacting negatively on food secudity in Greater Horn of Africa, *ITDGPractical Action-EA Peace Bulletin*, https://practicalaction.org/peace3-food-security, keywords = ,

Peters, A. J., E. A. Waletr-Shea, L. Ji, A. Viña, M. Hayes, and M. V. Svoboda (2002), Drought monitoring with NDVI–Based Standardized Vegetation Index, *Photogrammetric Engineering & Remote Sensing*, *68*, 71 – 75.

Pinzon, J. E., and C. J. Tucker (2014), A Non-Stationary 1981–2012 AVHRR NDVI3g Time Series, *Remote Sensing*, *6*(8), 6929, doi:10.3390/rs6086929.

Preisendorfer, R. W. (1988), *Principal Component Analysis in Meteorology and Oceanography*, Development in Atmospheric Science 17, Elsevier, Elsevier, Amsterdam .

Premoli, A., and P. Tavella (1993), A revisited three-cornered hat method for estimating frequency standard instability, *IEEE Transactions on Instrumentation and Measurement*, *42*(1), 7–13, doi:10.1109/19.206671.

Pricope, N. G., G. Husak, D. Lopez-Carr, C. Funk, and J. Michaelsen (2013), The climate-population nexus in the East African Horn: Emerging degradation trends in rangeland and pastoral livelihood zones, *Global Environmental Change*, *23*(6), 1525 – 1541, doi:http://dx.doi.org/10.1016/j.gloenvcha.2013.10.002.

Quiring, S. M. (2009), Developing objective operational definitions for monitoring drought, *Journal of Applied Meteorology and Climatology*, *48*(6), 1217–1229, doi:10.1175/2009JAMC2088.1.

Quiring, S. M., and S. Ganesh (2010), Evaluation of utility of Vegetation Condition Index (VCI) for monitoring meteorological drought in Texas, *Agriculture and Forest Meteorology*, *150*, 330 – 339, doi:10.1016/j.agrformet.2009.11.015.

Rajner, M., and T. Liwosz (2017), Analysis of seasonal position variation for selected GNSS sites in Poland using loading modelling and GRACE data, *Geodesy and Geodynamics*, *8*(4), 253 – 259, doi:http://dx.doi.org/10.1016/j.geog.2017.04.001.

Raziei, T., B. saghafian, A. A. Paulo, L. S. Pereira, and I. Bordi (2009), Spatial patterns and temporal variability of drought in Western Iran, *Water Resource Management*, *23*, 439–455, doi:10.1007/s11269-008-9282-4.

Rencher, A. C., and G. B. Schaalje (2007), *Linear Models in Statistics*, chap. Simple Linear Regression, pp. 127–136, second edition ed., John Wiley & Sons, Inc., doi:10.1002/9780470192610.ch6.

Rhee, J., J. Im, and G. J. Carbone (2010), Monitoring agricultural drought for arid and humid regions using multi-sensor remote sensing data, *Remote Sensing of Environment*, *114*, 2875 – 2885, doi:10.1016/j.rse.2010.07.005.

Richman, M. B. (1986), Rotation of Principal Components, *Journal of Climatology*, *6*(2), 293–335.

Rienecker, M. M., M. J. Suarez, R. Gelaro, R. Todling, J. Bacmeister, E. Liu, M. G. Bosilovich, S. D. Schubert, L. Takacs, G.-K. Kim, S. Bloom, J. Chen, D. Collins, A. Conaty, A. da Silva, W. Gu, J. Joiner, R. D. Koster, R. Lucchesi, A. Molod, T. Owens, S. Pawson, P. Pegion, C. R. Redder, R. Reichle, F. R. Robertson, A. G. Ruddick, M. Sienkiewicz, and J. Woollen (2011), MERRA: NASA's Modern-Era Retrospective Analysis for Research and Applications, *Journal of Climate*, *24*(14), 3624–3648, doi:10.1175/JCLI-D-11-00015.1.

Rieser, D., M. Kuhn, R. Pail, I. M. Anjasmara, and J. Awange (2010), Relation between GRACE-derived surface mass variations and precipitation over Australia, *Australian Journal of Earth Sciences*, *57*(7), 887–900, doi:10.1080/08120099.2010.512645.

Rodell, M., P. R. Houser, U. Jambor, J. Gottschalck, K. Mitchell, C. J. Meng, K. Arsenault, B. Cosgrove, J. Radakovich, M. Bosilovich, J. K. Entin, J. P. Walker, D. Lohmann, and D. Toll (2004), The Global Land Data Assimilation System, *Bulletin of the American Meteorological Society*, *85*(3), 381 – 394, doi:10.1175/BAMS-85-3-381.

Rojas, O., A. Vrieling, and F. Rembold (2011), Assessing the drought probability for agricultural areas in Africa with coarse resolution remote sensing imagery, *Remote Sensing of Environment*, *115*, 343 – 352, doi:10.1016/j.rse.2010.09.006.

Romilly, T. G., and M. Gebremichael (2011), Evaluation of satellite rainfall estimates over Ethiopian river basins, *Hydrology and Earth System Sciences*, *15*(5), 1505–1514, doi:10.5194/hess-15-1505-2011.

Rouault, M., and Y. Richard (2003), Intensity and spatial extension of drought in South Africa at different time scales, *Water SA*, *29*(4), 489–500, doi:10.4314/wsa.v29i4.5057.

Rousel, J. W., R. H. Haas, J. A. Schell, D. W. Deering, and J. C. Harlan (1974), Monitoring the vernal advancement and retrogradation (green wave effect) of natural vegetation, *NASA/GSFC Type III Final Report*, Greenbelt, MD.

Rowhani, P., O. Degomme, D. Guha-Sapir, and E. F. Lambin (2011), Malnutrition and conflict in East Africa: the impacts of resource variability on human security, *Climatic Change*, *105*(1), 207–222, doi:10.1007/s10584-010-9884-8.

Royston, P. (1992), Approximating the shapiro-wilk w-test for non-normality, *Statistics and Computing*, *2*(3), 117–119, doi:10.1007/BF01891203.

Rui, H., and A. McNally (2016), FEWS NET Land Data Assimilation System Version 1 (FLDAS-1) Products README, *NASA/GSFC/HSL*, pp. 1–18, Retreaved from: ftp://hydro1.sci.gsfc.nasa.gov/data/s4pa/FLDAS/FLDAS, On September 23 2016.

Saji, N. H., B. N. Goswami, P. N. Vinayachandran, and T. Yamagata (1999), A dipole mode in the tropical Indian Ocean, *Letters to Nature*, *401*, 360–363.

Sakumura, C., S. Bettadpur, and S. Bruinsma (2014), Ensemble prediction and intercomparison analysis of GRACE time-variable gravity field models, *Geophysical Research Letters*, *41*(5), 1389–1397, doi:10.1002/2013GL058632.

Salama, B. R. (1988), Groundwater resources of Sudan, *Rural Water Corporation*, *824SD76-474*, Accessed from:

http://www.ircwash.org/sites/default/files/824SD76-474.pdf on May 15, 2016.

Salifu, M., F. Aidoo, M. S. Hayford, D. Adomako, and E. Asare (2015), Evaluating the suitability of groundwater for irrigational purposes in some selected districts of the Upper West region of Ghana, *Applied Water Science*, pp. 1–10, doi:10.1007/s13201-015-0277-z.

Santos, J. F., I. Pulido-Calvo, and M. M. Portela (2010), Spatial and temporal variability of drought in Portugal, *Water Resource Research*, *46*(3), n/a–n/a, doi:10.1029/2009WR008071, w03503.

Scanlon, B. R., K. E. Keese, A. L. Flint, L. E. Flint, C. B. Gaye, W. M. Edmunds, and I. Simmers (2006), Global synthesis of groundwater recharge in semiarid and arid regions, *Hydrological Processes*, *20*(15), 3335–3370, doi:10.1002/hyp.6335.

Scheffran, J., and A. Battaglini (2011), Climate and conflicts: the security risks of global warming, *Regional Environmental Change*, *11*(1), 27–39, doi:10.1007/s10113-010-0175-8.

Schmidhuber, J., and F. N. Tubiello (2007), Global food security under climate change, *Proceedings of the National Academy of Sciences*, *104*(50), 19,703–19,708, doi:10.1073/pnas.0701976104.

Schneider, U., A. Becker, P. Finger, A. Meyer-Christoffer, M. Ziese, and B. Rudolf (2014), GPCC's new land surface precipitation climatology based on quality-controlled in situ data and its role in quantifying the global water cycle, *Theoretical and Applied Climatology*, *115*(1), 15–40, doi:10.1007/s00704-013-0860-x.

Schönemann, P. H. (1958), Varisim: A new machine method for orthogonal rotation, *Psychometrika*, *31*(2), 235–248, doi:10.1007/BF02289510.

Schreck, C. J., and F. H. M. Semazzi (2004), Variability of the recent climate of eastern Africa, *International Journal of Climatology*, *24*(6), 681–701, doi:10.1002/joc.1019.

Segele, Z. T., P. J. Lamb, and L. M. Leslie (2009), Seasonal-to-Interannual Variability of Ethiopia/Horn of Africa Monsoon. Part I: Associations of Wavelet-Filtered Large-Scale Atmospheric Circulation and Global Sea Surface Temperature, *Journal of Climate*, *22*(12), 3396–3421, doi:10.1175/2008JCLI2859.1.

Sellers, P. J., Y. Mintz, Y. C. Sud, and A. Dalcher (1986), A simple biosphere model (sib) for use within general circulation models, *Journal of the Atmospheric Sciences*, *43*(6), 505–531, doi:10.1175/1520-0469(1986)043⟨0505:ASBMFU⟩2.0.CO;2.

Selley, R. (1997), *African Basins*, Sedimentary Basins of the World, Elsevier Science.

Shapiro, S. S., and M. B. Wilk (1965), An analysis of variance test for normality (complete samples), *Biometrika*, *52*(3/4), 591–611.

Shapiro, S. S., M. B. Wilk, and H. J. Chen (1968), A comparative study of various tests for normality, *Journal of the American Statistical Association*, *63*(324), 1343–1372.

Sheffield, J., and E. F. Wood (2008), Global trends and variability in soil moisture and drought characteristics, 1950 – 2000, from observation-driven simulations of the terrestrial hydrologic cycle, *Journal of Climate*, *21*(3), 432–458.

Sheffield, J., G. Goteti, and E. F. Wood (2006), Development of a 50-year high-resolution global dataset of meteorological forcings for land surface modeling, *Journal of Climate*, *19*(13), 3088–3111, doi:10.1175/JCLI3790.1.

Sheffield, J., E. F. Wood, N. Chaney, K. Guan, S. Sadri, X. Yuan, L. Olang, A. Amani, A. Ali, S. Demuth, and L. Ogallo (2014), A drought monitoring and forecasting system for Sub-Sahara African water resources and food security, *Bulletin of the American Meteorological Society*, *95*(6), 861–882, doi:10.1175/BAMS-D-12-00124.1.

Shiferaw, B., K. Tesfaye, M. Kassie, T. Abate, B. Prasanna, and A. Menkir (2014), Managing vulnerability to drought and enhancing livelihood resilience in Sub-Saharan Africa: Technological, institutional and policy options, *Weather and Climate Extremes*, *3*, 67 – 79, doi:http://doi.org/10.1016/j.wace.2014.04.004, high Level Meeting on National Drought Policy.

Shiklomanov, I., and J. Rodda (2004), *World Water Resources at the Beginning of the Twenty-First Century*, International Hydrology Series, Cambridge University Press.

Shukla, S., A. McNally, G. Husak, and C. Funk (2014), A seasonal agricultural drought forecast system for food-insecure regions of East Africa, *Hydrology and Earth System Sciences*, *18*(10), 3907–3921, doi:10.5194/hess-18-3907-2014.

Siebert, S., J. Burke, J. M. Faures, K. Frenken, J. Hoogeveen, P. Döll, and F. T. Portmann (2010), Groundwater use for irrigation – a global inventory, *Hydrology and Earth System Sciences*, *14*(10), 1863–1880, doi:10.5194/hess-14-1863-2010.

Sigdel, M., and M. Ikeda (2010), Spatial and temporal analysis of drought in Nepal using standardised precipitation index and its relationship with climate indices, *Journal of Hydrology and Meteorology*, *7*(1), 59–74, doi:10.3126/jhm.v7i1.5617.

Souverijns, N., W. Thiery, M. Demuzere, and N. P. M. V. Lipzig (2016), Drivers of future changes in East African precipitation, *Environmental Research Letters*, *11*(11), 114,011.

Spinage, C. (2012), *African Ecology: Benchmarks and Historical Perspectives*, Springer Geography, Springer Berlin Heidelberg.

Stampoulis, D., K. M. Andreadis, S. L. Granger, J. B. Fisher, F. J. Turk, A. Behrangi, A. V. Ines, and N. N. Das (2016), Assessing hydro-ecological vulnerability using microwave radiometric measurements from WindSat, *Remote Sensing of Environment*, *184*, 58 – 72, doi:http://dx.doi.org/10.1016/j.rse.2016.06.007.

Steduto, P., T. C. Hsiao, E. Fereres, and D. Raes (2012), Crop yield response to water, *FAO Irrigation and Drainage paper No. 66*, Rome, FAO. Accessed from: http://www.fao.org/docrep/016/i2800e/i2800e00.htm on March 15, 2015.

Svoboda, M., M. Hayes, and D. Wood (2012), *Standardized precipitation index user guide*, World meteorological organization, WMO - No. 1090, Geneva, Accessed from: http://www.wamis.org/agm/pubs/SPI on March 15, 2015.

Swarzenski, W. V., and M. J. Mundorff (1973), Geohydrology of North Eastern Province, Kenya, *USGS, Water Supply Paper 1757-N*, Accessed from: http://pubs.usgs.gov/wsp/1757n/report.pdf on May 15, 2016.

Swenson, S., and J. Wahr (2009), Monitoring the water balance of Lake Victoria, East Africa, from space, *Journal of Hydrology*, *370*, 163–176, doi:10.1016/j.jhydrol.2009.03.008.

Swenson, S., D. Chambers, and J. Wahr (2008), Estimating geocenter variations from a combination of GRACE and ocean model output, *Journal of Geophysical Research: Solid Earth*, *113*(B8), n/a–n/a, doi:10.1029/2007JB005338, b08410.

Tadesse, T., M. Haile, G. Senay, B. D. Wardlow, and C. L. Knutson (2008), The need for integration of drought monitoring tools for proactive food security management in sub-Saharan Africa, *Natural Resources Forum*, *32*, 265 – 279.

Taffesse, A. S., P. A. Dorosh, and S. Asrat (2012), Crop production in Ethiopia: regional patterns and trends, *Research Note 11*, International Food Policy Research Institute, Addis Ababa, Ethiopia, Accessed from: http://www.ifpri.org/publication/crop-production-ethiopia-regional-patterns-and-trends on March 15, 2015.

Tallaksen, L., and H. van Lanen (2004), *Hydrological Drought: Processes and Estimation Methods for Streamflow and Groundwater*, Developments in water science, Elsevier.

Tapley, B., S. Belabour, M. Watkins, and C. Reigber (2004), The Gravity Recovery and Climate Experiment: Mission overview and early results, *Geophysical Research Letters*, *31*, 1 – 4, doi:10.1029/2004GL019920.

Tavella, P., and A. Premoli (1994), Estimating the instabilities of n clocks by measuring differences of their readings, *Metrologia*, *30*(5), 479.

Taylor, G. R., M. C. Todd, L. Kongola, L. Mourice, E. Nahozya, H. Sanga, and A. M. MacDonald (2012), Evidence of the dependence of groundwater resources on extreme rainfall in East Africa, *Nature Climate Change*, *3*, 374–378, doi:10.1038/nclimate1731.

Taylor, K. E. (2001), Summarizing multiple aspects of model performance in a single diagram, *Journal of Geophysical Research: Atmospheres*, *106*(D7), 7183–7192, doi:10.1029/2000JD900719.

Taylor, R. G., B. Scanlon, P. Döll, M. Rodell, R. van Beek, Y. Wada, L. Longuevergne, M. Leblanc, J. S. Famiglietti, M. Edmunds, L. Konikow, T. R. Green, J. Y. Chen, M. Taniguchi, M. F. P. Bierkens, A. MacDonald, Y. Fan, R. M. Maxwell, Y. Yechieli, J. J. Gurdak, D. M. Allen, M. Shamsudduha, K. Hiscock, P. J. F. Yeh, I. Holman, and H. Treidel (2013), Ground water and climate change, *Nature Climate Change*, *3*(4), 322–329, doi:10.1038/nclimate1744.

Technical Cooperation Department (2000), The elimination of food insecurity in the Horn of Africa: A strategy for concerted government and UN agency action - FINAL REPORT, *FAO Corporate Document Repository*, pp. 1–21, Accessed from: http://www.fao.org/docrep/003/x8406e/X8406e05.htm, on 27/04/2017.

The Editors of Encyclopædia Britannica (2017), East African Rift System, *Encyclopædia Britannica, inc.*, Retreaved from:https://www.britannica.com/place/East-African-Rift-System, On 29/06/2017.

Thenkabail, P., M. Gamage, and I. Institute (2004), *The Use of Remote Sensing Data for Drought Assessment and Monitoring in Southwest Asia*, IWMI Research Report, International Water Management Institute.

Toothaker, L. (1993), *Multiple Comparison Procedures*, no. 89 in Multiple Comparison Procedures, SAGE Publications.

Tucker, C., J. Pinzon, M. Brown, D. Slayback, E. Pak, R. Mahoney, E. Vermote, and N. El Saleous (2005), An extended AVHRR 8-km NDVI dataset compatible with MODIS and SPOT vegetation NDVI data, *International Journal of Remote Sensing*, *26*(20), 4485–4498, doi:10.1080/01431160500168686.

Tucker, C. J. (1979), Red and photographic infra-red linear combinations for monitoring vegetation, *Remote Sensing of Environment*, *8*, 127–150, doi:10.1016/0034-4257(79)90013-0.

United Nations (2015), World population prospects: The 2015 revision, key findings and advance tables, *Department of Economic and Social Affairs, Population Division, New York*, (Working Paper No. ESA/P/WP.241).

van den Dool, H., J. Huang, and Y. Fan (2003), Performance and analysis of the constructed analogue method applied to U.S. soil moisture over 1981–2001, *Journal of Climate*, *108(D16)*, 8617, doi:10.1029/2002JD003114.

van Huffel, S. (1997), *Recent Advances in Total Least Squares Techniques and Errors-in-variables Modeling*, SIAM Proceedings in Applied Mathematics Series, Society for Industrial and Applied Mathematics.

Verdin, J., C. Funk, G. Senay, and R. Choularton (2005), Climate science and famine early warning, *Philosophical Transactions of the Royal Society of London B: Biological Sciences*, *360*(1463), 2155–2168, doi:10.1098/rstb.2005.1754.

Villholth, K. G. (2013), Groundwater irrigation for smallholders in Sub-Saharan Africa – a synthesis of current knowledge to guide sustainable outcomes, *Water International*, *38*(4), 369–391, doi:10.1080/02508060.2013.821644.

Vinzi, V., W. Chin, J. Henseler, and H. Wang (2010), *Handbook of Partial Least Squares: Concepts, Methods and Applications*, Springer Handbooks of Computational Statistics, Springer Berlin Heidelberg.

Viste, E., D. Korecha, and A. Sorteberg (2013), Recent drought and precipitation tendencies in Ethiopia, *Theoretical Applied Climatology*, *112*, 535–551, doi:10.1007/s00704-012-0746-3.

Voll, J., and S. Voll (2016), *The Sudan: Unity and Diversity in a Multicultural State*, Routledge Library Editions: Sudan, Taylor & Francis.

von Storch, H., and F. W. Zwiers (1999), *Statistical Analysis in Climate Research*, Cambridge University Press: Cambridge.

Wahr, J., M. Molenaar, and F. Bryan (1998), Time variability of the Earth's gravity field: Hydrological and Oceanic effects and their possible detection using GRACE, *Journal of Geophysical Research-Solid Earth*, *103(B12)*, 30,205–30,229, doi:10.1029/98JB02844.

Wellfield, C., and G. S. British (2011), Groundwater and drought management project: regional groundwater monitoring network, *Transboundary*

aquifer report, Southern Africa Development Community, Accessed from: http://resources.bgs.ac.uk/sadcreports/sadc2011wellfieldbgstransboundaryaquifersinsadc.pdf on July 15, 2016.

Wichelns, D. (2014), Investing in small, private irrigation to increase production and enhance livelihoods, *Agricultural Water Management*, *131*, 163 – 166, doi:http://dx.doi.org/10.1016/j.agwat.2013.09.003.

Wilhite, D. A., and R. S. Pulwarty (2005), *Drought and Water Crises: Science, Technology, and Management Issues*, chap. Drought and Water Crises: Lessons Learned and the Road Ahead, pp. 389–398, CRC Press, Boca Raton,Florida.

Wilhite, D. A., M. V. Sivakumar, and R. Pulwarty (2014), Managing drought risk in a changing climate: The role of national drought policy, *Weather and Climate Extremes*, *3*, 4 – 13, doi:http://doi.org/10.1016/j.wace.2014.01.002.

Wilks, D. S. (2006), *Statistical methods in atmospheric sciences*, second ed., Academic press, Amsterdam.

Williams, A. P., and C. Funk (2011), A westward extension of the warm pool leads to a westward extension of the Walker circulation, drying Eastern Africa, *Climate Dynamics*, *37*(11), 2417–2435, doi:10.1007/s00382-010-0984-y.

Williams, A. P., C. Funk, J. Michaelsen, S. A. Rauscher, I. Robertson, T. H. G. Wils, M. Koprowski, Z. Eshetu, and N. J. Loader (2012), Recent summer precipitation trends in the Greater Horn of Africa and the emerging role of Indian Ocean Sea surface temperature, *Journal of Climate Dynamics*, *39*, 2307–2328, doi:10.1007/s00382-011-1222-y.

Wold, S., M. Sjöström, and L. Eriksson (2001), Pls-regression: a basic tool of chemometrics, *Chemometrics and Intelligent Laboratory Systems*, *58*(2), 109 – 130, doi:http://dx.doi.org/10.1016/S0169-7439(01)00155-1.

Wolter, K., and M. S. Timlin (2011), El Niño/Southern Oscillation behaviour since 1871 as diagnosed in an extended multivariate ENSO index (MEI.ext), *International Journal of Climatology*, *31*(7), 1074–1087, doi:10.1002/joc.2336.

Wouters, B., J. A. Bonin, D. P. Chambers, R. E. M. Riva, I. Sasgen, and J. Wahr (2014), GRACE, time-varying gravity, earth system dynamics and climate change, *Reports on Progress in Physics*, *77*, 41pp, doi:10.1088/0034-4885/77/11/116801.

Wu, H., M. J. Hayes, A. Weiss, and Q. Hu (2001), An evaluation of the standardized precipitation index, the China-Z index and the statistical Z-Score, *International Journal of Climatology*, *21*, 745–758, doi:10.1002/joc.658.

Xie, H., L. You, B. Wielgosz, and C. Ringler (2014), Estimating the potential for expanding smallholder irrigation in Sub-Saharan Africa, *Agricultural Water Management*, *131*, 183 – 193, doi:http://dx.doi.org/10.1016/j.agwat.2013.08.011.

Xu, H., C.-Y. Xu, H. Chen, Z. Zhang, and L. Li (2013), Assessing the influence of rain gauge density and distribution on hydrological model performance in a humid region of China, *Journal of Hydrology*, *505*, 1 – 12, doi:https://doi.org/10.1016/j.jhydrol.2013.09.004.

Yang, W., R. Seager, and M. A. Cane (2014a), The East African Long rains in Observations and Models, *Journal of Climate*, *27*, 7185–7202, doi:10.1175/JCLI-D-13-00447.1.

Yang, Y., D. Long, H. Guan, B. R. Scanlon, C. T. Simmons, L. Jiang, and X. Xu (2014b), GRACE satellite observed hydrological controls on interannual and seasonal variability in surface greenness over mainland Australia, *Journal of Geophysical Research: Biogeosciences*, *119*, 2245–2260, doi:10.1002/2014JG002670.

Yilmaz, M. T., M. C. Anderson, B. Zaitchik, C. R. Hain, W. T. Crow, M. Ozdogan, J. A. Chun, and J. Evans (2014), Comparison of prognostic and diagnostic surface flux modeling approaches over the Nile River basin, *Water Resources Research*, *50*(1), 386–408, doi:10.1002/2013WR014194.

Zaroug, M. G. (2000), Country pasture/forage resource profiles: Sudan, Retreaved from:http://www.fao.org/ag/agp/agpc/doc/Counprof/sudan/sudan.htm, On 22/06/2017.

Zhang, L., H. Dobslaw, T. Stacke, A. Güntner, R. Dill, and M. Thomas (2017), Validation of terrestrial water storage variations as simulated by different global numerical models with GRACE satellite observations, *Hydrology and Earth System Sciences*, *21*(2), 821–837, doi:10.5194/hess-21-821-2017.

Ziese, M., U. Schneider, A. Meyer-Christoffer, K. Schamm, J. Vido, P. Finger, P. Bissolli, S. Pietzsch, and A. Becker (2014), The GPCC drought index – a new, combined and gridded global drought index, *Earth System Science Data*, *6*(2), 285–295, doi:10.5194/essd-6-285-2014.

Zimmerman, F. J., and M. R. Carter (2003), Asset smoothing, consumption smoothing and the reproduction of inequality under risk and subsistence constraints, *Journal of Development Economics*, *71*(2), 233 – 260, doi:https://doi.org/10.1016/S0304-3878(03)00028-2.

Every reasonable effort has been made to acknowledge the owners of copyright material. I would be pleased to hear from any copyright owner who has been omitted or incorrectly acknowledged.

List of Figures

List of Tables